Torrefied Biomass for Large-Scale Electricity Generation

Paula McNamee

Submitted in accordance with the requirements for the degree of Doctor of Philosophy as part of the Integrated PhD with MSc in Low Carbon Technologies

May 2016

Doctoral Training Centre in Low Carbon Technologies,
Energy Research Institute, School of Chemical and Process Engineering,
University of Leeds

Declaration of Authorship

The candidate confirms that the work submitted is her own, except where work which has formed part of jointly-authored publications has been included. The contribution of the candidate and the other authors to this work has been explicitly indicated below. The candidate confirms that appropriate credit has been given within the thesis where reference has been made to the work of others.

The work contained in Chapter 7 and part of the work in Chapter 5 is based on the following publication:

McNamee, P., Adams, P.W.R., McManus, M.C., Dooley, B., L.I. Darvell, Williams, A., and Jones, J.M., *An Assessment of the torrefaction of North American pine and life-cycle greenhouse gas emissions,* Energy Conversion and Management. 113 (2016) 177-188.

I am the lead author of this paper and carried out all experimental work, characterisation and data elucidation in Chapter 5 with the exception of the cell wall contents determination which was performed by the Institute of Biological, Environmental and Rural Sciences at the University of Aberystwyth. I performed all of the mass and energy balance determinations and energy requirement calculations performed in Chapter 7 with the GHG emissions assessment a joint collaboration between myself and Dr Paul W.R. Adams at the University of Bath. Advice, help and guidance was provided by the other authors on this work.

The work contained in Chapter 6 is based on the following publication:

McNamee, P., Darvell, L.I., Williams, A., and Jones, J.M., *The combustion characteristics of high-heating-rate chars from untreated and torrefied biomass fuels*, Biomass and Bioenergy. 82 (2015) 63-72.

I am the lead authors this work and carried out all experimental work, characterisation and data elucidation with the exception of the chlorine contents determination and ICP-MS analysis which were performed in the University of Leeds Chemistry Department and Energy Resource Institute laboratories in the School of Chemical and Process engineering respectively. Advice, help and guidance was provided by the other authors on this work.

Acknowledgements

Firstly I would like to thank my supervisors Professor Jenny Jones, Dr. Leilani Darvell and Professor Alan Williams for their constant support, help and guidance throughout my PhD. None of this work would be possible without them and I will be forever grateful to them for letting me undertake this project.

I would also like to thank the members of my research group past and present- Ben Dooley, Patrick Mason, Yee-Sing Chin, Farooq Abubakar Atiku, Eddy Mitchell, Peinong Xing, Dr. Addy Saddawi, Dr. Bijal Gudka and Dr. Femi Akinrinola for their support and friendship throughout my PhD.

Several member of the university staff have also helped me during my research- Susanne Patel, Stuart Mickelthwaite, Sara Dona, Simon Lloyd, Ed Woodhouse, John Cran, Dr. Adrian Cunliffe, Karine Alves Thorne, James McKay, Emily Bryan-Kinns, Rachael Brown, David Haynes and Heather Strachan- who I would also like to thank. As well as members of staff at the University of Leeds, I would like to thank Dr. Paul Adams and Dr. Marcelle McManus at the University of Bath, who I worked with on some aspects of this research, for their help and for welcoming me in Bath.

I would also like to thank the Engineering and Physical Sciences research council (EPSRC) for my studentship and members of the Supergen Bioenergy Hub who I have worked with throughout my research.

Several members of the DTC in Low Carbon Technologies and beyond deserve special mention for their love, support and friendship throughout my PhD and for all the good times along away- Dave Allen, Holly Edwards, Clare Linton, Zarashpe Kapadia, Ramzi Cherad, Thom Best, Jo Robinson, David Jacques, Harriet Fletcher, Josh Cottom, Morgan Tatchell-Evans, Lloyd Davies, Stephen Chilton, Jamie Bright, Richard Riley, Aidan Smith, Dougie Phillips, Rob Bloom, Jannik Giesekam, Andy Dixon, Arthur Goodland, Rebecca Sheridan, Radka Jersáková, Florian Sturm, Scott Onder and last but by no means least Michael Smith.

Finally, I would like express deepest gratitude to my family- my mum, Jeanette, my dad, Patrick and my sister Karen (in addition to the newest members Sophie and Lewis!) for their endless love and constant support. My love for Jake also deserves a special mention in these acknowledgements- not a day goes by where I don’t think of you.

Abstract

Bioenergy is increasingly being used a means of combatting the effects of anthropogenic climate change in sectors such as the power industry. Problems can exist in utilising biomass fuels however such as high moisture contents and low calorific value when compared with fossil fuels. Torrefaction is a pre-treatment process that aims to address some of these issues. In this pre-treatment step, solid biomass is heated in an inert atmosphere to between temperatures between 200 and 300°C resulting in the loss of low-energy volatiles and moisture improving fuel chemical and physical properties and is the focus of this thesis work. Firstly, the effect of changing torrefaction temperature and residence time is investigated. Results show that torrefaction increases the calorific value of fuels via reduction in moisture and volatiles contents as a result of degradation of some of the lignocellulosic components- this also improving the grindability characteristics of torrefied materials- with these change more pronounced as conditions become more severe. Results further show that with increasing torrefaction severity, the solid product yields decrease while the liquid and gaseous products increase. The combustion properties of torrefied biomass is also investigated, with results showing that torrefaction reduces the reactivity of biomass fuels and that upon rapid devolatilisation, chars from torrefied fuels differ morphologically to those of untreated biomass and undergo a lesser degree of burnout. Results also show that promotion of nitrogen to the gas phase during rapid devolatilisation may be fuel dependent after torrefaction has been performed. Finally, the effect of torrefaction of supply chain GHG emissions is investigated where it was found that GHG savings can be made as a result of increased calorific value in torrefied materials. Emissions savings are maximised where heat integration of the combustion of the volatiles gases evolved during torrefaction is implemented and wood chips are used as utility fuel. Results also indicate that torrefaction favours long distance transport as a result of improved fuel properties.

Contents

List of Figures

List of Tables

Nomenclature

A	Exponential Factor
ADF	Acid Detergent Fibre
ADL	Acid Detergent Lignin
A_g	Surface Area
ar	As received basis
BET	Brunauer-Emmet-Teller method
BETTA	British Electricity Trading and Transmission Arrangements
C=O	Carbonyl group
C_2H_4	ethene
C-C	Carbon-Carbon bond
CCGT	Combined Cycle Gas Turbine
CEGB	Central Electricity Generating Board
CfD	Contract for Difference
CH_4	Methane
CHP	Combined Heat and Power
CM	Capacity Market
CO	Carbon Monoxide
CO_2	Carbon Dioxide
$Cp_{dry\ wood}$	heat capacity of dry pine
$Cp_{moisture}$	heat capacity of water
CPS	Cycles per second
$Cp_{torrefied\ wood}$	heat capacity of torrefied pine
$Cp_{wet\ wood}$	heat capacity of wet pine
daf	dry-ash free
db	Dry basis
DECC	Department of Energy and Climate Change

DNC	Declared Net Capacity
DTF	Drop Tube Furnace
DTI	Department of Trade and Industry
E	total emissions from the production of the fuel before energy conversion
E_A	Activation Energy
EC	European Commission
e_{ccr}	Emission savings from carbon capture and replacement
e_{ccs}	Emission savings from carbon capture and geological storage
EC_{el}	Total greenhouse gas emissions from the final energy commodity
EDX	Energy Dispersive X-ray Spectroscopy
e_{ec}	Emissions from the extraction or cultivation of raw materials,
e_l	Annualised emissions from carbon stock changes caused by land use change
EMR	Electricity Market Reform
e_p	Emissions from processing
e_{sca}	Emission savings from soil carbon accumulation via improved agricultural management
ESI	Electricity Supply Industry
e_{td}	Emissions from transport and distribution
EU ETS	European Union Emissions Trading Scheme
EU RED	European Union Renewable Energy Directive
e_u	Emissions from the fuel in use, that is greenhouse gases emitted during the combustion of solid and gaseous biomass
exp	Exponential
FFL	Fossil Fuel Levy
FiTs	Feed-In Tariffs

FPN	Final Physical Notification
GC	Gas Chromatography
gCO_2e	Grams of CO_2 equivalent
$gCO_2e/MJ_{electricity}$	Grams of CO_2 equivalent per MJ of electricity delivered
GCV	Gross Calorific Value
GHG	Greenhouse Gas
GW	Gigawatt
GWh	Gigawatt-hour
H_2O	Water
H_c	Heat of combustion
HCN	Hydrogen Cyanide
H-EB	Scottish Hydro-Electric Board
HFCs	Hydrofluorocarbons
HGI	Hardgrove Index
HGI_{equiv}	Hardgrove Index Equivalent
HHV	Higher Heating Value
HPLC	High Pressure Liquid Chromatography
H_{vap}	Enthalpy of vaporisation
ILUC	Indirect Land-use change
IPCC	Intergovernmental Panel on Climate Change
IPP	Independent Power Producer
IR	Infrared
k	reaction rate constant
$kgCO_2e/MWh$	Kilograms of CO_2 equivalent per megawatt-hour
kJ	Kilojoule
kPa	Kilopascals
Ktoe	Kilo-ton oil equivalent
LCA	Life-cycle Assessment

LCPD	Large Combustion Plant Directive
LHV	Lower Heating Value
LOLP	Loss of load probability
LUC	Land-use change
M/Z	Mass to charge ratio
mg	Milligram (10^{-3}g)
MJ	Mega-joule
Modt	Million oven dried tonnes
mol	moles
MW	Megawatt
MWh	Megawatt-Hour
MW_{th}	Megawatt Thermal
N_2	Nitrogen
N_2O	Nitrous oxide
NCV	Net Calorific Value
NDF	Neutral Detergent Fibre
NETA	New Electricity Trading Arrangements
NFFO	Non-Fossil Fuel Obligation
NG	Natural gas
NGC	National Grid Company
NH_3	Ammonia
nm	Nanometre (10^{-9}m)
NMR	Nuclear Magnetic Resonance Spectroscopy
NO	Nitric Oxide
NO_2	Nitrogen Dioxide
NO_x	Nitrogen Oxide
η_a	Aqueous phase mass yield
Ŋel	Electrical efficiency, defined as the annual electricity produced divided by the annual fuel input.

η_m	Solid phase mass yield
η_o	Organic phase mass yield
O_2	Oxygen
OFFER	Office of Electricity Regulation
OFGEM	Office of Gas and Electricity Market
OH	Hydroxyl Group
pf	Pulverised fuel
PFCs	Perfluorocarbons
PID	Proportional-Integral-Derivative
PM	Particulate Matter
P^n	Partial Pressure of Reacting gas
ppm	parts per million
PPP	Pool purchase price
PSP	Pool selling price
R	Universal Gas Constant
Rc	Overall chemical reactivity
REC	Regional Electricity Company
RF	Radiative Forcing
R_i	Intrinsic Reactivity
RO	Renewables Obligation
ROC	Renewables Obligation Certificate
SEM	Scanning Electron Microscopy
SF_6	Sulphur Hexafluoride
SMP	System Marginal Price
SO_2	Sulphur Dioxide
SSEB	South of Scotland Electricity Board
TC	Thermocouple
TC	Total Carbon

TCD	Thermal Conductivity Detector
TGA	Thermogravimetric Analysis
TIC	Total Inorganic Carbon
TOC	Total Organic Carbon
TP	Torrefied Pellets
UNFCCC	United Nations Framework Convention on Climate Change
UV	Ultra-violet
VOCs	Volatile Organic Carbons
VOLL	Value of lost load
W/m^2	Watts per metre squared
WC	Wood chips
WP	Wood Pellets
Wt%	Weight percent
Y_e	Energy Yield
Y_m	Mass Yield
µm	Micrometre (10^-

1 Thesis Overview and Research Objectives

1.1 Thesis Overview

This project investigates the use of torrefied biomass in large scale power generation and is comprised of three main bodies of research. The first investigates how different torrefaction reaction conditions whereby the temperature and residence time are changed affect the physical and chemical properties of biomass and how changing these conditions impact the mass and energy balance of the process. This was achieved by conducting laboratory based torrefaction experiments using a bench top reactor on two woody biomass fuels: pine and eucalyptus and changing the temperature and residence time (the time the wood is at the final temperature). A series of fuel analyses were then undertaken to determine the changes relative to untreated biomass. These changes to fuel properties upon torrefaction, such as increased calorific value and better grindability, are crucial to understand in order to ascertain any benefits that can be achieved. Investigation of these parameters at laboratory scale provide information on the specific behaviour of these fuels to this thermal pre-treatment and lead the way for process optimisation at larger-scales. The mass and energy balances i.e. the distribution of mass and energy from the parent fuel to the solid, liquid and gaseous torrefaction products was also investigated to understand the degree of change that takes place-under each condition.

Following this, research in to the combustion properties of torrefied biomass was investigated. During solid fuel combustion in high temperature boiler system, such as those encountered in large-scale power generation, pulverised fuel particles enter the boiler and are heated at rapid rates (10^4-10^5 K/s). During this process, the fuel particles first undergo drying and devolatilisation, followed by combustion of volatile gases, eventually producing char particles which then undergo combustion: the char combustion the slowest step which dictates the rate of reaction. To investigate the impact of fast heating rate devolatilisation on torrefied fuel char reactivity- fast heating rate, high temperature chars were prepared using a drop tube furnace (DTF) from torrefied and untreated willow and eucalyptus fuels. The heating rates (10^4-10^5 K/s) and temperature (1100°C) used in the DTF provide laboratory scale conditions as close as possible to pulverised fuel combustion in large scale power generation. From this, the oxidative reactivity of the chars and morphology of chars were further investigated. Investigation of the fate of nitrogen species (to determine potential NO_X emissions) during rapid devolatilisation as well as the potential impact of catalytically active potassium on devolatilisation are also

investigated. This body of work therefore attempts to investigate how torrefied biomass would behave in a large-scale boiler system.

The last section of research addresses of the effect of torrefaction on supply chain greenhouse gas (GHG) emissions. Including torrefaction as pre-treatment step in a bioenergy supply chain can lead to emissions savings from improvements in fuel properties e.g. increased calorific value lowering emissions on a per MJ of electricity delivered basis. Conversely, they can also contribute emissions as a direct result of the addition of the processing step. Investigating using a life-cycle approach allows the overall impact of torrefaction to be understood. To achieve this, a model was created to determine the energy requirements of the torrefaction of North American process (based on sensible and latent energy requirements). This was undertaken using the data from pine torrefaction experiments discussed above. This data was then incorporated in to a bespoke bioenergy chain in which pine is grown, torrefied and pelleted in North America before being shipped to the United Kingdom where it is used in large-scale power plant to produce electricity. The data are then compared to the exact same supply chain without torrefaction included for comparison. The life-cycle GHG emissions at each stage were calculated in accordance with the EU Renewable Energy Directive methodology.

The main research activities of this project are described above and can be found in Chapters 5-7 in this thesis. Before these results, an introduction to the recent history of the electricity supply industry in the UK is present in Chapter 2 which also includes some of the political and economic incentives presently operating in the UK for the deployment of biomass and other renewables in large scale power generation. The introduction also includes a discussion of biomass and its fuel properties. Following this, the literature review in Chapter 3 covers a detailed description of torrefaction and its impact on fuel properties, referencing other research studies in this area. The literature review also reviews the combustion properties of untreated and torrefied biomass, analysing some of the current studies in the field. A separate literature review describing the methodology used in the EU to calculate life-cycle GHG emissions in addition to studies which investigate the impact of torrefaction is included as part of Chapter 7.

This research is funded by the Engineering and Physical Sciences Research Council (EPRSC) (Grant Ref: EP/G036608). Some aspects of this research are supported by the EPSRC Supergen Bioenergy Hub [Grant Ref: EP/J017302/1].

1.2 Objectives

The specific objectives of this research are described below:

1) To understand the history of the electricity supply industry in the UK and the political drivers supporting the deployment of bioenergy on large scales to understand how renewable energy deployment has increased in recent time as well the incentives in place which allow large-scale deployment to take place.
2) To perform laboratory based torrefaction experiments using a bench-scale reactor on two fuels: North American pine (softwood) and eucalyptus (hardwood) employing a series of different reaction conditions by varying the temperature and residence times. This will ascertain the impact of changing conditions on the mass and energy balances of the processes.
3) To analyse the solid and liquid products from the torrefaction of pine and eucalyptus and determine the overall changes in physical and chemical fuel properties
4) To perform overall elemental balances for the species C, H and N during torrefaction
5) To prepare fast heating rate chars from untreated and torrefied (under 3 conditions) willow and eucalyptus fuels using a high temperature (1100°C) drop tube furnace
6) To determine the oxidation kinetics of high-heating rates chars produced from untreated and torrefied willow and eucalyptus
7) To determine the surface area and surface morphology of fast-heating rate biomass char particles
8) To determine the partitioning of nitrogen and potassium during fast heating rate devolatilisation
9) To determine the pyrolysis kinetics of untreated and torrefied willow and eucalyptus fuels
10) To model the energy requirements for the torrefaction of pine
11) To build a bespoke bioenergy supply from cultivation to end-user for the production of electricity from pellets from torrefied and untreated wood.
12) To determine the GHG emissions at each stage of production incorporating using the EU Renewable Energy Directive methodology

1.3 Tasks

The tasks to achieve the objectives listed above are presented below:

<u>Tasks to achieve objective 1:</u>

1a) to review the previous political incentives in place for the deployment of sustainable technologies in the UK

1b) to review the current and future political incentives and market mechanisms in place for the deployment of bioenergy in the UK

Tasks to achieve objective 2:

2a) to perform torrefaction experiments using a bench scale reactor on pine and eucalyptus fuels under various conditions changing the torrefaction temperature and residence time: 250°C for 30 minutes, 270°C for 30 and 60 minutes, and 290°C for 30 minutes)

2b) to perform an overall mass balance from determination of the solid and liquid product yields for each experiment

Tasks to achieve objective 3:

3a) to determine the changes in physical and chemical properties of solid products of torrefaction from:

- ultimate and proximate analysis
- higher heating value (experimental and estimated) determination
- changes in pyrolysis behaviour using thermogravimetric analysis (TGA)
- changes in surface morphology using scanning electron microscopy (SEM)
- determination of the grindability behaviour and particle size distribution
- surface area using the Brunauer, Emmett and Teller (BET) method
- changes in cell wall components

3b) to determine the elemental composition of the organic phase liquid products of torrefaction using ultimate analysis and estimation of its HHV.

3c) to determine the carbon content of the aqueous phase liquid products of torrefaction using total organic carbon (TOC) analysis.

Tasks to achieve objective 4:

4a) to determine the elemental balance of the species C, H and N using ultimate analysis of the untreated fuels, torrefied solid products and organic phase products and TOC analysis of the aqueous phase products

Tasks to achieve objective 5:

5a) to calibrate the DTF and oxygen analyser and develop a method to produce chars at the desired temperature and residence time

5b) to prepare fast-heating chars from untreated and torrefied willow and eucalyptus in a drop tube furnace (DTF)

5c) to perform isothermal experiments using TGA on the chars prepared to determine char oxidation kinetics

Tasks to achieve objective 6:

6a) to take SEM images of untreated and torrefied chars to determine changes in surface morphology during fast-heating rate devolatilisation

6b) to perform surface area analysis using the BET method to determine the apparent surface area of chars

Tasks to achieve objective 7:

7a) to perform ultimate analysis on the fuels and chars from untreated and torrefied willow and eucalyptus to determine the split of nitrogen during torrefaction and fast-heating rate devolatilisation

7b) to perform SEM analysis with energy dispersive x-ray spectroscopy (EDX) to acquire semi-quantitative information on changes in metal concentration during devolatilisation

Tasks to achieve objective 8:

8a) to determine the Arrhenius parameters for the pyrolysis of untreated and torrefied willow and eucalyptus using dynamic TGA

Tasks to achieve objective 9:

9a) to perform a mass and energy balance for the torrefaction of pine under selected conditions using the HHV, proximate and ultimate analysis determined experimentally (see Aim 3)

9b) to determine the sensible and latent heats required for drying and torrefaction of pine under the selected conditions

9c) to model the composition of the liquid products of torrefaction using the FG-Biomass model to determine their latent heat requirements

Tasks to achieve objective 10:

10a) to review the literature for information on forestry cultivation, harvesting and transport emissions in the production of pellets from torrefied and untreated wood for inputs in to a bespoke bioenergy supply chain

10b) to incorporate the energies required for torrefaction in to the bespoke bioenergy supply chain

Tasks to achieve objective 11:

11a) to determine the life-cycle GHG emissions according to the EU Renewable Energy Directive methodology

11b) to perform sensitivity analyses on uncertainties in the supply chain

1.4 Thesis Outline

Chapter 1 provides a thesis overview, the aims and objectives for this project work and a thesis outline.

Chapter 2 introduces the topic of climate change and international efforts to reduce the amount of anthropogenic GHGs in the atmosphere. It then discusses the emissions from the power sector before presenting a recent history of the electricity supply industry in the UK and previous incentives in place for generators of electricity from renewable technologies. The current and near-future incentives are then discussed before the topic of bioenergy is introduced in detail, covering the different types of biomass used in energy applications, the composition of biomass and conversion of biomass for energy. It then discusses the deployment of bioenergy in the UK and fuel characteristics before introducing some of the problems associated with biomass fuels and the topic of biomass pre-treatment to address some of these problems.

Chapter 3 contains a literature review and discusses the torrefaction process, its effect on biomass chemical and physical properties and mass and energy balances of the process. The combustion properties of untreated and torrefied fuels are then discussed, introducing the

extraction of kinetic parameters from experimental data and factors affecting char reactivity such as pyrolysis conditions and the presence of inorganic species. This chapter then discusses the oxidative reactivity of untreated and torrefied fuels and the fate of nitrogen during combustion.

Chapter 4 describes the fuels used in this study and experimental methods and techniques used as part of this project work including some theory of the instruments.

Chapter 5 presents an investigation in to the torrefaction of pine and eucalyptus fuels, which includes mass and energy balances of the processes, analysis of the products of torrefaction and its effect on fuel properties. This chapter fulfils objectives 2-4 of this work. As part of this work, pine and eucalyptus fuels were torrefied under 4 conditions (250°C for 30 minutes, 270°C for 30 and 60 minutes and 290°C for 30 minutes) and overall mass balances performed via determination of the solid (torrefied) product yield and the yields of aqueous and organic phase liquid products with permanent gases were calculated by difference. Analyses performed on the solid torrefied product (and the parent fuels) includes proximate and ultimate analysis, analysis of cell wall components, pyrolysis behaviour, grindability behaviour, surface area determination and high magnification images were taken using SEM. Analysis of the organic and aqueous phase products includes ultimate analysis and total organic carbon (TOC) determination respectively. These data were then used to determine overall elemental balances for C, N and H. The data collected for untreated and torrefied pine is later used in Chapter 7 as described below.

Chapter 6 covers objectives 5-9 in this thesis and investigates the combustion behaviour of chars prepared in a DTF from untreated and torrefied willow and eucalyptus. Each fuel has been torrefied under three conditions (270°C for 30 and 60 minutes and 290°C for 30 minutes). Each of the chars were prepared at 1100°C with a residence time of ~500ms in the DTF and were characterised, in addition to the parents fuels for their ultimate analysis and ash contents. The results of the nitrogen contents for the fuels and chars were used to determine the partitioning of N upon torrefaction and fast-heating rate devolatilisation. The surface morphology of the parent fuels and chars were also characterised using surface area analysis and SEM. The metals concentration of fuels was determined using ICP-MS and the metal concentration of the fuels and chars estimated using EDX. This was done to determine partitioning of K upon torrefaction and fast-heating rate devolatilisation. The pyrolysis behaviour of the fuels was also determined using TGA and the oxidative reactivity and intrinsic reactivity (with surface area analysis) of the chars determined using isothermal combustion experiments in a TGA.

Chapter 7 presents a study on the effect of torrefaction bioenergy supply chain GHG emissions. Using experimental data for the torrefaction of pine from chapter 5- the energy requirements

for each of the torrefaction conditions were modelled- these data then incorporated in to respective bioenergy supply chains, including all the appropriate steps from harvesting to end-use, to determine the life-cycle GHG emissions for the production of electricity using torrefied wood pellets. The supply chain scenarios involve the harvesting, torrefaction and pelleting of wood in North America before shipping to the UK and transported to a large power plant for use in electricity generation. The data for the different stages in the supply chain was derived from experimental and modelling work (e.g. in the case of the torrefaction energy requirements) or from information available in the literature and existing plant data such as the energy required for pelleting and the location for the torrefaction facility. The GHG emissions for each stage are calculated using the Renewable Energy Directive (RED) methodology and the overall emissions for each supply chain determined using a life-cycle approach. The life-cycle emissions are also compared with the emissions from a conventional (non-torrefied) supply chain to determine the difference in GHG emissions when torrefaction is included and sensitivity analysis performed to assess key assumptions and data uncertainties.

Chapter 8 presents the main conclusions of this research and discusses some suggestions for future work.

2 Introduction

2.1 Introduction

During the mid-18th century, the United Kingdom pioneered one of the most significant periods in global history where the development of manufacturing processes and advancement of engineering practises began to accelerate in what is known as the Industrial Revolution. This expansion in industrial development soon spread to mainland Europe and beyond and forms the foundation of the technologically advanced society we live in today. In order to power our continuing global development, an ever increasing amount of energy has been required, which has been sourced primarily from the cheap and widely available fossil fuels coal, oil and natural gas. Increased use of these fuels however has had a negative on the earth's climate as the release of energy from carbonaceous fossil-fuels results in the formation of carbon dioxide (CO_2) and other greenhouse gases (GHGs) to the atmosphere. To understand the threat anthropogenic GHGs pose, it is important to understand the natural flux of radiative forces in the earth's system in relation to the sun and the atmosphere.

2.1.1 The Natural Greenhouse Effect

The sun emits short wave (UV) radiation through the earth's atmosphere at an average incoming irradiance of 342 W/m^2 [1]. Some of this radiation is reflected back to the atmosphere by clouds and the earth surface however approximately half is absorbed by the earth's surface warming it up. In order to balance this incoming radiation, the earth emits some of this thermal energy back out in the form of long-wave infrared (IR) radiation. Of this emitted long-wave thermal radiation, some escapes the atmosphere and into space however some is absorbed by natural occurring 'GHGs' (in the absence of any anthropogenic inputs) in the atmosphere such as CO_2 and water vapour i.e. molecules that can absorb IR radiation [1]. These gases then scatter this IR radiation in all directions and effectively act as a 'blanket', resulting in an average earth temperature of around 15°C warmer than would result if these gases weren't present (the average earth temperature would be around 20-30°C cooler if these gases weren't present) [1]. The natural occurrence of these gases therefore allows for life to exist on planet earth.

2.1.2 The Enhanced Greenhouse Effect

While the natural occurrence of IR absorbing gases are necessary to sustain life on planet earth, human activity has resulted in additional GHGs in to the atmosphere. This has caused an

'enhanced greenhouse effect' where anthropogenic GHGs in the atmosphere have resulted in an increase of the earth's average temperature. This rise in temperature poses a severe environmental threat for several reasons such as rising sea levels and changes in climate activity. The key GHGs that present the most danger are CO_2, methane (CH_4), nitrous oxide (N_2O), hydrofluorocarbons (HFCs), perfluorocarbons (PFCs), and sulphur hexafluoride (SF_6) [2] with atmospheric concentrations of CO_2, CH_4 and N_2O increased to levels unprecedented in at least the last 800,000 years [3]. The effect of changing GHG concentrations in the atmosphere is measured via the change in Radiative Forcing (RF) in W/m^2. RF is defined as the change in average net radiation at the top of the troposphere relative to the year 1750 (the troposphere is the region of the lower atmosphere up to a height of 10km) [1]. A positive RF leads to surface warming while a negative RF leads to surface cooling. Figure 2-1 shows that the overall change in RF from all measured anthropogenic gases in 2011 (relative to 1750) is $2.29W/m^2$ [3]. In addition to GHGs, aerosols such as black carbon, which derive from incomplete fossil fuel combustion and burning biomass can also contribute to positive radiative forcing [4].

Figure 2-1 also shows the impact of each individual GHG where it can be seen that CO_2 has had the greatest impact on RF (since 1750) where it alone has caused an increase in RF of $1.68\ W/m^2$ [3]. This increases to $1.82W/m^2$ when emissions of other carbon-containing gas that contribute to increases in CO_2 concentrations are considered. During 1750-2011, cumulative anthropogenic emission of CO_2 have resulted in 555 GtC released in to the atmosphere [3]. At the time of writing, the monthly average concentration of CO_2 in the atmosphere, as measured at the Mauna Loa observatory in Hawaii, was 402.52ppm which has steadily increased since the late 1950s as shown in Figure 2-2 and considerably higher than the pre-industrial concentration of 280ppm [5].

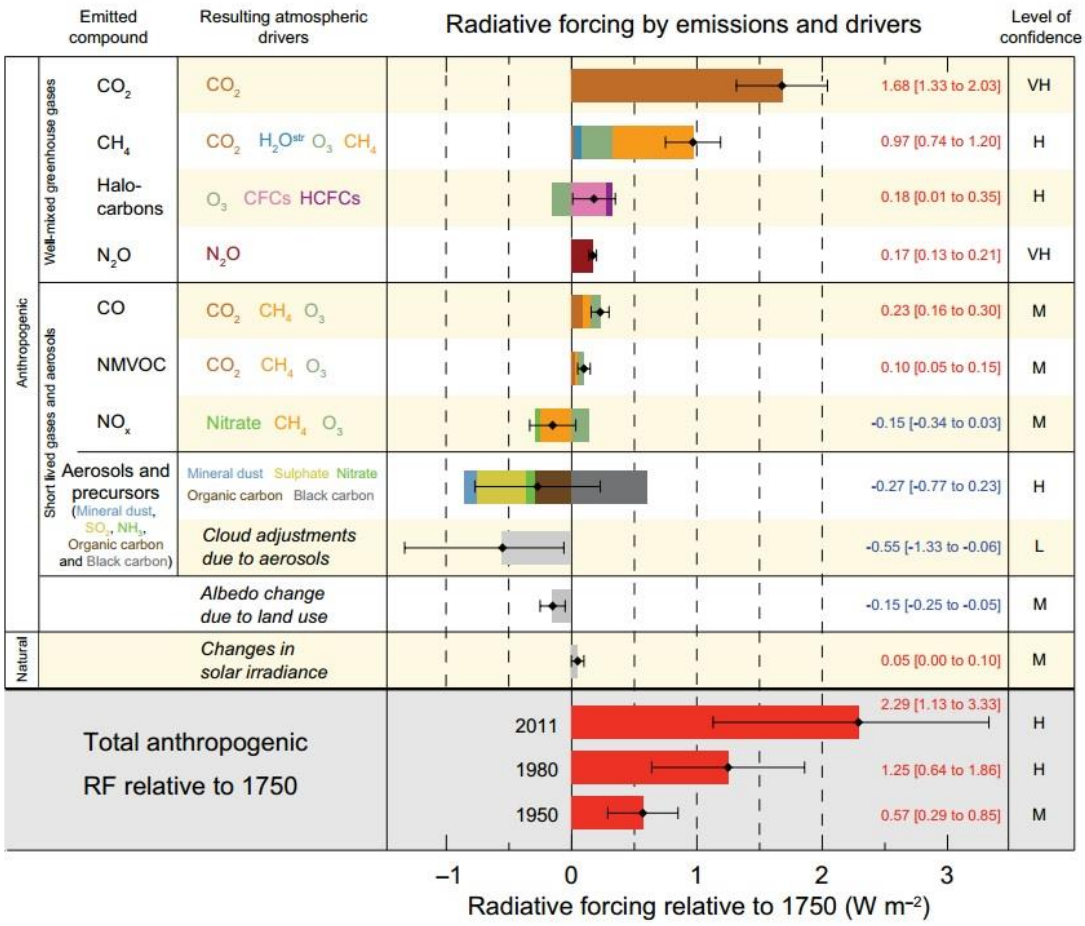

Figure 2-1: Radiative forcing estimates in 2011 relative to 1750 with uncertainties for the main drivers of climate change [3].

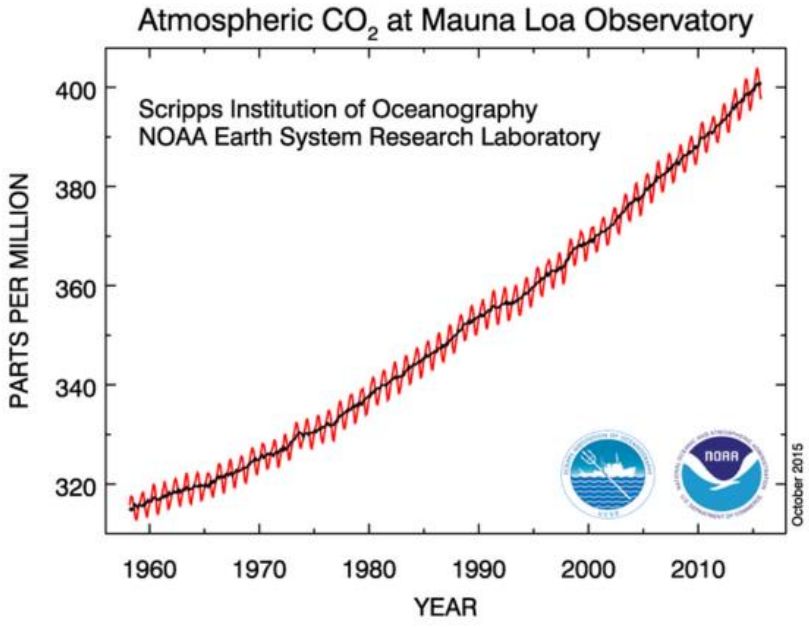

Figure 2-2 – Increase in atmospheric CO_2 concentration [6].

The use of energy (e.g. combustion of fossils fuels) represents the largest source of anthropogenic emissions to the atmosphere as shown in Figure 1-3 where CO_2 represents the greatest amount of GHGs [5]. Other sources of emissions include industrial processes and agricultural practises. The breakdown of CO_2 emissions by sector is also shown in Figure 2-3 and highlights some of the heaviest polluting industries. It can be seen that almost two-thirds of global CO_2 emissions in 2012 were sourced from electricity and heat production (42%) with the next heaviest polluter the transport sector which contributed 23% of global CO_2 emissions.

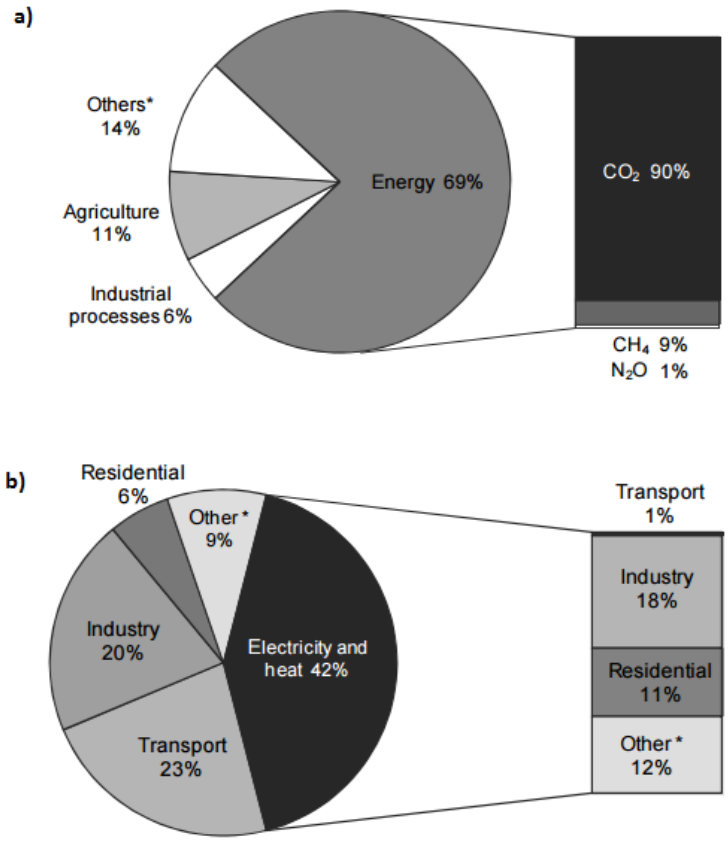

Figure 2-3: (a) Share of global anthropogenic GHGs in 2010, 'Others' include biomass burning, post-burn decay and N_2O emissions. (b) World CO_2 emissions by sector in 2012, 'Others' includes commercial and public services, agriculture and forestry. Both from [5].

2.1.3 International Efforts to combat the dangers of Climate Change

Awareness of the potential dangers of climate change has resulted in international and cross-governmental efforts to limit to the amount of anthropogenic GHGs emitted to the atmosphere. In 1992, the United Nations Framework Convention on Climate Change (UNFCCC) was formed and is an international treaty between member countries who aim to co-operatively consider what actions can be taken to limit the average global temperature and combat the dangers of

climate change [7]. One of the most important extensions of the 1992 UNFCCC is the signing of the Kyoto Protocol in 1997. This international agreement, ratified in 2005, commits state parties to reduce greenhouse gas emissions in their respective countries relative to 1990 levels (the 'baseline' year) during various commitment periods: the first period took place between 2008 and 2012 and the second currently underway from 2013-2020. The United Kingdom for example, who is a signatory to both the UNFCCC and Kyoto Protocol, had emissions reductions targets of 12.5% less than 1990 levels for the first commitment period for the six greenhouse gases listed in section 1.1.2 and achieved a reduction of 22.5%.

The party members to the UNFCCC regularly meet in what is known as Conference of Parties (COP) the first of which took place in 1995 in Berlin. During the 16th conference of parties held in 2010 in Mexico, included in the agreements was the commitment of governments to 'hold the increase in global average temperature below 2°C' relative to pre-industrial levels which has become the de facto target in international climate policy [8]. Overwhelming scientific evidence suggests that should we exceed a global average temperature of 2°C, which entails limiting the concentration of GHG in the atmosphere to no more than 450ppm [9], this will lead to considerable risks such as sea level rise, loss of valuable ecosystems, impacts on global food supply and large-scale disturbances of the current climate system [10]. The culmination of interdisciplinary scientific evidence to support the claim that anthropogenic activity has led to our changing climate lays with the Intergovernmental Panel on Climate Change (IPCC). The duty of this leading intergovernmental body, whose contributing members include thousands experts on climate change (on a voluntary basis), is to 'assess on a comprehensive, objective, open and transparent basis the scientific, technical and socio-economic information relevant to understanding the scientific basis of risk of human-induced climate change, its potential impacts and options for adaptation and mitigation' [11]. The IPCC publish 'Assessment Reports' which provide a clear and up to date view of the current state of scientific knowledge relevant to climate change which are highly regarded and provide the basis for action taken at governmental and international level.

It can be seen above that the rising GHGs emissions pose a severe threat to the earth's climate system and certain sectors are more responsible for others in their contribution to these rising emissions. Internationally, emissions from power generation (electricity and heat) are by far one of the greatest threats making it one particular sector where a change in practise could make a considerable difference. Domestically, here in the UK, emissions from the power sector accounted for 33% of total GHG emissions in 2013, of which almost 97% was attributed to CO_2

emissions (32% overall) [12]. The next section of this introduction is therefore dedicated to the electricity supply sector in the UK, providing a brief recent history and a discussion of the changing nature of this industry as climate change has risen on the political agenda.

2.2 Support for renewable energy in the UK

2.2.1 Privatisation of the Electricity Supply Industry (ESI)

Until the late eighties, the generation and transmission of electricity in the UK was a nationalised entity. In England and Wales, the transmission and generation of electricity was the responsibility of Central Electricity Generating Board (CEGB) [13] who sold electricity to 12 area boards under a tariff based upon its marginal costs. The 12 area boards in turn sold electricity to customers in their respective areas [14]. In Scotland, a vertically integrated system operated whereby electricity generation, transmission, distribution and supply were governed by two public companies: the South of Scotland Electricity board (SSEB) and the North of Scotland Hydro-Electric board (H-EB) who operated as regional monopolies in their respective districts [15]. During the early eighties however, the Conservative government's intentions to introduce legislative measures that would allow private companies to provide electricity became apparent with the rationale and strategy outlined a few years later in the form of the White Paper: 'Privatising Electricity' [14, 16]. At the end of the decade, the legislative foundations for restructuring of the electricity supply industry (ESI) were implemented with the Energy Act 1989 receiving Royal Assent on July 27th [15]. The main provisions of this Act were the change in ownership of electricity supply to private investors and the introduction of a competitive market and system of independent regulation [15]. In 1990, the restructuring of the ESI in England and Wales began with the transferal of CEGB assets to three generating companies: National Power, PowerGen and Nuclear Electric and one transmission company, The National Grid Company (NGC) [17]. Ownership of the NGC was split between 12 Regional Electricity Companies which replaced the 12 area boards as part of restructuring; the stake in the NGC each REC held proportional to its size. Trading under the new industry re-structure was enabled by the establishment of the 'electricity pool', one of the first mechanisms of its kind, as the main market mechanism governing how and at what price electricity is traded. Administered by the NGC, the electricity pool operated as a daily spot market where generators would submit 'bids' for how much electricity it will generate and at what price for each and every half hour the following day [18]. The bid price often reflected the demand of electricity e.g. in winter time when demand is high, generators could increase the bid price. In addition to these bids, generators would also declare the available capacity available for the next day. Once all bids had been submitted, the

NGC would forecast the expected demands and produce a merit schedule ranking all bids starting with the cheapest on top [18]. If there was over-capacity the most expensive bids (at the bottom of the merit schedule) were placed on standby (or even excluded). With varied demand throughout the day, units had to be brought online quickly with the lowest bidding generators brought online first and so on down the merit schedule. The 'System Marginal Price' (SMP) for any given half hour was therefore established as the most expensive bid brought online i.e. not the highest bid full stop. The generators were in turn paid the SMP; not their original bid price. The intention of the SMP was to reflect short term marginal cost of electricity however the SMP did not account for the covering the fixed costs of electricity generation at peaking capacity that failed to meet demand [19]. In order to account for the cost of capacity, an additional payment was paid to generators and calculated using the following equation:

$$\text{Capacity payment} = \text{LOLP} \times (\text{VOLL} - \text{SMP})$$

Where LOLP = loss of load probability and VOLL = value of lost load (set by the government) [19]. The capacity payment was therefore an administrative payment based on the potential disruption of electricity supply to generators who maintained marginal plant on the system that would have been otherwise closed [20]. The generators who were online at any given half hour period received both capacity payments and the SMP, the total of the two forming the 'Pool Purchase Price' (PPP); the price at which generators sold electricity to the pool. The PPP during the first half of the pool's existence was essentially controlled by two coal-fired power generators, PowerGen and National Power, as the low-cost but inflexible combined-cycle gas turbine and nuclear plants at the time often declared zero as their SMP to ensure their plant ran [20]. From the electricity pool, suppliers (RECs) and large customers purchased electricity at the 'Pool Selling Price' (PSP) which was equal to the PPP plus uplift costs, that covered the pool operating costs [18]. Regulation of the electricity pool was the responsibility of the Office of Electricity Regulation (OFFER). In Scotland, privatisation took place with the creation of Scottish Power and Scottish Hydro-Electric, replacing SSEB and H-EB respectively. After privatisation however, the vertically integrated market whereby both companies provided a full range of electricity provision that was in situ during public ownership remained [15].

By its very nature, pool electricity prices tended to be volatile providing uncertainty for generators and suppliers alike. To hedge against this, most of the electricity was in fact traded between generators and suppliers via bilateral contracts for difference (CfDs) [15] with 80-90%

of the electricity at this time hedged with CfDs, making most of the electricity at the time traded out with the electricity pool [19]. The CfDs were two-way agreements between generators and suppliers who agreed on a strike price for a fixed quantity of electricity, usually struck against the pool price of electricity [19]. When the strike price is below the pool price, the buyer (supplier) will pay the difference to the seller (generator). When it is above, the seller will refund the difference.

2.2.2 The Non-Fossil Fuel Obligation

In December 1990, the first steps in privatisation took place with the flotation of the 12 RECs entering the London Stock Exchange. The following year, 60% shares of the two fossil-powered generators (National Power and PowerGen) entered the stock market with the remaining 40% retained by the UK government [15]. Originally, the assets of the nuclear branch of the former CEGB, Nuclear Electric, were intended to be sold on the London Stock Market however the government realised after its proposal that privatisation of this sector would be too difficult and costly. As a result, its sell off was withdrawn and nuclear power generation at the time remained in public ownership [21]. The increased cost of running nuclear power plants in the UK still required financing however and in order to finance this generation within the newly privatised electricity sector, the UK government sought permission from the European Commission (EC) to subsidise 'non-fossil' electricity generation [22]. As a result, the Non-Fossil Fuel Obligation (NFFO), sanctioned by the EC, was introduced and mandated in the Electricity Act 1989 for a period of 8 years [23]. The obligation required RECs to purchase a portion of their electricity from non-fossil generators, at levels set by the Secretary of State. Generators producing non-fossil energy (NFFO generators) were awarded contracts as a result of success in a competitive bidding process; bidding a price per kWh for electricity generation within a particular technology band i.e. waste-to-energy producers bid against other waste-to-energy producers but not against wind projects. The Department of Trade and Industry (DTI), the body responsible for the awarding of the contracts and who decided on the total capacity and technologies that would be awarded, would take these bids and award contracts to the lowest bidders [23]. Once awarded, the RECs would purchase electricity from these generators a premium price, with the additional cost, relative to the PSP, paid to the RECs from the Fossil Fuel Levy (FFL); a tax imposed on fossil-based generators of electricity [24, 25]. The FFL was initially set at a rate of around 10% of the final electricity price for all fossil generators up until 1996 with most of this payment going to Nuclear Electric to cover it's £9.1 billion liabilities (note the profits from privatisation of the CEGB were just under £10 billion highlighting the need for the FFL) [26]. The Non-Fossil Fuel obligation (NFFO) was thus introduced as a means of subsidising nuclear generation [22]

however, in the government's request for subsidy; the request was called to finance 'non-fossil' generation and not nuclear generation specifically. Under the levy terms therefore payment could extend to other non-fossil generation; notably generation from renewable energy sources [21]. So while the NFFO was originally implemented as a support for non-fossil based generation, it effectively marks the first market-based incentive for renewable electricity generation in the UK which would in a few years become an important pioneering first step in the creation of market incentives for renewable deployment in response to the dangers of climate change [21].

Since its inception in 1990 there have been 5 rounds (Orders) of the NFFO; the contracts for first two rounds: NFFO1 and NFFO2 made in 1990 and 1991 respectively. Both of these were awarded for eight years while NFFO 3-5 deployed in 1994, 1997 and 1998 respectively, have contracts for a maximum of 15 years [22]. For the first order, almost 2 thirds of generating capacity were already operating and thus little competition was in place when bidding occurred. However the majority of renewable technologies bid under order 2 were new capacity [23]. Under the NFFO, payments for renewable generation were only given once plant were commissioned and so under NFFO2, where new plant were awarded relative to NFFO1, several projects essentially lost out as the time required for planning permission and high costs involved in the commissioning of new technologies e.g. new waste-to-energy plant ultimately meant that economic returns would not be seen by the end period of 1998 [23]. In response to this, extension of the NFFO was granted by the EC for NFFO3-5 and with it a 'grace' period to allow for planning permission and commissioning of up to 5 years followed by 15 years of premium payment. The extension of the NFFO for an additional 3 rounds was awarded covering renewable energy only [23]. Thus in 1994, for NFFO3 and beyond, there was significant hope for better integration of renewable technologies in the UK energy mix. In the third round of the NFFO, DNC of support was raised to 1500MW however in the following years it was to become clear that several issues were still problematic to the third order. These included a too low total cost cap resulting in the NFFO3 being too competitive in addition to too optimistic assessments of bid technologies despite the grace period allowance [23]. The fourth and fifth orders will be discussed later in the text.

2.2.3 Further restructuring and the 'dash for gas'

Throughout the 1990s, running parallel to the NFFO orders, further restructuring of the electricity market took place. In 1995, the National Grid company was floated on the stock market while a year later, parts of the state-owned nuclear plant were privatised [15]. In 1990, when privatisation took place, there were three major generators in England and Wales:

National Power, PowerGen and the state owned Nuclear Electric. However, enforced (then voluntary) divestment of capacity of the two main fossil generators (PowerGen and Innogy (National Power) to different generator, Eastern Electricity, also occurred during this time period to instil competition in the electricity market [15]. At the time also, previous European and UK restrictions that were in place for electricity generation from gas were lifted and from this, the introduction of new independent power producers (IPPs) (some part owned by RECs) entered the market; most of these IPPs combined cycle gas turbine (CCGT) generators [27]. Five years after privatisation, 15 CCGT generators were due to come online, displacing 25 million tonnes of coal in what was to become known as the 'dash for gas' which would ultimately have implications for the UK coal industry.

2.2.4 New Labour

In 1997, after 18 years of Conservative rule, the Labour government were voted in to parliament in the UK with an agenda for reform which had major impacts on energy policy and electricity market structure [22]. Following numerous policy reviews, the Labour government introduced a Utilities Bill in 1998, that when passed by the houses Parliament formed the Utilities Act 2000. The Bill included the merging of regulatory bodies of the electricity and gas markets in to one office: the Office of Gas and Electricity Market (OFGEM) and new powers for the regulatory authority and secretary of state. The Utilities Act 2000 also made provisions for 'New Electricity Trading Arrangements' (NETA); a new electricity market mechanism to replace the existing electricity pool following a review that found a number of problems existed. These included lack of competition in price setting (despite an influx of CCGT generation, these generators had long-term off-take contracts thus price setting was dominated by the main generators: PowerGen, National Power and Eastern [15]) which resulted in the creation of market powers and pool price manipulation [15]. As a result, NETA was introduced in March 2001 as the wholesale market with the bulk electricity sold via bilateral trading contracts between generators and suppliers and customers. Under the NETA system, the trade of electricity operated in a similar manner to other commodity markets as electricity became less centralised. Generators and buyers were able to directly trade without input from the system operator, note- previously in the pool system, the system operator utilised generators in a least cost manner whereas under bilateral trading contracts, the system operators utilises the prices agreed between generators and suppliers. Generators are also responsible for their own level of output whereas under the pool system, the NGC did this on the generators behalf. One of the main benefits to suppliers and generators under NETA are flexibility and security in trading where long-term contracts can be arranged between suppliers and generators but with the addition of 'short term power

exchanges' that can be struck on the day through spot markets [15]. To account for system imbalances, still under control of the NGC, bids are accepted 3.5 hours prior to real-time to balance any shortcomings in transmission (based on information provided by system participants to the NGC on their expected position for each half hour of each day one day prior to the day in question). The Act also put all customers on the same footing in the abolishment of a public electricity supplier with customers given the choice of which supplier they can source their electricity from as well as the separation of the former RECs (now in private ownership) into separate distribution and supply companies, which from a renewables perspective, undermined the legal basis of the NFFO [23]. Ultimately, renewable energy policy under the new government would require transferral in the new legislation or implementation of a new mechanism altogether.

2.2.5 Climate Change and the Renewables Obligation

During this time, climate change and the dangers of GHGs began to rise on the political agenda. As mentioned in section 1.1.3, five years before, the UK government signed the United Nations Framework Convention on Climate Change (UNFCCC) in Rio de Janeiro. It was during this time, concerns on increasing GHG emissions and the need to for stabilisation were first discussed by the global community together [28] leading to the signing of the Kyoto Protocol in 1997, marking the legally binding treaty in effect towards true global emissions reductions [29]. Now, the UK had legally binding targets to meet and thus deployment of renewable energy in to the mix was imperative. The final two orders of the NFFO (orders 4 and 5) were administered under the Labour government with NFFO4 announced in 1997 awarding new contracts of 1700MW DNC and NFFO5 contracts awarded the following years with 1177 MW DNC [23]. Despite this, the majority of the contracts were never developed, mainly due to too low bids and a low overall cost cap as well as other problems associated with the NFFO including its nature of 'picking winners' according to the NFFO banding. Any hope that the NFFO would substantially increase the use of renewable energy in to the mix failed to materialise with growth in renewables deployment only increasing 1% (from 2%-3%) during this time period [27]. As a result, the Utilities Act 2000 made provisions for new market- mechanism for incentivising renewable deployment, in line with the new electricity restructuring in the form of the Renewables Obligation (RO) [23]. Implemented in 2002, the RO became the main market mechanism for large-scale renewable energy deployment to replace the NFFO, requiring licensed suppliers of electricity to include a proportion of the electricity they produce from eligible renewable technologies [30]. The original target for the amount of electricity produced for renewable technologies was 3% for the period 2002-2003 which was to increase incrementally each year

until 20% of electricity was generated from renewable technologies by 2020 [31]. The scheme currently operates by generators receiving 'Renewable Obligation Certificates' (ROCs) proportional to the amount of electricity they generate from renewable technologies. These ROCs are then sold with (or without) their output to suppliers who in turn receive a premium on top of the wholesale price of electricity. The duty is then placed on the supplier to demonstrate to Ofgem the ROCs they have acquired to show their compliance with the RO. If insufficient ROCs are presented by the suppliers, they then pay a penalty known as the 'buy-out price' which are then collected and distributed on a pro-rata basis by Ofgem to the suppliers who presented their obliged number of ROCs. The recycling of the buyout fund was included in the scheme to lower RO costs for suppliers for compliance [31]. As a market-based scheme there is no fixed price for a ROC as they are tradable commodities and so the price per ROC is negotiated between the suppliers and generators. Each supplier's obligation is the total annual supply provided multiplied by the level of obligation (ROCs per MWh).

When the RO was first introduced, ROCs issued were 'technology neutral' (set at 1 ROC/MWh generated) [32]. This was set in place to avoid the favouring particular technologies. However owing to the competitive nature of electricity market and the higher costs and risks associated with less mature renewable technologies, those that offered low risk and investment that were currently in deployment notably onshore wind and landfill gas were preferentially taken up [31]. This left other technologies, such as dedicated biomass plant, behind as insufficient support was provided. Other aspects of the original RO were also unfavourable such as no guaranteed fixed contracts with suppliers resulting in higher costs from uncertainty risks as well as difficulties for new entrants in to the scheme; again attributed to high investment risks [30, 33]. Revisions to the RO were thus implemented including the introduction of a guaranteed 'headroom' which, operated by DECC, provided a set margin between the predicted generation (equating to the supply of ROCs) and the level of obligation (equating to the demand for ROCs). This was set in place to avoid surplus supply occurring which would turn crash the value of ROCs. Revision of the RO also occurred amidst new domestic and European political drivers aimed at tackling the dangers of climate change. In the UK, the Climate Change Act received royal assent in 2008 which binds the UK to reduce GHG emissions by 80% relative to 1990 levels by 2050 [34]. The UK was also given shorter term emissions reductions targets in 2009 in the form of the European Directive to produce 15% of its energy from renewable sources by 2020 as part of an overall EU target of 20% by the same year [35]. One of the key changes to the RO was the introduction of technology banding under the Renewables Obligation Order 2009 to give support to less developed technologies as well as fixed rates for generators from 2009-2013 to provide income

certainty [30]. The structure of this banding reflected the maturity of the technologies providing additional support for those in the development stage. For example, landfill gas was supported with 0.25 ROCs for every MWh generated as this was a mature technology, while Wave and Tidal projects were awarded 2 ROCs for every MWh to reflect high upfront and commissioning costs [36]. This banding review thus introduced a 'multiple-fractional ROC approach'; awarding more, equal or less than 1 ROC/MWh depending on the technology [33]. The Renewables Obligation Order 2009 also made provisions for the Secretary of State to make banding reviews every four years to ensure cost-effectiveness of support levels and to help bring forward technologies ensuring capacity is delivered [37]. The first review took place in 2010 for the period 2013-2017 through analysis of deployment scenarios and generation costs. As a result, a new banding scheme for the period 2013-2017 was introduced in line with phase III of the EU Emissions trading scheme (discussed below). Details of these bands, specifically those pertaining to biomass deployment are discussed later in this introduction.

2.2.6 The EU Emissions Trading Scheme

While the RO requires electricity providers to source a portion of their generated energy from renewable energy, high-emitting industry sectors are also included in the EU Emissions Trading scheme; a European-wide 'cap and trade' system which limits the volume of greenhouse gases that can be admitted by power plants, factories and other heavy industrial works [38]. Implemented in 2005, the scheme covers over 11,000 energy installations accounting for around 45% of EU (plus Iceland, Liechtenstein and Norway's) GHG emissions. The volume of GHG emissions which can be emitted are set or 'capped' each year with parties involved receiving or purchasing allowances equating to the volume of emissions they are allowed to emit. One allowance = the right to emit 1 ton of CO_2 or the equivalent emissions for nitrous oxide (N_2O) and perfluorocarbons (PFCs) [38]. If a company has a surplus of left-over allowances, they can keep them to use for subsequent years or sell them to other companies who can in turn buy from sellers from approved projects. When a company emits 1 ton of CO_2 (or equivalent) covered by the scheme, an allowance is surrendered. Fines are imposed on those whose emissions supersede their allocated or purchased allowances. The overall cap on emissions is then reduced each year; from 2013 onwards the reduction equating to 1.74% resulting in a 21% reduction by 2020; causing emissions to gradually fall. The incentive therefore is for heavy emitters to implement more efficient practises or deploy less-carbon intensive technologies to avoid paying heavy fines for over-emitting.

At this time then, heavy emitters were affected by multiple policy instruments; the legal requirements to include renewables from the RO while reducing CO_2 and other GHGs at minimal cost as part of the EU ETS. It is beyond the scope of this study to analyse interactions between these two measures however it must be noted that while both schemes endeavour to achieve the same outcome, an increase in renewables deployment subsequently frees up the number of allowances; in turn reducing the cost of carbon [39].

2.2.7 Electricity Market Reform

The most recent reform of the electricity market in the UK until recent times was thus the creation of the NETA trading system in England and Wales. In 2005 however Scotland was incorporated in to the trading arrangements with the creation of the British Electricity Trading and Transmission Arrangements (BETTA) creating a single British wholesale electricity market [40]. As part of this incorporation, the NETA system extended to Scotland and introduced more competition in the Scottish wholesale market also allowing Scottish generators to sell their electricity south of the border [40]. The BETTA market operates in the same manner as the NETA system whereby generators are paid for the electricity they generate by suppliers who in turn sell this electricity on the retail market to consumers- the price determined directly between sellers and buyers through bilateral trading agreements [41, 42]. The market operates on the basis of rolling half hourly slots in which generators contract with customers one hour ahead of their actual supply (known as 'gate-closure') and declare their settlements to the National Grid with their Final Physical Notification (FPN) - with charges enforced if generators or suppliers deviate from their FPN levels [43]. The BETTA (and NETA) system has thus operated successfully for generators who could come on-line quickly and ensure electricity when required and has delivered on key objectives such as affordability [41]. However, as government energy strategies have evolved with decarbonisation now at the forefront of energy policy, current electricity market mechanisms are not congruent with the introduction of low-carbon technologies in to the energy mix which are intermittent or inflexible in nature. As mentioned above, the UK is bound by legal framework to reduce its GHG emissions; a challenging feat considering the deployment of renewable technologies must ensure capacity while keeping costs to a minimum. Difficulty in ensuring capacity is particularly important at this time owning to the decommissioning of several major existing coal plants due to non-compliance with the emissions restrictions set in place by the Large Combustion Plant Direct (LCPD) [44]. As part of this revised 2001 European directive, combustion plants, and other major industrial works, with a thermal capacity ≥50MW licensed after 1987 have legislative restrictions in place to control the

emissions of sulphur dioxide (SO_2), nitrogen oxides (NO_x) and particulate matter (PM) across Europe. Plant listed before this year have three options presented to them [45]:

1) Opt-in: by complying with new emissions limits by retro-fitting flue gas treatment equipment
2) Opt-out: 20,000 hours of operation permitted between January 1st 2008 and 31st December 2015
3) Close before 1st January 2008

Six coal powered plants in the UK chose to opt-out which will result in the eventual removal of 8.7GW of capacity in entirety at the end of 2015 [46]. It is essential therefore to ensure not only that additional capacity is available during this time, but also that capacity is produced using cleaner technologies. It is predicted that the electricity sector will need to attract investment in the region of £110 billion to replace and upgrade measures by 2020 [47]. Investment in renewable technology however is accompanied by uncertainties including price risk and ensuring secure delivery. In order to ameliorate these issues raised above and assist the transition to a low carbon economy, the UK government has introduced an Electricity Market Reform (EMR); the framework of which is incorporated in the Energy Act 2013 [48]. The main objectives of this Act of Parliament are not only to set decarbonisation targets and secure investment and supply of low carbon technologies but also to keep costs to taxpayers and energy bills as low as possible. In fulfilling the objectives set out in the EMR, two new market mechanisms have been introduced: Feed-in tariffs (FiTs) with Contracts for Difference (CfD) and Capacity markets (CM).

2.2.8 Contracts for Difference (CfDs)

The first market mechanism in place as part of the EMR are feed-in tariffs with Contracts for Difference; the primary aim of these to promote investment in low carbon technologies by reducing the risk of potential changes in electricity prices. CfDs are private law contracts between low carbon generators and the government owned Low Carbon Contracts Company (LCCC). The scheme operates by ensuring a fixed return price for generation with generators being paid the difference between the 'strike price' which reflects the cost of investment in a particular low carbon technology and the 'reference price' – a measure of the market price for electricity in the market [49]. The strike price is a pre-agreed price for electricity which will remain constant throughout the duration of a contract between the holder and the generator. CfDs ensure a guaranteed rate of return regardless of fluctuations in market electricity prices. If

the price falls below the strike price, the generators are subsidised and if the price of electricity is higher than the strike price, the generator will pay back the difference relative to the agreed strike price (Figure 2-4):

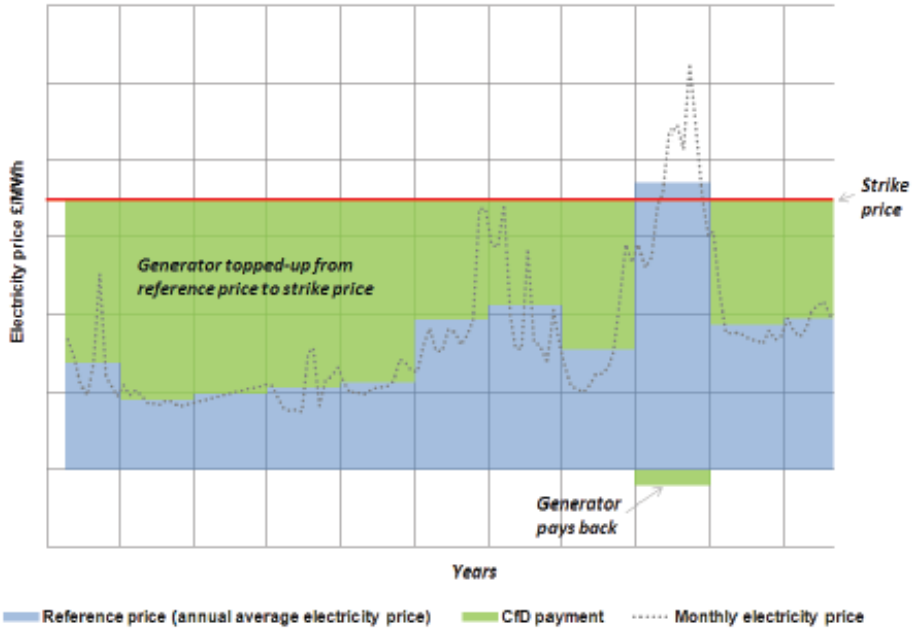

Figure 2-4 – Operation of CfD payments under the new Electricity Market Reform

2.2.8.1 Capacity Market

In addition to CfDs, a Capacity Market will be introduced to secure UK energy power supply through financial incentives to capacity providers to provide reliable capacity at peak times. The introduction of a Capacity Market is required not only in light of changes to current capacity via closures of plant affected by the LCPD but also amidst the challenge of decarbonisation of the grid. As there will be an increase in the deployment of intermittent or inflexible resources such as wind power and nuclear respectively there is a need to ensure enough power is available should these technologies fail to provide. The capacity market introduced will run alongside the 'normal' energy market and will operate through a system where the amount of capacity needed, four years in the future in the case of the UK, will be auctioned to potential providers. Bidders in the auction known as 'capacity providers' can then enter in to the auction, using their operating costs as their bid price, to provide capacity at this future date during times of 'stress'. In exchange for providing capacity, providers are paid through steady capacity payments and must pay a penalty if they fail to provide capacity when required [49].

There are four stages of the new EMR with Stage 1 currently underway at the time of writing. Until 2017, CfDs will run alongside the RO with competitive industries (Pot 1) entering a competitive auction to determine the strike price. Less mature technologies (Pot 2) are at present stage receiving support at administrative strike prices. Capacity auctions also took place for the parallel capacity market in 2014 which will be operational in Stage 2 from 2018. In Stage 3, for the 2020s period, it is expected that technologies will continue to mature, resulting in technology neutral auctions with Stage 4 (late 2020s) resulting in all generators to compete without intervention [49].

While the RO is currently in place to encourage development in renewable technologies, the scheme will close to new entrants in 2017, although participants operating in the scheme will receive subsidies for the duration of the scheme (until 2037). At the present time however, entrants wishing to invest and supply renewable technology have the choice of whether to enter the RO or CfDs. It is useful at this stage therefore to briefly highlight the impact the RO has had on renewable electricity generation in the UK from 2002 (the beginning of the RO). Figure 2-5 shows the contribution of renewables to electricity generation in the UK from 2000-2014. It can be seen that the contribution of renewables has increased from 3% in 2002 to 19% in 2014 which indicates the RO has been successful in diversifying the energy mix. However, the government has chosen to change the way in which new renewable generators are financed; swapping from a subsidy scheme which tops up the wholesale cost of electricity (RO) to a system where generators receive long-term contracts under variable payments between a fixed strike price and reference price (wholesale price) for renewable electricity generation (EMR). It is beyond the scope of this work to analyse the implications of these changes which in reality are very complex however general some points and conclusions can be made regarding the transition. The RO has been successful in integrating renewable energy however the government's rationale behind the implementation of the EMR is that guaranteed rates of return through CfDs will help incentivise renewable generators to invest. This differs from the RO where the lack of contractual obligations between suppliers and generators under RO mean, in simple terms, that both are exposed to long-term price risks. It is also noteworthy to point out that under the EMR, 'low carbon generators' can receive CfDs as opposed to the renewable generators. This effectively allows technologies such as nuclear or fossil generation with CCS to receive fixed payments.

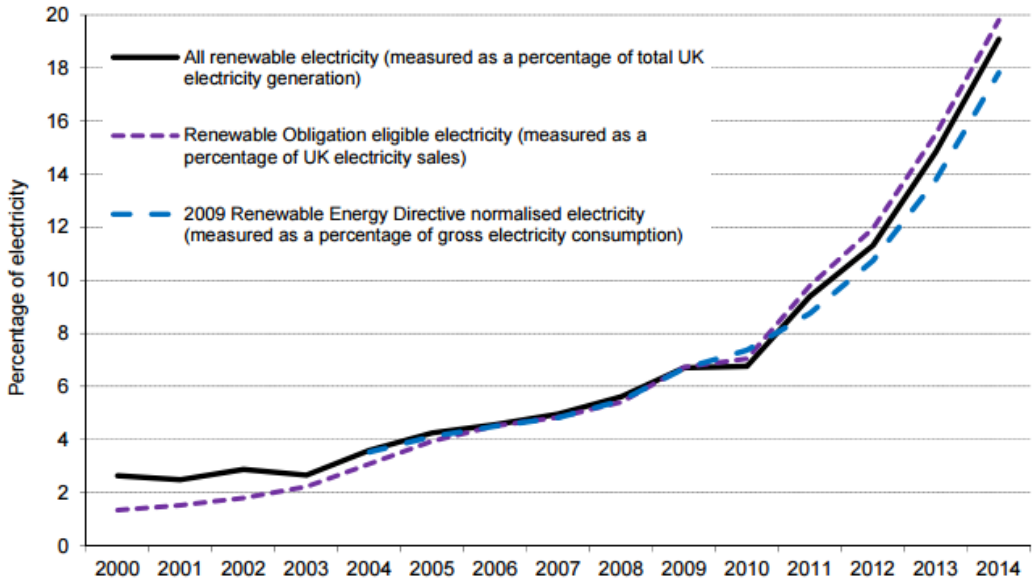

Figure 2-5 – Growth in electricity generation from renewable sources since 2000 [50]

Regarding the RO, some of the different eligible renewable technologies are briefly mentioned earlier in the text however the focus of the next section will be to report on the deployment of bioenergy, specifically solid biomass, as well as an introduction to what constitutes biomass and its suitability as a fuel. Presented in Figure 2-11 in the next section are some statistics on the changing nature of biomass utilisation in the UK since the beginning of the RO from co-firing to dedicated biomass (in dedicated plant and converted plant) which demonstrates how these technologies have changed as ROC allowances have developed.

2.3 Bioenergy

Biomass is a term used to describe the organic material found in plants which derive from photosynthetic processes [51]. Within the chemical bonds of this organic material is the energy from sunlight which, when broken (as a result of combustion or other processes), release their chemical energy. The energy within these bonds has been utilised by man for millennia as a source of heat and light and thus represents one of the oldest uses of fuel for energy [52, 53]. Worldwide, bioenergy accounts for 50EJ of total global primary energy use and 1.5% of the world electricity today [54]. It is an important source of energy in developing countries with almost two-thirds of global biomass used for cooking and heating applications in these areas. The remaining use of biomass is considered as 'modern usage' in high efficiency systems for heat and power generation [55]. The use of bioenergy for large-scale heat and power in modern times did not take place until the 1990s as a means of co-firing with coal to reduce SO_x and NO_x

emissions however it is now recognised as an extremely important source of energy based on its potential for GHG abatement. As a fuel, it can be loosely considered 'carbon-neutral' in the sense that any carbon released from conversion processes is biogenic i.e. any carbon released is the same carbon produced via photosynthesis thus there is no 'net' increase of CO_2 to the atmosphere. It also a very versatile source of energy being the only form of renewable energy that can exist solid, liquid or gaseous form [56]. When compared with other sources of renewable energy, biomass is attractive option being a carbon carrier that can be stored and brought on-line when required and so alleviates issues of intermittency associated with solar and wind technologies for example.

In 2012, the UK government published the UK Bioenergy Strategy which highlighted the importance of using bioenergy in meeting its low carbon objectives [57]. Underpinning the strategy are four main principles which aim ensure that the use of bioenergy delivers genuine carbon reductions, that delivery is done cost-effectively, that support for bioenergy maximises benefits across the economy and that when required policy-makers should assess and respond to impacts of increased deployment [57]. The use of bioenergy is thus utilised in the UK in line with renewable energy policy and subsidies discussed above in line with the principles set out in the bioenergy strategy.

2.3.1 Types of Biomass

The term biomass is used for all organic matter derived from plants however different types of can be sub-categorised depending on its source e.g. virgin biomass or waste biomass. Table 2-1 shows the major biomass types that can be used in energy applications. Some of these are commonly used for heat and power applications with forest/woody biomass, energy crops, forest residues and sawdust (in the form of pellets) representing a large proportion of the solid biomass utilised. Forest/Woody biomass and their corresponding waste products (forest residues and sawdust) derive from vascular plants whose perennial stem is above ground [58].

Woody biomass can be herbaceous or non-herbaceous depending on whether the leaves and stem die at the end of growing season (herbaceous e.g. wheat) or live all year round (non-herbaceous e.g. trees: pine, oak). Energy crops are annual or perennial crops whose cultivation purpose is solely to produce solid, liquid or gaseous forms of energy [59] (e.g. short rotation coppice willow, eucalyptus). The make-up of these types of biomass is, in basic terms, a mix of predominantly organic materials in the form of lignocellulose (which make up the cell wall) and

extractives with small amounts of inorganic materials (ash). With regards to thermochemical conversion for energy, the lignocellulosic constituents represent the most important fraction of biomass and so will be discussed in more detail below.

Group	Sub class.	Example
Virgin Biomass	Terrestrial Biomass	Forest Biomass Grasses Energy Crops Cultivated Crops
	Aquatic Biomass	Algae Water Plants
Waste Biomass	Municipal Waste	Solid Waste Sewage Landfill gas
	Agricultural Waste	Livestock Manure Crop residues
	Forest Residues	Bark, leaves and branches
	Industrial Waste	Demolition wood Sawdust Waste oil/fat

Table 2-1 - Different types of biomass used for in energy applications; adapted from [58].

2.3.2 The Plant Cell

In woody biomass and energy crops, the cell wall protects the cytoplasm which is responsible for cell functions. The cell wall itself is made up of a primary outer layer and multiple inner secondary layers providing structural support (as well as protection) with individual cell walls separated by a middle lamella which acts as a glue joining the cells together (Figure 2-6).

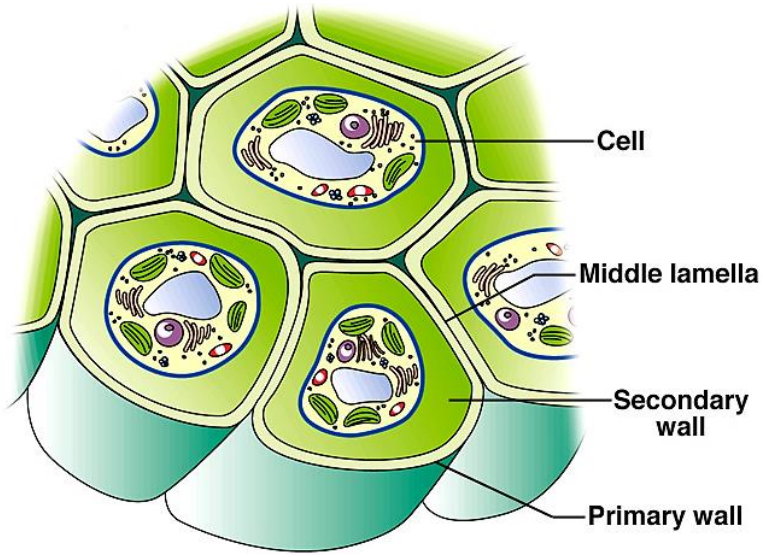

Figure 2-6 - Structure of typical plant cell [60]

The cell wall is composed of the main lignocellulosic components: hemicellulose, cellulose and lignin with each layer containing a different proportion of each. The primary cell wall is made up of hemicellulose, cellulose and pectin [61]. The secondary cell wall, inside the primary cell wall is split in to three layers, S_1, S_2 and S_3 with the distribution of lignocellulosic components shown in Figure 1-6.

The S_2 layer is the thickest layer and is composed of thick macrofibrils of cellulose microfibrils which hydrogen bond to a hemicellulose network. The orientation of the S_2 is perpendicular to the S_1 and S_3 layers; these two layers composed of mainly hemicellulose and cellulose with lignin increasing in weight percent as the distance towards the cell decreases [61].

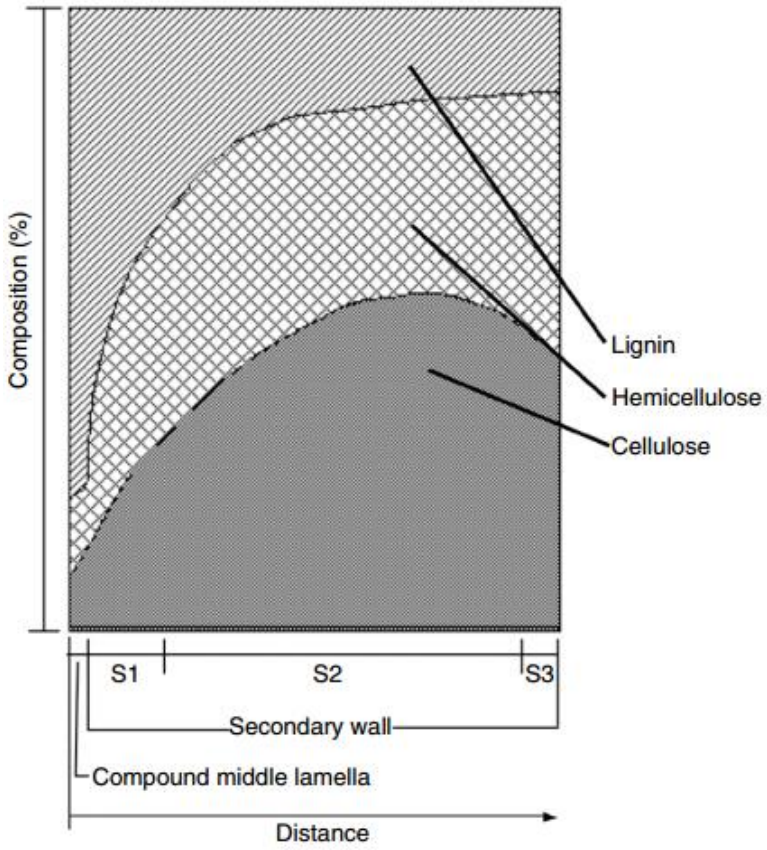

Figure 2-7 - Lignocellulosic composition of the middle lamella and secondary cell walls in plant cells [58].

Figure 2-8 shows the chemical structure of each of the lignocellulosic components. Each will be described in more detail below.

2.3.2.1 Cellulose

Cellulose is a long chain, crystalline polymer composed mainly of repeating d-glucose units with the generic formula $(C_6H_{10}O_5)_n$. The hydroxyl functional groups (-OH) contained in glucose monomers form hydrogen bonds with oxygen molecules on the same and neighbouring chains forming microfibrils with high tensile strength [62]. Cellulose has a high degree of polymerisation (~10,000) and provides structural integrity in the cell wall.

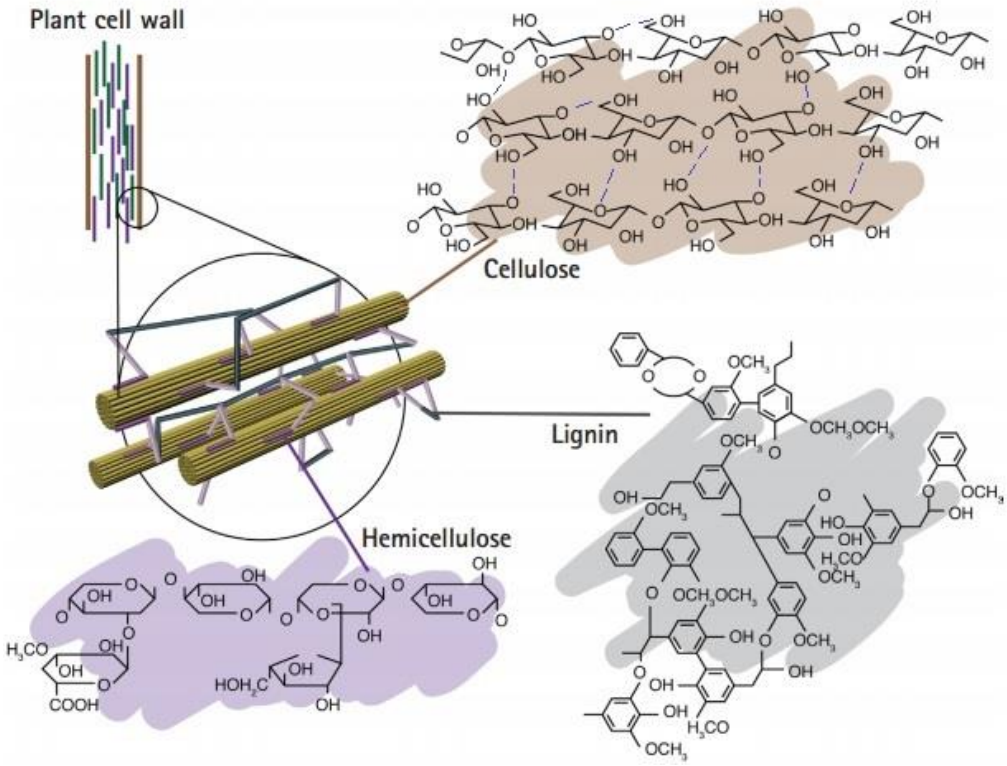

Figure 2-8 - Lignocellulosic composition of the plant cell wall showing cellulose, hemicellulose and lignin [62]

2.3.2.2 Lignin

Lignin is a highly branched, amorphous, cross-linked polymer that serves as an embedding material for cellulose in the secondary cell wall [63]. Unlike cellulose, there is no exact structure for lignin and it is relatively hydrophobic and aromatic [62]. The main lignin subunits found in woody biomass are guaiacyl (4-propenyl-2-methoxy phenol) and syringyl (4-propenyl-2,5-dimethoxy phenol) which derive from the *trans*-coniferyl and *trans*-sinapyl alcohols respectively [61]. These units exhibit extensive cross-linking and produce high-molecular weight materials that are rich in carbon. Different types of wood contain different proportions of the guaiacyl and syringyl moieties. Softwoods (e.g. pine, spruce) are characterised mainly by syringyl units while hardwoods (e.g. eucalyptus) contain both guaiacyl and syringyl units.

2.3.2.3 Hemicellulose

Hemicellulose is an amorphous, non-crystalline, polymeric structure of which there are several different types. The type of hemicellulose depends on the sugar monomers (monosaccharides) that make up the structure however all hemicelluloses share a low degree of polymerisation (~50-200) and are structurally very weak [58]. Typical sugars that make up different

hemicelluloses include d-xylose, d-galactose, l-arabinose and d-mannose (shown in Figure 1-8) and vary depending on the type of wood [64]. The sugar monomers in hemicellulose are characterised by β-(1->4) linkages corresponding to an equatorial configuration at C1 and C4 [64] (Figure 2-9).

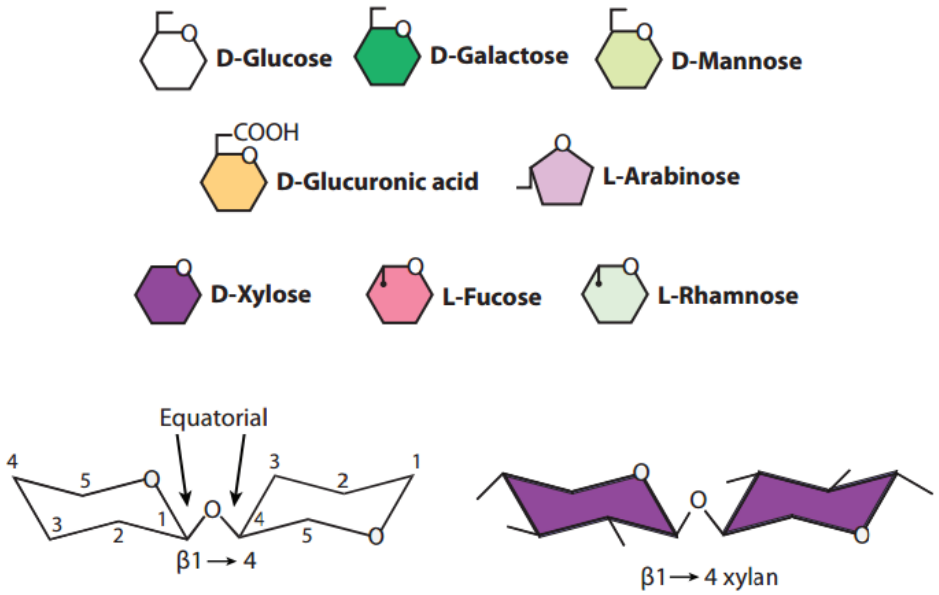

Figure 2-9 - Typical sugar monomers found in hemicellulose and their characteristic linkage shown with xylan as an example. Adapted from [64].

Hemicelluloses contain a high-degree of branching and possess side chains containing acid and ester functional groups (amongst others) which are very easy to remove and are released as volatiles upon degradation. The main hemicellulose found in hardwoods is xylan which is composed mainly of xylose monomers. Softwoods on the other hand are composed mainly of (galacto)glucomannan, composed of d-mannose and d-galactose sugars, followed by xylan and arabinoglucuronoxylan which is composed of xylose, l-arabinose and d-glucuronic acid [65]. Approximate amounts of these monomers in softwoods and hardwoods are shown in Table 2-2.

	Cellulose (%)	Lignin (%)	Hemicellulose (%)		
			Glucomannan	Arabinogalactan	Xylan
Hardwood	43-47	18-26	2-5	1	20-35
Softwood	39-43	26-32	5-15	2	7-15

Table 2-2 – Typical lignocellulosic compositions for hardwoods and softwoods [58]

2.3.3 Biomass conversion

In order to utilise the energy contained in biomass, it must undergo conversion. There are two main routes to achieve this: biochemical conversion and thermochemical conversion. During biochemical conversion, biomass is broken down by the action of bacteria or enzymes and includes anaerobic/aerobic digestion and fermentation [58]. During thermochemical conversion, biomass is converted using heat, producing different amounts of solid, liquid and gaseous products depending on the process conditions. Three of the main types of thermochemical conversion are combustion, pyrolysis and gasification; a brief description of each is discussed below.

Combustion of biomass represents one of the simplest thermochemical conversion methods that can be utilised for energy. When biomass undergoes combustion, it reacts with oxygen to produce heat, water and carbon dioxide. A simple equation (assuming complete combustion) is shown below:

$$C_xH_yO_z + O_2 \rightarrow H_2O + CO_2 + \text{Heat}$$

The biomass combustion sequence can broadly be split in to 4 different steps as shown in Figure 2-10 although overlap between steps does occur. During the first step, biomass particles heat up and undergo drying as moisture is released. During the second step the dried particle undergoes pyrolysis which is thermal degradation in the absence of air [66]. This involves the release of permanent and volatile gases during which the porosity of the particle increases. The third step involves the combustion of the volatile gases released in step 2 until the final step which is combustion of the residual char. The final step is the slowest step and thus determines the overall rate of biomass combustion. A more detailed description of biomass combustion and rates of decomposition will follow in the literature review so a short introduction is only presented here.

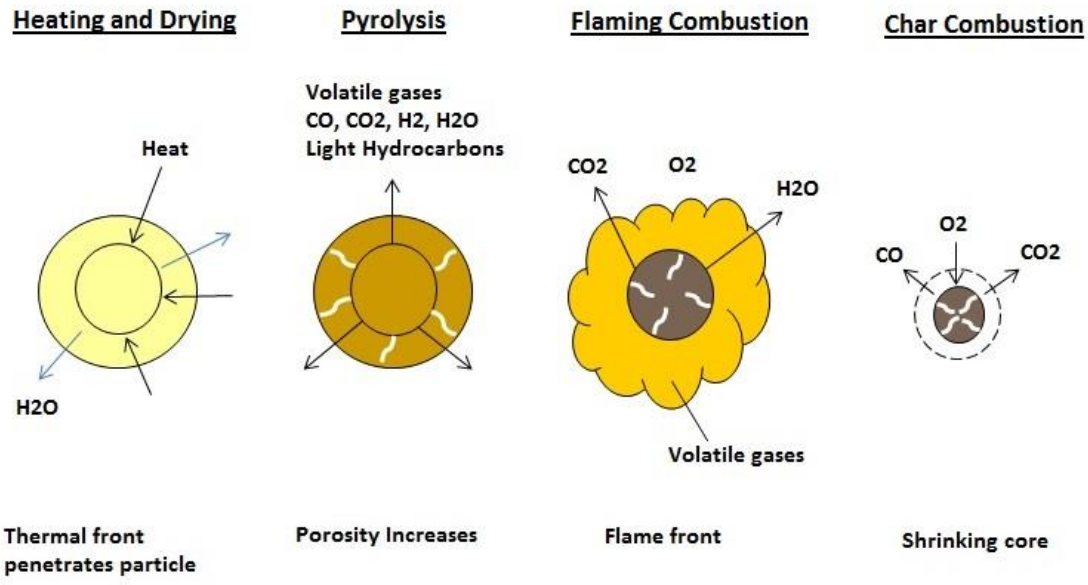

Figure 2-10 - Stages of biomass combustion

During pyrolysis, as a standalone process, biomass is heated to a specific temperature in the absence of oxygen to produce solid, liquid and gaseous product which will vary depending on the final temperature, residence time and heating rate. In fast pyrolysis, the main product is liquid and in slow pyrolysis, the main products are solid (charcoal) and gas. The liquid products in fast pyrolysis are also known as bio-oil containing degradation products of lignocellulose, including anhydrosugars, acids, aldehydes and phenolic compounds and up to 20% water [58].

Gasification is concerned with the conversion of solid or liquid biofuels into a gaseous product that can be used as a fuel or chemical feedstock [58]. It differs from combustion in the sense that when solid or liquid biofuels undergo combustion, the energy contained within the chemical bonds is released. During gasification, the aim is to contain the energy within the chemical bonds of the product gas to be utilised at a later date [58].

2.3.4 Deployment of bionenergy

Of the 13,556 ktoe equivalent of renewable energy consumed in the UK in 2014, 72.2% was generated using bioenergy as shown in Figure 2-11 [67]. As mentioned earlier, the main platform for biomass support in the UK is the RO with different levels of support allocated depending on the type of technology. One of the technologies that feature heavily is biomass combustion, and there is RO support for combustion of biomass in dedicated plant, in conversion from existing

coal plant and co-firing with coal. As ROCs were originally technology neutral, co-firing was a favoured technology due to relatively small upfront costs.

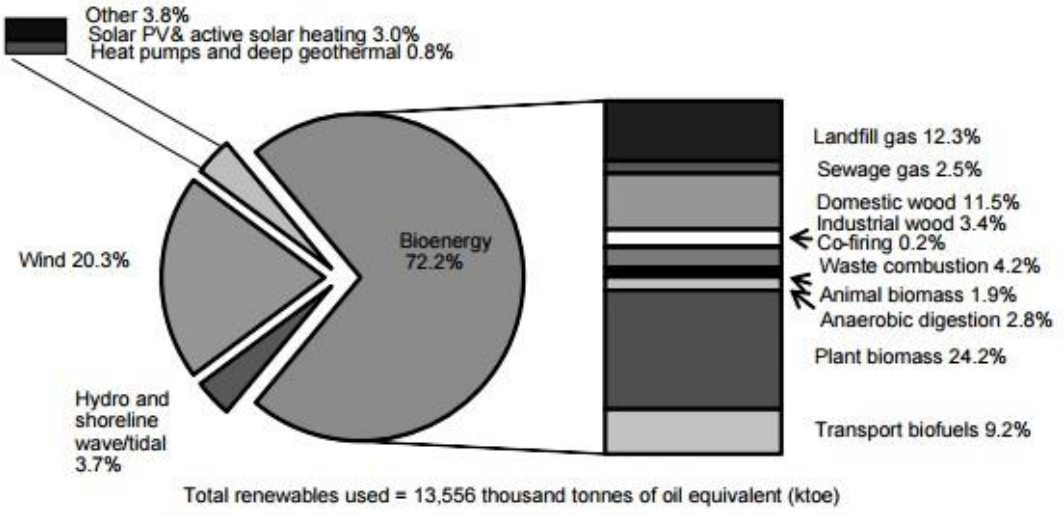

Figure 2-11 – Renewable energy by consumption in the UK in 2014 [67]

Despite this, some restrictions were in place for co-firing including the volume of ROCs a supplier could receive from this technology which was placed at 25% of the supplier's total obligation. This was done to avoid over deployment which would in turn crash the price of the ROC [68]. With respect to co-firing, several revisions have taken place since 2002 including original proposals to fade-out co-firing as it was deemed a short term solution, implemented to incentivise development in bioenergy supply chains. Phasing out was postponed however to provide stability to biomass growers to 2016 and retention of co-firing under the RO was selected as it was recognised as having a large impact on emissions reductions [68]. The support for co-firing and other bands for biomass combustion for the current 2013-17 period is shown in Table 2-3.

There have also been changes to the grandfathered support some of these technologies receive. Grandfathering operates by suppliers receiving a constant level of support throughout the technology's participation in the scheme that were first awarded. Grandfathering for low-range co-firing was never in place and in 2013 grandfathering was extended to mid-range firing and conversion on a unit by unit basis i.e. if a plant unit moves from mid to high range co-firing, the mid-range levels would no longer be grandfathered and grandfathered support for high-range would occur at the time of conversion [70].

Band	2013/14 ROC support	2014/15 ROC support	2015/16 ROC support	2016/17 ROC support
Co-firing (low-range*)	0.3	0.3	0.5	0.5
Co-firing (mid-range**)	0.6	0.6	0.6	0.6
Co-firing (high-range***)	0.7	0.9	0.9	0.9
Co-firing (low-range) with CHP	0.8	0.8	1.0	1.0
Co-firing (mid-range) with CHP	1.1	1.1	1.1	1.1
Co-firing (high-range) with CHP	1.2	1.4	1.4	1.4
Co-firing of reg. bio-liquid	0.3	0.3	0.5	0.5
Co-firing of reg. bio-liquid with CHP	0.8	0.8	1.0	1.0
Co-firing of reg. energy crops (low-range*)	0.8	0.8	1.0	1.0
Co-firing of reg. energy crops (low-range*) with CHP	1.3	1.3	1.5	1.5
Conversion† (station/unit)	1	1	1	1
Conversion† (station/unit) with CHP	1.5	1.5	1.5	1.5
Dedicated biomass	1.5	1.5	1.5	1.4
Dedicated biomass with CHP	2	2	1.9	1.8
Dedicated crops	2	2	1.9	1.8

* Less than 50% co-fired in a unit (minimum threshold 15%)
** 50 - < 85% biomass co-fired in a unit
*** 85 - < 100% biomass co-fired in a unit
† 100% biomass

Table 2-3 – Bioenergy combustion technologies supported under the RO during 2013-17 period [69]

In 2014 however DECC announced that grandfathering would no longer be upheld for co-firing and conversion although plant that had already made significant investment would still receive grandfathered support. DECC also announced a 400MW cap on new dedicated biomass builds to prevent over deployment. The impact these changes have had on bioenergy deployment in recent years is the shift in from co-firing to stand-alone combustion as shown in Figure 2-12.

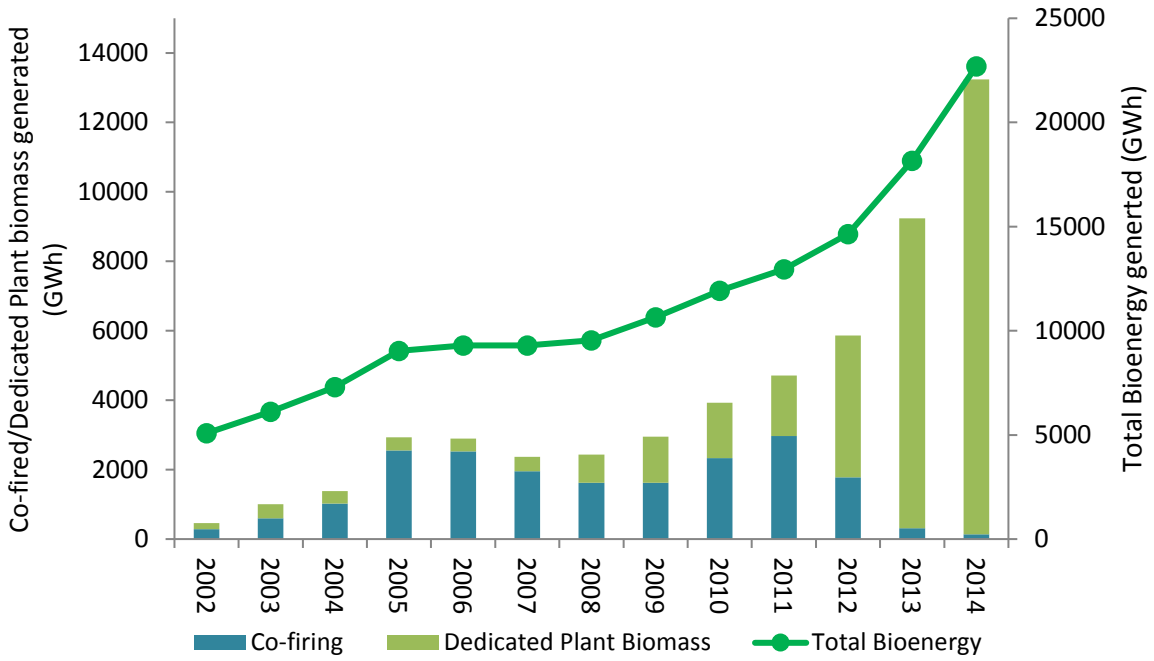

Figure 2-12: Generation from co-firing, dedicated plant biomass and total bioenergy generation in the UK from 2002 to 2014. Data taken from [67, 71-73]

This increase in dedicated biomass and reduction in co-firing is largely due to the conversion of existing coal plant to biomass as in the case of Drax, Tilbury and Ironbridge power stations, details of which are shown in Table 2-4 who have received support under the RO. Tilbury and Ironbridge are now closed and closing respectively under the LCPD (see section 1.2.7), however Drax is in the process of converting a third unit to 100% biomass and has opted to receive support under the new EMR with CfDs for units 2 and 3 while continuing to receive support for its first converted unit under the RO [74].

	Owner	Capacity (MW)	Conversion year	Status
Drax 1	Drax Plc	660	2013	Running
Drax 2	Drax Plc	660	2014	Running
Drax 3	Drax Plc	660	Expected 2016	Under Construction
Ironbridge B	E-On	1000	2013	Closing end 2015
Tilbury B	RWE	1428	2011	Closed

Table 2-4 – Details of large-scale biomass plant in England

During 2013-14 alone, generation from dedicated biomass plant rose by 4176 GWh to 131,405 GWh (excluding co-firing) as a result of conversion of a second unit at Drax Power Station; in addition to other smaller installations during the 2013-14 periods as shown in Figure 2-12. In terms of solid biomass used, this increase corresponded to 5.4 million tonnes, a 62.2% increase

from the 3.3 million tonnes used in 2012-13 [75]. The main fuel used in biomass generation is woody biomass with smaller contributions from energy crops and waste products such as straw and palm kernel expeller as shown in Figure 2-13.

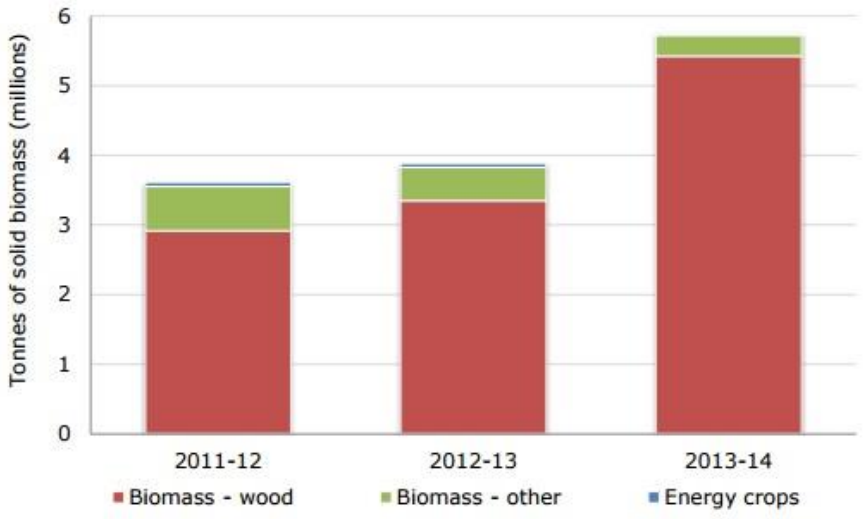

Figure 2-13 – Type of biomass used in power generation [75].

It is projected that by 2020 the solid biomass requirement for electricity will be between 9 and 16 Modt/year [76]. The increase in biomass consumption is beyond the biomass resources available in the UK (for comparison the total wood harvest for *all* wood products is approximately 5.3Modt/year [76]) and as a result, imports of biomass from outside the UK are increasingly being sought to meet demand. Figure 2-13 shows that during 2013-14, biomass imports were the dominant source of fuel utilised with 79% of biomass sourced from oversees and more than half the total biomass consumed deriving from North America (~ 3 million tonnes) [75].

Whilst utilising imports from abroad is currently satisfying the UK's demand for solid biomass, it must be sourced in a sustainable manner. Shipping of biomass from across the Atlantic for example will impact the life-cycle GHG emissions in the supply chain which must fall within regulatory limits. Understanding supply chain emissions and the sustainability limits set in place for using biomass are extremely important when evaluating its potential and practical use in the UK. As a result, these are discussed later on in this thesis (Chapter 7) in a separate literature review.

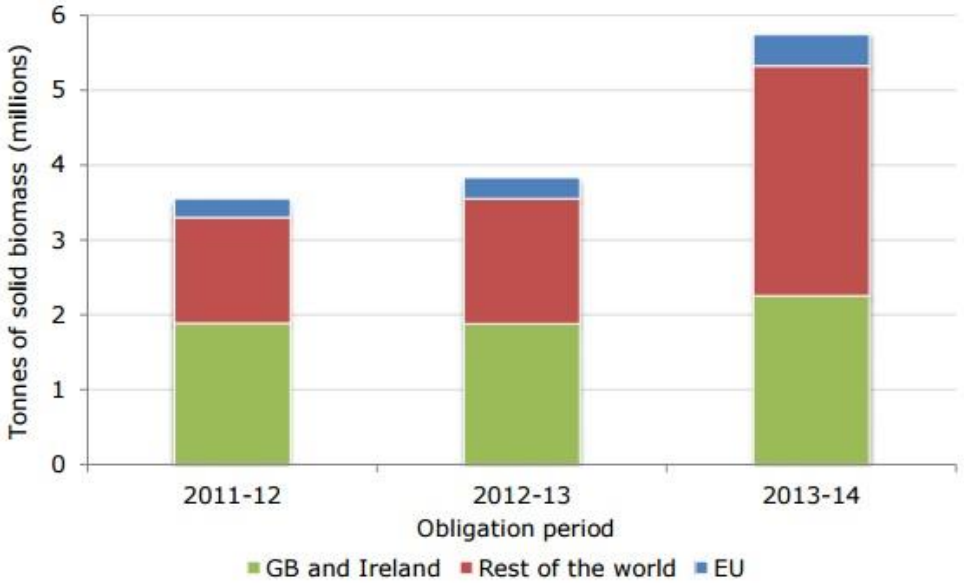

Figure 2-14 – Sources of biomass used in power generation [75]

2.3.5 Fuel characteristics

2.3.5.1 Moisture Content and Calorific Value

Different properties of biomass have an effect on how they behave as fuels. Two properties, which have a particularly important effect, are the calorific value and moisture content; the two are closely linked as the greater the moisture content, the lower the calorific value. The moisture content of freshly harvested biomass can be 50% (as received) and so drying of biomass prior to combustion is often essential owing to the energy required to overcome the latent heat of vaporisation (H_{vap}). In a combustion chamber, if the moisture content is too high, the energy required to overcome the H_{vap} can reduce the flame temperature to the point where combustion is non spontaneous [77].

The calorific value of biomass provides information on the amount of energy released when biomass undergoes complete combustion. There are two main terms used to describe this: the gross calorific value (GCV) and the net calorific value (NCV). The gross calorific value (or Higher Heating Value (HHV)) is described as the heat released during combustion, per unit mass of fuel, under the constraints that the energy required to convert liquid water to steam is recovered. The net calorific value (or Lower Heating Value (LHV)) is the same as above excluding the energy recovered from condensation and is subsequently always lower than the GCV [66].

GCVs are often used in the literature however NCVs describe the energy available in real-life systems. In an industrial boiler for example, the energy recovered from condensation of moisture does not occur in practise. The calorific value is a function of the organic species present in biomass and the moisture content.

2.3.5.2 Ultimate and proximate analysis

Knowledge of the organic species weight percent can be derived from ultimate analysis of solid fuels which describes the organic components in terms of their basic elements. In addition to ash, moisture and some other elements such as Cl these elements make up the empirical composition of biomass:

$$C + H + N + S + O + Cl + Ash + Moisture = 100\%$$

Carbon and oxygen are the most prevalent elements in biomass typically making up 30-60% and 30-40% of the dry matter respectively [77]. Hydrogen typically makes up 5-6% of the dry matter of biomass with nitrogen, sulphur and chlorine normally providing <1% of dry matter, although some biomass do contain more of these latter species [77]. The energy content of biomass is derived mainly from the carbon as well contribution from the hydrogen, nitrogen and sulphur while oxygen contributes no useful energy to biomass fuels. Oxygen also has the effect of consuming some of the hydrogen content in biomass (i.e. the hydrogen is oxidised) which further reduces the energy content. Thus, the higher the carbon content and lower the oxygen content of the biomass, the greater the calorific value. This effect is notable when comparing biomass to carbon-rich fuels such as coal. Van Krevelen diagrams, which plot atomic H/C ratios against O/C ratios, are often used to classify coals. As O/C ratios reduce, the calorific value increases. Figure 2-15 shows the Van Krevelen diagram of the coalification from biomass to anthracite. While ultimate analysis quantifies the individual organic elements, proximate analysis characterises the biomass by quantifying the components of moisture, volatile matter, ash and fixed carbon.

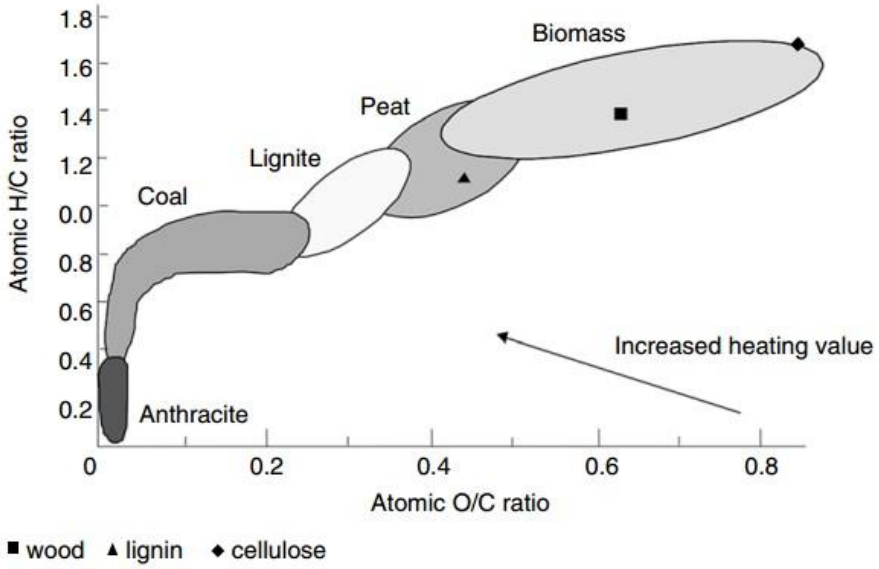

Figure 2-15 – Van Krevelen diagram showing the H/C vs O/C atomic ratios for biomass and coal [58]

Moisture, discussed above, is a main component of fresh biomass and derives mainly from absorption from the ground whilst standing. In biomass it exists in two forms: inherent moisture and free moisture; both linked with the equilibrium moisture content (EMC) which is a function of relative humidity [58]. Inherent moisture is the moisture contained in biomass when it is in equilibrium with relative humidity of its environment and is normally contained within the cell wall [78]. Free moisture is moisture that is in excess of the EMC and is normally outside the cell wall [58]. Volatile matter is the matter that is released when biomass is heated to 550°C usually in the form of condensable and non-condensable vapours [79]. Ash refers to the inorganic elements present in biomass. These include major essential elements: K, Na, Mg and Si and minor species: Mn, Fe, Mo, Cu and Zn [80] and do not contribute any energy value to biomass fuel. Fixed carbon is the carbon retained in the char once the volatile matter has been released.

2.3.6 Problems with biomass as a source of energy

The subsidies in place for bioenergy show the level of interest in using this fuel for energy applications and as a carbon carrier; it can be utilised in similar manner to coal. There are several issues associated with using bioenergy that can place some limitations on its deployment however. Some of these are already mentioned above, notably high oxygen concentrations and significant moisture contents that reduce the fuel's energy content. When comparing calorific values with coal directly, biomass contains much less energy per unit mass which means that more mass is required to provide a given amount of energy. The moisture content of biomass

also causes problems during storage as the biomass can grow mouldy and disintegrate signifying economic losses. Other problems include a tendency of biomass to undergo low temperature ignition during processing and conveying as well as self-heating during storage which can lead to spontaneous combustion [81]. The propensity for biomass to form dust layers during handling also presents a risk as these may lay on hot machinery [81]. Storage of biomass also presents a danger as gases such as CO, CO_2, CH_4 and N_2O can be emitted from heaped piles which can cause both health risks and environmental problems [82]. The lignocellulosic structure of biomass can also cause problems in pulverised fuel applications, particularly co-firing with coal in existing plant, as biomass does not readily break down in to small particles with ease and reduces the mill capacity owing to its fibrous nature [83].

2.3.7 Pre-treatment of Biomass

Pre-treatment of biomass can be implemented to address some of the issues presented above. Treatment of biomass in one way or another is normally implemented prior to use in energy application (e.g. drying) however other treatments that make significant changes to the lignocellulosic structure of biomass can be utilised to improve handling, storage and energy conversion. Pre-treatment of biomass can be broadly grouped in to 4 different types:

- Mechanical
- Chemical
- Biological
- Thermal

Mechanical pre-treatment involves the comminution of lignocellulosic components via methods such as chipping, grinding and milling [84]. Chemical pre-treatment involve the disruption of the biomass structures via chemical reactions of which there are several different methods [85]. These include acid and alkaline hydrolysis which alter the structure through hydrolysis of hemicellulose and lignin components [85]. Other chemical pre-treatments include oxidative delignification which converts lignin polymers to e.g. carboxylic acids with an oxidising agent such as hydrogen peroxide [85]. Combinations of these two pre-treatments, mechanical and chemical, can also be employed; one example being steam explosion. This process involves treating biomass with hot steam under pressure before explosive decompression which ruptures the fibrous structure [86]. Biological pre-treatment utilises micro-organisms to degrade hemicellulose and lignin [84] while thermal pre-treatment utilises heat to break down the lignocellulosic structures. One type of thermal pre-treatment is torrefaction which affects some the properties of biomass raised above (e.g. decreasing the volatiles and moisture content)

creating a fuel with improved chemical and physical properties. The pre-treatment step will be discussed in great detail in the next chapter as it forms the basis of this research, covering the principles of torrefaction, torrefaction mechanisms and its effect on fuel properties and product distribution i.e. the split of solid, liquid and gaseous products. The effect of torrefaction on the combustion properties of biomass is also introduced in more depth as these effects are also investigated in this work. Finally, the effect of torrefaction on biomass sustainability, in particular supply chain GHG emissions is also investigated with a separate literature review which can be found in Chapter 7. Specific details of this work carried out in relation to these points raised above can be found at the end of the literature review and in the aims and objectives in Chapter 3.

2.4 Conclusion

Climate change as a result of anthropogenic activity poses a severe threat to the earth's system. Increased energy use since the beginning of the industrial revolution has led to increase in the amount of GHGs in the atmosphere, increasing the earth's average temperature. One of the key contributors to anthropogenic GHGs is in power generation which accounts for just over a third of total GHG emissions. Increased awareness of these dangers has led to inter-governmental efforts to lower anthropogenic emissions and prevent the increase of the earth's average temperature below 2°C.

In the United Kingdom, several changes have taken place in the electricity supply industry since privatisation in the early 1990s including the introduction of government incentives to increase the deployment of sustainable technologies. The current market-based mechanism takes the form of the renewables obligation, with current participants receiving subsidies proportional to the amount of renewable electricity they generate. The RO is closed to new participants (current participants will still receive subsidies until 2030), being replaced with a feed-in tariff with contracts for difference as part of the electricity market reform.

One type of fuel currently being used to combat climate change is bioenergy: this being the utilisation of the energy contained within the organic material found in plants. One of the oldest forms of energy known to man, biofuels represents a key resources being carbon carriers that can be brought on-line when required and can exist the solid, liquid and gaseous state. Bioenergy is also a key technology as it can be loosely considered 'carbon-neutral' at the point

of combustion as there is no net release of CO_2 to the atmosphere. When used in thermochemical conversion, it is the cell wall components- hemicellulose, cellulose and lignin- that represent the most important constituents- each varying in composition and structure (e.g. crystalline or non-crystalline) depending on the type of fuel. One of the key routes of thermochemical conversion for biomass currently deployed in the UK is combustion on large-scales for power (and heat) generation- this technology current receiving subsidies under the RO. While the use of biomass on large-scales has several favourable qualities e.g. easy incorporation in to existing coal supply chains, there are several inherent problems associated with biomass. These include high moisture content, low calorific value and poor grindability when compared with fossil-based fuels. Several pre-treatments can be considered to address these issues which can be mechanical, chemical, biological or thermal in nature depending on the pre-treatment selected. One particular thermal pre-treatment that has undergone increased attention in recent years is torrefaction. This pre-treatment process is discussed in detail in the next chapter and forms the basis of this thesis work.

3 Literature Review

3.1 Introduction

The term torrefaction derives from the French *torréfier* which translates as the verb 'to roast'. Its perhaps most well-known application is in the coffee industry where fresh green coffee beans are roasted, or torrefied, to produce the darkened beans that can be ground up and used to make drinkable coffee. In recent years however its application using biomass has grown as a means of improving fuel properties. The process involves the heating of biomass at slow heating rates (<50°C/min) to a temperature between 200-300°C in the absence of oxygen and holding for a chosen residence time typically less than one hour. During torrefaction, free moisture is driven off during the drying stage up to 100°C and above 200°C the 'torrefaction reaction' begins with degradation of lignocellulosic structures. The extent to which each of the three lignocellulosic components, hemicellulose, cellulose and lignin, undergo degradation is related to the torrefaction temperature and residence time, however hemicellulose is the most affected as this is the least thermally stable component [87]. The breakdown of these components results in the evolution of reaction water, permanent gases and low-molecular weight volatile species which contain relatively small amounts of energy relative to the loss of mass resulting in energy densification in the solid residue. This energy densification is one of the key benefits of torrefaction as it produces a fuel with a higher calorific value relative to the untreated fuel. The loss of moisture during drying contributes to the increase in calorific value however its loss effectively lowers the number of hydroxyl (-OH) functional groups present in the biomass which reduces the torrefied biomass' ability to form hydrogen bonds with external sources of moisture since this can cause problems during storage of untreated (non-torrefied) biomass is seen as another benefit of torrefaction. The degradation of hemicellulose also improves the grindability in torrefied fuels, as the cellulose fibrils are no longer bound by this component resulting in easier particle size reduction which is beneficial in pulverised fuel (pf) combustion. A brief overview of torrefaction and some of the benefits of the process are described above however these will be discussed in more detail below. This literature review is split in to two sections, the first of which focusses on the torrefaction reaction and its influence on fuel properties. This first section directly relates to the work in Chapter 5 of this thesis where the torrefaction of pine and eucalyptus is presented and covers literature pertaining to Objectives 2-4 in this project, which focuses on torrefaction directly. The second half of this literature, beginning at Section 3.2, focusses on the combustion of torrefied fuels and is described in greater detail in its respective section.

3.1.1 The Torrefaction process

The torrefaction process can be described as a series of steps as shown in Figure 3.1 which include heating of the biomass, dwell stages and a final cooling stage [88]:

1) **Initial heating** - This stage represents the initial heating of the biomass to the drying temperature (~100°C). Toward the end of this stage, free moisture in biomass begins to evaporate.
2) **Drying** - Free moisture is driven off at a steady rate and the biomass temperature remains constant. This stage is the most energy intensive in terms of heat demand owing to the high enthalpy of vaporisation for moisture [58].
3) **Post-drying & intermediate heating** – After the drying stage, the biomass is heated to the desired torrefaction temperature with the onset of torrefaction occurring when the temperature of the biomass exceeds 200°C. Above this temperature, the biomass starts to lose solid mass.
4) **Torrefaction** – This is the key stage where the lignocellulosic materials undergo the most significant change. Devolatilisation of hemicellulose and to an extent cellulose and lignin takes place during the heating period and continues during the dwell stage at the 'torrefaction temperature' resulting in mass loss. Torrefaction temperature is a selected temperature (which may also be a peak temperature) that is maintained for a desired residence time. Above 250°C, torrefaction becomes mildly-exothermic [89] reducing the need for external heat (not including heat losses).
5) **Cooling** - Once torrefied, the biomass is cooled down upon exit from a torrefaction system, exposure of hot biomass with oxygen in the air may result in spontaneous combustion [58]. During cooling, the solid biomass undergoes no further mass loss although some re-absorbed reaction water may evaporate during this stage [90].

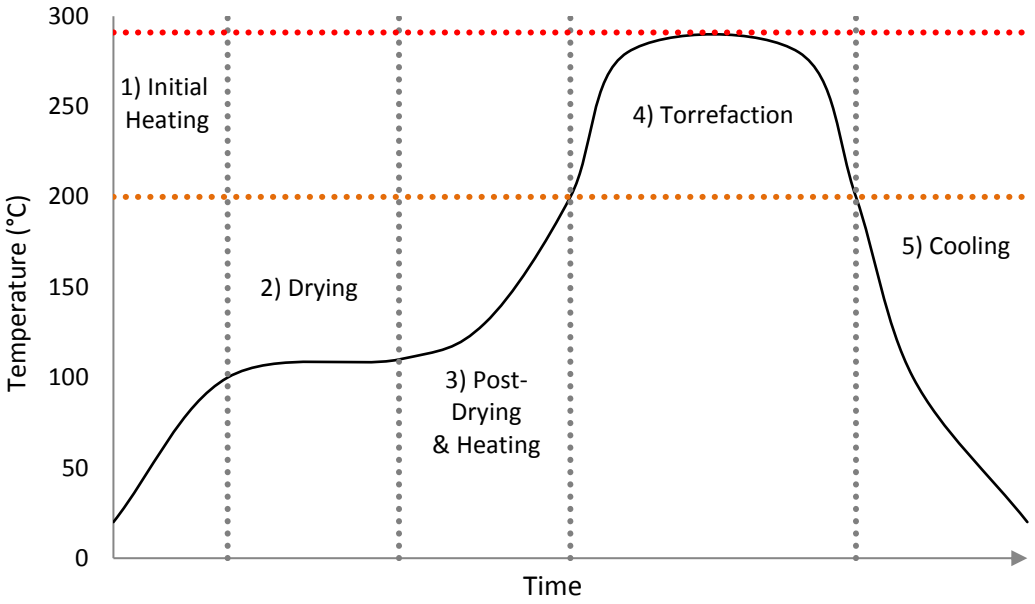

Figure 3-1 – Schematic of the torrefaction steps with temperature and time

3.1.2 Pyrolytic behaviour of lignocellulose

During torrefaction, hemicellulose, cellulose and lignin undergo different chemical transformations as a result of their distinct chemical and thermal reactivities [91]. Knowledge of the pyrolytic behaviour of these materials is crucial in understanding the reactions that take place during torrefaction as it has been suggested that pyrolysis (and by extension torrefaction) of any biomass can be considered as the superposition of these three components [87] in the absence of any synergistic effects. Numerous studies have been carried out on the thermal treatment of individual cell wall species to understand the degree of mass loss that occurs, to develop kinetic models for predicting pyrolytic behaviour and to evaluate the mechanisms of decomposition and evolution of species. Yang et al. [87] studied the pyrolysis of hemicellulose, cellulose and lignin using thermogravimetric analysis (TGA) with the individual components showing different rates and degrees of mass loss. As shown in Figure 3-2, hemicellulose undergoes degradation most readily with greatest rate of mass loss occurring between 220 and 315°C. In their study, cellulose was the most resistant to thermal degradation at lower temperatures with significant mass loss only occurring above 315°C. Lignin showed mass loss across the widest range however its rate of mass loss was much slower highlighting a resistance in thermal decomposition.

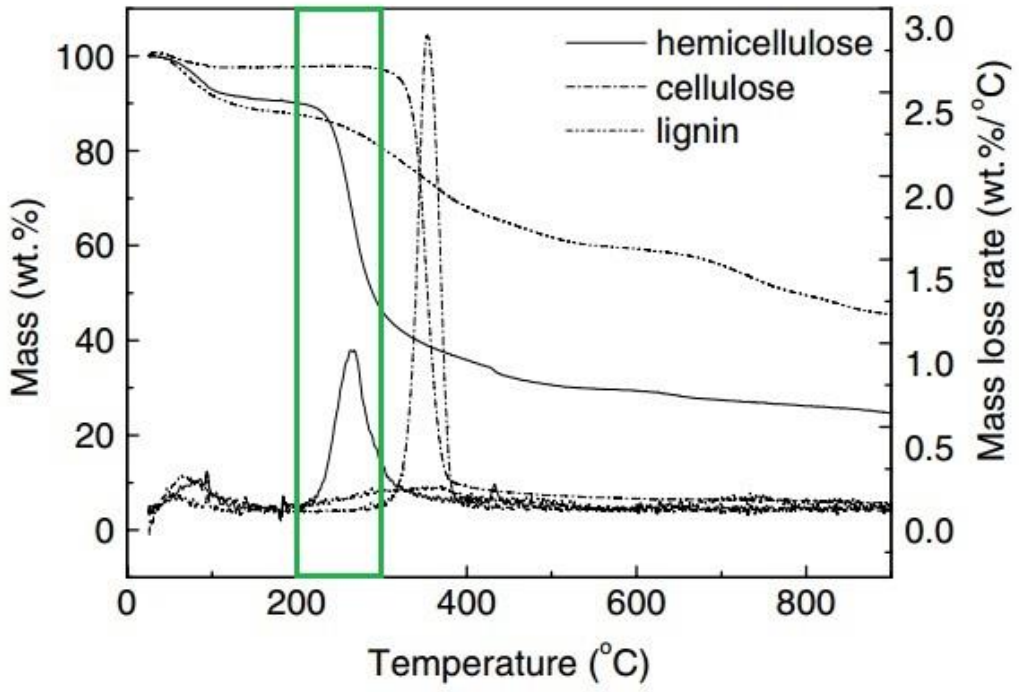

Figure 3-2 – Pyrolysis of hemicellulose, cellulose and lignin using thermogravimetric analysis with the torrefaction range outlined in green. Adapted from: [87].

Chen et al. performed a similar study on the individual components however the authors employed a range of torrefaction temperatures: 230°C, 260°C and 290°C with a residence time of 1 hour using TGA [92]. In the case of hemicellulose, rapid mass loss occurred upon reaching each of the torrefaction temperatures with degree of mass loss increasing from 2.74% to 37.96% from the mild (230°C) to medium (260°C) conditions. The most severe condition, 290°C, resulted in a 58.93% mass loss. Cellulose underwent only small degrees of mass loss under the mild and medium conditions in this study (1.05% and 4.43% respectively) however under the severe condition, 44.82% of the cellulose was degraded. Note this mass loss occurs at lower temperatures than the temperature at which Yang et al. [87] observed significant mass loss and is mostly likely due to the effect of residence time of one hour as the pyrolysis by Yang et al. employed a dynamic programme with no dwell periods. The mass loss of lignin was found to be 1.45, 3.12 and 6.97% for the mild, medium and severe conditions respectively.

3.1.3 Torrefaction chemistry

The differences in rates and degree of mass loss for each of these components can be attributed to their chemical structures. As hemicelluloses exist as amorphous structures with little crystallinity and numerous side branches, this allows for easier thermal degradation during

torrefaction. During torrefaction, hemicellulose degradation can start as low as 150°C however major decomposition does not occur until above 200°C. Above this temperature, 'intact hemicellulose' undergoes depolymerisation via hydrolysis or thermal chain scission to produce 'reacting' hemicellulose [62]. Shen et al. [93] propose that during pyrolysis of xylan (the main hemicellulose found in hardwood), cleavage of glycosidic bonds results in the in the formation of unstable 1,4-anhyrdo-D-xyopyranose which acts as an intermediate according to the following mechanism (Figure 3-3):

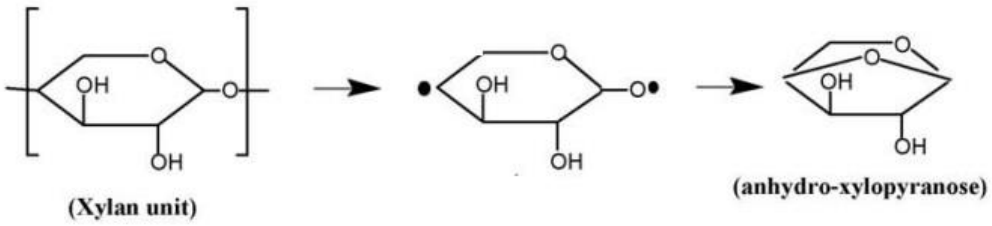

Figure 3-3 – Initial mechanism for the decomposition of xylan during pyrolysis [93]

The reacting monosaccharides (single monomer units) and oligosaccharides (3-9 monomer units) formed during depolymerisation are then decomposed by acid and radical reactions to produce a range of compounds that re-combine to produce torrefied hemicellulose [62]. Water evolved during these reactions can be used to depolymerise hemicellulose or release acids via hydrolysis of acetyl groups bonded to the hemicellulose fraction. As mentioned in section 1.3.2.3, the hemicellulose composition of softwoods and hardwoods differ in terms of the sugar monomers that make up the hemicellulose structure. As a result, the effects of torrefaction of different hardwood and softwood species may ultimately be different. Werner et al. studied the pyrolysis behaviour of different polysaccharides that comprise the hemicellulose components in softwoods and hardwoods [94]. The two main polysaccharides found in hardwoods and softwoods, xylan and glucomannan respectively, showed different behaviours under pyrolytic treatment (Figure 3-4). Glucomannan exhibited gradual mass loss beginning around 220°C and peaking at 320°C while xylan exhibited maximum mass loss in two stages; one at ~245°C and another at ~290°C. The onset of mass loss for xylan was also lower than glucomannan, beginning around 210°C. Ramiah provides further support for this notion from thermogravimetric analysis of xylan and glucomannan. In his study, the onset of glucomannan pyrolysis occurred at lower temperatures however xylan exhibited less thermal stability overall resulting in greater rates of mass loss as the temperature reached around 230°C [95]. Differences in the pyrolysis profiles of softwoods (pine) and hardwoods (eucalyptus) can be found in Section 5.3.4 of this thesis, were

the results of the pyrolysis of pine and eucalyptus in a TGA are shown. As the polysaccharides attributed to softwoods and hardwoods differ chemically, their pyrolysis products will also be different. Details of species evolved are discussed later in the text.

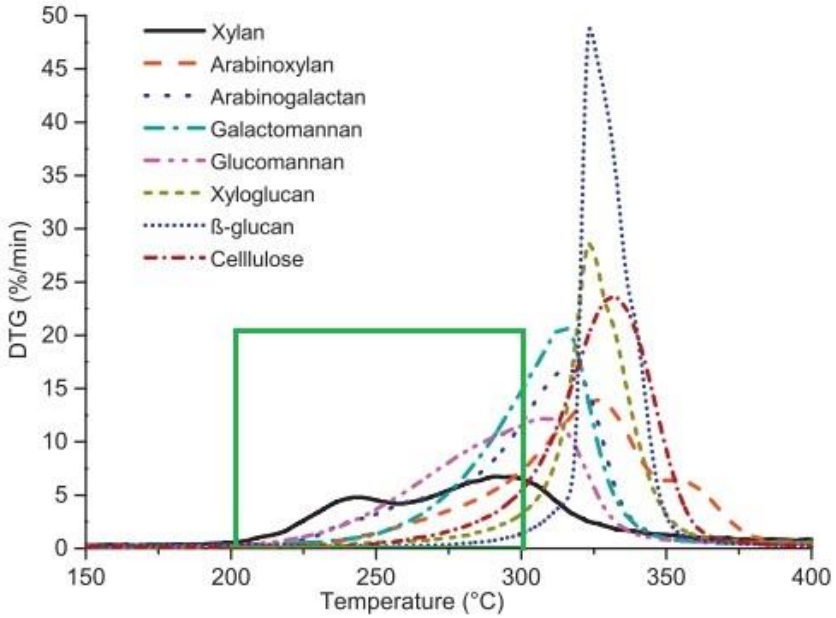

Figure 3-4 – Derivative mass loss curves for pyrolysis of polysaccharides. Green line represents the torrefaction temperature region. Adapted from [94]

In the torrefaction temperature range, the decomposition reaction of cellulose is dominated by decreasing degree of polymerisation [96] however degradation resulting in notable mass loss can occur at highest torrefaction temperatures as shown in thermogravimetric study performed by Chen at al. [92]. During depolymerisation, the cellulose polymeric structures undergo cleavage at the glycosidic bonds to produce some glucose monomers or 'active cellulose' [97]. Degradation of the active cellulose produces anhydrocellulose and levoglucosan according to the mechanism shown in Figure 3-5 [98]. In this mechanism, levoglucosan is formed via a glucosan radical where the hydroxyl moiety on the C6 transfer a proton to the C1 cation forming a 1-6 oxygen bridge [98].

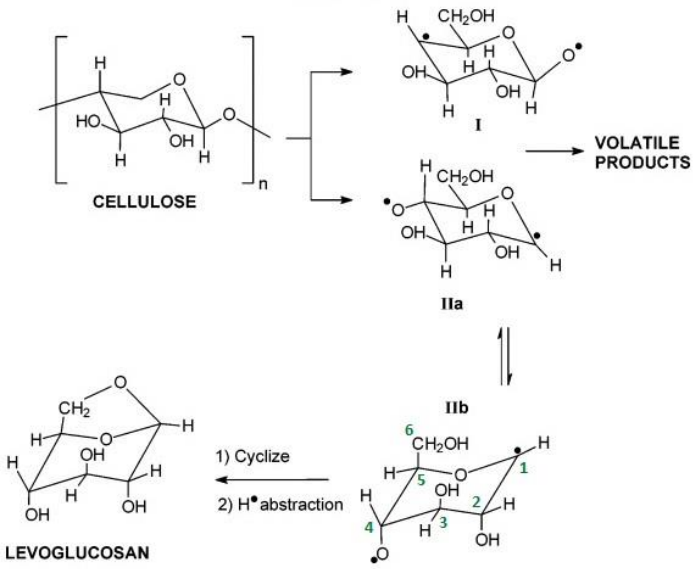

Figure 3-5 - Mechanism of low-temperature pyrolysis of cellulose. Adapted from [98].

Mass loss attributed to lignin occurs over the widest temperature range; however in the torrefaction temperature range significant mass loss does not occur. At higher temperatures (>280°C) lignin decomposes via cleavage of ether bonds and scissioning of C-C bonds [62]. Lignin decomposition results in the production of char more so than holocellulose as lignin is more difficult to dehydrate [98].

3.1.4 Torrefaction reaction rates

As shown above, in the torrefaction temperature range, the main changes and mechanism for torrefaction of biomass is largely represented by the changes in the hemicellulose (and to some extent cellulose). Owing to the number and complexity of reactions that occur during thermal degradation of these components, kinetic models have focussed on simplified mechanisms that use a semi-global approach, using mass loss of these components as a means of understanding rates of decomposition [97]. Di Blasi and Lanzetta [99] propose that for hemicellulose decomposition, the reaction occurs via a two-step mechanism on the assumption that conversion of hemicellulose occurs under pure kinetic control and semi global mechanisms can be applied. The first step involves the depolymerisation of the hemicellulose at temperature below 250°C leading to re-arranged polysugar structures and the evolution of moisture as a result of bond scission at glycosidic bonds [100]. The second step is decomposition of the monosaccharides and oligosaccharides formed as a result of depolymerisation (Stage 1) resulting in the formation of char, CO_2, CO and moisture in addition to the release of light

volatiles from fragmentation of the carbon structure [88]. Prins et al. aimed to verify this approach using isothermal thermogravimetric analysis of a hardwood sample (willow) to determine a global reaction mechanism for torrefaction [101]. The authors accurately predicted the mass loss during torrefaction, in the absence of transport limitations, according to the following mechanism (Figure 3-6):

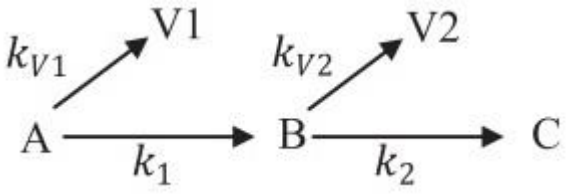

Figure 3-6 – Torrefaction reaction mechanism

Where A represents the parent fuel, B the solid intermediate and C and torrefied product and k_1, k_2, k_{v1} and k_{v2} are the Arrhenius kinetic parameters (a discussion of the Arrhenius parameters will follow later in relation to the kinetics of biomass combustion). As a global approach was applied, the lignocellulosic components are grouped together as represented by A, B and C and the total mass of solid product at any given time is the sum of these. Similarly, the mass of evolved species is the sum of volatiles evolved during each reaction: V1 and V2. The authors determined that the rate of decomposition of A to B to be much faster than the rate of decomposition of B to C and thus attributed the first mechanism to be dominated by hemicellulose decomposition and the second to dominated by cellulose decomposition. The authors do note that while this global approach can be applied for torrefaction of biomass, several factors can influence the rates of decomposition including the type of the biomass i.e. softwood or hardwood as discussed above. In their study, it is known that the hemicellulose composition of hardwoods and softwoods differ and so their decomposition rates may vary.

3.1.5 Changes in structure

While the reaction kinetics for torrefaction can be elucidated from thermogravimetry, determination of structural changes of the three lignocellulosic components before and after torrefaction and determination of the species evolved using analytical techniques can provide information on reactions that occur during thermal treatment. In the case of the former, Melkior et al. use ^{13}C NMR spectroscopy in their study on untreated and torrefied wood samples to

understand the changes in structure via changes in resonance for carbons assigned to the different lignocellulosic components [102]. With regards to hemicellulose, the authors found depletion in signal for the carbon assigned to acetyl groups (carbonyl and methyl groups) with increasing torrefaction severity. From plotting the integrals of these carbon signals as a function of torrefaction temperature, the authors quantitatively determined the loss of these carbons during treatment (Figure 3-7a). These changes in signal can possibly be attributed to the devolatilisation of the side branches containing the acetyl functional group with increasing torrefaction severity.

The authors also observed a reduction in the C1 carbon signal, representative of the C1 involved in axial β-1-4 ether linkages, in hemicellulose and cellulose. Using the same quantitative methodology as above they determined the loss of these carbons to begin around 245°C (Figure 3-7b). As it is known hemicellulose undergoes degradation at lower temperatures than cellulose, the C1s assigned to hemicellulose can be evaluated by comparison with temperature at which carbons exclusive to cellulose begin to reduce; this appears to occur at higher temperatures (Figure 3-7b). The resonance for carbons attributed to cellulose remains largely identifiable with increasing torrefaction temperature until 300°C where the spectrum (not shown) was notably different as all cellulose carbons decreased drastically. The behaviour of the signal integrals attributed to crystalline and amorphous cellulose carbons did however reveal information on chemical restructuring during torrefaction. Figure 3-7c shows an increase in crystalline cellulose with a reduction in amorphous cellulose suggesting that cellulose is partially re-crystallised up to around 260°C. Following this, at elevated temperatures, there is a rapid decrease in the integral corresponding to crystalline cellulose.

For lignin, differences in changes in resonance for C3 and C5 of etherified (i.e. those involved in β-1-4 structures) and non-etherified syringyl subunits provide information on the behaviour of lignin during torrefaction. As torrefaction temperature increases, there is a decrease in resonance for etherified C3 and C5 syringyl carbons which could be due to depolymerisation via cleavage of β-1-4 bonds or demethoxylation of syringyl units producing guaiacyl - note guaiacyl structures have only one methoxyl in the para position while syringyl has methoxyl groups in both para (3 and 5) positions. The etherified C3 and C5 syringyl carbons and methoxyl group carbons exhibited similar behaviour: both are relatively stable up to 200°C, before a marked degradation. This suggests that demethoxylation of syringyl is the dominant mechanism above 200°C (Figure 3-7d). As the demethoxylation of syringyl subunits led to an increase in resonance

for carbons attributed to guaiacyl, this further suggests that demethoxylation of etherified syringyl units mainly occurs at one position (either C3 or C5). In the case demethoxylation of guaiacyl, it is suggested by the authors to occur above 245°C as while the signal for guaiacyl C3 and C5 plateaus at this temperature, there is a reduction in resonance for methoxyl group carbons. Above 245°C, the resonance for non-etherified syringyl and guaiacyl increased while that of etherified syringyl and guaiacyl decreased suggesting that depolymerisation of lignin occurs above this temperature. These findings are in agreement with the studies on thermogravimetric analysis of lignin shown above as the low gradual weight loss may be attributed to demethoxylation of lignin subunits while the higher temperature degradation may be due to cleavage of C-C bonds after depolymerisation.

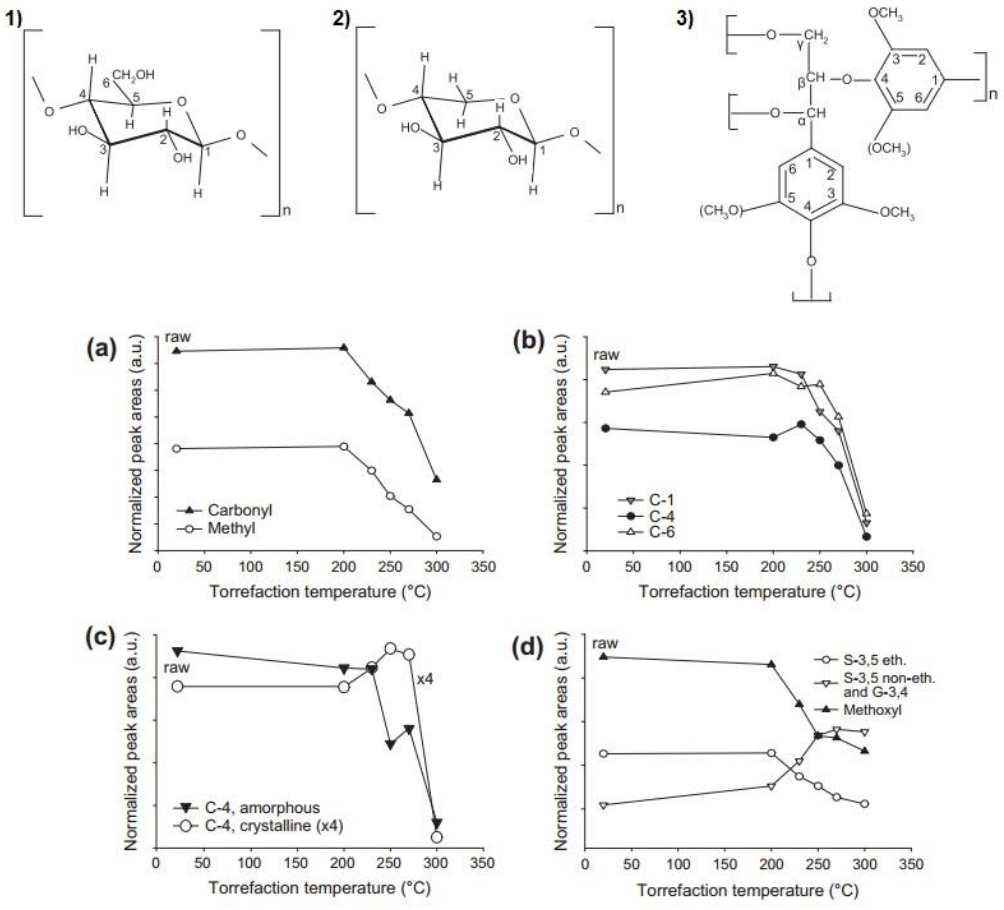

Figure 3-7 – 1) Hemicellulose monomer, 2) Cellulose monomer, 3) Cross-linked lignin subunits. Integrals from ^{13}C NMR vs temperature for a) acetyl groups (hemicellulose), b) C1, C4 and C6 carbons (hemicellulose and cellulose), c) C4 crystalline and amorphous (cellulose) d) Guaicyl and Syringl carbons: methoxyl carbons and aromatic carbons (Lignin). Taken from [102].

Changes in structure upon torrefaction can also be determined using Fourier Transform Infrared Spectroscopy (FTIR). Park et al. used FTIR to determine changes in the torrefaction of loblolly pine chips at three torrefaction temperatures: 270°C, 300°C and 330°C, in form of pellets blended with potassium bromide (KBr) [91]. The authors observed a reduction in C=O adsorbance for bonds attributed to carbonyl groups in the torrefied samples which could be attributed to deactylation during thermal treatment. The authors also observed an increase for C=C stretching vibrations associated with aromatic structures suggesting these increase upon torrefaction as a result of degradation of hemicellulose and cellulose i.e. the lignin weight percent increases. This notion further supported by an increase in intensity of C-O stretching bonds which can be attributed to non-etherified guaiacyl. This increased intensity is agreement with the study by Melkior et al. who suggest cleavage of β-1-4 bonds occurs at higher temperatures in line with the temperatures used in this study.

3.1.6 Mass and Energy Balance

During torrefaction, decomposition of biomass results in a combination of solid, liquid and gaseous products. The main products of torrefaction are shown in Figure 3-8 and are formed as a result of the reactions that take place described above. The relative yield of each phase varies depending on the temperature and residence time of the torrefaction condition. As a general rule however, the higher the temperature or residence time, the lower the solid phase yield and the higher the liquid and gaseous phase yield.

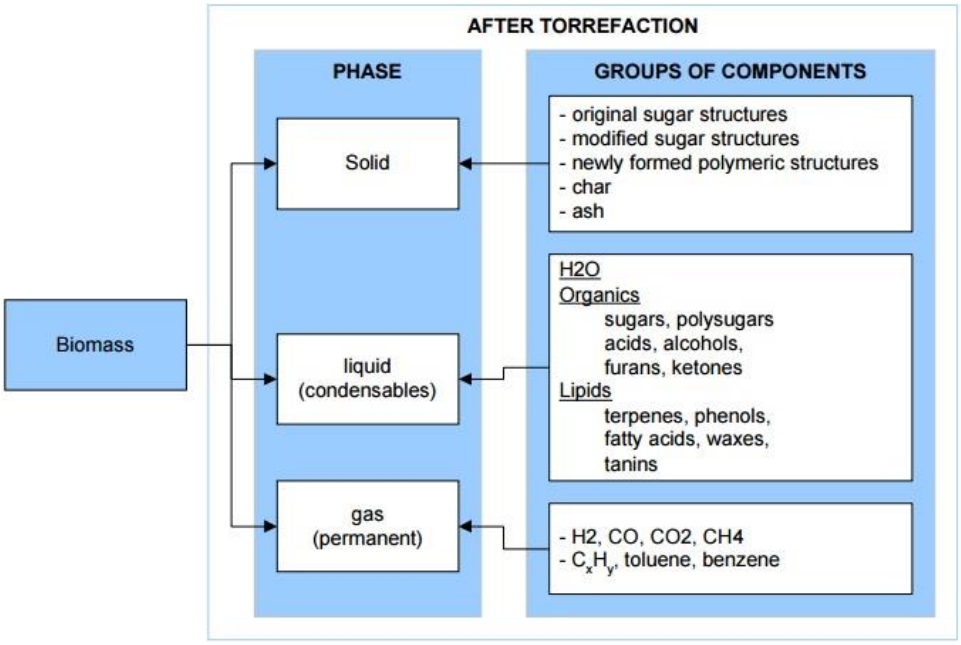

Figure 3-8 – Products formed during torrefaction [103]

The solid products of torrefaction exist as a combination of the original sugar structures, modified structures and newly formed polymeric structures [103]. The solid product also contains chars of the parent fuel as well as ash, which increases as a result of organic matter loss. The liquid products of torrefaction can be split in to three main groups: reaction water (in addition to free moisture released during drying), organics and lipids. Some of the liquid products are often referred to as condensable liquids as they only exist in the gaseous phase at torrefaction temperatures and exist in the liquid state at standard temperature and pressure (STP), thus can be condensed upon exiting the torrefaction reactor. The organic fraction represents a host of species that evolve during the devolatilisation and carbonisation reactions described above and include, amongst others, acids, alcohols and ketones. The lipid fraction contains species that are present in the original biomass structure that may evaporate during torrefaction. This fraction is therefore not technically a reaction product as they have not evolved through a reaction mechanism. The gases, sometimes denoted as permanent gases, represent the gases that exist in this phase at STP and include species such as CO and CO_2 as well as other light volatiles e.g. methane (CH_4) and ethene (C_2H_4) present in small amounts. While the objective of torrefaction is to retain as much energy in the solid yield, some energy will be lost in the species evolved however some species evolved do not contain any useful energy namely water and CO_2. Thus, the mass and energy yields for the torrefaction process are one of the main parameters in evaluation of the torrefaction process. As defined by Bergman et al. [88] these are calculated using the following equations:

$$Y_M = \frac{m_{torrefied\ fuel\ (dry\ basis)}}{m_{\ untreated\ fuel\ (dry\ basis)}}$$

$$Y_E = Y_M \left(\frac{LHV_{torrefied\ fuel\ (dry\ basis)}}{LHV_{untreated\ fuel\ (dry\ basis)}} \right)$$

Where Y_M = the mass yield, $m_{untreated\ fuel\ (dry\ basis)}$ = mass of the untreated fuel entering the torrefaction reactor on a dry basis, $m_{torrefied\ fuel\ (dry\ basis)}$ = mass of the torrefied fuel exiting the torrefaction reactor, Y_E = is the energy yield, $LHV_{torrefied\ fuel\ (dry\ basis)}$ = the LHV of the torrefied fuel on a dry basis and $LHV_{untreated\ fuel\ (dry\ basis)}$ = the LHV of the parent fuel on a dry basis. While the mass and energy yields can be represented on an as received basis, it is commonplace to report the mass and energy yields on a dry basis as the moisture content for a particular fuel entering a torrefaction system may differ. Also, these equations above describe the mass and energy yield with respect to the solid phase however the yields can be applied to the liquid and gaseous phases also. The mass and energy yield for the solid product is often the most interesting as it is ultimately the product that is further utilised however an understanding of the overall mass and energy balance of the torrefaction process is imperative for optimising process parameters.

The overall mass and energy balance for the torrefaction of woodcutting at 280°C for 17.5 minutes is shown in Figure 2-9. In this case, there was a 12.5% mass loss which corresponded to a 5.1% loss of original energy in the parent fuel. The second largest mass yield belonged to the reaction water followed by the organic phase. The lipid phase contained the second highest amount of energy followed by the organic phase and permanent gases.

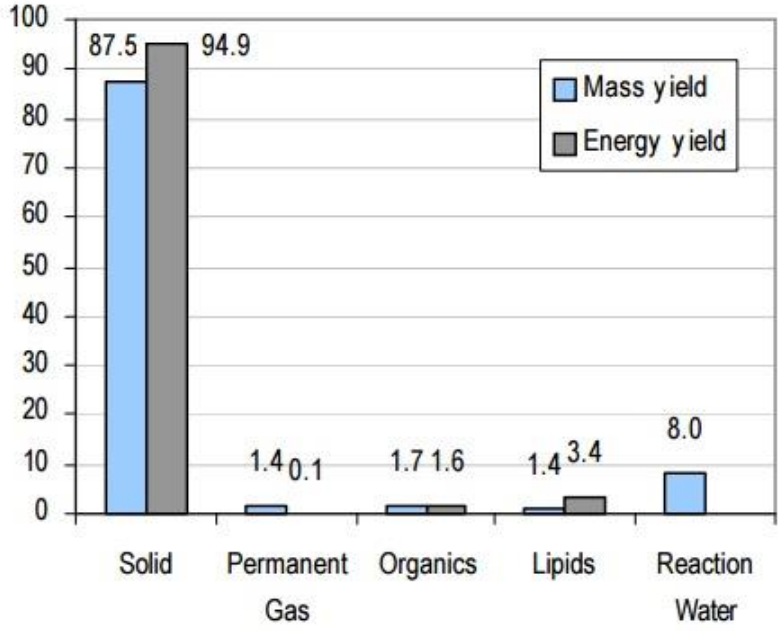

Figure 3-9 – Overall mass and energy balance for the torrefaction of wood cutting at 280°C for 16.5 minutes [103].

Prins et al. [104] performed mass balances for the torrefaction of three different types of biomass: willow (hardwood), larch (softwood) and straw (agricultural residue) under different process conditions. Their results, summarised in Figure 3-10, show that solid mass yield decreased with increased temperature and residence time. In comparing willow and larch, larch resulted in greater solid yield than willow under the same torrefaction conditions. For example, during torrefaction at 250°C for 30 minutes, the solid mass yield was highest for larch (~97%) followed by willow (~87%) then straw (~85%). The differences in the reactivity of willow and larch could be attributed to differences in hemicellulose composition- as xylan undergoes degradation more readily than glucomannan, there is an expected greater mass loss for the willow fuel. Even at the most severe torrefaction treatment for larch (270°C for 15 minutes), there was still 90% solid mass yield while the solid yield for willow dropped to ~78%. Nevertheless, differences in reactivity cannot be attributed solely to differences in structure as other factors such as the presence of catalytically active potassium may affect reactivity (the catalytic effect of potassium is discussed later in relation to combustion).

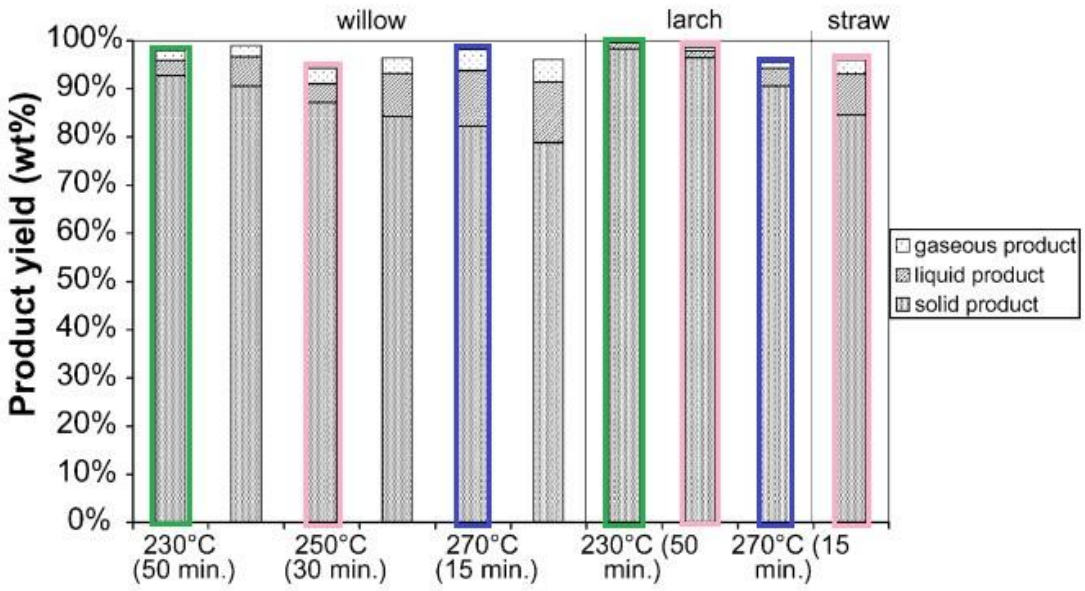

Figure 3-10 – Overall mass balance for the torrefaction of willow, larch and straw. The coloured outlines represent the same treatments for different fuels: Green = 230°C/50 minutes, Pink = 250°C/30 minutes and Blue = 270°C/15 minutes. Adapted from [104].

Bridgeman et al. [105] also studied the torrefaction of willow and wheat straw at 4 different torrefaction conditions (230, 250, 270 and 290°C for 30 minutes) and found comparable solid mass yields: 95.1, 80.6, 79.8 and 72.0% with increasing torrefaction severity for willow while wheat straw's yields were 91.0, 82.6, 71.5 and 55.1%. Bridgeman et al. also reported the energy yields for each torrefaction condition whereby the differences between mass and energy yield increased with increasing torrefaction severity leading to an increase in energy densification i.e. Energy Yield/Mass Yield. For example, for willow torrefaction, the energy densification ratio for 250°C/30 minutes was 1.02 whereas for 290°C/30 minutes the ratio is 1.1. This can be attributed to a greater increase in HHV with increasing torrefaction severity which will be discussed in a later section on improvements to fuel properties.

The impact changing torrefaction temperature and residence greatly influences the distribution of mass to the solid, liquid and gaseous phases. Similarly, the same set of conditions for two different fuels can yield different distributions of these products due to different fuel chemistries. These changes are investigated in Chapter 5 of this thesis where four chosen torrefaction conditions: 250°C for 30 minutes, 270°C for 30 and 60 minutes, and 290°C for 30 minutes have been performed on a softwood (pine) and hardwood (eucalyptus) fuels. This allows investigation of the effect of changing temperature on the distribution of the solid, liquid

and gaseous products where the residence time stays the same (i.e. 250, 270 and 290°C for 30 minutes). It also allows to determine the influence of residence time where the temperature stays the same (i.e. 270°C for 30 and 60 minutes) on product distribution. These results can be found in Section 5.3.2 and also allow for comparison of the effect of torrefaction on two different fuel types. The energy yields for the solid and organic phases of torrefaction can be found in Sections 5.3.2 an 5.3.6 helps understand the degree of energy retained in the solid phase, in which a high energy retention is desirable from a fuels perspective. These areas of work aim to fulfil the first second objective of this thesis

3.1.7 Condensable and non-condensable products of torrefaction

As described above, the torrefaction process yields solid, liquid and gaseous products. Prins et al. [104] in their study of the torrefaction of willow and larch, also quantified the liquid and gaseous species evolved during torrefaction using high-pressure liquid chromatography (HPLC) and gas chromatography (GC) respectively. For the liquid (or condensable) species evolved, the most abundant product formed for both wood types was reaction water, derived from dehydration reactions. For willow, the next most abundant liquid product was acetic acid followed by smaller amounts of formic acid and methanol. For larch, formic acid was the second greatest liquid products save for the most severe torrefaction condition where lactic acid was the second greatest yield. The overall liquid yields were lower for larch than willow (see above). The evolution of acetic acid and methanol can be ascribed to devolatilisation of the acetyl and methoxyl groups on the hemicellulose fraction which are released as acetic acid and methanol respectively.

The non-condensable gases measured by Prins et al. for both fuels included predominantly CO_2 and CO with trace amounts of hydrogen and methane although the authors note the amounts of these latter two gases are negligible. CO_2 was the most abundant gas produced which increased with the torrefaction severity. CO on the other hand was only produced in small amounts in the mildest conditions but did increase under the most severe conditions. While CO_2 can be attributed to decarboxylation of the acid groups in wood, CO evolution cannot be ascribed to these mechanisms hence the authors denote the presence of CO to the reaction of CO_2 and steam with porous char as the temperature increases. This could explain why more CO is measured at higher torrefaction temperatures.

Nocquet et al [106] also studied the composition of liquid and gaseous species evolved from the torrefaction of beech wood at 4 different conditions: 220, 250, 280 and 300°C for 180 minutes. The author noted the main species to be water, formaldehyde, acetic acid, furfural, CO_2 and CO, all of which comprised 70% of the liquid and gaseous yields. In general for all conditions, of the 70%, 30-50% was water, 15% was permanent gases and the remaining amount 'dry' condensable species. In comparing the change in liquid component yields between torrefaction conditions, the water yield showed the greatest increase in yield i.e. greater difference between conditions, with increasing torrefaction severity. For example from 280°C to 300°C, the water yield increased by 10%. This could possibly be attributed to evolution of hydroxyl groups on the cellulose which can decompose at the highest torrefaction temperatures. The authors also compared the product yields from beech wood with the torrefaction of the individual lignocellulosic components to determine the sources of each product with the following findings: CO and CO_2 mainly derived from the hemicellulose which is the only source of formic acid. Formaldehyde derived mainly from cellulose and lignin, due to hydroxymethyl groups present on these structures, while methanol derived from xylan and lignin from the methoxyl groups on these structures. Acetic acid was not measured in the torrefaction of any individual components however it is known acetic acid is produced as a result of hydrolysis of acetyl groups on the hemicellulose and in this study, these groups were removed during extraction.

In this project, the liquid products of the torrefaction of pine and eucalyptus were determined as part of the mass balance quantification. Due to instruments constraints, determination of the actual species present was not performed however the split between polar and non-polar liquid products is determined and presented in Section 5.3.6**.** Achieved using extraction of the liquids yield with dichloromethane (which dissolves the non-polar species) this provides information on how different torrefaction conditions affect the mass yield of polar species which will be mainly water and non-polar species. Increased yields of non-polar species are indicative of the presence of species possibly arising from the carbon rich non-polar lignin fraction of biomass. These species may results when torrefaction temperature or residence time is greater which may allow for degradation or evaporation of species in lignin to take place. Analysis and determination of the liquid products fulfils part of Objective 3 of this work.

3.1.8 The effect of torrefaction on fuel properties

3.1.8.1 Proximate and ultimate analysis and calorific value

The evolution of moisture, volatile and gaseous species during torrefaction results in the concentration of carbon in the solid fuel with the preferential loss of oxygen and hydrogen bonded to oxygen (i.e. oxidised hydrogen as part of hydroxyl groups) which has the effect increasing the calorific value. These changes are observed upon ultimate and proximate analysis of untreated and torrefied fuels with subsequent determination of the higher heating value, and have been measured in a number of studies e.g. [105, 107-111]. Ibrahim et al. studied the effect of torrefaction on willow and eucalyptus fuels under three conditions: 270°C for 30 and 60 minutes and 290°C for 30 minutes [107]. In the case of willow, torrefaction under the mildest condition reduced the volatiles content from 84.8% to 73.8% and also lowered the moisture content from 6.0% down to 3.9%. The fixed carbon content increased from 15.2% to 26.2%. As torrefaction severity increased, these changes became more pronounced. The higher heating values (HHVs) calculated in this study increased from 19.4MJ/kg to 24.2MJ/kg from untreated to condition 290°C/30 minutes as a result of these chemical changes. Arias et al. also observed these changes in eucalyptus upon torrefaction at a number of conditions [112]. For example, torrefaction at 240, 260, and 280°C reduced the moisture content of eucalyptus from 6.5% to 2.1, 2.0 and 1.9% respectively while volatiles content decreased from 84.0% to 75.4, 69.6 and 69.0%. The HHVs of the fuels increased with torrefaction severity from 19.4 MJ/kg for untreated eucalyptus to 22.2, 22.7 and 23.4MJ/kg for each respective condition. Peng et al. in their study of the torrefaction of range softwood residues at 280°C for 52 minutes also measured the increases in calorific value which increased from 19.4, 20.4 and 19.5MJ/kg for untreated spruce, fir and pine respectively to 21.5, 2.1 and 22.3 MJ/kg [113]. The tendency of oxygen (and hydrogen) removal and preferential retention of carbon upon torrefaction has been measured in a number of studies. Figure 2-11 highlights these changes for a range of untreated fuels and their torrefied counterparts on a Van Krevelen plot.

With torrefaction, the H/C and O/C ratios decrease. Torrefaction has the effect therefore of making fuels more ‘coal-like’ as their position on the Van Krevelen plot moves towards the area where the ratios for coal predominantly lie. It is interesting to note from Figure 3-11 too that the ratios for hardwoods (willow, eucalyptus and Leucaena) are lower than the softwoods (spruce, fir and pine) which can be attributed to the their differences in hemicellulose reactivity discussed above.

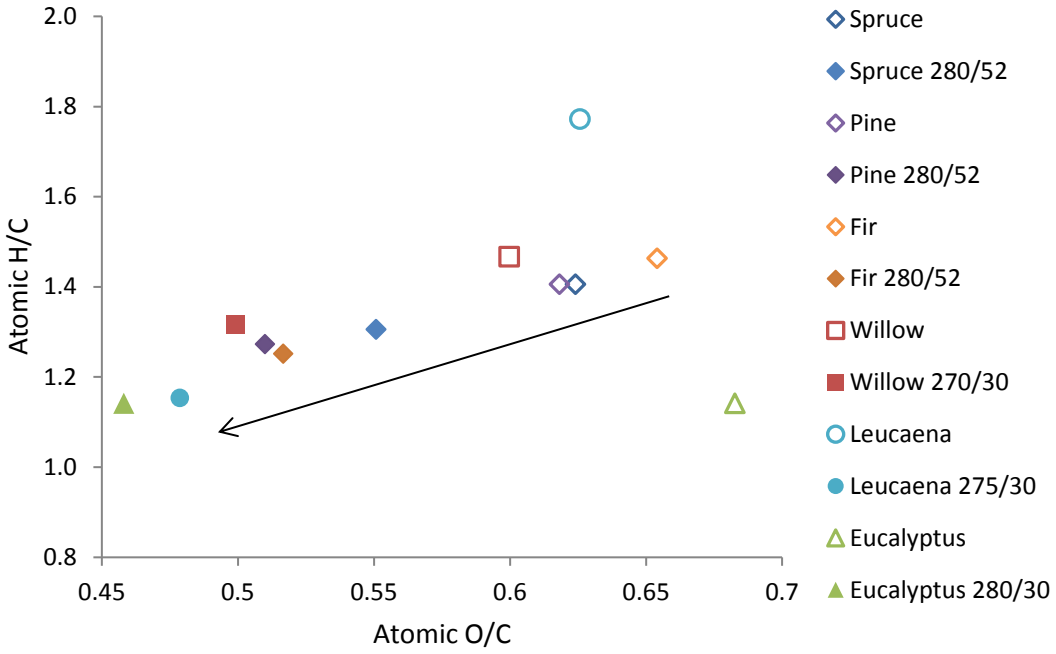

Figure 3-11 – Van Krevelen plot for selected untreated and torrefied fuels. Torrefaction conditions denoted as Temperature/Residence time. Spruce, pine and fir (diamonds) taken from [113], Willow (squares) taken from [105], Leucaena (circles) taken from [114], Eucalyptus (triangles) taken from [112].

Proximate and ultimate analysis of solid fuels are fundamental in understanding their inherent nature and potential behaviour as fuels and in this instance provide information on the changes which take place upon torrefaction. The proximate and ultimate analysis of both untreated and torrefied pine and eucalyptus used the torrefaction experiments in Chapter 5 can be found in Section 5.3.5.1. A Van Krevelen diagram is also presented in Figure 5-8 to emphasis the changes in H/C and O/C ratios, more specifically increase in C weight percent and decrease in H and O weight percent. Analysis of the solid products fulfils the remainder of Objective 3 in this project.

The effect of torrefaction on the changes on carbon, hydrogen and oxygen content receive considerable attention as a result of their impact on the fuel energy content, however the effect of torrefaction on the nitrogen content of fuels receives much less focus. Nitrogen in biomass fuels is mostly in the form of linear and cyclic N-compounds in the form of proteins [115]. Knowledge of the nitrogen content is important owing to the potential emissions of NO_x that can be released during combustion which are subject to strict legislation and must fall within regulatory limits [46]. NO_x emissions from biomass combustion can arise from three main sources: thermal NO_x, prompt NO_x and fuel NO_x. Fuel NO_x is the main source of NO_x emissions

from biomass combustion in large-scale boilers and is generated through the oxidation of nitrogen that is chemically bound to the fuel matrix [116]. Thus, the quantity fuel NO_x emissions are directly related to the nitrogen content of the fuel. Jones et al. studied the loss of nitrogen upon torrefaction of willow and observed that shorter residence times (10 minutes) favoured the retention of nitrogen in the solid fuel as no nitrogen was released in the volatile phase as calculated from nitrogen mass balance [117]. The longer residence time used in their study however (60 minutes) resulted in 40% loss of nitrogen in the volatile phase.

As knowledge of the partitioning of N during torrefaction is lacking in the current literature and to understand any potential changes in N content in more detail, a mass balance determining the fate of N is presented in Section 5.3.7.2**.** In this mass balance, the N content of each of the torrefied pine and eucalyptus fuels presented in Chapter along with the corresponded tar phases were determined as a percentage of the original N content of the untreated fuels. Any remaining N unaccounted for is therefore released to the gas phase and is calculated by difference. The N balance therefore provides information on the behaviour of N when torrefaction conditions are changed. Determination of the N balance, in addition to C and H balances aims to cover Objective 4 in this project which is overall elemental balance of the these elements during torrefaction.

3.1.8.2 Colour and Morphological changes

One of the most obvious visual changes that occur during torrefaction of biomass is the change in colour from light to dark brown; this colour becoming increasingly darker as the temperature and residence time increases. The enrichment of carbon and the loss of oxygen and hydrogen results in this effect as shown by Bridgeman et al. in Figure 3-12 below [83].

Figure 3-12 - Images of untreated and torrefied willow = a) untreated willow, b) willow (230-250°C/10 minutes) c) willow (230-250°C/30 minutes) d) willow (290°C/10 minutes) e) willow (290°C/60 minutes)

Changes in surface morphology are apparent when scanning electron microscopy methods are used to analyse the products of torrefaction. Ibrahim et al. performed SEM analysis on untreated and torrefied willow and eucalyptus in their study and showed that with torrefaction, the bulky fibrous structure of raw biomass changes, becoming more fibrous with deep fissures apparent on the surface [107]. Chen et al. also studied surface changes in untreated and torrefied eucalyptus (300°C for 1 hour) using high magnification SEM images [118]. Cross sectional image showed that torrefaction resulted in the loss material in the cellular structure of the treated materials as shown in Figure 3-13.

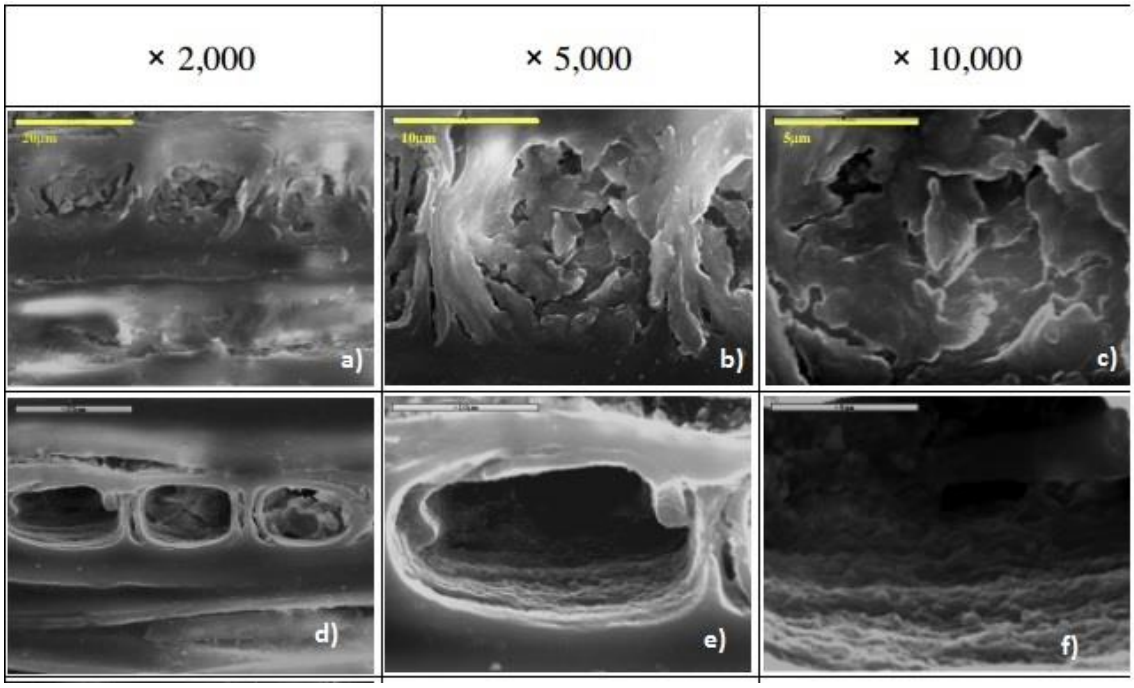

Figure 3-13 – Cross-sectional images of untreated (a, b and c) and torrefied eucalyptus (d, e and f) at different magnifications. Taken from [118].

Images of each of the untreated and torrefied pine and eucalyptus fuels presented in Chapter 6 can be found in Section 6.2.1.2 while images of torrefied Pine can be found in Section 5.3.5.5. The photograph images in Section 5.3.5.1 provide strong visual evidence of the changes that take place during torrefaction while the SEM images show in greater detail structure changes to the biomass particles upon torrefaction.

3.1.8.3 Grindability and particle size

It is shown above that the breakdown of the lignocellulosic components has a marked effect on the structure of the resultant torrefied fuels. As the hemicellulose binds the cellulose fibrils in biomass, and it is this component that undergoes the most change, there is a tendency for torrefied biomass to become more fibrous as it loses its original structure which can result in smaller particle sizes and reduced energy requirements when grinding the torrefied materials. Several studies have focussed on the grindability of torrefied fuels, for example [83, 112, 119, 120]. Repellin et al. [120] studied the energy required to grind untreated and torrefied wood chips (spruce and beech) to a fine powder and performed a particle size distribution on the resultant powders. The authors observed that the grinding energy required for torrefied beech and spruce was considerably lower than the energy required for grinding of the untreated chips as shown in Figure 3-14. The authors also noted the energy required for grinding of untreated beech and spruce to be around 1/6th of the LHV of these fuels, which has significant implications when viewed on an energy input basis. Results of the particle size distribution on the ground samples showed that for spruce wood, there was a decrease in the average particle size of 237µm for untreated to 219µm under the mildest torrefaction condition (160°C for 5 minutes). Increasing the torrefaction temperature resulted in even smaller average particle sizes: 193µm for spruce torrefied at 220°C for 5 minutes and 137µm for a torrefaction temperature of 280°C for 5 minutes. Concerning beech, the opposite trend was observed at the lowest torrefaction temperatures however, with a reduction in average particle when compared to untreated beech only measured once the torrefaction temperature reached 200°C.

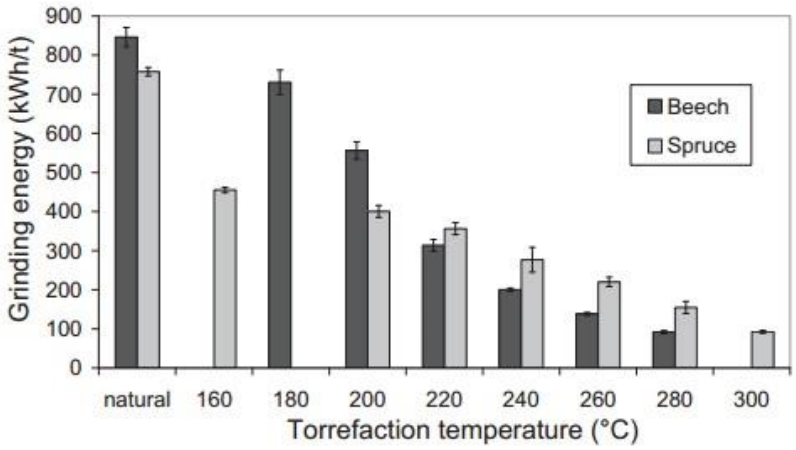

Figure 3-14 – Energy required for the grinding of untreated and torrefied beech and spruce [120].

Bergman et al. [103] also evaluated the net electricity consumption of grinding untreated and torrefied fuels, determining the energy required to reduce willow, larch and beech and their torrefied counterparts to an average particle size of 0.2mm. The authors observed that a reduction in power consumption of up 80% could be achieved with torrefaction.

An indicator often used to measure the grindability of coal is the Hardgrove Grindability Index (HGI). This standardised methodology involves grinding 50g of coal for 60 revolution with a particle size distribution between 600µm and 1.18mm in a purpose built Hardgrove Grindability machine [121]. The mass of ground material that passes through a 75µm sieve is measured and plotted on a calibration curve created with four reference materials with known HGI values to determine the HGI of the sample being analysed. The general principle is that the greater the amount of mass that passes through the sieve, the easier the particle is to grind which corresponds to a higher HGI value. As this testing requires specialised equipment and large sample sizes which aren't feasible at laboratory scales, a modified version of the HGI has been developed in which the grindability of biomass samples can be measured producing an $HGI_{equivelent}$ value. The details of the modified HGI test ($HGI_{equiv.}$) are described in the experimental methodology section later in the text (see Section 4.4.6). Bridgeman et al. used this adapted methodology to determine the $HGI_{equiv.}$ value for untreated and torrefied willow and miscanthus samples [83]. The authors observed poor grindability behaviour for the untreated fuels corresponding to an $HGI_{equiv.}$ of 0 with only noteworthy changes observed when long residence times and higher temperatures were deployed: torrefaction of willow and miscanthus at 290°C for 60 minutes resulted in HGI_{equiv} values of 51 and 79 respectively while the same residence time at 240°C resulted in HGI_{equiv} values of 10 for willow and 11 for miscanthus.

In order to ascertain changes to the grinding behaviour of biomass upon torrefaction, the HGI_{equiv} values for untreated and each of the torrefied pine fuels were determined. These can be found in Section 5.3.5.3 in addition to a particle size distribution for these fuels in Section 5.3.5.4.

3.2 Combustion properties of untreated and torrefied fuels

3.2.1 Introduction

The application of torrefied biomass in combustion systems requires an understanding of the combustion behaviour of these fuels. Comparing the behaviour of untreated and torrefied fuel

during combustion enables an understanding of the effect torrefaction has on combustion properties. As torrefaction changes the physical and chemical properties of the fuel, for instance reduced volatiles contents, it is expected that the combustion characteristics of the torrefied fuel will change with a most obvious change being the reduction in reactivity. Measurement of fuel reactivity, on laboratory-scales, predominantly focusses on determination of the Arrhenius parameters with thermogravimetric analysis (TGA) the technique often employed to determine the reaction rates governing combustion. Determination of these reaction rates often involves analysis of the rates of pyrolysis (decomposition) and char combustion separately. As noted in Section 1.3.3 combustion of biomass can be broadly split in to 4 stages, of which the last stage, char combustion, is the slowest step which effectively controls the overall rate of combustion i.e. it is the rate determining step. Studying char combustion separately therefore requires preparation of chars by completing the pyrolysis (thermal decomposition) or devolatilisation step first. Char preparation can be done using TGA however this technique often uses slower rates (of the order 10-100°C/minute) and lower temperatures (up to 900°C) relative to those found in an industrial boiler for example. As a result, high temperature (e.g. >1000°C) fast-heating rate (e.g. 10^4-10^5°C/second) chars can be prepared using equipment such as a drop tube reactor which mimics industrial systems more closely. A drop tube reactor, which will be explained in more detail in Section 4.5, is a heated reactor in which biomass particles are inserted and travel through in an entrained flow at fast rates under high temperatures from which chars can be collected at the end. Chars prepared using a drop tube furnace, which as mentioned above reflect the conditions in a large-scale power plant boiler more closely, can then be further analysed for their the chemical reactivity in oxygen (discussed in greater detail below). Several factors affect can char reactivity including whether chars are prepared under slow or fast heating rates in addition to influence of mineral matter, notably potassium, which may catalyse char combustion. The conditions under which chars are prepared can also have an impact on the partitioning of nitrogen where the fast heating rates and high temperatures used in a drop tube furnace may promote the release N to the gas phase or retain in the char. Understanding how these conditions affect nitrogen become significant when NOx emissions are considered. This second section of this literature review reflects the work shown in Chapter 6 in this thesis where the combustion behaviour of chars prepared in a drop tube furnace from untreated and torrefied willow and eucalyptus fuels is the focus. The topics introduced in this section introduction are discussed in more detail below.

3.2.2 Pyrolysis of untreated and torrefied fuels

Pyrolysis (thermal decomposition in inert atmosphere) or devolatilisation (thermal decomposition in air) of biomass occurs during the early stages of biomass combustion and begins around 160-250°C [122]. The devolatilisation step during biomass combustion is significant as volatile content of biomass contributes about 70% of the heat of biomass [122]. Similar to torrefaction, pyrolysis can give rise to a number of different products: solid, liquid and gas which vary depending on the pyrolysis conditions as a result of decomposition of the original biomass and secondary reactions involving the volatile products [123]. For example, fast heating to temperatures between 750 and 800°K with short vapour residence times favour the production of tars (bio-oil) in a process commonly known as fast pyrolysis while fast heating to temperatures encountered in pf boilers (>1500°K) in combustion system favour the production of gases such as CO, CO_2 and light VOCs via cracking of the volatile products evolved [122]. In rapid heating systems, char yields decrease as the temperature increases; for example chars yields are roughly 8-28% for fast pyrolysis compared with 20-40% for slow pyrolysis [123]. Knowledge of the rates of release of volatiles, their composition and amount of volatiles during pyrolysis is important in terms of modelling biomass combustion as these factors influence flame ignition and stability [124]. In determining the rates of biomass pyrolysis, slow heating of thermally thin biomass particles (<90μm) using TGA is often employed. Under these conditions heat and mass transfer effects, which would nominally affect larger solid biomass particles, are largely removed, and so kinetic analysis is simplified [124, 125]. From a pure kinetic perspective, the rate of a reaction is often found to be proportional to the molar concentrations of the reactants raised to a simple power and can be derived from the rate law. Included in the rate law is the rate constant, k, a characteristic of the reaction being studied which quantifies the reaction and can only be derived from experimental data [126]. The thermal decomposition of biomass occurs via a number of different reactions pertaining to the degradation of the main lignocellulosic components, hemicellulose, cellulose and lignin. As several reactions are occurring at different rates during decomposition, to derive rate laws for each reaction is extremely complex and, as a result, a global one-step mechanism is often employed using the initial mass of sample as the 'concentration' of the reactant. This widely used 'reaction-rate constant method' uses data from TGA experiments to derive the pre-exponential factor, A, and activation energy E_A, assuming the reaction rate constant follows the Arrhenius function [124]:

$$k = A \exp\left(-\frac{E_A}{RT}\right)$$

Where R is the universal gas constant (8.134 J/mol K) and T is the temperature (°K). During pyrolysis experiments in the TGA, biomass samples are heated in an inert environment at low heating rates up to 900°C during which time biomass will lose mass. If the experiments are performed an inert environment (e.g. nitrogen) the mass loss curve with time approximate to a single linear relationship while if the experiments are performed in air, the curve will show the initial curve mass loss (devolatilisation) followed by a second curve or 'knee' at higher temperatures corresponding to char combustion. If the weight loss curve with time is assumed to be the result of one global first-order reactions then k can be described by following equation:

$$k = -\frac{1}{(m-m_{\infty})}\frac{dm}{dt}$$

Where m is the initial mass, m_{∞} is the chosen terminal mass and dm/dt is the change in mass with time (derivative) during that reaction. The values for A and E_A can then be calculated via integration of the Arrhenius equation where A and E_A are found by the intercept (ln A) and slope (E_A/R) of a plot of ln k vs. 1/T [124]:

$$\ln k = \ln A - \frac{E_A}{RT}$$

The reaction-rate constant method is just one method that can be used to derive pyrolysis kinetics and yield reaction rates when a small portion of the mass loss curve is examined i.e. when conversion is small. At high conversion rates, diffusion will begin to contribute to the mass loss curve characteristics. Details of other methods for deriving kinetic parameters can be found in e.g. [124] and [127].

Several studies have looked at the pyrolysis behaviour of untreated and torrefied materials to determine the changes pre-treatment have on fuel reactivity. Arias et al. [112] studied the combustion behaviour in air of untreated eucalyptus and eucalyptus torrefied at 240, 260 and 280°C for one hour. The derivative mass loss curves for untreated and torrefied fuels showed a

'shoulder' in the temperature range 220-300°C which has decreased in the 240°C pyrolysis curve and disappeared in the 260 and 280°C samples; this can be attributed to the degradation of hemicellulose during torrefaction (Figure 3-15). The authors derived kinetic parameters for pyrolysis of the fuels using the mathematical model proposed by Agrawal and Sivasubramanian [128]. The authors calculated untreated eucalyptus to have the lowest activation energy (87 kJ/mol) which increased with increasing torrefaction severity: 240°C for 1 hour: E_A = 106 kJ/mol, 260°C/1 hour: E_A = 113 kJ/mol and 280°C/1 hour: E_A = 119 kJ/mol highlighting that the biomass had become less reactive as a result of torrefaction with differences becoming less pronounced as torrefaction severity increased. Saddawi et al. [129] also derived Arrhenius parameters for untreated and torrefied willow, eucalyptus, miscanthus and wheat straw samples (torrefied at 290°C for 1 hour) from pyrolysis experiments in a TGA under a flow of helium. Similar to Arias et al, the derivative mass loss curves or the torrefied fuels lost the 'hemicellulose shoulder' presents in the untreated samples and the activation energies for the untreated fuels increased from 79.0, 95.6, 110 and 62.9 kJ/mol for willow, eucalyptus, miscanthus and wheat straw respectively to 130, 141, 151 and 90.4 kJ/mol respectively. While the activation energy serves as indicator of reactivity, it is important to note that this parameter alone does not serve as an absolute indicator of reactivity. The pre-exponential factor plays a significant role and thus determination of the reaction rate constant for a selected temperature serves as an indicator at the temperature selected.

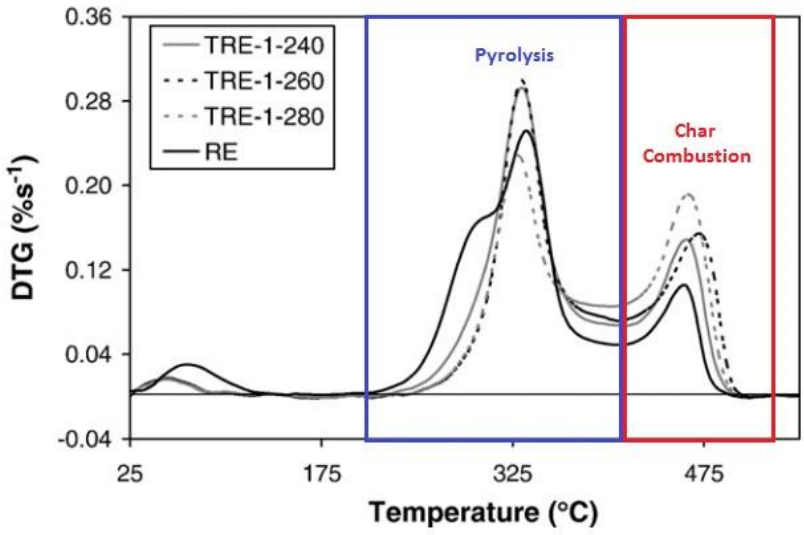

Figure 3-15 – Combustion of untreated and torrefied eucalyptus with the pyrolysis range outlined in blue and char combustion range outlined in red. Adapted from [112].

While slow heating rate TGA analysis is a widely used technique employed to derive the kinetic biomass pyrolysis, the relatively slow heating rates are not in fact akin to most real-life boiler scenarios (especially in the case of pf combustion) and thus is often criticised as a result of its lack of applicability [124]. In particular the heating rate of pyrolysis affects the char reactivity and this will be discussed in more detail below.

The reaction rate constants for the pyrolysis of untreated and torrefied willow and eucalyptus fuels used in this study can be found in Section 6.2.2.1 of this thesis. Determination of these parameters, similar to the studies from Arias et al. and Saddawi et al. described above, aims to show that torrefaction has resulted in a reduction in reactivity of the fuels due to the loss of volatiles materials enriched in oxygen. Determination of the pyrolysis reaction rates of untreated and torrefied willow and eucalyptus directly covers objective 9 in this project.

3.2.3 Kinetics of char combustion

As introduced in Section 2.3.3 the char combustion stage of biomass combustion is the rate-determining step during combustion and thus governs the overall rate of reaction. Chars from biomass represent 10-30% of biomass by weight and their combustion form important pathways for the release of species such as nitrogen and inorganic components [122]. Conversion of char differs from pyrolysis, as it is a heterogeneous reaction where the surface of the particle is the location for chemical reactions. As a result, reacting gases, e.g. oxygen in the case of combustion diffuse on to the surface of the char where they react with active site carbon atoms on the surface of the particle (C_f). Fundamentally, the reaction of oxygen with surface carbon atoms consists of a number of different adsorption and desorption reactions, which include [123]:

1) $2\ C_f + O_2 \rightarrow 2\ C\ (O)$
2) $C\ (O) \rightarrow CO$
3) $C\ (O) \rightarrow CO_2 + C_f$

Reaction 1 represents the chemisorption of oxygen on to the free active sites on carbon surface to form a carbon-oxygen activated complex: C (O). Reactions 2 and 3 represent desorption of

CO and CO_2. The reactivity of a char particle is therefore sensitive to a number of processes including [130]:

- Mass transfer (by diffusion) of gases from the bulk gas phase to the carbon surface
- Adsorption of reacting gases on the surface
- Chemical reactions on the surface and formation of absorbed products
- Desorption of absorbed products
- Mass transport (by diffusion) of gaseous products away from the carbon surface

Excluding chemical reactions, all of these processes are mass transport effects [123]. The slowest of these processes governs the rate of char conversion and is dependent on a number of process parameters and carbon properties including temperature, pressure and particle size in the case of process parameters and porosity, active site concentration and catalytic impurities in the case of carbon properties. With respect to the kinetics of char combustion, while each of these reactions will have governing reaction rate constants, a common method applied is a global one-step reaction to describe the conversion of char during oxidation. Derivation of the kinetic parameters can be performed using TGA under dynamic conditions where a ramped heating programme is applied to biomass samples or under isothermal conditions. Also using TGA, this latter method involves firstly the heating char samples, which have been externally prepared in a drop tube for example, or in the TGA in an inert environment (e.g. nitrogen) to a desired temperature before introduction of an oxidising gas which results in a mass loss in a mass loss vs. time TGA plot. It is important to note at this stage the motive for knowledge of the kinetics biomass char combustion which is essentially for the design of combustors [131]. Determination of the kinetics of the char combustion under real-life systems is however difficult to derive from experimental conditions on laboratory scales as the mass/heat transfer-controlled conditions would reflect the laboratory set-up instead of the true combustion rate [131]. As a result, it is common practise to determine the kinetics at lower temperatures (300-400°C) and extrapolate the resultant kinetic data to higher temperatures. As a result, the overall chemical kinetics of char conversion are determined and represented by the following equation:

$$R_c = -\frac{1}{W}.\frac{dm}{dt}$$

Where R_c is the overall chemical reactivity (apparent first order rate constant) at the temperature (K) in g/s. g, W is the initial mass of carbon and dm/dt is the maximum rectilinear rate of weight loss [130]. The reactivity, or rate constant, k, can be derived from a number of isothermal analyses of char samples at different temperatures from which a plot of ln k vs. 1/T will yield a straight line and the Arrhenius parameters E_A and A can be derived (described above) provided the reactions that take place are the result of one or more first order reactions. As mentioned above, this technique uses relatively low temperatures and so the reactivity determined is the 'chemical reactivity' where at low temperatures, chemical reaction rates are slow with respect to diffusion and the reactant gas concentration is uniform throughout the bulk of the carbon particle. Thus, reaction rates are chemically controlled over the accessible surface and the activation energy is the true chemical activation energy. Reactions that occur in this temperature regime are denoted as Zone 1 reactions (Figure 3-16 and 3-17). As the gas concentration in Zone 1 reaction is uniform throughout the char particle, the order with respect to oxygen, n, tends to be 0 [131]. This can be ascribed to the carbon-oxygen reactions described above, as at low temperatures reactions 2 and 3 are the rate determining steps. For faster reaction rates at higher temperatures, diffusion of oxidising gases in to and out of the pore spaces may be controlling factor (due to different degrees of porosity which can be affected by pyrolysis conditions) and are denoted as Zone 2 reactions where the rate of char conversion may be controlled by a combination of chemical reactions and diffusion of gases in to and out of the pore spaces (Figure 3-16). For Zone 2 reactions the reactant gas concentration decreases in the particle (Figure 3-17). For even faster reactions rates at higher temperatures, Zone 3 reactions, char conversion is controlled by the diffusion of gases to the external carbon surface only in which a boundary layer exists where gas concentrations deplete from the bulk value. For these high temperature reactions (>700-800°C) the order with respect to oxygen tends to be 1 [131].

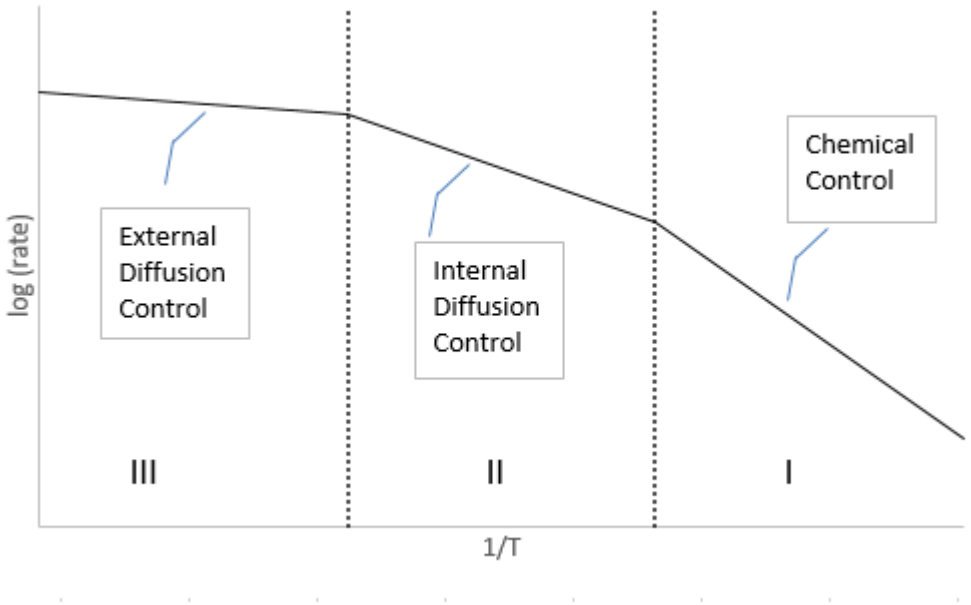

Figure 3-16 – Zone 1, 2 and 3 reactions shown on an Arrhenius Plot.

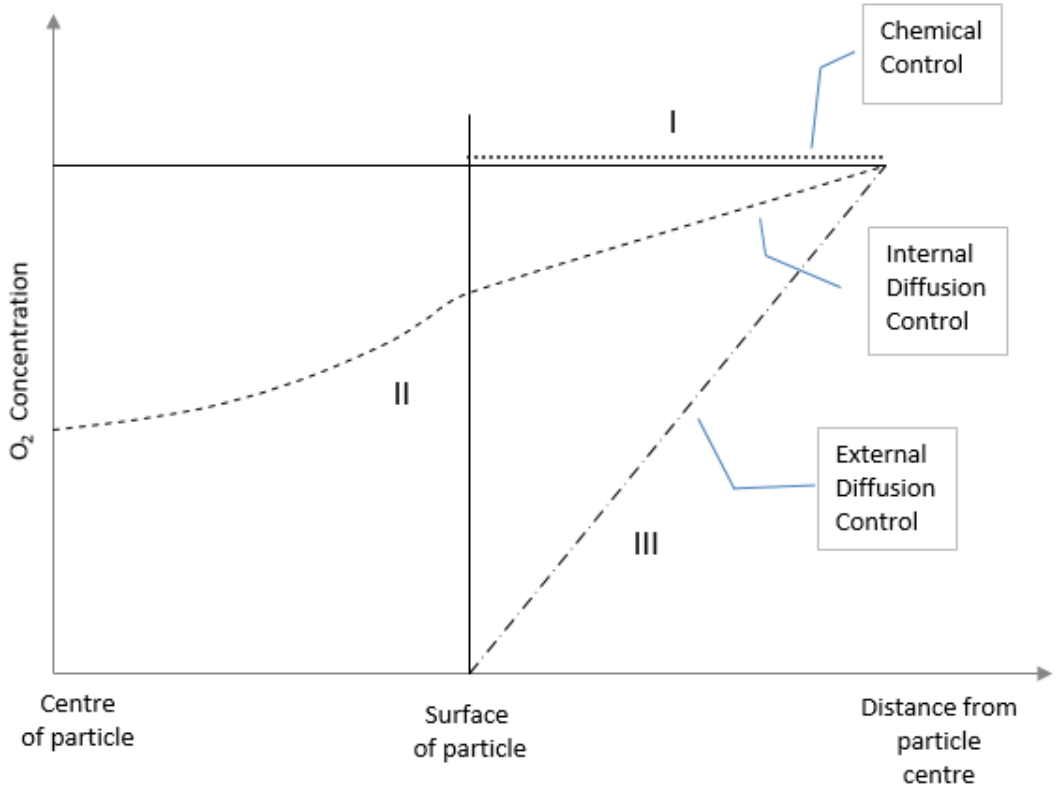

Figure 3-17- Zone 1, 2 and 3 reactions shown with changes in O_2 concentration

In this project, the chemical reactivities for chars prepared in a drop tube furnace from untreated and torrefied willow and eucalyptus fuels is presented with three torrefaction conditions for each fuel. These can be found in Section 6.2.2.2. Chars from each fuel were individually prepared

in a drop tube furnace from which a series of isothermal (single temperature) TGA runs were performed to determine the rate constant for each temperature. Following this, Arrhenius parameters were determined (as described above) and the chemical reactivities at higher temperature determined via extrapolation. The overall aim therefore was to prepare chars under 'boiler like' devolatilisation conditions thus improving on TGA char preparation methods and to determine how torrefaction conditions affect char reactivity. This piece of work aims to fulfil objectives 5 and 6 described in Chapter 1.

While the overall chemical reactivity of char conversion is described above, the reactivity of char per unit surface area in the absence of any mass transfer restrictions [132] is expressed as the intrinsic reactivity according to the following equation:

$$R_i = k\, P^n\, A_g^{-1}$$

Where R_i is in the intrinsic reactivity in $g/m^2.s\ Pa$, k is chemical reactivity, P is the partial pressure of the reacting gas, n is the reaction order with respect to oxygen and A_g is the surface area (m^2/g). The intrinsic reactivity provides information on the rates of reactions taking place on the available active sites on the surface of biomass particles and the magnitude of surface area available for reaction is directly related to porosity. The porosity of particles is highly influenced by the pyrolysis conditions in which chars are prepared which is discussed in the text shortly. When torrefied fuels undergo pyrolysis, the changes in porosity and particle morphology may be different when compared to the pyrolysis of their untreated analogues. As torrefaction can be described as 'mild pyrolysis' and as such torrefied fuels have already undergone some degree or thermal treatments. As such, the intrinsic reactivities may be different for chars prepared from untreated and torrefied fuels. To determine the effects torrefaction on char reactivity, the intrinsic reactivities of the untreated and torrefied drop tube chars were also determined and can be found in Section 6.2.2.2. The intrinsic reactivity of a char particle requires knowledge of the surface area of the particle which will be discussed shortly in the text.

3.2.4 Factors affecting char reactivity

3.2.4.1 Effect of Pyrolysis conditions

The reactivity of pyrolytic chars depends on their porosity and morphological structure which can alter as a result of release of volatiles from the particle during pyrolysis. To clarify, the pyrolysis conditions, that is the temperature and residence time, affect how and to what extent volatile species in biomass are lost from the particles.. High heating rates are expected to produce more porous and thus more reactive chars than those produced under slow heating rates as a result of the increase in exposed surface areas on the particle for surface reactions from rapid release of volatile material [133]. When biomass particles are subjected to fast heating rates, there can be overpressure in the particles and coalescence of smaller particles which leads to formation of large cavities and thus exposed surface area for. On the contrary, slow heating rates allows for volatile material to escape through 'natural porosity' resulting in no significant cellular changes. . This effect was observed by Guerrero et al. who studied the reactivity of eucalyptus chars prepared under slow rates in a fixed reactor in the temperature range 600-900°C and chars prepared under fast heating rates in a fluidised bed reactor at 800 and 900°C [134]. SEM images of the slow and high heating rate chars are shown in Figure 3-18. It can be seen that in the slow heating rate chars there is evidence of cracks on the surface which can be attributed to slow release of volatiles. The fast-heating rate chars however show evidence of large cavities with a more open structure. In comparing the physical differences between slow and fast heating rate chars, it can be seen that there can be significant differences in particle morphology which will directly impact their reactivity. These differences provide justification for the need to study the reactivity of chars produced at fast heating rates (i.e. in a drop tube) compared with slow heating rates (i.e. in a TGA) when trying to extract information on how fuel may behave in industrials boilers. Using slow heating rates, the char produced, to a lesser extent, won't reflect those found in large-scale boilers unlike drop tube chars.

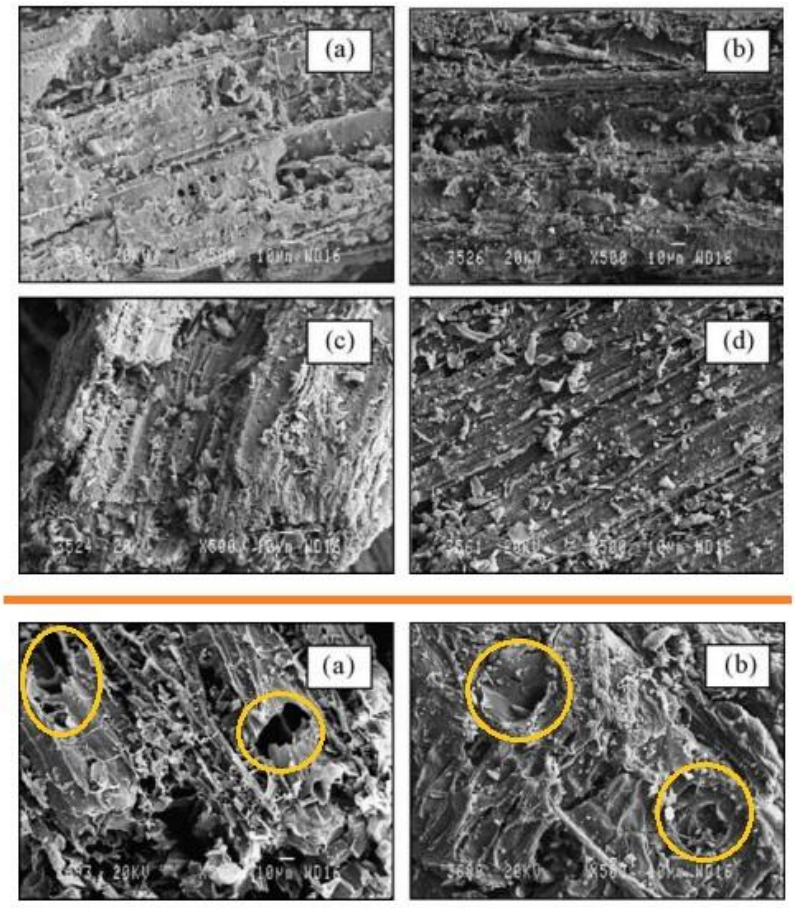

Figure 3-18 – SEM images for slow heating rate eucalyptus chars (above the orange line a-d) and high heating rate eucalyptus chars (a-b showing porosity inside the amber circles). Taken from [134].

To emphasise how pyrolysis conditions affect char particles further, Biagini et al. [135] also present SEM images of high-heating rate cacao shells and olive cake prepared in a drop tube reactor under nitrogen flow at 500 and 800°C for olive cake and 600 and 800°C for cacao shell to determine changes in final pyrolysis temperature. When compared to the parent fuel, the chars prepared at the lower temperatures showed some evidence of pores on the surface and the presence of small vesicles that were not present originally. At 800°C however, for both chars, the presence of vesicles had largely disappeared while deeper pores were visible on the surface and the particles were more rounded. The authors explain these effects as when the biomass particle heats up, the particle softens allowing for gases to escape through natural porosity however these natural pores can become clogged with volatile material generating overpressure and forming bubbles (as was observed in the 500 and 600°C chars) which can burst (as was observed in the 800°C chars). The bursting of these bubbles can then cause changes in the shape of the particles while the thermal decomposition of the chemical bonds can cause particle shrinkage or possible fragmentation. This rounding and increased porosity in high heating rate

chars has been observed by a number of researchers for a variety of fuels e.g. pine [136], forest residues, wood chips and rice husk [137] and wheat straw [138].

Analysis of the effect of fast-heating rate high temperature conditions used for the preparation of chars from torrefied fuels is less prevalent in the current literature and so merits further study. As mentioned above, implementing torrefaction as a pre-treatment step before pyrolysis (and ultimately combustion) may alter the resulting char particles and so should be investigates. To determine these changes, and fulfil some of the actions outlined in Objective 7, SEM images of the char particles prepared in a drop tube furnace from untreated and torrefied willow and eucalyptus can be found in Section 6.2.1.2 of this thesis

While SEM provides largely qualitative data on the change in surface morphology of char particles, measurement of the surface area of char particles can provide more quantitative information on the surface available for reactions and allows for determination of the intrinsic reactivity. Measurement of the surface area for char particles can be performed in a number of ways however typical measurement of char surface areas usually involve analysis of adsorption isotherms (volume of gas adsorbed vs. relative pressure) where an inert gas is adsorbed on to the surface of the char particles. From these plots, the surface area can be determined from the amount of gas required for a monolayer of coverage i.e. a layer one molecule thick. One method commonly uses the adsorption of N_2 at cryogenic temperatures (77°K) and application of the Brunauer-Emmett-Teller (BET) method [139] in the relative pressure range 0.05-0.3 P/P_0 to determine the apparent surface area (the BET methodology is described in Section 4.4.5).

Pottmaier et al. [138] report the BET surface areas with nitrogen as the adsorbate for rice husk and wheat straw chars prepared at different temperatures (900, 100 and 1300°C) in a drop tube furnace. The authors report for wheat straw, the surface area increases from 1.86 m^2/g to 6.9m^2/g for the 900°C chars increasing to 19.0 and 30.7 m^2/g for the 1100 and 1300°C chars respectively. For rice husk, the parent fuel had a measured surface area of 2.18m^2/g with the highest surface are char measured at 900°C as 79.6m^2/g and decreasing to 25.4 and 13.5 m^2/g for 1100 and 1300°C respectively. In the case of the chars, the surface area increased by an order of magnitude which can possibly be attributed to increased porosity (also evident from SEM images shown in their study) and cavities formed during rapid pyrolysis. In the case of rice husk, the decrease in surface area is postulated by the authors to potentially be result of melting of

the pore structures at elevated temperatures. As a result, determination of apparent surface can provide more robust information on the impact of pyrolysis conditions as higher temperatures may not directly correspond to increase surface exposure as was discovered by Pottmaier et al. where the highest temperatures resulted in lower measured surface areas relative to the lower temperatures in the case of rice husks.

Yuan et al. [140] also report the BET surface areas for chars prepared in a furnace from rice straw, chinar leaves and pine sawdust at 800, 1000 and 1200°C. The apparent surface areas reported rice straw and chinar leaves range from 85.5-133.9 m^2/g and 186.1-225.3m2/g respectively with increasing temperature. The pine straw char surface areas measured were considerably lower; the highest surface area measured was 47.5m^2/g for chars prepared at 800°C and the lowest 8.9m^2/g at 1200°C – the authors similarly attributing this decrease in surface area to melting of the particles at higher temperatures.

Although surface area analyses can provide quantitative information on the extent of surface exposure, caution was be administered, as some techniques may not reflect the true surface. This can be the case when nitrogen is used as the adsorbate gas to determine the surface area of particles dominated by micropores (<2nm) dominate. As classical manometric surface area analysis takes place with reactions cells submerged in liquid nitrogen (77°K) to maintain constant temperature at nitrogen's saturation vapour pressure [141], activated diffusion of nitrogen molecules in to the micropores can be problematic as equilibrium pressure may not be achieved in the designated time [142]. This effectively 'undershoots' the apparent surface area derived from the BET equation as the measured monolayer coverage is too low. This effect is highlighted when comparing surface area measurements using another adsorbate gas such as CO_2. Some researchers have postulated that CO_2 is a better adsorbate gas in the surface area analysis of carbonaceous materials due to its ability to fill more microporosity as a result of its higher polarizability [142, 143]. Della Rocca et al. [144] measured the surface areas of hardwood biomass chars prepared at 623 and 1123K using N_2 (using BET) and CO_2 (using the Dubinin Rudushkevich equation). The ratios of CO_2/N_2 measured surface areas were in some cases were as high as 245 however some of the surface areas measured yielded similar results where it could be the case where the CO_2/N_2 ratios are lower, that micropores aren't present on the surface.

While there are differences observed in measured surface areas using different adsorbate gases, it would be imprudent to assume CO_2 is exclusively suited to analysis of biomass chars. One reason for this is due to the fact that measured surface is highly dependent on degree of burnout which can affect the nature of the pores on biomass particle surfaces; some authors suggest nitrogen adsorption is in fact better suited for biomass particles which have undergone a degree of burnout [143].

Analysis of the surface areas of the chars prepared from torrefied fuels is performed in this study for two primary reasons. Firstly, to ascertain any changes to the surface area relative to untreated fuels and secondly, to determine the intrinsic reactivies (described above). These can be found in Section 6.2.1.1 of this thesis and fulfil Objective 7 of this work. While there have been numerous studies characterising biomass chars under various pyrolysis conditions, there are fewer studies dedicated to the high temperature pyrolysis of torrefied biomass although more studies are emerging. Li et al, analysed the mass loss during char formation of torrefied palm kernel shell (TPKS) (torrefied at 220, 250 and 300°C for 30 minutes) pyrolysed in a isothermal plug flow reactor (IPFR) at 500, 700 and 900°C for a number of residence times ranging from 0.1-1 second (heating rate was 10^4-10^5°C/s) [145]. The authors then used the ash tracer method to determine the degree of mass loss at the varying conditions. Results showed that longer residence times equated with greater mass loss for each fuel. However the most severely TPKS underwent the least degree of mass loss followed by the 250°C treatments for each pyrolysis temperature and residence time as shown in Figure 3-19. For example, at 900°C and a residence time of 0.5 seconds, the mass loss of 220, 250 and 300°C TPKS was 30, 19 and 10% respectively. The authors also pyrolysed untreated PKS (UPKS) which showed an even greater degree of mass loss where the same temperatures and residence times were used e.g. the mass loss at 900°C for 0.5s was 78%. Torrefaction thus has the effect of lowering the reactivity of the biomass fuel.

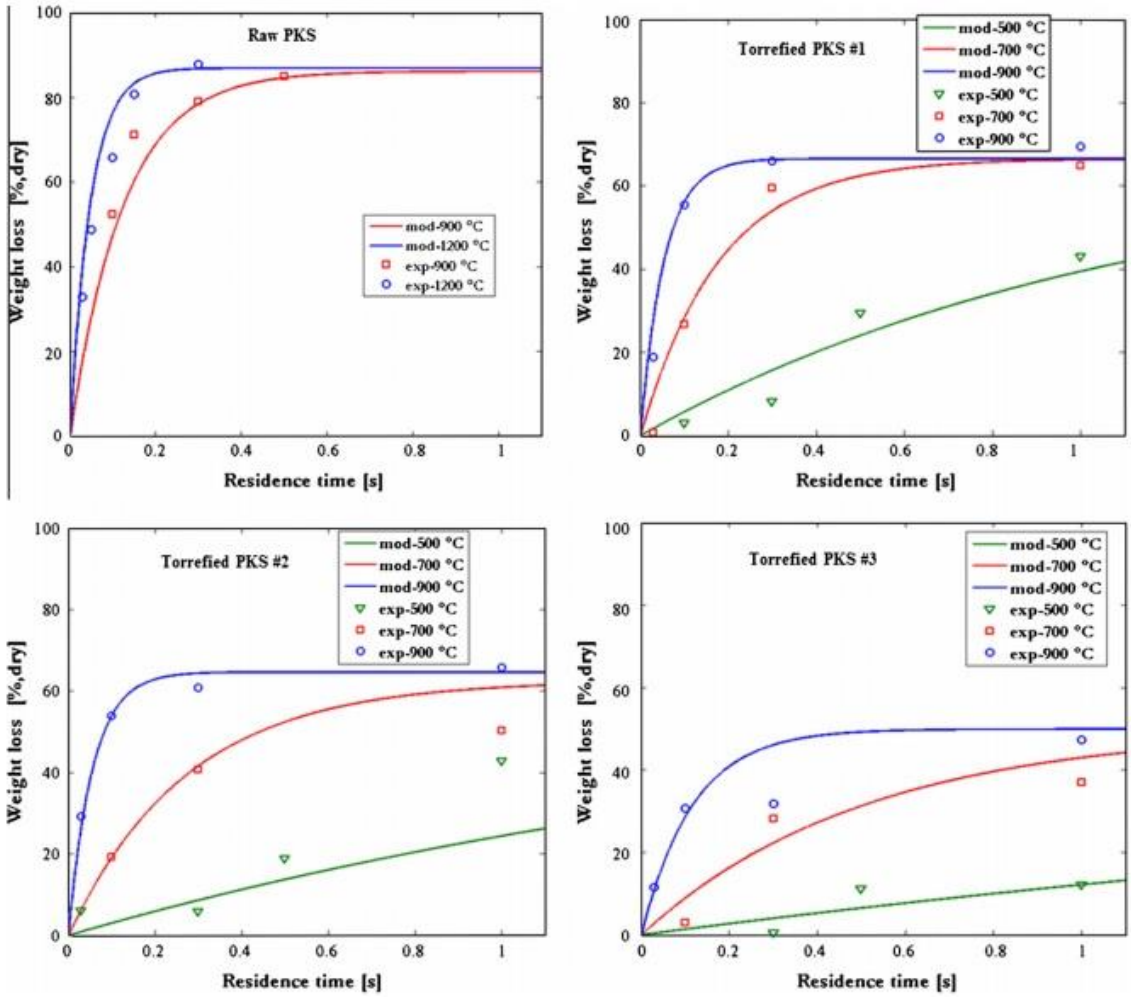

Figure 3-19 – Mass loss for rapid devolatilisation of untreated and torrefied PKS [145].

3.2.4.2 Effect of inorganic species

Pyrolysis conditions affect the devolatilisation and char reactivity however the inorganic species present in biomass can also affect the reactivity of biomass during combustion. One of the most important species is potassium (K), which is absorbed through the root system and transported to all areas of the plant [146], is known to have a catalytic effect on the pyrolysis and char combustion stages [77, 146, 147]. Olsson et al. studied the release of K during pyrolysis of wheat straw using a surface ionisation method [148]. The authors showed small amounts of potassium are released at low temperatures (180-500°C) which they ascribed to decomposition of the organic structure; thus representing the loss of K bound to the organic matrix. The authors found however that the majority of K was released at high temperatures (>500°C) from the inorganic ash component during char combustion, which increased when higher chlorine (Cl) contents were found in the straw samples. This is due to the fact that the most abundant K species found to be released during straw char combustion was potassium chloride (KCl). Westburg et al. also

observed this in their study of distribution of potassium and chlorine between the solid and vapour phases during combustion of wood chips [149].

The potassium content of the parent fuels and chars were determined in this work using two techniques: inductively coupled plasma mass spectrometry (ICP-MS) for the parent untreated and torrefied fuels and energy dispersive x-ray analysis (EDX) for the drop tube furnace chars. Specific details of these techniques can be found in Section 4.4.9 in the experimental methodology. These determinations were performed to firstly, ascertain any changes in K content during torrefaction and then secondly to calculate the rate of potassium evolved during pyrolysis in the drop tube furnace. These can be found in Section 6.2.1.3 of this work and aim to cover part of Objective 8.

3.2.5 Chemical reactivity of chars from untreated and torrefied biomass

Section 3.2.3 presents the fundamentals of determining the chemical reactivity of chars from untreated and torrefied fuels. This section presents some studies available in the literature on determinations of the chemical reactivies of chars prepared from biomass fuels.

Di Blasi [123], in her review paper, presents chemical reaction rates for the char combustion of a variety of biomass fuels shown in Figure 3-20. The studies shown on the Arrhenius plot employ a range of pyrolysis conditions and use different techniques for determination of oxidative reactivity e.g. dynamic or isothermal analysis. For instance, the line corresponding to 176 on the Di Blasi plot corresponds to the study performed by Adanez et al. [150] who pyrolysed pine in a fluidised bed reactor at 850°C before char oxidation experiments in air using TGA. The activation energy and pre-exponential factor determined were 140kJ/mol and 3.8 x $10^7 s^{-1}$ respectively. Janse et al. [131], corresponding to line 134 on the Di Blasi plot, used isothermal oxidation using TGA analysis of pine sawdust char pyrolysed on wire gauze (heating rate of at least 300°K/s) to at various final temperatures (500 and 600°C) and varying residence times (20, 60 and 100s).

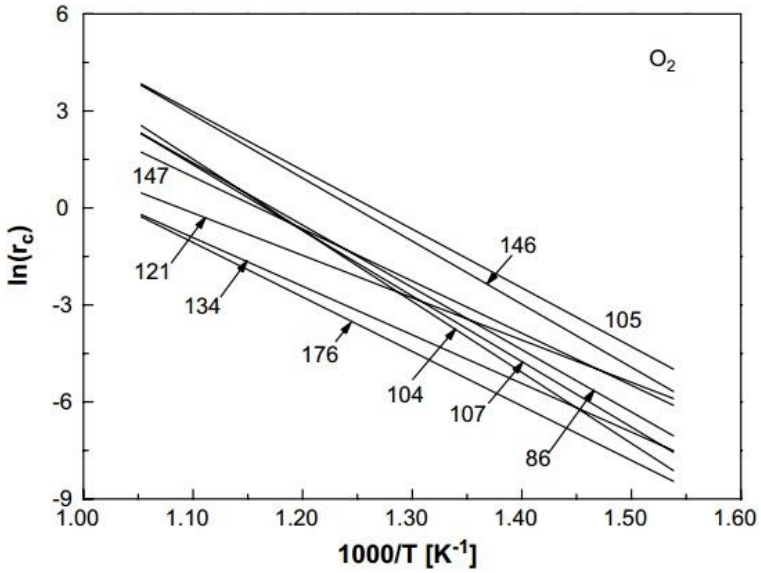

Figure 3-20 – Chemical reactivity for various biomass samples [123].

In this study, the authors used a variety of oxygen concentrations ranging from 2.25-36% in TGA analysis however Di Blasi notes that these studies are only strictly applicable to the environments in which the studies were performed. Mason et al. [151] also determined the Arrhenius parameters for char combustion of pine, eucalyptus and willow and found their activation energies to be 94, 113 and 70 kJ/mol respectively.

There has been much less focus on the char combustion properties of torrefied materials, especially those pyrolysed at high heating rates to high temperatures although some studies have been performed. Jones et al. [117] studied the combustion properties of torrefied willow and compared them with the combustion properties of untreated willow and bituminous coal. Chars from untreated and torrefied willow (2 torrefaction conditions: 290°C for 10 minutes for particles less <10mm and 30 minutes for particles >20mm respectively) were prepared using a pyroprobe under helium flow at a heating rate of 1000°C/s to 1000°C and held for 30 seconds and the oxidative reactivity determined using both dynamic (heating rate 10°C/min) and isothermal (range 360-420°C) conditions. Using the reaction rate constant method, the authors determined the reactivity at 400°C, k_{400}, and found the reactivity decreased with increasing torrefaction severity. The authors postulate the lower reactivity to be as a result of lower and different composition of volatile contents in the torrefied material: the chars from torrefied material have a larger fraction of higher molecular weight volatiles which will result in lower porosity and lower reactivity. However, the measured surface area for the torrefied chars was

larger when compared to raw willow chars (279m^2/g compared with 157m^2/g) and so lower reactivity cannot be attributed to a decrease in porosity. The authors report the intrinsic reactivity of untreated and torrefied willow compared with some bituminous coals as shown in Figure 3-21. It can be seen that the biomass chars are more reactive than the chars produced from a variety of coals however it is important to note that the torrefied char reactivity has moved downwards towards the region of coal reactivity. Bridgeman et al. [105] also studied the reactivity of single particles of untreated and torrefied willow during combustion in a methane flame by determining the length of time required to achieve particle burnout. Results showed that for char combustion, untreated willow burned out faster than the torrefied samples, the greatest disparity shown when particle mass was larger. As the size of the particles reduced however, the differences in reactivity became less.

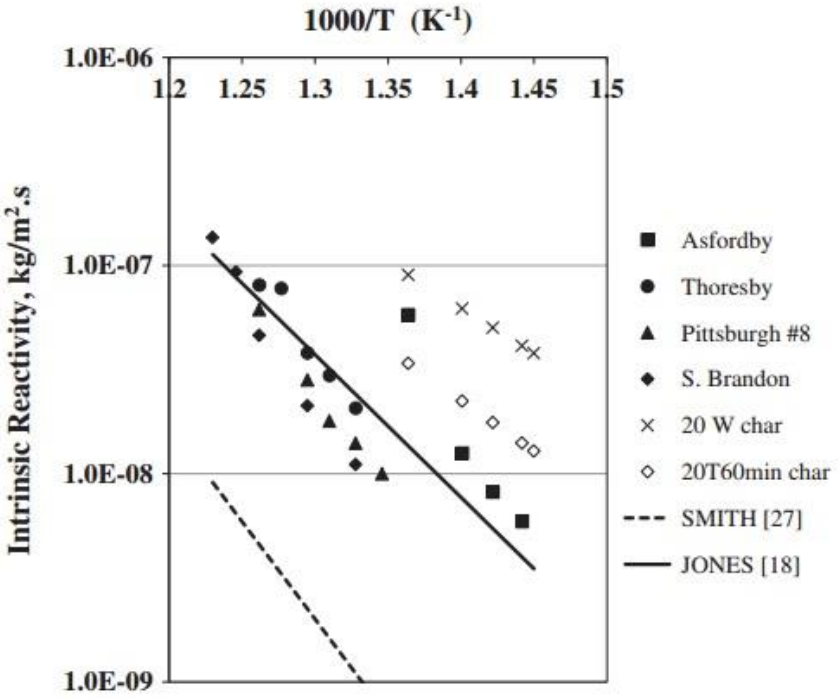

Figure 3-21 – Intrinsic reactivities of untreated willow, torrefied willow and some bituminous coals [117].

3.3 The fate of nitrogen during combustion

As discussed in Section 3.1.8.1 knowledge of the fate of nitrogen during biomass combustion is important with regards to potential NO_x emissions that may arise- NO_x the umbrella term for nitrogen oxides. The main NO_x species that pose environmental and human health concerns that can arise from combustion of biomass fuels is nitric oxide (NO) which can undergo oxidation to

nitrogen dioxide (NO_2) in the atmosphere. NO_x emissions in the atmosphere can cause problems including acid rain and eutrophication which can have subsequent effects on soil and water quality [152]. NO_2 also has major implications on human health where at high concentrations can cause inflammation of airways [152]. NO_x also act as 'indirect' greenhouse gases as while they don't affect the earth's radiative balance, they catalyse tropospheric ozone formation. Under the EU Large Combustion Plant Directive discussed earlier in section 1.2.7 restrictions are placed on the amount of NO_x (and SO_x and soot) that can be emitted from large industrial plant. These emissions restrictions are shown in Table 3-1.

		NO_x emissions limit values (mg/N m^3)*		
	Fuel	50-100 MW_{th}		> 500 MW_{th}
Existing plant (until 2016)	Solid fuel	600		500
Existing plant (after 2016)	Solid fuel	600		200
	Fuel	50-100 MW_{th}	100-300 MW_{th}	> 300 MW_{th}
New build plant	Biomass	400	300	200
New build plant	Solid fuel	400	200	200

*Daily mean values (references oxygen contents are 6% for solid fuels)

Table 3-1– NOx emissions limit values under the Large Combustion Plant Directive [45].

Figure 3-22 shows how nitrogen distributes between the solid, tar and char phases during combustion [153]- the distribution of N to each phase varying depending on conditions such as heating rate, residence time etc. The formation of NO_x can occur via several reactions including oxidation of the NO_x pre-cursors: ammonia (NH_3) and hydrogen cyanide (HCN) released during devolatilisation and through direct oxidation of char nitrogen. The NO_x pre-cursors, NH_3 and HCN can derive from char-N and oxidise to NO however it is reported in smaller quantities (up to 20%) [154] than direct oxidation of char-N.

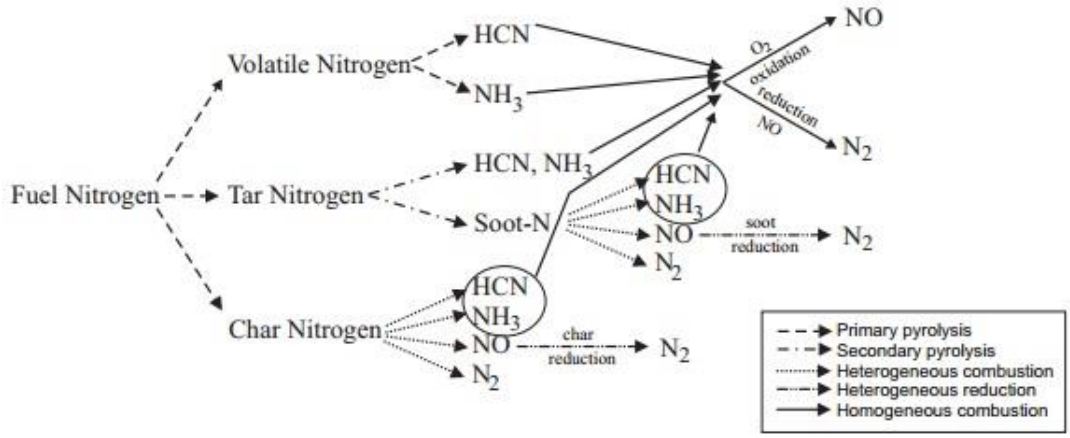

Figure 3-22 – Fate of Nitrogen during biomass combustion [153]

Low NO_x strategies in place in industrial-scale boilers operate via removal of nitrogen species released in the volatile phase thus release of nitrogen to the vapour phase during combustion is highly desirable. Subsequently however, nitrogen retained in the char phase is therefore undesirable as it is char-N which that poses a threat to potential NO_x emissions to the atmosphere. Knowledge therefore, of the partitioning of nitrogen to the volatile phase during rapid pyrolysis can provide information on how fuels will behave in real life systems. With respect to the fate of nitrogen and the combustion of torrefied fuels, there is still relatively little information available. In the same study discussed above, Jones et al. [117] also studied the partitioning of nitrogen during torrefaction of willow, the authors also studied the partitioning of nitrogen during rapid pyrolysis of the untreated and torrefied samples. The authors found similar retention of N in the char phase for untreated and torrefied willow: 41-42% for untreated and 41.2% for willow torrefied at 290°C for 10 minute and 44% for willow torrefied at 290°C for 60 minutes.

Ndibe et al. [155] studied the emissions characteristics of the combustion of torrefied biomass (spruce, pine and forest residues) in 6% oxygen in a 20kW drop tube furnace to determine the influence of torrefaction on NO_x emissions. In this study, a drop tube furnace temperature of 1200°C was used and various atmospheric conditions selected: unstaged combustion where the overall stoichiometric ratio was 1.15 and air-staged combustion where burner stoichiometric ratio was reduced to 0.75. NO_x emissions were measured online at the furnace outlet. The concentration of NO_x detected for the torrefied fuels, untreated white wood (spruce, pine and

forest residue), coal (El-Cerrejon) and a blend of coal and torrefied spruce are shown in Figure 3-23.

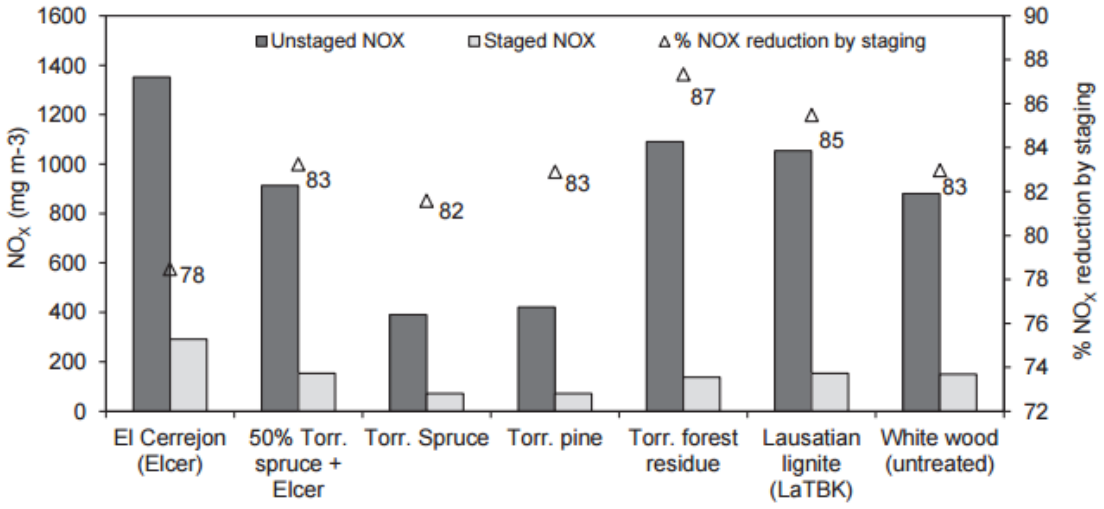

Figure 3-23 – NOX concentrations in flue gas at the furnace exit for the various fuels under unstaged and air-staged combustion conditions. Percentage reduction during staging is determined from comparison to unstaged combustion concentrations.[155]

Results show that the NO_x emissions for unstaged combustion for torrefied pine and spruce are lowest (420 and 400 mg/m^3 NO_x) and coal the highest (1350 mg/m^3 NO_x). The authors note the correlation between fuel-N contents and NO_x emissions where greater fuel-N contents corresponded with greater emissions- the torrefied spruce, torrefied pine and El Cerrejon fuel-N contents 0.2, 0.2 and 1.64 % dry-ash free (daf) respectively. Interestingly, the white wood fuel-N contents is 0.35% daf which is greater than the torrefied fuels N contents (except torrefied forest residue which has an N-content of 0.45% daf)- suggesting that N could be lost during the torrefaction process although this would be more conclusive if compared with untreated spruce and pine singularly. The results also show that air-staged NO_x reduction strategies work well for all fuels presented; reducing the NOx emissions for each of the torrefied fuels 82-87%.

The fate of nitrogen during fast heating high temperature pyrolysis in a drop tube furnace has been performed in this work. The methodology takes the form of determination of the N contents of the parent untreated and torrefied fuels and the chars using elemental analysis and then performing a material mass balance. From this, the amount of N retained in the char and the amount evolved in the drop tube furnace can be determined. This can be found in Section 6.2.1.4 of this this thesis and fulfils the remaining objectives included in Objective 8.

3.4 Conclusions

Torrefaction is promising pre-treatment process that has received increased attention in the past few years to address some of the issues commonly associated with biomass fuels. Parameters of interest include how the different torrefaction process conditions affect the chemical and physical properties of biomass as well the behaviour of torrefied fuels during combustion. At present, torrefaction technologies are not deployed on commercial scales and so more information is still required at laboratory level to optimise the process for potential future application in large-scale generation. This includes information pertaining to the overall mass and energy balances of the torrefaction process for specific fuels as well as the resultant changes in the physical and chemical properties that occur as a result of torrefaction. The torrefaction conditions selected will affect the fuel under treatment in different ways- with higher temperatures and residence times resulting in greater solid mass loss and increased gas and liquid yields. Changes in the solid, liquid and gas yields and the physical and chemical properties of each are greatly influenced fuel type (e.g. softwood or hardwood) and the associated degrees of thermal stability of the cell wall components which vary in relative concentration and composition depending on the type of fuel. As a result, it is necessary to optimise the conditions for each type of biomass through changing process parameters and determining the effects of torrefaction on product yields and fuel properties. This process of optimisation through determination of the effects of torrefaction forms the basis of Chapter 5 in this thesis. In this chapter the torrefaction of two fuels, North American pine and eucalyptus, under 4 conditions (250°C for 30minutes, 270°C for 30 and 60 minutes and 290°C for 30 minutes) is investigated. The investigation involves determination of the overall mass balances of the torrefaction reaction for each fuel via determination of the solid and liquid phase yields with the permanent gas yields determined by difference. In this chapter, a number of physical and chemical properties of the torrefied product are characterised including ultimate and proximate analysis, changes to cell wall components, grindability behaviour, pyrolysis behaviour and surface and morphological changes. The organic phase liquid products are also characterised for their elemental composition using ultimate analysis and the carbon content of the aqueous phase liquids products is determined using total organic carbon (TOC) analysis. These data are also used to determine the overall elemental balance of the process for each condition to determine the partitioning of the elements C, H and N. Regarding the elemental balances; the partitioning of N of particular interest owing to potential NO_x emissions can arise from fuel-N. As mentioned above, determination of these parameters is essential for process optimisation, which must be determined with accuracy at laboratory level before scaling-up to large scales is considered. The variety of analyses performed on the torrefied fuels in addition to the

determined mass and elemental balances provide novelty in this work as few torrefaction studies combine all of these analyses together.

Information on the behaviour of torrefied biomass fuels in environments which mimic pf combustion is also limited. These include analysis of the oxidation kinetics of torrefied biomass chars prepared at high-heating rates in drop tube furnaces since most studies have largely focussed on untreated biomass fuels leaving a gap in the current knowledge. The fate of species such as nitrogen and potassium during high-heating rate devolatilisation are also largely unknown, especially for torrefied fuels, and requires investigation owing to their importance with regards to potential NO_x emissions and the catalytic effect on char reactivity respectively. The investigation of these unknowns is undertaken in Chapter 6 of this thesis whereby fast heating rates chars from untreated and torrefied fuels prepared under 3 conditions (270°C for 30 and 60 minutes and 290°C for 30 minutes) were prepared using a drop tube furnace (DTF). The oxidative reactivity for each of the chars was determined isothermally using TGA. As the devolatilisation (and pyrolysis) conditions can affect char reactivity, a number of analyses were also employed to investigate char morphology. These include SEM and surface area determination; this latter technique also used to determine the intrinsic reactivity of the chars. The investigation of the partitioning of N and K between the fuels and chars is also investigated and achieved using the data from elemental analysis and SEM-EDX respectively. The combination of these studies above provides a detailed account of the behaviour of torrefied materials (and their untreated analogues) under conditions similar to boiler configuration and provides the crucial primary investigation before any scale-up processes can be considered. As the information on the parameters listed above are lacking from the current investigations on torrefied fuel combustion behaviour, this chapter makes for an interesting and original study.

Uncertainties also remain on the effect of torrefaction on bioenergy supply chain greenhouse gas emissions. While torrefaction aims to improve the chemical and physical properties of the resultant fuel which can have a positive effect on supply chain logistics (i.e. lower moisture contents and improved energy density) it is an overall endothermic process which can require an external energy input where the heat integration of combustion of volatile gases does not meet demand- this discussed in subsequent chapters. Analysis of any potential 'trade-off' between energy inputs and enhanced fuel properties must therefore be understood. As mentioned in Section 1.3.4 the use of biomass for energy applications must be done sustainably. This covers a wide range of considerations such as supply chain GHG emissions (which must fall

under regulatory limits to qualify for subsidies) and the type of fuel and land the fuel is sourced from- with limitations placed on using land with high carbon stock for example. Knowledge of the GHG emissions profiles of incorporating torrefaction in to bioenergy supply chains is necessary to ascertain its effects, both directly and indirectly on life-cycle GHG emissions- for example more land may be required for production of torrefied material however the improvements to fuel properties may 'offset' this increase. An introduction to the sustainability aspects of using bioenergy with a focus on life-cycle GHG emissions is covered in Chapter 7 of this thesis with its own literature review. Following this, and using data on the torrefaction of North American pine from Chapter 5, the energy requirements for each of the torrefaction conditions performed was determined as part of an LCA study on the life-cycle GHG emissions associated with the production of electricity from torrefied wood pellets using the methodology laid out in the EU RED methodology. This was achieved by building bespoke supply chains and assessing the GHG emissions at each stage of production in which biomass is harvested, torrefied and pelleted in North American and transported to the UK for use in a power plant. The results are also compared with conventional (i.e. non-torrefied wood pellets) to determine how torrefaction affects life-cycle GHG emissions. In determining the energy requirements for each of the torrefaction conditions based on real-life experimental data and adopting the RED methodology to assess GHG emissions is an original piece of work as to the author's knowledge, no other study of its kind has been performed.

4 Experimental Methodology

4.1 Introduction

This chapter describes the experimental procedures and instruments used as part of this research. The chapter begins with a brief description of the samples used before discussing the torrefaction experiments using the bench scale reactor, providing information on the bench-scale reactor itself and operating procedure used in during torrefaction. The chapter then discusses some of the sample preparation equipment required for some analyses before discussing the experimental techniques and instruments used, information on operation and some instrument theory. The chapter ends by describing equipment used in combustion and pyrolysis studies, namely the drop tube furnace, and the methodology used to determine isothermal oxidation and pyrolysis kinetics.

4.2 Samples

For the torrefaction work presented in Chapter 5, two fuels were utilised: North American Pine and Eucalyptus. Each of these fuels were used in the bench-scale torrefaction experiments and take the form of 5-30mm wood chips for pine and 20-40mm wood chips for eucalyptus. Images of the untreated fuel chips used in Chapter 5 are shown in Figure 4-1. For the study on chars prepared in a drop tube furnace presented in Chapter 6, different fuels were used than those utilised in Chapter 5. The fuels used in Chapter 6 are untreated and torrefied willow and eucalyptus fuels which were obtained from a previous study performed in my research group [107]. It must be noted therefore that the eucalyptus fuels used in Chapters 5 and 6 are different eucalyptus fuels. The fuels used in this study by Ibrahim et al. were willow and eucalyptus wood chips which were torrefied under 3 conditions- 270°C for 30 and 60 minutes and 290°C for 30 minutes. These torrefaction conditions were chosen by Ibrahim et al. as they had been determined in previous studies [105] to result in improvements in fuel physical and chemical properties (i.e. increase in HHV and lowering of volatiles content) while the extent of mass and energy loss remained within suitable limits. These conditions also provide information on the impact of changing temperature and residence during torrefaction. In using conditions 270°C for 30 and 60 minutes, the impact of residence time on torrefaction can be determined while comparing 270°C for 30 minutes and 290°C for 30 minutes, the influence of temperature can be determined. The GHG emissions assessment in Chapter 7 utilises the data for the torrefaction of pine discussed in Chapter 5.

Figure 4-1 – The fuels used in Chapter 5 of this study: pine (left) and eucalyptus (right).

4.3 Torrefaction experiments

4.3.1 Bench Scale Reactor

Torrefaction experiments were performed using a three zone horizontal tube furnace with an internal diameter of 75mm and 750mm in length as shown in Figure 4-2**.** The central heating zone is controlled using a Eurotherm Model 2416 PID controller with the zones either side controlled using Eurotherm Model 2216e PID controllers.

During torrefaction experiments, heating rates, dwell periods and final temperatures were programmed using the centre 2416 PID controller which served as a master controller to the side 2216e slave controllers ensuring uniformity across the furnace during experiments. A PID diagram of the tube furnace is shown also shown in Figure 4-4.

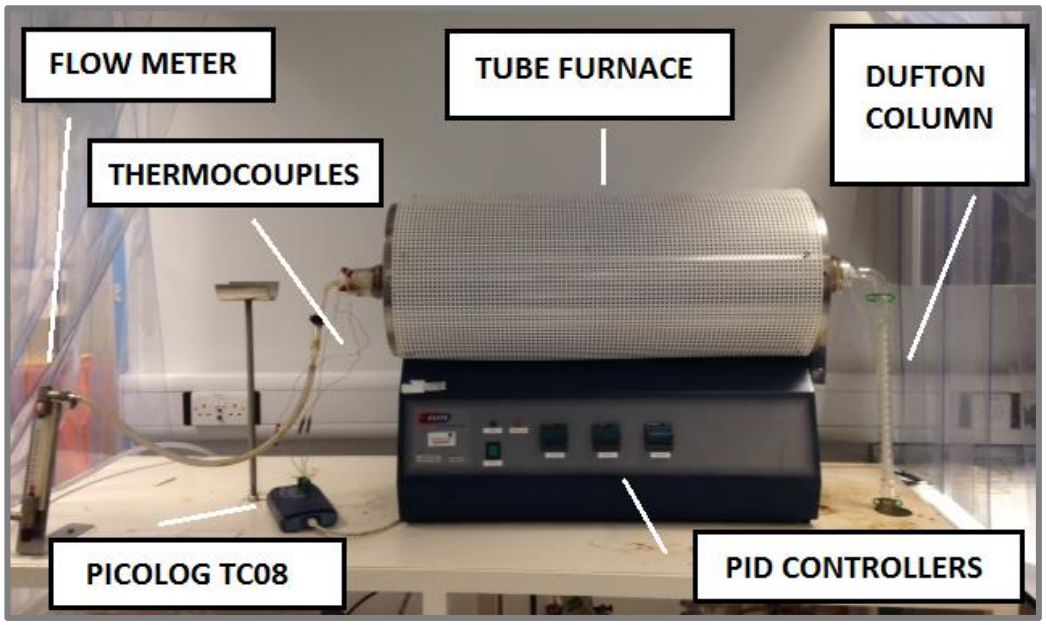

Figure 4-2 – Bench scale reactor used in torrefaction experiments

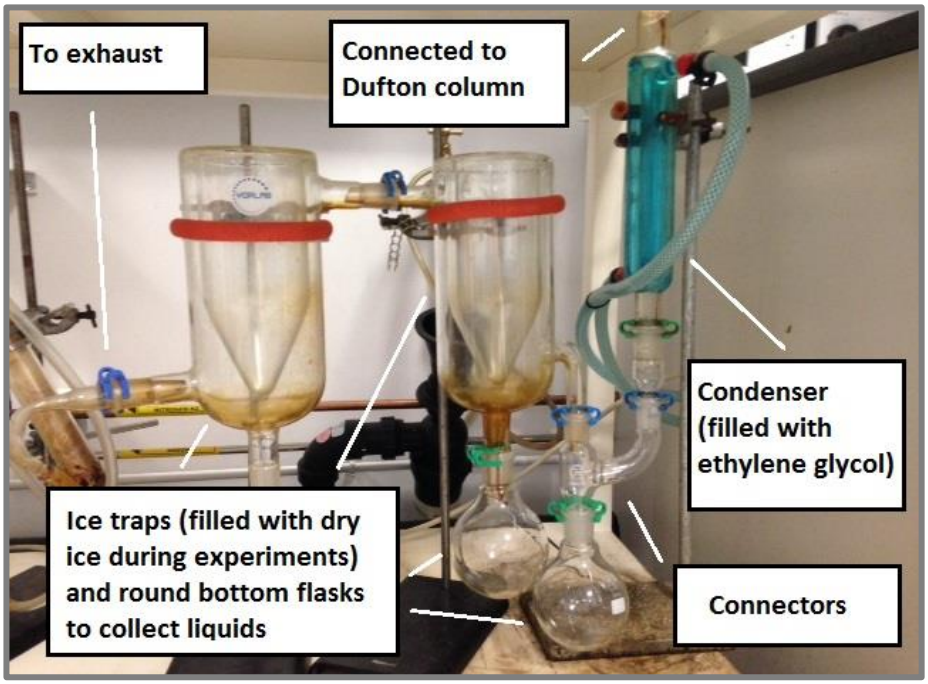

Figure 4-3 – Glassware beneath torrefaction rig for collection of condensable liquids

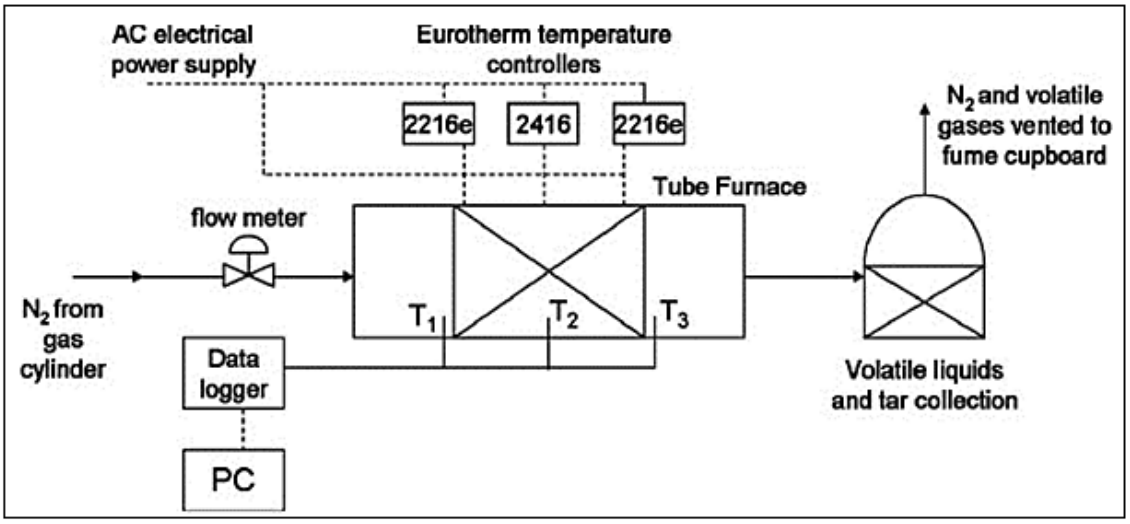

Figure 4-4 – PID diagram of the bench-scale torrefaction reactor

The tube furnace accommodates a borosilicate reactor tube with diameter of 60mm and 800mm in length with sample supports 200mm from one end allowing sample to be introduced via the other the end. The tube was designed so that the centre 400mm can accommodate sample for torrefaction experiments, the sample region having an approximate volume of 1130cm^3. Quickfit (B60) sockets can then be fitted and clipped in place at each end of the reactor tube. The front end of the tube is fitted with a B60 quickfit cone containing one central gas inlet tube and three surrounding inlets fitting three thermocouples. The three thermocouples were placed at 20cm intervals in the reactor tube; the shortest thermocouple measuring the temperature of the gas inside the reactor tube while the middle and longest thermocouples measured the temperature in the bulk of the sample. The temperatures measured by the thermocouples were monitored using a pico-logger connected to a PC. Nitrogen was supplied from a gas cylinder and controlled using a valve and flow meter through the central gas inlet tube. The other end of the reactor tube fits a B60 quickfit socket which narrows into a 90° bent outlet with a 24/29 male cone. Attached to this was 30mm Dufton column which connected to a double surface condenser tube. The outer surface of the condenser was filled with ethylene glycol supplied from a chiller pump which was kept at -5°C during experiments. During torrefaction experiments heavy (i.e. high molecular weight) liquid products (e.g. tars) collected in the B60 connector while lighter liquids and gaseous products travelled down the Dufton column and through the condenser. Connected beneath the condenser is a series of round bottom flasks connected to two ice traps which were filled with dry ice during experiments; the condensable liquid subsequently collecting in the round bottom flasks. The majority of liquid products from torrefaction were collected in the first round bottom flask beneath the condenser flask during experiments however the additional flasks were in situ to ensure all condensable products were

retrieved. Connected to the final ice trap was a piece of tubing which allowed for permanent gases (non-condensable) to escape through a fume hood. The glassware used for collection of the condensable liquids is shown in Figure 4-3.

4.3.2 Operating Procedure

Before each torrefaction experiment, around 100g of wood chips were weighed. A glass wool plug was then inserted in to the reactor tube up to the sample supports followed by the sample which was gently packed in to the reactor tube. Another glass wool plug was then inserted in to the reactor tube after and up to the sample. The tube was then half-inserted in to the tube furnace with the outside portion supported by a stand. A small film of lubricant was rubbed on to outside of the front end B60 connector hosting the thermocouples and inserted in to the reactor tube ensuring the thermocouples were correctly positioned in the 'empty' gas space and in two areas in the bulk of the sample. The reactor tube was then inserted in to the tube furnace allowing for the other end to sit slightly outside the furnace. From here, the second B60 connector, also with a thin film of lubricant, was connected to the other end of the reactor tube and clipped in place followed by the Dufton column and condenser. The chiller pump filling the condenser was then set at -5°C. At this point, a beaker was placed underneath the condenser which was open to the atmosphere at this stage. The nitrogen supply was then switched on at a flow rate of 1.2L/min and allowed to flow for 10 minutes at ambient temperature. A heating programme was then applied to the master PID controller with a heating rate of 10°C/min to 150°C and programmed to dwell for 60 minutes once this temperature was reached. This drying stage was performed to ensure the biomass samples were completely dried (loss of free moisture) before torrefaction experiments. Once the 60 minute drying stage was complete, the beaker from beneath the condenser, now filled with free moisture lost during drying, was removed and the series of pre-weighed round bottom flasks and ice traps filled with dry ice connected. The master PID controller was then programmed to heat the tube furnace at a rate of 10°C/minute to a selected final torrefaction temperature and dwell for a designated residence time. The torrefaction conditions (final temperatures and residence times) used in the torrefaction of North American pine and eucalyptus are shown in Table 4-1. The residence time in this instance was taken to begin when the gas temperature reached the final torrefaction temperature.

Condition	Final Temperature (°C)	Residence Time (minutes)
250-30	250	30
270-30	270	30
270-60	270	60
290-30	290	30

Table 4-1 – Torrefaction conditions used in this work

These torrefaction conditions were selected for several reasons. As mentioned in Section 2.1, these conditions have previously been reported to provide improvements to fuel properties while the extents of mass and energy loss are not too severe. These conditions also allow for assessment of the impact of changing temperature (for conditions 250, 270 and 290°C for 30 minutes) and residence time (for conditions 270°C 30 and 60 minutes) on the mass and energy balances of the processes. In comparing these, it can be elucidated which parameter has a greater overall effect. Furthermore, these conditions also match those used by previous researchers in this research group [105] [107] and thus also help contribute to a greater body of work.

The addition of the mildest condition, 250°C for 30 minutes, in addition to those selected by Ibrahim et al. was done to enhance the subject knowledge on the torrefaction of fuels at lower conditions which may be used in commercial applications. Milder torrefaction conditions may be desired in a commercial setting as they will have lower overall energy demands (and costs) but also as severe conditions can potentially impact the utilisation of torrefied fuels when preparing wood pellets for further application. These topics are touched upon this section however will be discussed in greater detail later in Section 7.7.5.2 where the assessment of torrefaction on supply chain GHG emissions is investigated.

Once the residence time was complete, the back-end B60 connector was disconnected and the reactor tube containing the torrefied material was quickly removed from the tube furnace and quenched with a greater flow of N_2 gas to cool the sample down more quickly. The B60 connector was then placed in a large beaker to collect the heavy tars that had deposited in it (i.e. those that hadn't flowed through the Dufton column and condenser). Following this, around 10mL of dichloromethane (DCM) was poured down the Dufton column to collect any lighter tars still remaining in spiral fractional column which flowed down the condenser and into the round bottom flasks. The liquid products in the round bottom flask now formed two layers: a bottom aqueous layer containing reaction water and organic polar species and a top layer containing

DCM and dissolved non-polar organic species. Note that the water contained in the aqueous layer contains only *reaction* water as the *free* moisture lost during the drying stage was collected separately in the beaker. Once all the liquid products were collected in the round bottom flasks, they were carefully removed and stoppered. Some DCM was then added to the beaker containing the tars from the B60 connector to dissolve them before adding them to the round bottom flask containing the liquid products. All of the liquid products were then added to a separating funnel and left to stand to allow both layers to completely separate. Following this, the two separate layers were collected in separate previously weighed glass vials. The lower aqueous layer collected in the vial was then weighed and the difference from the empty vial recorded. The organic layer containing DCM was then weighed and then left open in a fume hood for 24 hours to allow the DCM to evaporate until its mass remained constant. Once the torrefied material in the reactor tube had cooled down, the torrefied chips were carefully removed and weighed. Once the DCM in the vial containing the organic layer was evaporated and at constant mass, it was weighed and the difference taken from the empty vial was recorded.

4.3.3 Mass Balance determination

Following torrefaction experiments, an overall mass balance was performed using the experimental mass yields for the solid and liquid products with the mass of the permanent gases determined by difference. The following equations were used to calculate the mass yields:

$$\text{Solid yield } (\eta_m) = \frac{\text{Mass of torriefied material (exiting the torrefaction rig)}}{\text{Mass of untreated material (entering the torrefaction rig)}} \times 100$$

$$\text{Aqueous yield } (\eta_a) = \frac{\text{Mass of aqueous phase}}{\text{Mass of untreated material (entering the torrefaction rig)}} \times 100$$

$$\text{Organic yield } (\eta_o) = \frac{\text{Mass of organic phase}}{\text{Mass of untreated material (entering the torrefaction rig)}} \times 100$$

$$\text{Permanent Gas yield} = 100 - \text{solid yield} - \text{aqueous yield} - \text{organic yield}$$

The gas yields in this work were calculated by difference due to instrument constraints and therefore were unable to quantified using gas chromatography. Each of the torrefaction experiments were performed in duplicate to ensure results from mass balance experiments could be evaluated accurately. The duplicate results produced excellent correlation providing confidence in mass balance determinations. The results of the overall mass balances for the torrefaction of pine and eucalyptus torrefied under each of the conditions shown in Figure 5-2 are presented and discussed in Chapter 5.

4.3.4 Energy Yield

The energy yields for the solid and organic phases were also calculated to determine the amount of energy recovered in each of these products. The energy yields were determined according to the following equations:

$$\text{Energy yield (solid phase)} = \eta_m \, x \, \frac{\text{HHV torrefied material}}{\text{HHV untreated material}}$$

$$\text{Energy yield (organic phase)} = \eta_o \, x \, \frac{\text{HHV organic phase}}{\text{HHV untreated material}}$$

The HHVs correspond to the higher heating values for untreated, torrefied and organic phases and their determination is discussed below in section 4.4.4**.** Results of the energy yields for the solid and organic phases can be found in Sections 5.3.5.2 and 5.3.6 respectively.

4.4 Fuel characterisation

Following torrefaction, the torrefied samples and their untreated counterparts were characterised using a number of different analyses to determine the changes to the fuel chemical and physical properties. A description of the analyses used and sample preparation steps is present below.

4.4.1 Sample preparation

Some of the fuel characterisation analyses required preparation of the samples to smaller sizes prior to analysis. Information on the specific sizes required pertaining to each analysis are

discussed in each respective section however the instruments used for size reduction are discussed below.

4.4.1.1 Retsch SM300 Cutting Mill

Untreated and torrefied wood chips were reduced to smaller size particles (<20mm) using a Retsch SM300 cutting mill shown in Figure 4-5. The wood chips were introduced via a hopper in to the top of the mill before coming in contact with the rotor. Here the biomass is comminuted between three stainless steel blades of the rotor (at 1300rpm) and the stationary double acting cutting bars inserted in the mill before passing through a sieve with a desired size aperture (20mm, 10mm or 4mm). The particles are then collected in a glass jar with cyclone suction ensuring the smallest particles are collected.

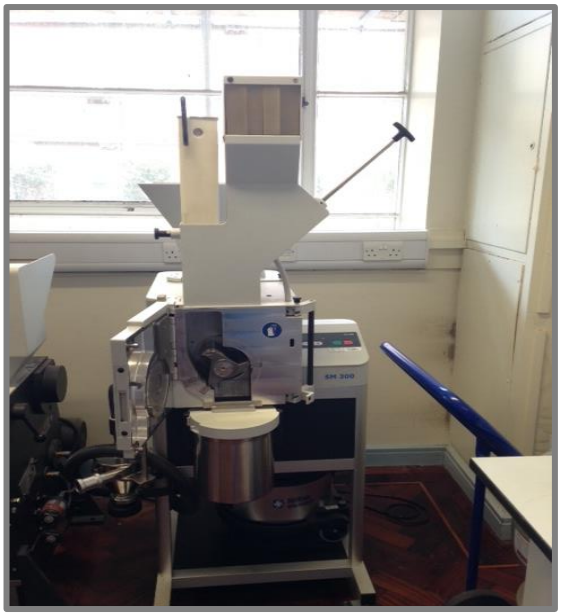

Figure 4-5 – Retsch SM300 Cutting Mill

4.4.1.2 Retsch PM100 Planetary Ball Mill

If requiring further particle size reduction, the biomass particles (after reduction in the cutting mill) could be pulverised using a Retsch PM100 planetary ball mill shown in Figure 4-6. This consisted of a 250mL stainless steel grinding jar in which the biomass samples were added with 15 x 20mm stainless steel balls. Once in place, the jar is then closed and arranged eccentrically on the sun wheel of the ball mill where it is clamped using a safety catch. The mill is then programmed (with a desired time and rpm) in which the grinding jar rotates about its own axis and in the opposite direction around the common axis of the sun wheel. The combination of frictional forces and impact of the grinding balls pulverise the biomass particles.

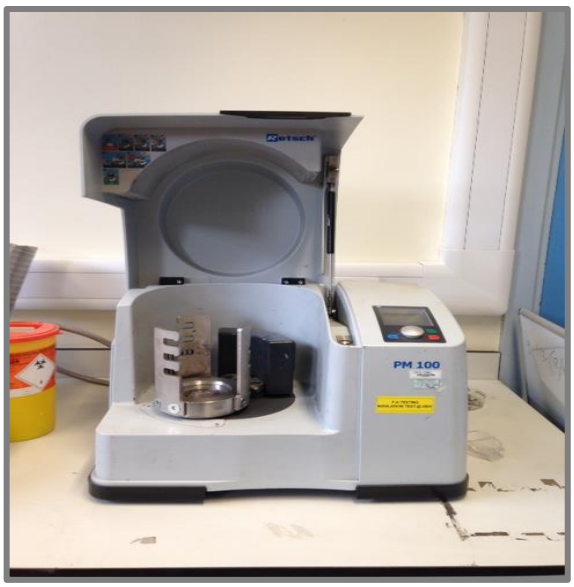

Figure 4-6 – Retsch PM100 Planetary Ball Mill

4.4.1.3 Retsch AS 200 Basic Vibratory sieve shaker

Different size fractions of milled torrefied and untreated biomass samples were obtained using a Retsch AS 200 sieve shaker as shown in Figure 4-7. Different aperture size sieves are stacked (largest on top) with a base at the bottom and the sample poured in to the top sieve. The sieves are then placed on the sieve shaker and clamped in place via a metal plate with two metal rods either side of the sieves. The sieve shaker can then be programmed to for a desired residence time and amplitude of shaking.

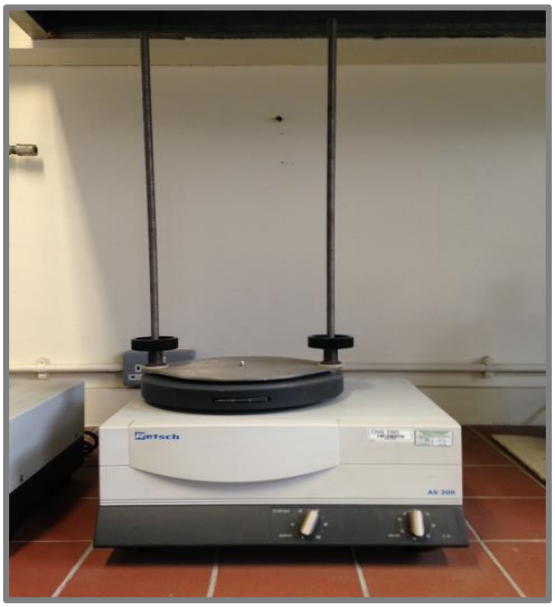

Figure 4-7 – Retsch AS 200 Basic vibratory sieve shaker

4.4.1.4 Spex 6770 Freezer Mill

For analyses that required very small particle sizes (<90µm), a Spex 6770 freezer mill was used to cryogenically mill the samples as shown in Figure 4-8. The use of cryogenic conditions ensured the biomass samples do not fractionate during milling maintaining homogeneity across the sample. Before milling, a few grams of cutting milled sample were added to a polycarbonate grinding vial with a stainless steel end plug. A stainless steel impactor was added to the vial before it was sealed with another stainless steel plug at the other end. The vial was then placed in to the grinding chamber and mill filled with liquid nitrogen. Additional vials could then be placed in a pre-cooling chamber to be milled after the grinding chamber vial was complete. The mill was then programmed to set the number of cycles the mill will go through, the pre-cooling time, run time and cool time (all in minutes) and the grinding rate (in cycles per second (CPS)). Once complete, the grinding vial is removed and allowed to warm up. Following this, the cryo-milled sample is removed from the vial and placed on a 90µm sieve on top of a sieve base. The sample was then gently brushed and the sample passing through the sieve (size fraction of <90µm) was collected for future analysis.

Figure 4-8 – Spex 6770 freezer mill

4.4.2 Proximate analysis

All untreated and torrefied fuels were characterised for their moisture, ash and volatiles contents in duplicate according to the following European Standards: BS EN 14774-3:2009

(moisture) [156], BS EN 14775:2009 (ash) [157], BS EN 15148:2009 (volatiles) [158]. The fixed carbon contents were determined by difference. These analyses were performed to characterise the fuels and to determine the changes in moisture, ash, volatiles and fixed carbon upon torrefaction under each condition. Each of these determinations will be discussed in more detail below.

4.4.2.1 Moisture Content Determination

For moisture content determination, the untreated and torrefied fuels to be analysed were cutting milled and sieved to obtain a size fraction of <1mm. Following this, a number of glass dishes and their lids were dried at 105°C in an oven (until constant mass) and then removed and allowed to cool to room temperature in a desiccator. Once cooled, the dishes and lids were weighed following which approximately 1g of each sample to be analysed was added to two respective dishes (duplicate) and weighed. The uncovered dishes containing sample and their lids were then dried at 105°C for 3 hours (until constant mass). Once completed, the lids were placed on the dishes before removal from the oven and allowed to cool to room temperature in a desiccator. Once cooled, the dishes with sample and lids were weighed and the moisture content, $\mathrm{M_{ad,}}$ expressed as a percentage by mass, for each sample was determined according to the following formula:

$$\mathrm{M_{ad}} = \frac{\mathrm{m_2 - m_3}}{\mathrm{m_2 - m_1}} \mathrm{x}\ 100$$

Where,

m_1 = the mass of the empty dish and lid (g)

m_2 = the mass of the dish plus lid plus sample before drying (g)

m_3 = the mass of the dish plus lid plus sample after drying (g)

4.4.2.2 Volatiles Content Determination

Prior to analysis, all fuels to be analysed were cutting milled and sieved to obtain a size fraction <1mm. Before analysis, 4 silica crucibles and their lids were placed in a stand and inserted in to a Carbolite VMF (+PID/CHIM) furnace at 900 (±10) °C for 7 minutes. The crucibles and lids in the stand were then removed and allowed to cool to room temperature on thermo-resistant plate before storage in desiccator. Once cooled, the crucible and lids were weighed after which

approximately 1g of each sample was added to two respective crucibles (duplicate), the lids replaced and weighed again. The charged crucibles were then inserted back in to the cool stand and inserted in to the oven at 900 (±10) °C for 7 minutes. After this, the stand and crucibles were removed and placed on the thermo-resistant plate to cool to between 30 and 50°C before further cooling to room temperature in a desiccator. The crucible, lids and resultant chars were then re-weighed and the volatiles content, V_d, expressed as a percentage by mass on a dry basis was determined using the following equation:

$$V_d = \left[\frac{100(m_2 - m_3)}{m_2 - m_1} - M_{ad}\right] x \left(\frac{100}{100 - M_{ad}}\right)$$

Where,

m_1 = the mass of the empty crucible and lid (g)

m_2 = the mass of the crucible and lid and test portion before heating (g)

m_3 = is the mass of the crucible and lid and contents after heating (g)

M_{ad}= is the moisture content, as a percentage of mass, in the sample being analysed determined according to BS EN 14774-3:2009 (see section 4.4.2.1)

4.4.2.3 Ash Content Determination

As for the moisture and volatiles determinations, the ash content determination required all samples to be <1mm in size. Prior to analysis, a number of ceramic dishes were dried at 105°C until constant mass and stored in a desiccator to cool to room temperature. After drying, approximately 1g of each sample was added to two respective dishes (duplicate) and inserted in to a cool furnace. The temperature was then gradually raised to 250°C at a heating rate of 7.5°C/min. The samples were then held at this temperature for one hour to allow the volatiles to leave before sample ignition. The samples were then heated, at a rate of 10°C/min, to 550 (±10) °C where the samples were kept at this temperature for two hours. Once completed, the dishes, now containing ash, were removed and allowed to cool on a heat-resistant plate for 10 minutes before further cooling to room temperature in a desiccator. As soon as the crucibles reached room temperature, they were then re-weighed and the ash contents, A_d, of each sample, expressed as a percentage by mass on a dry basis, were calculated using the following equation:

$$A_d = \left(\frac{m_3 - m_1}{m_2 - m_1}\right) \times 100 \times \left(\frac{100}{100 - M_{ad}}\right)$$

Where,

m_1 = the mass of the empty dish (g)

m_2 = the mass of the dish and test portion (g)

m_3 = is the mass of the dish and ash (g)

M_{ad}= is the moisture content, as a percentage of mass, in the sample being analysed determined according to BS EN 14774-3:2009 (see section 4.4.2.1)

4.4.2.4 Fixed Carbon Content determination

The fixed carbon content, on a dry basis, was determined using the results of the volatiles and ash determinations using the following formula:

$$FC_d = 100 - V_d - A_d$$

4.4.3 Ultimate analysis

The elements C, H, N (and S for) untreated and torrefied biomass samples and the tar products from torrefaction were determined using a CE Instruments Flash EA 1112 Series elemental analyser (Figure 4-9) using the methodology laid out in the European Standard BS EN 15104:2011 [159]. These analyses were performed to characterise the fuels for the elemental composition, to determine the changes in elemental composition after torrefaction and to perform elemental, mass and energy balances for each torrefaction experiment.

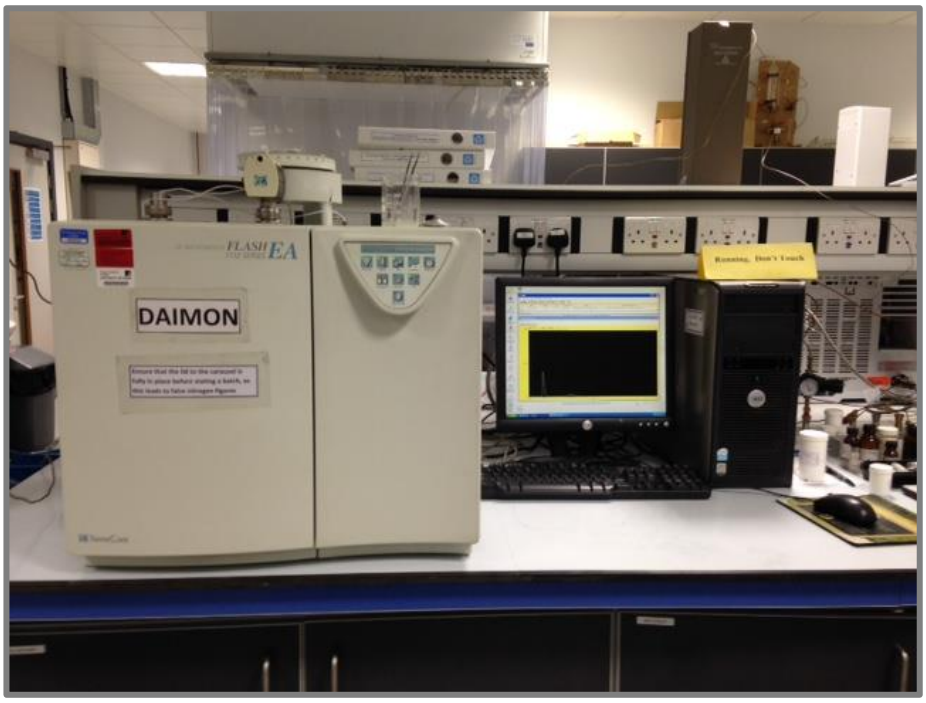

Figure 4-9 – CE instruments Flash EA 112 Series elemental analyser

Prior to analysis, gas leak tests were performed and the instrument was set at 900°C. During the heating period, approximately 2.5mg of each of the calibration standards and solid biomass samples (cryomilled and sieved to obtain a sample size <90µm) were added to small tin capsules respectively, weighed and folded. The calibration standards used during analysis were: atropine, methionine, cysteine, sulphanilamide and 2, 5-Bis (5-tert-butyl-benzozazol-2-yl) thiophene (BBOT). For the tar samples, approximately 3mg of sample was added in drops to a tin capsule, weighed and folded before insertion in to another tin capsule and folded again. For every ten samples, a calibration standard was prepared (as above) to be analysed as an unknown to ensure the results for the sample unknowns are valid.

Once prepared, the standard and sample information (i.e. IDs and weights) were input using the analyser software and the samples were placed in the auto-sampler with a blank (i.e. a tin capsule with no sample or standard) added first followed by the calibration standards then the biomass and tar samples. The solid samples were each performed in duplicate and the tar samples in triplicate. During analysis, the standards and samples in turn fall in to the reactor chamber where an excess of oxygen is introduced and the samples are combusted in the combustion tube (containing quartz wool and metal catalysts) to produce gases CO_2 (and CO), H_2O and N_2 (and NO_x). These reaction gases are then swept through the combustion tube, via a helium carrier gas, to the reduction tube (at a cooler temperature: ~650°C) where the gases are

swept over copper to remove excess oxygen and to reduce any NO_x to N_2 (via oxidation of the copper to copper oxide) and over copper oxide at the end of the reduction tube to convert any CO to CO_2. These gases then undergo mixing before entering a gas chromatography (GC) column where they separate at different rates. Once the gases exit the column, they are detected by a thermal conductivity detector (TCD) in the order N_2, CO_2 then H_2O. For analysis of sulphur contents, the samples were analysed using a singular CHNS combustion/reduction tube. The products of sulphur combustion are SO_2 and SO_3; the copper in the reactor tube used to reduce any SO_3 combustion products to SO_2. The SO_2 gases exit the GC column after H_2O. The results of the CHNS are obtained on an as received basis. These were converted to a dry and dry-ash-free (daf) basis using the following equations:

$$\text{Wt\%}_{\text{dry (C,N,S)}} = \text{Wt\%}_{\text{ad}} \times \frac{100}{100 - \text{M}_{\text{ad}}}$$

$$\text{Wt\%}_{\text{dry (H)}} = \left(\text{Wt\%}_{\text{ad}} - \frac{\text{M}_{\text{ad}}}{8.937}\right) \times \frac{100}{100 - \text{M}_{\text{ad}}}$$

$$\text{Wt\%}_{\text{daf (C,N,S)}} = \text{Wt\%}_{\text{ad}} \times \frac{100}{100 - \text{A}_{\text{ad}} - \text{M}_{\text{ad}}}$$

$$\text{Wt\%}_{\text{daf (H)}} = \left(\text{Wt\%}_{\text{ad}} - \frac{\text{M}_{\text{ad}}}{8.937}\right) \times \frac{100}{100 - \text{A}_{\text{ad}} - \text{M}_{\text{ad}}}$$

Where,

$\text{Wt\%}_{\text{dry (C,N,S)}}$ = the dry basis for carbon, nitrogen and sulphur

$\text{Wt\%}_{\text{dry (H)}}$ = the dry basis for hydrogen

$\text{Wt\%}_{\text{ad}}$ = the weight percent as determined from elemental analysis

M_{ad} = the moisture content as determined by proximate analysis

$\text{Wt\%}_{\text{daf (C,N,S)}}$ = the dry ash free basis for carbon, nitrogen and sulphur

$\text{Wt\%}_{\text{daf (H)}}$= the dry ash free basis for hydrogen

A_{ad} = the ash content as determined by proximate analysis.

8.937 = the mass ratio of H_20/H_2

The oxygen contents, on a dry and dry ash free basis, were determined using the following equations:

$$\mathrm{O\%_{dry}} = 100 - \mathrm{C\%_{dry}} - \mathrm{H\%_{dry}} - \mathrm{N\%_{dry}} - \mathrm{S\%_{dry}} - ash$$

$$\mathrm{O\%_{daf}} = 100 - \mathrm{C\%_{daf}} - \mathrm{H\%_{daf}} - \mathrm{N\%_{daf}} - \mathrm{S\%_{daf}}$$

4.4.4 Higher Heating Value Determinations

The higher heating values for all untreated and torrefied biomass samples were determined either experimentally using bomb calorimetry or estimated using the Friedl correlation [160]. These experiments were performed to characterise the original heating values of the untreated fuels and to determine the changes after torrefaction. Knowledge of the HHVs was also necessary to perform energy balances of the torrefaction reactions performed. Descriptions of these methods are presented below.

4.4.4.1 Bomb Calorimetry

The higher heating values of the untreated and torrefied pine samples (See Chapter 5) were determined experimentally using a Parr 6200 Bomb Calorimeter (Figure 4-10) using the methodology set out in the European standard BS EN 14918: 2009 [161]. Prior to analysis, around 10mL of ultra-high quality (UHQ) water was used to rinse the inside of the bomb body. The calorimeter can was then filled with exactly 2000g of deionised water and placed in the calorimeter jacket. Around 0.5g of sample was weighed in the sample cup and 10cm of ignition wire was wrapped around the two electrodes of the bomb lid creating a bent 'U' shape. The filled sample cup was then placed in the sample head just beneath the wire and the lid placed in to the bomb body and screwed in gently.

The bomb was then filled with oxygen and then set in place at the bottom of the calorimeter can. The lid of the instrument containing a stirrer (to maintain even distribution of water) and thermometer was then closed submerging these in to the water and the instrument started. Once started, the ignition wires are gradually heated via the two electrodes until the sample ignites resulting in combustion of the sample. The heat released from combustion results in a temperature change in the water in the calorimeter can measured using the thermometer

attached to the lid. The heat of combustion, H_C (or HHV) of the sample is then calculated by a substitution procedure in which the heat released by the sample being analysed is compared with the heat released from the combustion of a calibrant (benzoic acid) with a known heat of combustion. Each of the samples analysed were performed in duplicate and the average values reported in Section 5.3.5.2.

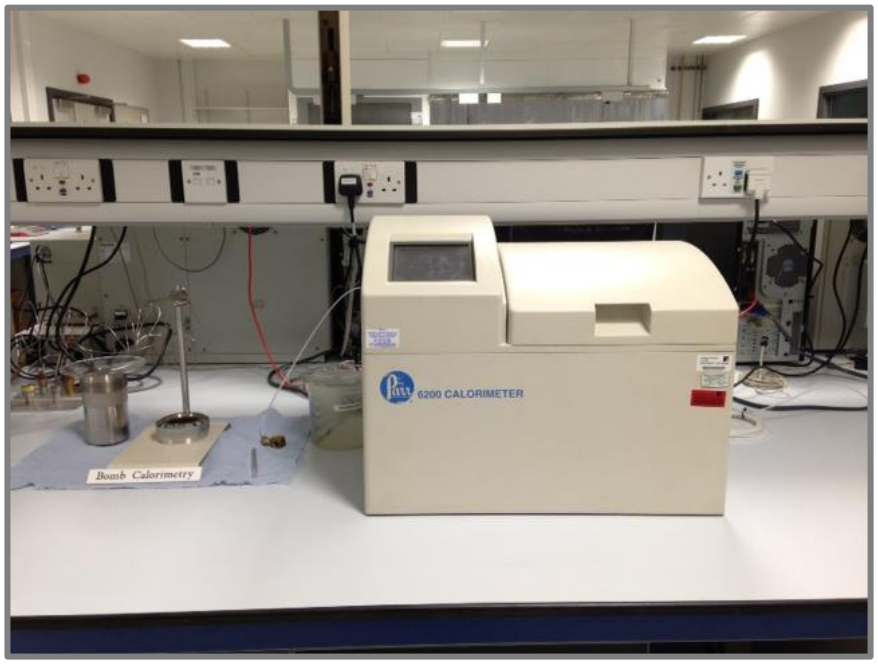

Figure 4-10 - Parr 6200 Bomb Calorimeter

4.4.4.2 Friedl estimation of HHV

The higher heating values of the untreated and torrefied pine and eucalyptus fuels were estimated using the correlation derived by Friedl et al. [160]. In their study, the authors used 122 biomass samples with known elemental composition (C, H, N, O, S, Cl and ash on a dry basis) to calculate two regression models: an ordinary least square regression model (OLS) and a particle least square regression model (PLS) for the prediction of HHV from the elemental composition shown below:

$$\text{HHV (OLS model)} = 1.87C^2 - 144C - 2820H + 63.8C \times H + 129N + 20147$$

$$\text{HHV (PLS model)} = 5.22C^2 - 319C - 1647H + 38.6C \times H + 133N + 21028$$

The authors found both models yielded almost identical results thus produced a model with an average of both, resulting in a final model for HHV prediction as follows:

$$HHV = 3.55C^2 - 232C - 2230H + 51.2C \times H + 131N + 20600$$

This final model was used to estimate the HHVs (in MJ/kg) of the untreated and torrefied pine and eucalyptus and can be found in Section 5.3.5.2.

4.4.5 Total Organic Carbon (TOC)

The total organic carbon contents of the aqueous phase products of torrefaction were determined using a Hach Lange IL550 TOC analyser as shown in Figure 4-11. This analysis was performed to determine the distribution of carbon to the aqueous phase during torrefaction in the overall carbon elemental balance (See Section 5.3.7.1)

Before analysis, the aqueous phase samples were diluted 100x to ensure the sample concentrations were within calibrated range of the instrument (high concentration variant range: 10-1000ppm). Following this, around 10mL of each sample was added to respective sample vials and a stirrer bar added to each. These were then placed in auto-sampler and the instrument started. The TOC method utilised in these experiments was the differential method whereby the total inorganic carbon (TIC) is determined via its reaction with acid at room temperature to form carbon dioxide which then passes through a non-dispersive infrared detector. The total carbon (TC) is then determined by the combustion of organic carbon and thermal decomposition of inorganic carbon. The total organic carbon (TOC) is derived from the difference between TC and TIC. In this instance, the TIC contents of each sample was zero, thus the TC = TOC. Results of the TOC analysis for the aqueous phase products from the torrefaction of pine and eucalyptus can be found in Section 5.3.6

Figure 4-11 - Hach Lange IL550 TOC analyser

4.4.6 Grindability Test – Hardgrove Grindability Index equivalent

Grindability tests were performed on untreated and torrefied pine to determine the changes in milling performance upon torrefaction. The test employed in this study was the revised Hardgrove Grindability Index (HGI) method as described by Jones et al. [121] which is a modification of the British Standard HGI determination BS 1SO 5074:2015 [162] used to determine the HGI of hard coal. In the British Standard method, 50g of air dried coal with particle size distribution 600µm – 1.18mm is ground for 60 revolutions in a bespoke Hardgrove instrument. The mass of particles that then passes through a 75µm sieve is then measured and the HGI determined by comparison of this mass on a calibration curve of mass passed through vs. HGI for coals with known HGIs. While this method is standardised and objectively simple, drawbacks include the need for bespoke expensive instrumentation and large amounts of sample required [162]. Thus, the revised 'Hardgrove Grindability Index equivalent ($HGI_{equiv.}$)' was employed as described below.

4.4.6.1 Calibration

The calibration used to determine the $HGI_{equiv.}$ was obtained from a previous study [83]. To describe the calibration methodology however, approximately 1000g of four coals with known HGI values: 35, 49, 66 and 92 were each ground using a Retsch Cutting mill SM100 with a 4mm screen. These were each sieved to obtain a particle size distribution of 600µm – 1.18mm.

Following this, 50cm^3 of sample was measured using a measuring cylinder and its mass recorded – note the HGI_{equiv} uses a smaller *volume* while the HGI standard test uses a greater *mass* (50g). The 50cm^3 standards were then placed in a 250mL stainless steel milling cup with 15x20mm stainless steel balls and ground for 2 minutes at 165rpm using a Retsch PM100 planetary ball mill. This ground sample was then sieved for 5 minutes on a 75µm sieve and two fractions weighed once completed. If there is loss of > 0.5g the test was aborted and repeated. The mass passing through the sieve was calculated according to the following equation:

$$\mathrm{m} = \mathrm{m_v} - \mathrm{m_1}$$

Where,

m_v = the mass of the 50cm^3 sample

m_1= the mass of sample collected on the sieves.

The process for each coal standard was repeated three times and an average calculated. The results were then used to plot a calibration for the mill of HGI vs. mass pass through the 75µm sieve as shown in Figure 4-12.

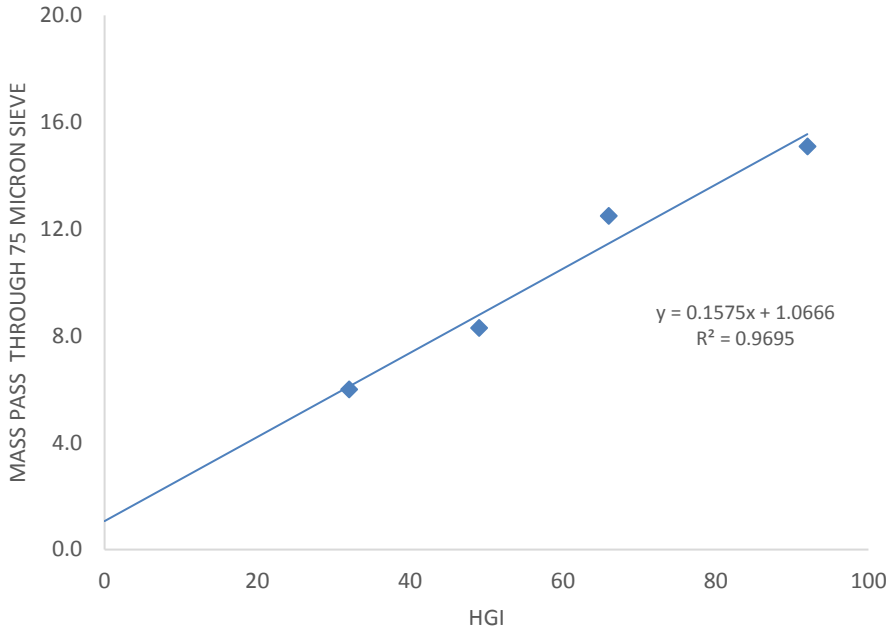

Figure 4-12 - Calibration of coals with known HGI to determine the $HGi_{equiv.}$ of untreated and torrefied pine

4.4.6.2 Testing of biomass fuels

Testing of the untreated and torrefied biomass fuels involves repeating the measuring, weighing and grinding steps discussed above in section 4.4.6.1. The HGI_{equiv} of the fuels is then determined from the mass passing through the 75µm sieve and the calibration curve.

4.4.7 Particle Size Distribution

Particle size distributions for untreated and torrefied pine were also performed to further determine the grindability characteristics of these fuels beyond that of the HGI_{equiv} tests. This involved the same grinding process as described above for the HGI_{equiv} tests however the samples were sieved on a series of sieves with size fractions: 600, 355, 212, 150, 75 and 53µm. The samples were sieved on a sieve shaker for 5 minutes following which the masses of sample left on each sieve were weighed and recorded as a percentage of the original mass of the sample. A particle size distribution was then plotted with each point taken as the average particle size between two sieve size fractions e.g. 477.5µm = (600 + 355)/2. The result of the particle size distribution for untreated and torrefied pine can be found in Section 5.3.5.4.

4.4.8 Surface Area Analysis

The specific surface areas of untreated and torrefied biomass fuels presented in Chapter 5 and the untreated and torrefied fuels and chars (char preparation discussed below in Section 4.5) presented in Chapter 6 were determined using a Micromeritics Tristar 3000 and Quantachrome Nova 2200 respectively (Figure 4-13). The methodology used in surface area determination was the Brunauer-Emmett-Teller (BET) [139] method with nitrogen as the adsorbing gas. The surface areas for the untreated and torrefied fuels were determined to assess any changes to the surface on the biomass particles upon torrefaction. The char surface areas were analysed firstly to determine the changes to the surface upon rapid devolatilisation and secondly to determine the intrinsic reactivity of the chars.

Figure 4-13 - Quantachrome Nova 2200 (left) and Micromeritics Tristar 3000 (right)

Prior to analysis, the untreated and torrefied fuel samples were weighed in their reaction tubes before degassing under N_2 flow at atmospheric pressure at 150°C for 2 hours. The de-gassing preparation step is essential to remove any absorbed moisture or contaminants on the surface that may interfere with analysis. The samples were then weighed again to determine the change in mass (i.e. loss of surface impurities) after de-gassing. For the chars, the same pre and post de-gassing weighing was performed however the samples were de-gassed under vacuum (in the

Nova de-gassing station) for 1 hour at 90°C before the temperature was raised to 300°C and the samples de-gassed for a further 3 hours. Following this, the sample tubes were screwed in to their respective stations and the Dewar flask, in which the sample tubes are to be submerged, filled with liquid nitrogen. The samples tubes are then evacuated and then submerged in the liquid nitrogen once evacuation is complete. At the beginning of analysis, the sample is exposed to a small volume of nitrogen gas (at its liquefaction temperature: 77K). These gas molecules may then be attracted to the surface of the sample by its intrinsic surface energy and become physisorbed i.e. physically adsorbed. This adsorption occurs as a result of the attractive (and repulsive) forces between individual adsorbate molecules and the atoms on the surface of the sample. The energy of the forces of physisorption do not exceed 40-50 kJ/mol thus are relatively very weak and physisorbed molecules can be removed via decreasing the pressure/increasing the temperature. As the pressure in the cell is increased, the quantity of gas molecules approaching the surface at any given time increases thus the quantity adsorbed increases i.e. adsorption is a function of increasing pressure. As pressure in the cell increases further; this results in monolayer (one molecule thick) and multilayer coverage. The coverage of adsorbate molecules on the surface of a sample are plotted on an adsorption isotherm which is defined as the quantity of gas adsorbed vs. the relative pressure. Note the relative pressure is used in plotting the adsorption isotherm (not the absolute pressure) and is defined as the ratio of absolute pressure (p) to the saturation pressure (p_0); the saturation pressure defines as the vapour pressure of a pure liquid.

The specific surface areas are thus estimated using the BET method [139] mentioned above which is an extension of the Langmuir model. The BET equation is shown below and describes the isotherm in which the quantity of gas adsorbed is a function of relative pressure:

$$q_a = \frac{q_m \, C \, p}{(p_0 - p)[1+(C-1)p/p_0]}$$

Where,

q_a = quantity adsorbed for a given relative pressure

q_m = quantity of gas required to produce a monolayer

p = absolute pressure

p_0 = saturation pressure

C = constant associated with adsorption energy

To derive the specific surface area, the BET equation is plotted in its linear form shown below:

$$\frac{p}{q_a(p_0 - p)} = \frac{1}{q_m C} + \frac{C-1}{q_m C}\frac{p}{p_0}$$

If the data from the adsorption isotherm conforms to the BET model, plotting the left hand side of this equation against relative pressure will yield a plot with a linear region (in the nominal region 0.05-0.3 p/p_0) in which q_m and C can be determined. From this, the specific surface area is determined using the following equation:

$$\text{Specific surface area} = \frac{q_m \sigma N_a}{m}$$

Where,

q_m = quantity of gas required to produce a monolayer

σ = the cross sectional surface area of nitrogen at 77K (0.162 nm^2/molecule [163])

N_a = Avogadro's number

m = the mass of sample used during analysis

Full adsorption isotherms were analysed for both the chars and fuels and the equilibrium time for the fuels and chars set at 1 and 2 minutes respectively. The specific surface areas were derived from the multipoint (3-5 point) BET plots with a linear correlation ≥ 0.995.

4.4.9 Scanning Electron Microscopy (SEM) and Energy Dispersive X-ray spectroscopy (EDX)

SEM images of untreated and torrefied biomass fuels and chars were taken using a Carl Zeiss EVO MA15 scanning electron microscope shown in Figure 4-14. Semi-quantitative metals (specifically potassium) concentration determination on the fuels and high-heating rate chars from untreated and torrefied willow and eucalyptus was performed using Energy dispersive x-ray spectroscopy using an Aztec Energy EDX system (on the Carl Zeiss EVO MA15) with AELEOS software for data analysis. Images for both fuels and chars were acquired to ascertain any changes to surface morphology during torrefaction of fast devolatilisation.

Prior to SEM imaging, a small amount of the fuels and chars (~2mg) were each coated on an adhesive sticker on an aluminium stub. The samples were then spluttered with a gold coating to create a conductive layer across the sample to prevent charging during analysis as a non-conductive surface can build up a static negative charge which interferes during imaging. Where EDX was employed, the samples were ground using a pestle and mortar and prepared as above. Once prepared, the samples were screwed into the imaging platform inside the instrument chamber and set under vacuum. Images of varying magnification were then acquired with an incident electron beam of 20kV across different segments of the stubs using either secondary electrons or backscattered electrons (these described below) to acquire images. For EDX analysis, a similar technique was employed whereby the metals concentrations for various segments of the stub were determined at random and average value taken for a given sample.

During SEM analysis, a beam of electrons is focussed on to the sample within the chamber induced from an electron gun (cathode). The electrons are finely focussed on to the sample using an anode and series electromagnetic condenser lenses. The electrons then scan the sample (left to right and up and down) depending on the degree of magnification selected i.e. greater magnification = smaller scanning area.

As the electron beam hits the sample, depending on the mode of analysis selected, either secondary electrons (SE) or back-scattered electrons (BSE) are released. In the case of the former, when the electron beam hits the sample, the sample absorbs the electrons and gives off its own electrons. These electrons are attracted to a positively charged faraday cage and then hit the detector. The detector then uses the information from these electrons to create an image

on a computer screen. In the case of back-scattered electron imaging, the electrons from the beam hit the sample and are reflected back out of the sample on to a detector attached to the pole piece (above the sample). These electrons penetrate deeper than secondary electrons.

Figure 4-14 - Carl Zeiss EVO MA15 scanning electron microscope

During EDX analysis, the incident electron beam penetrates even deeper in to the sample where it may hit an inner-shell electron of a sample atom in the ground state. When the incoming electron beam is greater than the binding energy of inner-shell electrons (~few hundred electron volts for inner-shell excitation [164]), this can result in excitation creating an electron hole or vacancy. The presence of an inner-shell vacancy creates instability in the atom resulting in an outer energy level (or shell) electron 'jumping' to fill the vacancy. As the outer energy level electron jumps, it emits energy in the form of an x-ray. The shells are characterised according to the Rutherford-Bohr atomic model, from inside outwards starting with the letter K then L, M and so on; each of these corresponding to the principle quantum number *n* (principle electron shell: n = 1(K), n = 2(L), n = 3(M) etc.). The electrons in each of these shells are further characterised by their orbital angular momentum quantum number *l*, which determine the shape of an orbital (i.e. s, p, d, f orbitals etc.) and its value is dependent on principle quantum

number with the relationship: *n-1* where it can take the value zero (unlike the principal quantum number). Thus, electrons in the K shell with n = 1 can have an *l* value of 0, when n = 2 (M shell), l = 0 or 1 and so on. The electrons are characterised further according to their magnetic quantum number (m_l) which determine the number of orbitals and their orientation within a subshell; its values dependent on the angular momentum quantum number *l* where, given a specific value for *l*, m_l is an interval ranging from *+l* to *–l.* For example for n = 2 and *l* = 0 and 1, m_l can have the values -1, 0 and 1. The final quantum number, m_s, is the electron spin quantum number and designates the direction of electron spin either *+1/2* or *-1/2* and is not governed by another quantum number. Figure 4-15 shows a schematic of the inner shells present in an atom where for example in Shell L (n = 2), three subshells exists according to the magnetic quantum number *l*. According to the Pauli Exclusion Principle no two electrons in inner shells can occupy the same quantum state simultaneously and so the jumping of these electrons from outer to inner shells is thus characteristic according to their quantum state and thus their position within the atom. Subsequently, the x-rays released are characteristic in energy and wavelength to the atom (and thus element) and specific shells in which they take place. The x-rays emitted are characterised by these shell and subshell transitions e.g. if an electron is excited from the K subshell, and is filled with an L-shell electron, the x-ray is characterised as a K-α x-ray. If it is filled by an M-shell electron, the x-ray is a K-β x-ray. An example of the transitions and x-ray emissions are shown in Figure 4-15 above where the Roman and Greek letters and numbers characterise the transition between subshells.

It is important to note that Roman letters and numbers attributed to x-ray emissions are associated with their relative intensities as opposed to their orderly sequence within the atom (this nomenclature was assigned when the atomic structure of atoms was much less well understood) [164]. The x-rays emitted are then detected by an x-ray detector following which EDX spectra are generated specific to individual elemental shell transitions. A spectral range of 0-20kV can detect elements from boron to uranium and the higher the atomic number, Z, the greater the number of peaks on an EDX spectra. The data from the EDX spectra can that be used to estimate a weight percent of each of these species in the sample.

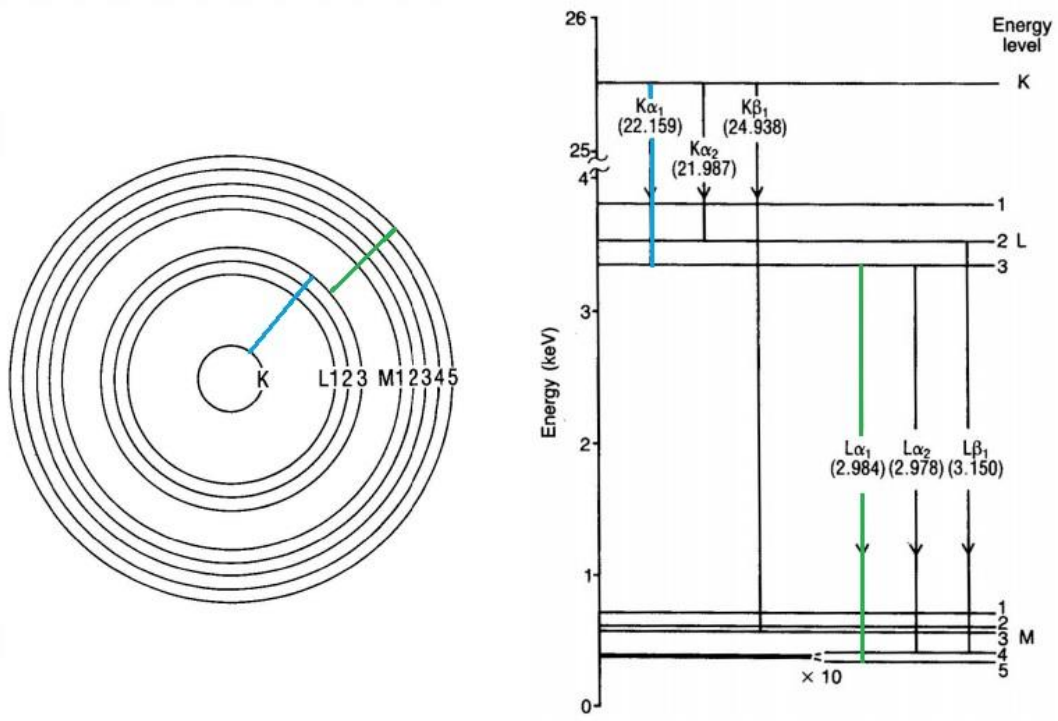

Figure 4-15 – Schematic of atomic inner electron shells (left) and energy level diagram for silver showing characteristic x-ray emissions between subshells where the arrows denote direction of vacancy (right). The blue and green lines on both images correspond to the same vacancy transitions respectively. Edited from [165]

4.4.10 Inductively Coupled Plasma Mass Spectrometry (ICP-MS)

The untreated and torrefied willow and eucalyptus samples which are discussed in Chapter 5 were analysed for their total metals concentration using a Perkin Elmer Elan DRCe ICP-MS shown in Figure 4-16. The principle metal of investigation is potassium (K) to determine the changes in concentration upon torrefaction. Before analysis, the solid samples were digested using an Anton Parr Multiwave 3000 Microwave. This was done by adding approximately 0.2g of sample inside Teflon digestion vessels and adding 10mL Nitric acid using an automatic pipette. The vessels were sealed and transferred to the microwave where by a bio-char digestion programme was employed. This 3-stage programme involves systematically ramping the samples to 200°C over a time period of 70 minutes. Once complete, the samples were cooled and transferred to a fume cupboard where they were vented slowly and allowed to stand for 10 minutes to allow all of the acidic NO_x vapours to exit the vessels. The samples and seals were then rinsed with UHQ water and diluted gravimetrically to 50mL in centrifuge tubes. The diluted samples were then inverted 10 times to ensure mixing and allowed to stand for 24 hours. Before ICP-MS analysis (on the day of analysis) the samples were diluted 100x to ensure concentrations lay

within the limits of detection of the instrument. The potassium metals concentrations for the untreated and torrefied willow and eucalyptus fuels can be found in Section 6.1.3.1.

Figure 4-16 – Perkin Elmer Elan DRCe ICP-MS

During ICP-MS analysis, the digested samples are introduced as aerosol droplets to a high temperature (6000-10000°K) argon plasma. This plasma dries the aerosol and ionises components in the sample creating positively charged particles (+1/+2 charge). These particles are then directed at the mass filtering device which in this instance is a quadrapole made up of four parallel rods with pairs of rods in different planes. All of the rods are electrodes with both direct current (DC) and alternating radio frequency current (AC/RF) voltages, with opposite pairs of rods having the exact same voltage profile. One pair (of opposing rods) contains a positive charge supplied from the DC which can be alternated to negative (and back to positive) by the AC based on the selected AC/DC voltage ratios applied. These pairs of rods serve as 'high mass filters' in which heavy molecules or elements (high mass) travel through the centre of the quadrapole as a result of the alternating current while the lighter species 'crash' in to the poles as their light mass allows for quick trajectory change when the current is negative. The other pair of rods is supplied with a negative charge from the DC which can alternate from negative to positive from the AC. These serves as 'low mass filters' where by the lighter species travel through the quadrapole and the heavy species crash in pole as their trajectory cannot be changed as quick i.e. when the current is negative their electrostatic attraction pulls the species towards the pole. In brief, the positive rods remove species below a certain mass/charge (M/Z)

ratio and the negative rods remove species above a certain M/Z ratio. Working in combination, these create a 'spiral flow' of ions through the quadrapole whereby the species travel through to the detector which counts individual ions exiting the quadrapole. The ions striking the detector hit an active surface called a dynode which releases electrons to hit a second dynode creating a cascade of electrons until a pulse is generated. By counting these electrons, the instrument counts the number of ions hitting the first dynode thereby identifying the number of ions with a specific M/Z ratio. Thus, the varying voltage can be applied to a specific or range of M/Z ratios in which a mass spectrum of number of ions vs. M/Z can be derived and the elements determined.

4.4.11 Determination of Cell Wall Components

Knowledge of the absolute and relative amounts of each of the cell wall components: hemicellulose, cellulose and lignin before and after torrefaction allows for the understanding of how torrefaction at a given temperature and residence time affects the biomass sample. The holocellulose (hemicellulose and cellulose) and lignin contents were determined from gravimetric measurements of Neutral Detergent Fibre (NDF), Acid Detergent Fibre (ADF) and Acid Detergent Lignin (ADL) based on the Van Soest method [166] using a Gerhardt fibrecap system [167]. The analyses were carried out by the Institute of Biological, Environmental and Rural Sciences (IBERS) at the University of Aberystwyth. All of the untreated and torrefied pine and eucalyptus samples in Chapter 5 were analysed for these components.

During analysis, the NDF contents are determined which correspond to the cell wall components (hemicellulose, cellulose and lignin) corrected for ash. This is determined after refluxing in a neutral buffered detergent solution for one hour [167]. The ADF contents which correspond to cellulose and lignin (corrected for ash) are determined after refluxing the samples in a solution of cetyltrimethylammonium bromide (CTAB) in 2M sulphuric acid [167]. ADL was determined via treatment of the ADF with 72% sulphuric acid (H_2SO_4) to dissolve the cellulose fraction to determine the lignin weight percent [167]. Thus, the hemicellulose, cellulose and lignin contents were calculated according to the following equations:

$$\text{Hemicellulose (\%)} = \text{NDF (\%)} - \text{ADF (\%)}$$

$$\text{Cellulose (\%)} = \text{ADF (\%)} - \text{ADL (\%)}$$

Lignin (%) = Acid treatment of ADF (%)

In addition to the ADL contents, the Klason lignin contents were determined. These contents were determined as some authors have noted that small amounts of acid-soluble lignin may be lost during the ADF treatment step of the ADL method [168] although this is more prevalent in grasses as opposed to woody biomasses [169]. The Klason lignin contents were determined using a standard two-step hydrolysis procedure by hydrolysing 0.5g of sample with 5mL of 72% H_2SO_4 for two hours at room temperature and stirring the sample every 15 minutes. Following this, the samples were then diluted with 140mL water and refluxed for 4 hours. The acid insoluble material was then recovered by filtration, washed several times with water (to remove excess acid), dried and then weighed and corrected for ash. The ash contents for all analyses were determined after heating in a muffle furnace at 600°C for 4 hours.

4.4.12 Chlorine contents determination

The chlorine concentrations of untreated and torrefied willow and eucalyptus were determined by the analytical department in the Department of Chemistry at the University of Leeds. The chlorine contents were determined by titration with mercury nitrate ($HgNO_3$) to ascertain the changes in chlorine concentration upon torrefaction.

4.5 Preparation of fast-heating rate chars at high temperature using a drop tube furnace (DTF)

4.5.1 Drop Tube Furnace (DTF)

Chars from each of the untreated and torrefied biomass fuels were prepared using a Drop Tube Furnace (DTF). The DTF was designed and commissioned by Dr Leilani Darvell and fabricated by Elite Thermal Systems consists of an alumina tube of 1400mm (L) x 65mm (I.D) inserted in to an electrically heated furnace as shown in Figure 4-17. The furnace is 1165mm and inside is a 610mm heated reaction zone is controlled using three independent PID controllers. Within the heated reaction zone is a measured 455mm isothermal zone- a schematic of which is shown in Figure 4-18.

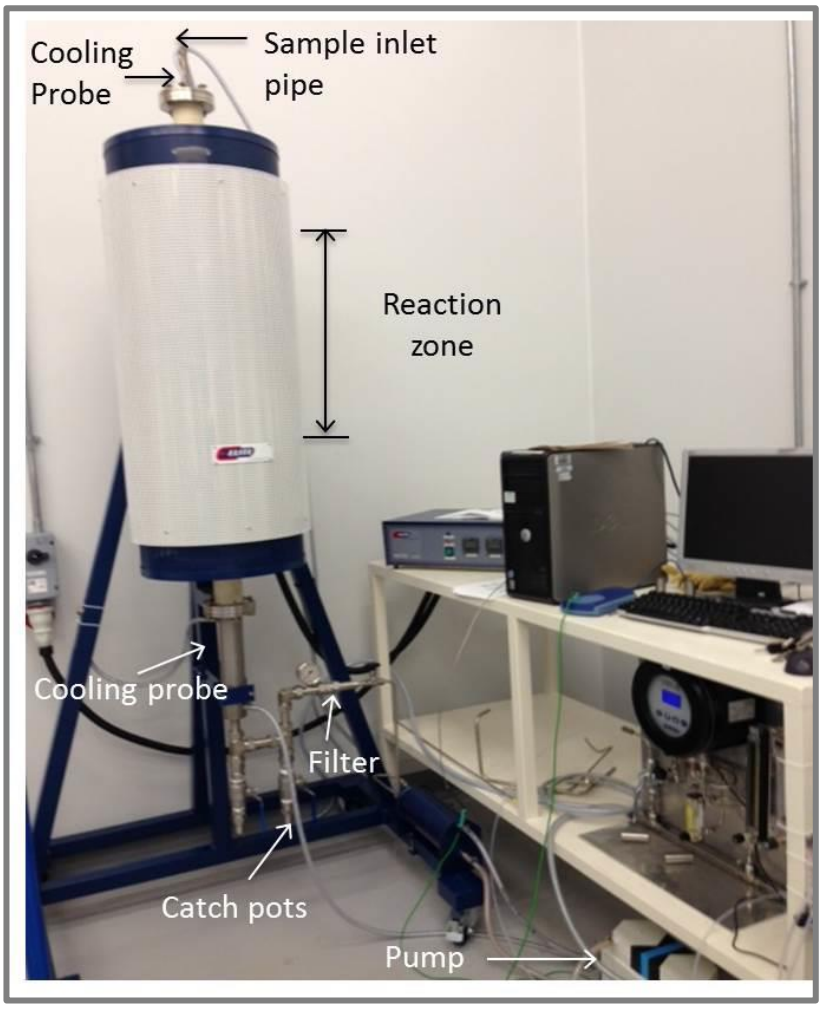

Figure 4-17 – Schematic of drop tube furnace used to prepare fast-heating rates chars from untreated and torrefied biomass fuels

To the top of the furnace is the sample inlet pipe where the biomass particles are introduced. Just beneath the sample inlet is the primary gas inlet which is supplied with pure nitrogen gas (from a manifold) and controlled using a flow meter. The gas is pulled through the reactor by a pump; this process also pulls some air through the top of the reactor (from the sample inlet pipe) introducing some oxygen to the system. The oxygen concentrations in the reactor tube are controlled using a needle valve beneath the furnace and monitored using an oxygen analyser. To the bottom of the furnace is the cooling jacket which is supplied by cooled ethylene glycol via an inlet pipe connected to a chiller pump. The cooling liquid enters the cooling jacket at the bottom of the furnace, is pumped to the top of the furnace to cool sample inlet pipe region and cooling probe (down to just above the heated reaction zone) before it is pumped back down to the chiller pump via a heat exchanger.

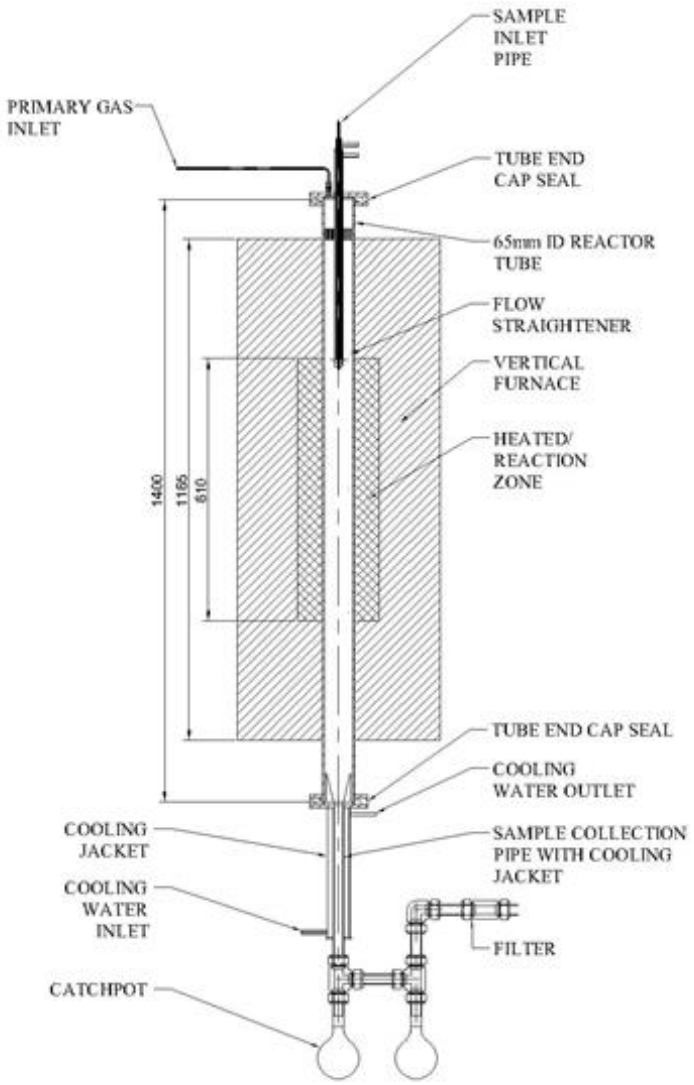

Figure 4-18 – Schematic of drop tube reactor showing internal structure and heating zones

Beneath the cooling jacket are two catch-pots where char samples are collected. These catch pots are connected to Swagelok piping containing a filter to prevent any small particles flowing through the gas. This pipe then connects to the same heat exchanger (as the chiller pipe) and on to a manifold containing a Mitchell Instruments XTP601 paramagnetic oxygen analyser (Figure 4-19) before exiting via an exhaust. The oxygen analyser required at least 300mL of gas throughput in order to operate which is controlled using a flow meter on the analyser manifold.

Figure 4-19 – Mitchell Instruments XTP601 paramagnetic oxygen analyser used to monitor oxygen concentrations during char preparation and flow meter to control gas flow.

4.5.2 Temperature profiling of the DTF

During commissioning and prior to char preparation experiments, temperature profiles were taken of the inside of the alumina furnace tube to ensure the isothermal temperature range remained consistent and ensure the heating elements were working effectively. This was achieved using a K-type thermocouple inserted into the top of the DTF via the sample inlet and measuring the temperature profiles every 15cm. During temperature profiling the nitrogen gas was switched on and the oxygen concentration maintained at 1 ±0.1 % to mimic the conditions during char preparation. The temperatures were recorded using a Picolog recorder and the temperatures at each height interval recorded every second for one minute and the average values reported. The temperature at which chars were prepared during analysis was 1100°C and a temperature profile for this temperature is shown below in Figure 4-20. The average temperature measured by the thermocouples was 1062 ±33°C.

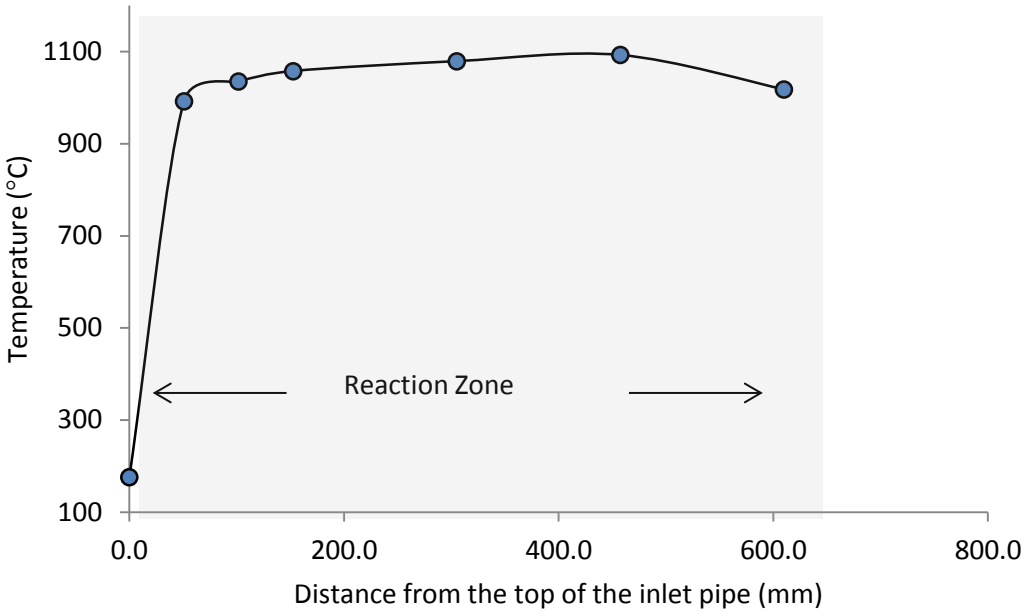

Figure 4-20 – Temperature profile for the reaction zone in the DTF (Set point 1100°C)

4.5.3 Calculation of particle residence time in the DTF

An assumption of the DTF is that the particles are small enough that they have the same velocity of the gases flowing through the furnace. An initial flow rate of N_2 gas in to the DTF was set at 16.74 dm^3/min and controlled using a flow meter. Thus, the mean velocity of gas was calculated according to following equation:

$$V_{mean} = 16.84 dm^3/min \,/\, ((0.65 m^2.\pi)/4) = 50.74 \text{ dm/min}$$

Where:

$16.84 dm^3$/min = N_2 flow rate at 20°C

$((0.65 m^2.\pi)/4)$ = Cross-sectional area of the drop tube

This mean velocity corresponds to the velocity of gas at room temperature (20°C) however in the heated zone in the drop tube furnace the temperature is 1100°C. Therefore, the gas flow at 1100°C was calculated according to the following equation:

$$Q_{1100°C} = 16.84 dm^3/min \times (1373°K/293°K) = 78.91 \text{ } dm^3/min$$

From this, the mean velocity of gas at 1100°C was determined according to the following:

$$V_{mean} = 78.91 dm^3/min / ((0.65 m^2.\pi)/4) = 78.91 \text{ dm/min} = 0.396 \text{ m/s}$$

The residence time in the drop tube was therefore calculated using the following:

78.91 dm^3/min = N_2 flow rate at 20°C

($(0.65 m^2.\pi)/4$) = Cross-sectional area of the drop tube

The particles are assumed to flow through the centre line of the tube where in a laminar flow (described below) the centreline velocity is twice the mean velocity. Therefore, the residence time in the heated zone in drop tube was then calculated using the following equation:

$$\text{Residence time (s)} = (0.61m)/ (2*0.396 \text{ m/s}) = 0.77s$$

Where:

0.61m = the theoretical heated zone

0.396m/s = the mean velocity of gas

The flow rate in to the drop tube is representative of a 100% N_2 flow and so the addition of 1% O_2 in to the gas flow was accounted for. This was done by firstly calculating the flow of oxygen:

$$\text{Flow of 1\% oxygen in 100\% } N_2 = 16.84 dm^3/min*(1/100) = 0.164 dm^3/\text{minute}.$$

The flow of oxygen from the air (as oxygen is supplied from via the inlet) was then calculated as the percentage oxygen in the air is known as 21%. Hence,

$$\text{Air flow} = 0.164 \text{ } dm^3/min / 0.21 = 0.802 \text{ } dm^3/min$$

This was then subtracted from the original flow calculation (in 100% N_2) to give a final flow rate of 16.05 dm^3/min N_2. With a flow rate of 16.05dm^3/min N_2, this equates to a residence time of 0.8s (using the methodology above) in the theoretical 0.61m reaction zone. From the

temperature profile measurements shown above however, the heated isothermal reaction zone was measured as 0.455m in length. The corresponding residence time in the isothermal reaction zone (from the 0.77ms) was thus determined as 0.57s.

The viscosity, v, of N_2 at 1100°C was calculated using Sutherland's formula as 4.824×10^{-5} Pa S from which the Reynolds number was calculated using the following equation:

$$N_{Re} = V_{mean} * 0.065 * \frac{\rho}{\nu} = 129$$

The Reynolds number was calculated as 129 which is characteristic of laminar flow i.e. $N_{Re} < 2600$.

4.5.4 Operating Procedure

Before preparation of fast heating rate chars, untreated and torrefied (270-30, 270-60 and 290-30) fuels obtained from a previous study, see Ibrahim et al. [107] were milled using a Retsch SM1000 cutting mill to reduce wood chips down to smaller particle size. These were then sieved using a Retsch AS 200 vibratory sieve shaker and sieves to obtain a size fraction of 212-355µm. Before preparation of the chars, around 6-8g of sample was dried overnight in an oven at 80°C.

The three PID controls were then programmed to 1100°C at a heating rate of 10°C/minute. The nitrogen gas was then switched on and the rig allowed to rise in temperature. Once at temperature, the oxygen analyser was calibrated using a 2 point calibration between 0-5% oxygen. A 0% oxygen environment was achieved by flooding the system with an increased flow of N_2 gas to analyser, allowing time for equilibration and setting this as 0% oxygen. The 5% oxygen environment was then established by switching the gas flow source from the nitrogen to a 5% oxygen in nitrogen calibration gas canister (BOC gases). These gases were then given time to equilibrate before the second calibration point was input. Once complete, the nitrogen flow was switched back and set at a flow rate of 16L/min and an oxygen concentration of 1% set in the reactor tube. The vacuum pump ensured biomass particles, once introduced under these conditions, flowed isokinetically through the reactor. With a 16L/minute flow of nitrogen at

1100°C, the residence time of the particles in the isothermal heating zone was calculated to be ~600ms as shown above. The 1% oxygen concentration was selected to allow for combustion of volatile species in the biomass during devolatilisation but not the char species and to prevent biomass and tar sticking to the inside of the alumina tube.

Once the system was fully prepared, biomass particle were inserted in to the top of the DTF at a rate of 4g/hour. During analysis, the oxygen concentration was monitored whereby if the 1% deviated greater than 0.1%, the concentration was re-stabilised using the needle control valve. At the end of analysis, the chars were removed from the catch pots and stored in a glass vials in a desiccator until further analysis.

4.5.5 Theoretical char yield and burn-off (ash tracer method)

Owing to the nature of biomass fuels containing very high volatiles contents, the majority of the sample entering the DTF vaporised to the gas phase making char yield estimations difficult. As a result, char yields for each drop tube experiment were estimated using the ash tracer method according to the following equation:

$$\text{Char yield} = \frac{\text{Ash in fuel (dry basis)}}{\text{Ash in char (dry basis)}} \text{ x } 100$$

The method uses the ash contents of the parent fuel (from proximate analysis) and the ash content of the char (from TGA analysis) and assuming a 100g initial mass of fuel (thus the ash weight percents can be used as mass values).

Due to the 1% oxygen concentration as well as high oxygen concentrations in biomass, it is possible for the chars to burn in the DTF. As a result, the degree of char burn-off was also determined. This method uses the char yields from the ash tracer method and the theoretical char yield which is the fixed carbon and ash content of the parent fuel i.e. all volatiles and moisture lost according to the following equation:

$$\text{Char Burn off} = \frac{\text{Theoretical char (FC \& ash)} - \text{ash tracer char yield}}{\text{Char (FC \& ash)}} \text{ x } 100$$

4.6 Isothermal Oxidation kinetics experiments

The isothermal oxidation kinetics of the chars prepared in the DTF were determined using a TA QA 5000 IR thermogravimetric analyser shown in Figure 4-21. Prior to analysis, the platinum weighing pans of the TGA were cleaned in a Bunsen burner flame to burn off any residual fragments remaining from previous experiments. Once cooled, any excess ash was brushed off following which the pans were tared in the instrument. Approximately 2mg of char was finely ground using a pestle and mortar, added to the TGA pans and placed in to the auto-sampler.

The instrument was then programmed for individual isothermal runs. Initially, temperature in the TGA was set at 0°C and the balance flow was set at 100mL N_2; the balance flow in place to maintain a positive pressure in the balance chamber to prevent decomposition products from contaminating the sensitive balance mechanism. The system was then kept at equilibrium for 5 minutes before the balance flow was set at 20mL/min. The purge flow i.e. the 'interacting' gas (initially N_2 gas) through the furnace, which flows horizontal to the sample was set at 20mL/minute throughout the experiment. The system was allowed to equilibrate for 5 minutes before the temperature was then raised (via IR bulbs) to 100°C at a heating rate of 20°C/minute and held for 20 minutes. The sample was then heated further to the desired combustion temperature (discussed below) and held at this temperature for 30 minutes. The purge flow was then switched from N_2 gas to air to allow for oxidation of the char samples to take place. The temperatures for isothermal oxidation of the chars from untreated biomass ranged from 300-360°C while the temperatures for oxidation of the chars from torrefied biomass were slightly higher (owing to decreased reactivity) and ranged from 320-400°C. These temperatures were maintained for 60-120 minutes following which the temperature was ramped to 900°C and held for 5 minutes.

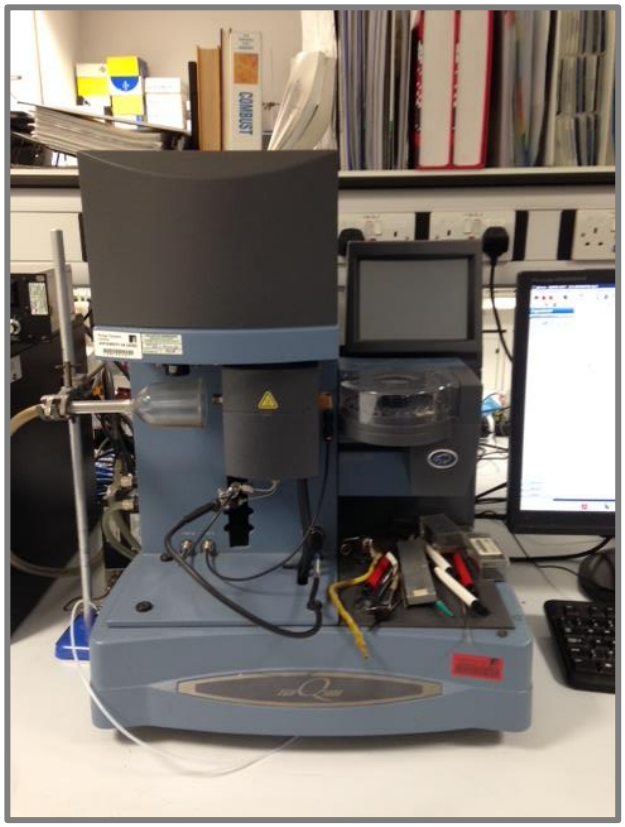

Figure 4-21 - TA QA 5000 IR Thermogravimetric Analyser

4.6.1 Chemical reactivity

The sampling interval during experiments was 0.5 seconds/point and from the data acquired the mass loss was converted to weight percent and plotted against time in seconds. These plots were acquired for each char at each oxidation temperature e.g. chars from willow 270-30 at 320°C, 340°C etc. The plots for each of the chars can be found in Appendix A**.** Using these data, the overall chemical reactivity, for each temperature according to the following equation:

$$R_c = -\frac{1}{W_0} \cdot \frac{dm}{dt}$$

Where,

R_c = the overall chemical reactivity (s^{-1})

W_0 = the mass of carbon (corrected with ash weight percent removed)

$\frac{dm}{dt}$ = the maximum rectilinear rate of weight loss

Using the reaction rate constants and temperatures an Arrhenius plot (ln K vs. 1/T) for each char was plotted to determine the Arrhenius parameters: activation energy (E_a) and pre-exponential

factor (A). This is derived from the Arrhenius equation and tsking the natural logarithm according to the following equations:

$$k = A.\, e^{-E_a/RT}$$

$$\ln k = \frac{-E_a}{R}\frac{1}{T} + \ln(A)$$

Where,

k = reaction rate constant

e = exponential function

A = pre-exponential factor

E_a = activation energy

R = Universal Gas constant

T = temperature

ln = natural logarithm

Figure 4-22 shows the Arrhenius plot for chars prepared from Willow 270-30 (all other Arrhenius plots can be found in Appendix A). From the slope of the line and y-intercept, E_a and A, were determined respectively.

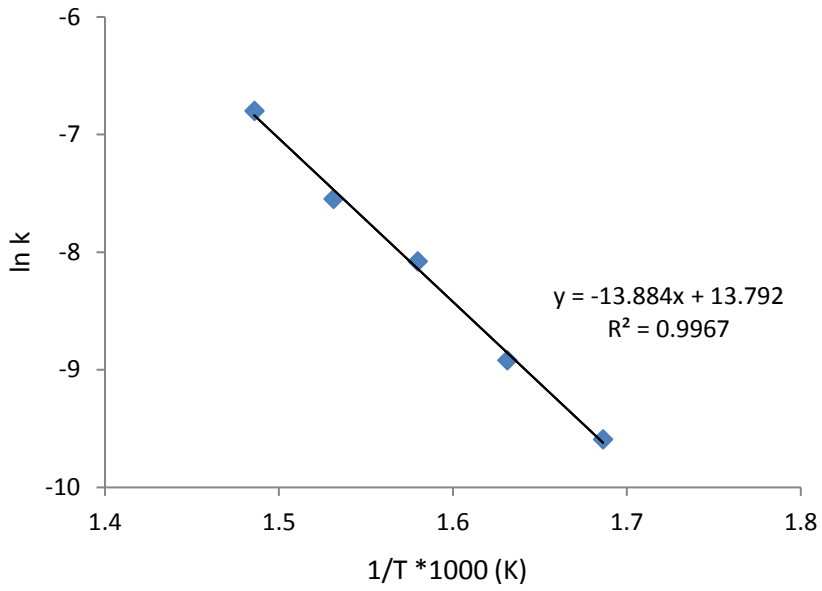

Figure 4-22 – Arrhenius plot for the oxidation of fast-heating rates chars from Willow 270-30.

Once the Arrhenius parameters were determined, the chemical reactivity at higher temperatures could be extrapolated via feeding the parameters back in to the Arrhenius equation at the desired temperatures. The Arrhenius parameters and results of the chemical reactivity extrapolated to higher temperatures for chars prepared from untreated and torrefied willow can be found in Section 6.2.2.

4.6.2 Intrinsic reactivity

The intrinsic reactivity, defined as the reactivity per unit surface area in the absence of any mass transfer restrictions [132] can be determined by the following equation:

$$R_i = \frac{k\,P^n}{A_g}$$

Where,

R_i = the intrinsic reactivity

k = the reaction rate constant

P^n = the partial pressure of the reacting gas

A_g = the specific surface area

The intrinsic reactivities for the chars from untreated and torrefied willow and eucalyptus were calculated using the reactivities, the partial pressure of reacting gas, in this instance = 101.325kPa/21.278kPa, the numerator and denominator corresponding to standard atmospheric pressure and PO_2 respectively and the specific surface areas determined using the BET method (described above). The intrinsic reactivities for the chars can be found in Section 6.2.2.

4.7 Pyrolysis studies of untreated and torrefied biomass fuels

The pyrolysis behaviour of the untreated and torrefied biomass fuels were also investigated as part of this work. For the untreated and torrefied willow and eucalyptus fuels discussed in chapter 6, the decomposition behaviour and reaction rate constants for pyrolysis of fuels were derived while the decomposition behaviour was established for the untreated and torrefied pine and eucalyptus discussed in Chapter 5.

4.7.1 Pyrolysis experiments

Pyrolysis experiments were performed using a QA2000 IT thermogravimetric analyser. Prior to experiments, the samples were cryogenically milled using a Spex 6770 freezer mill and a size fraction of <90μm obtained. Around 5mg of sample was then added to the tared platinum pans and inserted to the TGA auto-sampler. The pyrolysis programme was then input in which the purge flow (N_2 gas) was set at a rate of 20mL/minute and balance flow was set at a rate of 100mL/minute with the temperature kept isothermal for 5 minutes. Following this, the balance flow rate was set to 20mL/minute and the system kept isothermal for a further 5 minutes. The temperature was then ramped to 105°C at a heating rate of 10°C/minute and kept isothermal for 15 minutes. Following this, the temperature was ramped to 900°C at a heating rate of 10°C/minute. Once reached, the temperature was maintained for 15 minutes before the purge flow switched to air to burn off the sample. The sampling interval during experiments was 0.5 seconds/point and from the data acquired the mass loss was converted to weight percent and plotted against time in seconds.

4.7.2 Pyrolysis kinetics

For untreated and torrefied willow and eucalyptus (Chapter 6) the kinetics of pyrolysis were determined. The method employed was the 'reaction rate constant method' (similar to char oxidation experiments) in which the pre-exponential factor and activation energies are derived using the Arrhenius equation. Firstly, if the weight loss curve with time is assumed to be the result of one apparent first order reactions then k' can be derived using the following equation:

$$k' = -\frac{1}{(m - m_T)}\frac{dm}{dt}$$

Where,

k' = reaction rate constant

m = is the initial mass

m_T = is the terminal mass (taken at 550°C)

$\frac{dm}{dt}$ = derivative mass loss with time

An Arrhenius plot for on the onset of mass loss, where the percentage mass loss is <5%, yields a straight line from which the activation energy and pre-exponential factors can be derived. The reaction rate constant for a given temperature e.g. 300°C = k_{300} can be derived using this temperature, E_a and A in the Arrhenius equation. The Arrhenius plot for the pyrolysis of willow 270-30 is shown in Figure 4-23.

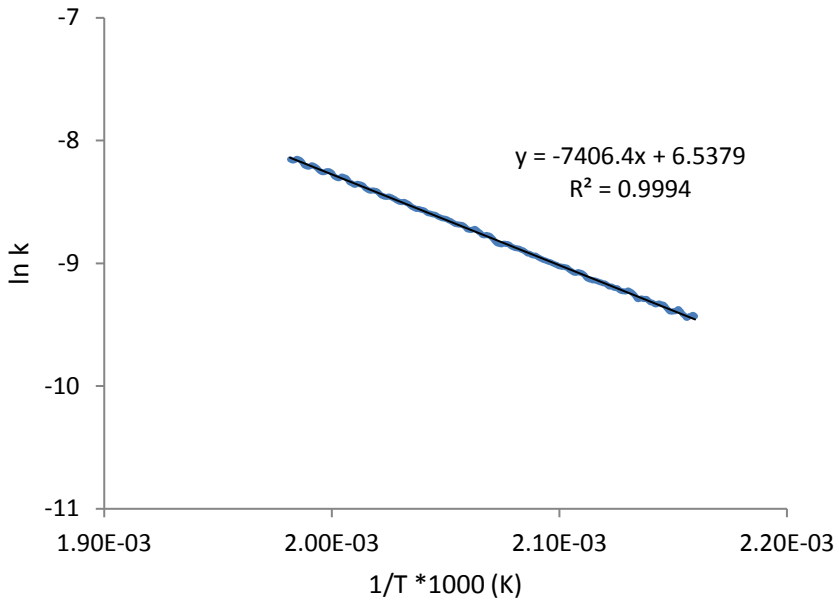

Figure 4-23 – Arrhenius plot for the pyrolysis of Willow 270-30

5 The Torrefaction of Pine and Eucalyptus

5.1 Introduction

As discussed in Chapter 2 torrefaction of biomass aims to alleviate some of the problems associated with raw biomass to produce a fuel with enhanced chemical and physical properties. This chapter investigates the torrefaction of two wood sources, North American pine and eucalyptus to provide a detailed description of the torrefaction process in terms of mass and energy balances as well as analysis of the products of torrefaction. Understanding and analysing torrefaction of fuels on a laboratory scale is an important primary step when determining the optimum conditions for the torrefaction of a given fuel and must be understood fully prior to any scaling up process. While research of the torrefaction of fuels is present in the literature, few studies provide the necessary holistic view to the process that is attempted in this study. This chapter therefore provides a well-rounded analysis of the torrefaction of pine and eucalyptus by providing detailed mass and energy balances, descriptions of the physical and chemical changes that occur during torrefaction as well an elemental balance for species C, H and N for each condition.

5.2 Experimental

Two fuels, pine and eucalyptus, were torrefied using a bench scale reactor by the methodology explained in Section 4.3. The conditions for torrefaction are shown in Table 5-1.

Nomenclature in text	Temperature (°C)	Residence Time (minutes)
250-30	250	30
270-30	270	30
270-60	270	60
290-30	290	30

Table 5-1 - Torrefaction conditions used in this study

The solid products of torrefaction were analysed for proximate analysis, ultimate analysis, pyrolysis behaviour, HGI equivalent, particle size distribution, BET surface area and images of the sample were taken using scanning electron microscopy. The procedures for each of these analyses are described in in Section 4.4. The liquid products of torrefaction, the aqueous phase

and organic phase, were analysed for TOC and ultimate analysis respectively by the procedures also explained in Section 4.4

5.3 Results and Discussion

5.3.1 Temperature Profiles

The temperature profiles for the torrefaction of pine under each condition are shown in Figure 5-1. Similar temperature profiles were obtained for torrefaction of eucalyptus under the same conditions and so these profiles are also representative of the torrefaction of eucalyptus. In each case, TC 1 (TC = thermocouple) corresponds to the temperature of the gas in the reactor tube whilst TC 2 and 3 correspond to thermocouples located inside the fuel under treatment and represent the temperature of the fuel. In some cases, a lag in the temperature inside the fuel is observed (conditions A and B) relative to the temperature of the gas during the drying stage which can be attributed to the endothermic drying reactions.

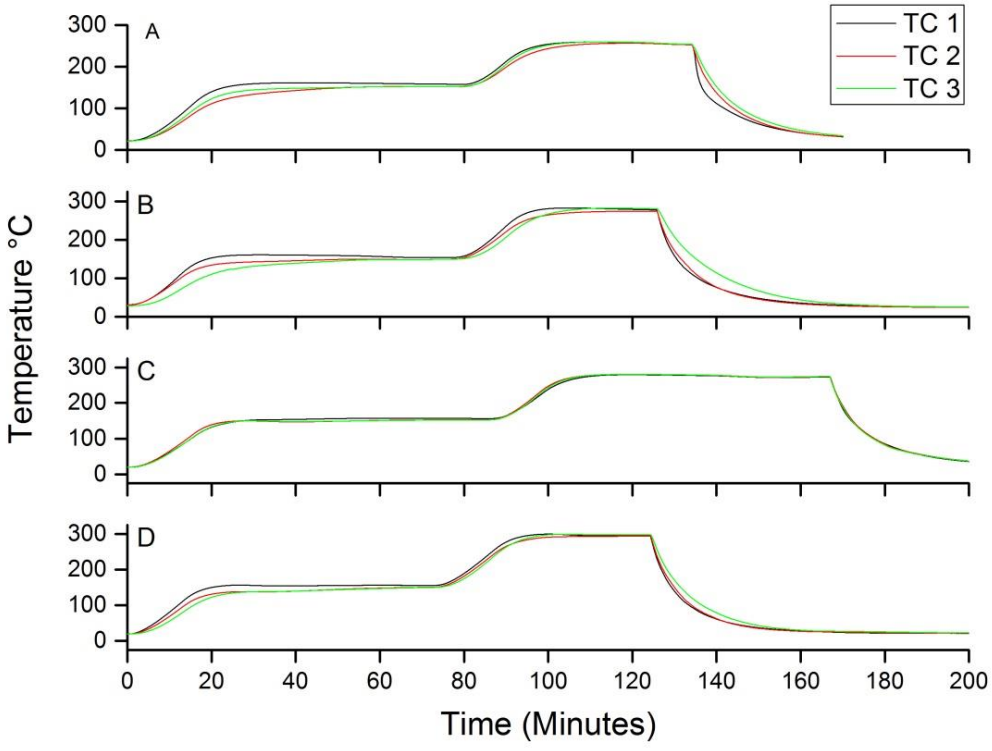

Figure 5-1 - Temperature profiles for torrefaction of pine under condition 250-30 (A), 270-30 (B), 270-60 (C) and 290-30 (D)

The residence time for torrefaction is often quoted in the literature to begin when the temperature of the fuel reaches 200°C. In these experiments however, the residence time was taken to begin when the temperature of the gas reaches the desired final temperature- this method was chosen to keep conditions for different fuels the same for direct comparison e.g. for example for condition 250-30, the residence times for pine and eucalyptus are the exact same providing a 'like-for-like' comparison. Nevertheless, Table 5-2 compares the residence times in which the residence time begins when the gas temperature reaches the torrefaction temperature (column 2) alongside the residence time taken to begin when the fuel reaches 200°C (column 1) - the latter expectantly greater. Table 5-2 also shows the residence times taken when the temperature in the fuel reaches the torrefaction temperature (column 3) - showing the time taken for the temperature measured in the fuel to 'catch-up'. For the conditions at lower temperatures and residence times (conditions 250-30 and 270-30) the residence time which begins when the fuel reaches final temperature (column 3) is notably lower than the residence time that begins when the gas temperature reaches torrefaction temperature (column 2) - this time difference shorter for more severe conditions (270-60 and 290-30). Table 5-2 also shows the maximum temperature observed in the fuel during torrefaction experiments (column 4). While there is a lag during the heating of the biomass owing to heat transfer effects and endothermic reactions taking place, when the final temperatures are reached, torrefaction can become exothermic and release heat e.g. for eucalyptus at 290-30, the maximum temperature reached in fuel was 304°C showing that heat is being released during torrefaction reactions.

Condition	1 Residence time beginning when fuel reaches 200°C (min)	2 Residence time beginning when gas reaches final temperature (min)	3 Residence time beginning when fuel reaches final temperature (min)	4 Maximum temperature recorded in the fuel (°C)
P250-30	45	31	25	259
E250-30	42	33	23	254
P270-30	40	34	18	275
E270-30	37	32	21	278
P270-60	72	60	62	281
E270-60	61	55	49	278
P290-30	42	31	28	297
E290-30	43	34	30	304

Table 5-2 - Residence times and maximum temperatures for each condition during torrefaction

At the end of each of torrefaction run, when the reactor tube was quickly removed and quenched with a higher flow of nitrogen to prevent further reaction there is a sharp decrease in temperature which can be clearly observed on the profiles. From this, the end of the residence time can be reliably determined. The next section will discuss the effect these different conditions have on the overall mass balance of the torrefaction reaction.

5.3.2 Overall Mass balance

The products of torrefaction reactions consist of solid, liquid and gaseous fractions which vary in abundance depending on the torrefaction conditions and the type of fuel. For each condition, an overall mass balance was performed from collection of the solid and liquid products with the permanent gaseous products calculated by difference. The solid product is comprised of the torrefied solid fuel particles with the condensable liquid products split in to an aqueous phase and a tar phase (via extraction with dichloromethane as described in Section 4.3.2). The results of the mass balance for pine and eucalyptus are shown in Figure 5-2 with results shown on a dry basis.

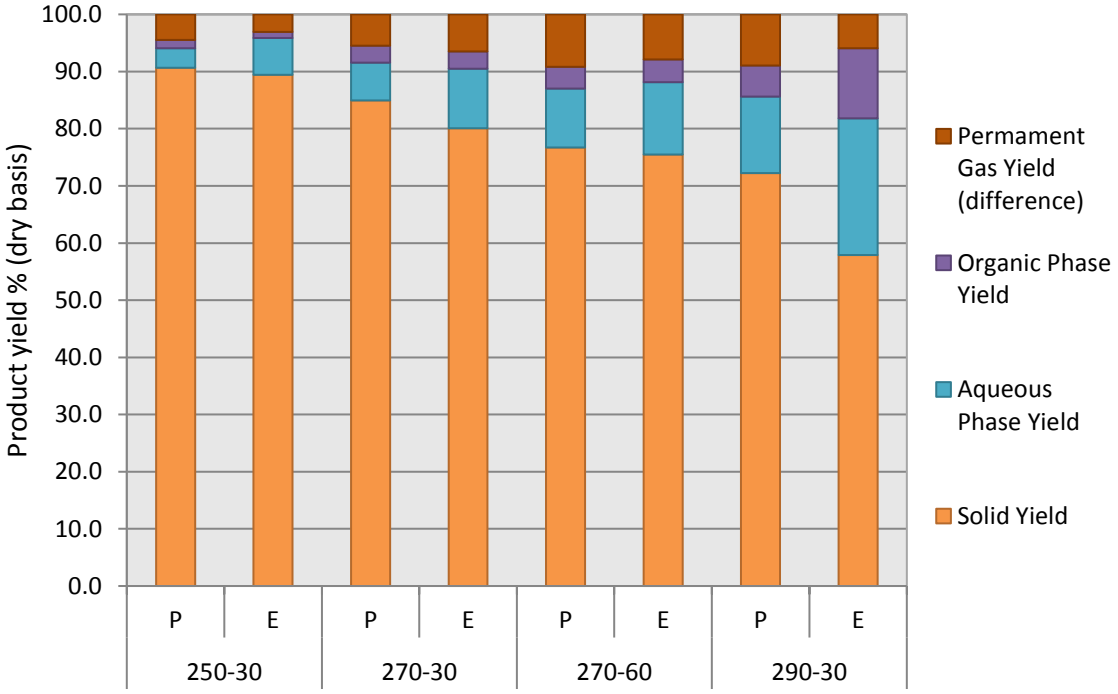

Figure 5-2 - Overall mass balance or the torrefaction of pine and eucalyptus under different conditions: (P = pine, E = eucalyptus)

For both pine and eucalyptus, under all conditions, the solid fraction represents the greatest proportion of the mass yield followed by the aqueous phase then the organic tar phase. The

solid yield decreases with increasing torrefaction severity with a corresponding increase in liquid and gas yields. This trend has been observed by other researchers [111]. While this trend is followed, it is important to point out the difficulty in attaining 100% retrieval of solid and liquid products of torrefaction. The fibrous nature of torrefied biomass, which will be discussed later, results in the creation of small particles that may be lost during collection. It can also be difficult to collect all of the liquid products of torrefaction as well owing to nature of liquid samples however special care was taken to maximise the retrieval of all products upon completion of each torrefaction run.

For pine fuels, increasing the torrefaction temperature by 20°C from 250°C to 270°C under the same residence time corresponds to a greater dry mass loss of 5.7% from (90.7% to 84.9%) with an increase in liquid product by a similar amount (4.9% and 9.6% respectively). For the more severe conditions, 270-60 and 290-30, the dry solid mass yield decreases to 76.2% and 72.3% respectively with greater yield of liquid products of 14.1% and 18.8%. For eucalyptus increasing the torrefaction temperature from 250°C to 270°C with 30 minutes residence time results in a 9.4% increase in dry solid loss from 89.4% to 78.8% respectively and a 5.9% increase in total (aqueous and organic) liquids yield. The solid and total liquids yields for eucalyptus torrefied at 270-60 are 75.5% and 16.7% respectively and 57.9% and 36.1% for the solid and liquids yield at 290-30.

The effect of changing the residence time and temperature on torrefaction yields can be shown when comparing the yield distribution upon changing one parameter i.e. changing the residence time in the case of 270-30 and 270-60 and temperature for 270-30 and 290-30. Table 5-3 shows the change in each product from the milder torrefaction 270-30. For both fuels, temperature has a greater effect on torrefaction yields than residence time and is in agreement with other researchers [105, 107].

	Change from condition 270-30	Pine	Eucalyptus
Solid	270-60	-8.25	-4.59
	290-30	-12.71	-17.55
Aqueous	270-60	+3.72	+2.25
	290-30	+6.80	+13.46
Organic	270-60	+0.80	+0.94
	290-30	+2.43	+9.21

Table 5-3 - Percentage point change in solid, aqueous and organic phases yields (percentage points) from condition 270-30 to 270-60 and 290-30.

When comparing pine and eucalyptus directly, the dry solid yield for pine is greater than eucalyptus for each condition with greatest disparity between results at condition 290-30. There is an increase in the aqueous phase for eucalyptus relative to pine under each condition with tars following the same trend save for the mildest condition where pine torrefied at 250-30 produced slightly more tar. While it is clear that temperature plays a greater role than residence time on yield distribution overall for both fuels, it can be seen that residence time has a greater relative effect on pine than eucalyptus. In spite of this, overall eucalyptus shows greater apparent reactivity relative to pine. The marked changes between the yields of these fuels, an indicator of reactivity, can be attributed to the lignocellulosic composition of these fuels. Pine and eucalyptus are a softwood (coniferous) and hardwood (deciduous) respectively, and as a result contain a different distribution of the three main constituents of biomass cell walls: hemicellulose, cellulose and lignin. On average, the hemicellulose content of softwoods and hardwoods are 20-32% and 18-25% respectively; for cellulose, 35-50% and 40-50% respectively and the lignin content is 25-35% and 18-25% respectively [101]. Differences in the composition of these components, notably hemicellulose, as discussed in the literature review also affect the reactivity of these fuels. Results of the changes in cell wall components are discussed below.

5.3.3 Changes in cell wall components with torrefaction

The results of the changes in lignocellulosic compositions are shown in Figure 5-3 with moisture and ash contents included (which will be discussed later). For untreated pine, the hemicellulose, cellulose and lignin weight percents are 11.9, 49.8 and 26.7 % respectively. The share of lignocellulosic components for untreated eucalyptus are 9.76, 57.6 and 17.5% for hemicellulose, cellulose and lignin respectively. As expected, pine has a greater amount of hemicellulose than eucalyptus, while eucalyptus has a greater amount of cellulose relative to pine owing to the typical distribution of these components in softwoods and hardwoods [101]. Untreated pine

also has a greater amount of lignin than eucalyptus. Under torrefaction at 250-30, the hemicellulose content decreased for both fuels to 5.7 and 4.6% for pine and eucalyptus respectively. This corresponded with an increase in cellulose and lignin weight percent: cellulose increased by roughly 4 percentage points for both fuels to 53.9 and 62.3% for pine and eucalyptus respectively while lignin increased by 5-6 percentage points for both fuels to 31.6 and 23.7% for pine and eucalyptus respectively. At 250°C therefore some of the hemicellulose is lost during the torrefaction process while some is still retained in the fuel. While some of the cellulose and lignin may be lost at this low temperature, the overall increase in weight percent suggests that at 250-30 this temperature is too low for any significant mass loss. These changes agree with the torrefaction studies on individual components performed by Chen et al [92] discussed in section 2.1.2 which show hemicellulose mass loss as low as 220°C while there was no notable cellulose mass loss until 290°C and negligible mass loss of lignin. When the torrefaction conditions are increased to 270-30 the hemicellulose content of pine and eucalyptus decrease further, to 2.2% for pine while for eucalyptus virtually all of the hemicellulose had degraded to 0.6%. The greater loss of hemicellulose for eucalyptus compared with pine can possibly be attributed to differences in hemicellulose composition. Xylan, the main polysugar found in hardwoods is known to be more reactive than glucomannan, the main polysugar found in softwoods. As discussed in section 2.1.3, the pyrolytic behaviour of these polysugars is different as shown from TGA studies in which xylan not only degrades more than glucomannan in the torrefaction temperature ranges, but it loses more mass at lower temperatures than glucomannan serving as an indicator of reactivity.

With attention on cellulose and lignin, there is an increase to 54.8 and 36.1% respectively for pine. While lignin increases for eucalyptus 270-30, there is a slight decrease in cellulose weight percent compared with 250-30 as 61.9%. This suggests that some of the cellulose may be starting to degrade at 270°C for eucalyptus. Still at 270°C but with a longer residence time of 60 minutes, the hemicellulose content for pine reduces to 0.45% and is almost zero (0.6%) for eucalyptus. Under condition 270-60, the cellulose content for pine has started to decrease to 52.3% when compared to 270-30 with eucalyptus cellulose further decreasing to 58.4%. Note that the change in mass loss at 270-60 is greater for pine than eucalyptus which is in agreement with these changes.

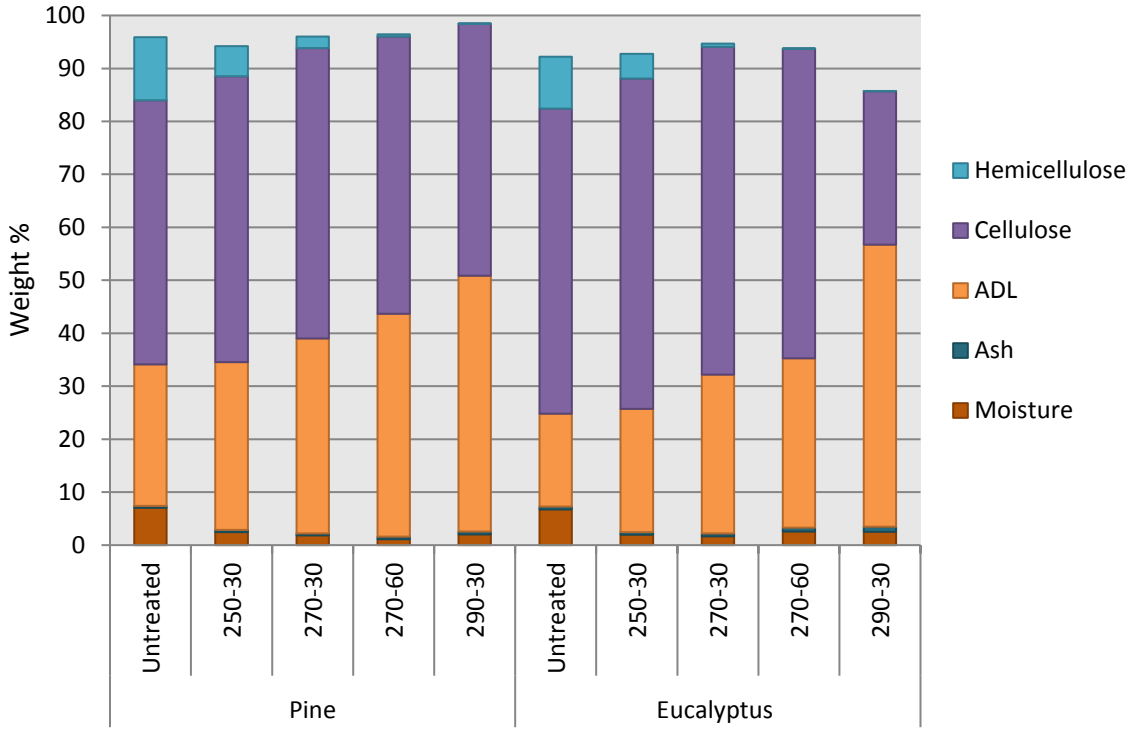

Figure 5-3 – Changes in lignocellulosic composition for untreated and torrefied pine and eucalyptus

Under condition 290-30 all of the hemicellulose has been degraded for both fuels. The cellulose for pine has decreased even further to 47.5% with lignin increasing to 48.3%. However the case for eucalyptus is more interesting. At 290-30 the cellulose content has decreased drastically by almost 30% compared with 270-60 to 28.9%. The lignin content correspondingly increased from 32% at 270-60 to 53.2%. Under this condition, it may be the case that cellulose has undergone extensive degradation and begun to carbonise. Note that in the studies performed by Chen et al [92], 44.82% of the cellulose had degraded at 290°C. It is also worth noting too that during the torrefaction of eucalyptus at 290-30, the maximum temperature measured by the thermocouples in the reactor was 304°C (Table 5-2) which could result in the changes observed for this fuel.

5.3.4 Pyrolysis of untreated and torrefied fuels

The pyrolysis behaviour of these fuels also provides information on the impact torrefaction has on lignocellulosic components in the pine and eucalyptus. Figure 5-4 and Figure 5-5 show the pyrolysis behaviour (derivative mass loss vs. temperature) of untreated and torrefied pine and eucalyptus respectively. For untreated pine, appreciable mass loss begins around 220°C which is in agreement with other studies as the range at which hemicellulose pyrolysis begins [87]. The

rate of mass loss peaks around 330°C which is represented predominantly by cellulose decomposition [87]. The onset of hemicellulose decomposition for untreated pine is lower than untreated eucalyptus which is agreement with Ramiah et al [95] who showed glucomannan, the main hemicellulose in softwood to be less thermally stable than xylan, the main hemicellulose in hardwoods. For the pyrolysis of the torrefied fuels, the onset of mass loss occurs later i.e. hotter than the untreated pine and the shift to the right (higher temperature) increase slightly with increasing torrefaction severity.

The temperature of maximum rate of mass loss has also shifted to the right for 250-30 and 270-30 and slightly further for 270-60 and 290-30. Interestingly, when considering the results of the lignocellulosic analysis of the torrefied fuels, at condition 270-60 and 290-30 the cellulose weight percent had started to decrease. The higher peak temperature and onset of mass loss for these fuels could possibly be explained by the loss of some of the less thermally stable cellulose products formed during torrefaction at these conditions. This would result in the remainder of the more thermally stable cellulose in the 270-60 and 290-30 pine which would lose mass at higher temperatures during pyrolysis.

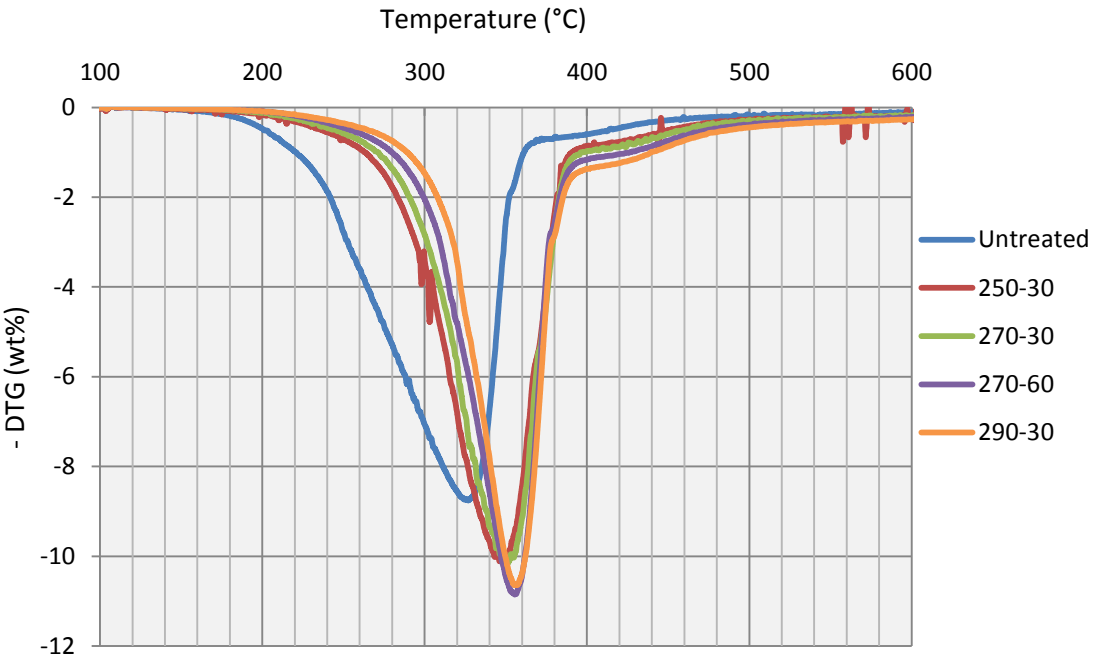

Figure 5-4 - Pyrolysis behaviour of untreated and torrefied pine

For untreated eucalyptus, shown in Figure 5-5, a shoulder is clearly present on the derivative curve which can be attributed to hemicellulose decomposition. When compared with untreated pine (Figure 5-4), the relative intensity of this peak is lower which is possibly due to the fact that eucalyptus has less hemicellulose than pine. The differences in composition i.e. mainly xylan (80-90 wt. %) for eucalyptus and glucomannan (60-70 wt. %) for pine may account for differences in rate of mass loss. The study performed by Werner et al. on the pyrolysis of various polysugars found in hemicellulose (discussed in section 2.1.3), showed that xylan decomposition was characterised by two distinct peaks, the onset of each beginning at around 220 and 260°C. This is in agreement with the pyrolysis of untreated eucalyptus in this study where two regions of notable mass loss are observed up to 300°C: one beginning around 220°C following by a second rapid mass loss beginning around 250°C. The shoulder decreases for eucalyptus 250-30, where the mass loss shifts to higher temperature (240-250°C), highlighting the loss of some of the more reactive hemicellulose materials during torrefaction under this condition. Note from the results of lignocellulosic analysis that the hemicellulose content of the eucalyptus 250-30 has approximately halved. The pyrolysis results therefore suggest that some of the least thermally stable components of hemicellulose have been removed during treatment 250-30 while the more thermally resistant components have been retained in the fuels; these are decomposed above 250°C during pyrolysis.

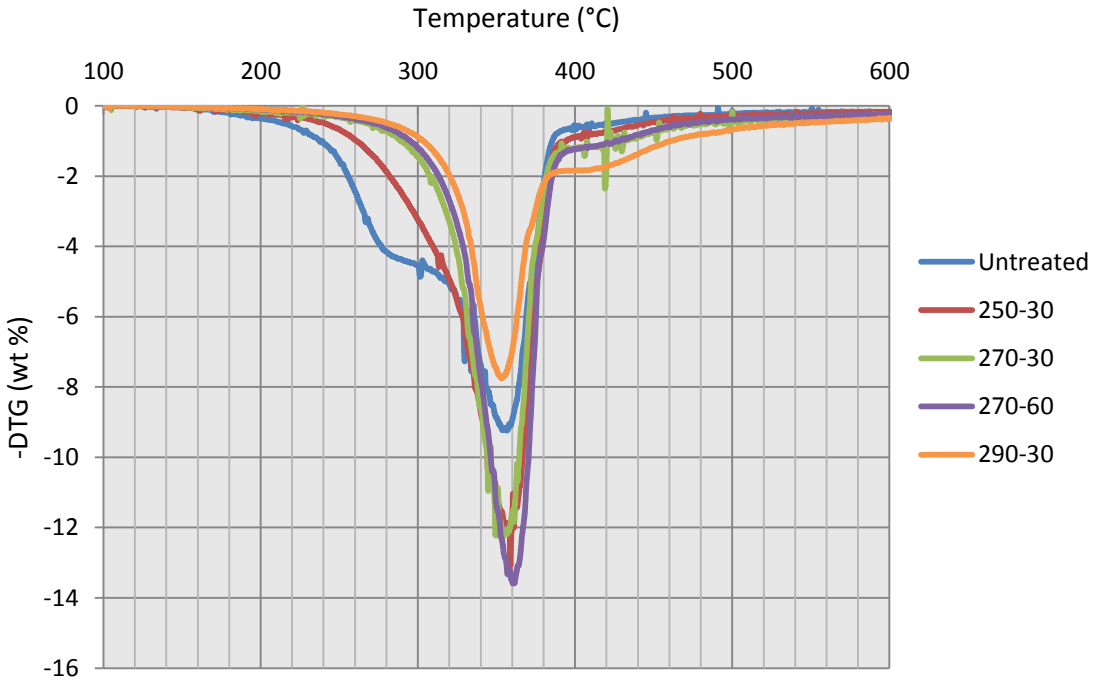

Figure 5-5 - Pyrolysis behaviour of untreated and torrefied eucalyptus

The degree of mass loss attributed to cellulose decomposition is also greater for eucalyptus 250-30, which is expected as the weight % of cellulose has increased for this fuel. Interestingly for eucalyptus 270-30 and 270-60, the greatest change in mass loss does not occur until after 300°C. Results from lignocellulosic analysis for these fuels show that almost all of the hemicellulose has been degraded. For eucalyptus 290-30, the intensity of the derivative curve for cellulose is the lowest and the mass loss attributed to lignin decomposition shows the greatest rate of change. Again, this is in agreement with the composition of lignocellulose in eucalyptus 290-30 where the cellulose and lignin contents of these fuels are lowest and highest respectively out of all the fuels.

The degradation of the components affects the overall mass balance (and energy balance which will be discussed in the next section) of the torrefaction process. Several authors have reported global mass balances for solid, liquid and gaseous products from the torrefaction of a range of woody (hardwood and softwood) and herbaceous biomasses e.g. [88, 104, 111, 114, 170, 171]. Medic et al. [111] report on the torrefaction of corn stover at various torrefaction temperatures and conditions. The author's findings agree with those found in this study where the solid mass yield decreases with increasing torrefaction severity and increasing condensable liquids and non-condensable gases. Pach et al. [171] report an extensive list of solid, liquids and permanent gas yields from the torrefaction of a range of fuels. A summary of selected fuels and conditions from this study, and other studies is shown in Table 5-4. In comparing the results of studies number 1 and 3 where the same condition was applied to pine (softwood) and birch (hardwood), the solid mass yield is greater for pine than birch highlighting the differences observed during torrefaction on softwoods and hardwoods [171]. This effect is further shown in Bergman et al. (numbers 8-13) where the solid mass loss is greater more for hardwood (willow) relative to softwood (larch) [88].

In comparing the results from this study (numbers 15-22) and literature studies directly, for pine 270-60, the yields of solid and liquid products (76.7 and 14.1% respectively), are comparable with the 280-60 results from the study by Pach et al [171] (number 2 in the table)- with liquid yields in the Pach study slightly greater due to the slightly warmer torrefaction temperature. While the yields are comparable, the calculated permanent gas yields for 270-60 in this study are greater than the permanent gas yield in the Pach study (9.2% compared with 2.1%). Although these fuels are not the exact same and have been performed in different laboratories using different equipment, it could be expected that 270-60 permanent gas yields should be lower

than the 280-60 gas yields owing to the milder process conditions. As the gas yields in these experiments are calculated by difference, this could be result of losses during recover and extraction of liquid (and solid) products which are accounted for in the permanent gas yield.

	Torrefaction conditions			Yield of Products (Wt % dry)			Reference
	Fuel	Temperature (°C)	Res. Time (min)	Solid	Liquid	Gas†	
1	Pine	250	60	88.2	10.8	1.0	[171]
2	Pine	280	60	78.1	19.8	2.1	[171]
3	Birch	250	60	85.5	12.8	1.7	[171]
4	Corn Stover	250	30	84.4	4.1	1.4	[111]
5	Corn Stover	300	20	57.4	13.3	2.7	[111]
6	Leucaena	250	30	72.0	24.1	3.9	[114]
7	Leucaena	275	30	54.3	40.0	5.6	[114]
8	Willow	230	50	91.5	5.9	2.1	[88]
9	Willow	250	30	82.5	10.0	3.3	[88]
10	Willow	270	15	79.0	13.5	4.4	[88]
11	Larch	230	50	97.0	1.6	0.3	[88]
12	Larch	250	30	92.0	3.6	0.8	[88]
13	Larch	270	15	89.0	8.0	1.3	[88]
14	Straw	250	30	82.0	10.0	3.0	[104]
15	Pine	250	30	90.7	4.9	4.5*	-
16	Pine	270	30	84.9	9.5	5.5*	-
17	Pine	270	60	76.7	14.1	9.2*	-
18	Pine	290	30	72.8	18.8	8.9*	-
19	Eucalyptus	250	30	89.4	7.5	3.1*	-
20	Eucalyptus	270	30	80.6	13.8	6.5*	-
21	Eucalyptus	270	60	75.5	16.7	7.9*	-
22	Eucalyptus	290	30	57.9	36.1	5.9*	-

† Permanent gases, * calculated by difference

Table 5-4 - Overall mass balances for selected studies (1-14) and torrefaction experiments performed in this research (15-22)

5.3.5 Analysis of Products of Torrefaction

5.3.5.1 Analysis of Solid Products

Torrefaction produces solid, liquid and gaseous products which vary in abundance depending on the degree of severity. Within these fractions it is important to determine the characteristics of each to help determine the chemical and physical changes relative to the parent fuel. Images of the untreated and torrefied pine and eucalyptus are shown in Figures 5-6 and 5.7 respectively. It can be seen that with torrefaction the fuel turns from very pale brown to brown, and this colour become darker as torrefaction progresses. This is due to the loss of oxygen and

enrichment of carbon which will be explained in more detail from results of ultimate and proximate analysis. In comparing pine and eucalyptus under the same torrefaction conditions, the eucalyptus fuels appear to be darker. For example, condition 290-30, eucalyptus is very dark brown when compared with pine. As the composition of eucalyptus 290-30 is predominantly carbon rich lignin, this would explain this appearance of this fuel.

The results of the proximate analysis for untreated and torrefied pine and eucalyptus solid fuels are shown in Table 5-5. It can be seen that upon torrefaction the moisture and volatiles content decrease while the fixed carbon and ash contents increase. The decrease in moisture can be attributed to the loss of bound moisture from evaporation while the decrease in volatiles with increasing severity is mainly due to the decomposition of hemicellulose and to an extent cellulose.

	Condition	Moisture % (ar)	Volatiles (% db)	Ash (% db)	FC (% db)
Pine	Untreated	7.08	83.78	0.34	15.89
	250-30	2.43	81.66	0.45	17.89
	270-30	1.86	79.64	0.35	20.01
	270-60	1.13	76.35	0.47	23.18
	290-30	2.02	72.78	0.55	26.66
Eucalyptus	Untreated	6.75	83.32	0.53	16.15
	250-30	1.96	79.72	0.5	19.78
	270-30	1.70	75.23	0.52	24.25
	270-60	2.59	72.49	0.69	26.83
	290-30	2.51	60.1	0.96	38.94

ar = as received basis, db = dry basis

Table 5-5 – Proximate analysis for untreated and torrefied pine and eucalyptus

Figure 5-6 - Images of untreated pine (U) and pine torrefied under condition 250-30, 270-30, 270-60 and 290-30.

Figure 5-7 - Images of untreated eucalyptus (U) and eucalyptus torrefied under condition 250-30, 270-30, 270-60 and 290-30.

For both untreated fuels, the moisture, volatiles and fixed carbon contents are comparable while eucalyptus has a slightly higher dry weight percent of ash. Upon torrefaction, the volatiles content of eucalyptus is lower than pine under each condition, which is agreement with the overall mass balance: there is a greater solid mass loss and increase in liquids yield for eucalyptus, where the volatiles lost during torrefaction are distributed amongst the liquid and gas phases. This also agrees with the relative losses of hemicellulose where greater amounts are lost. For eucalyptus 290-30, the marked decrease in volatile and increase fixed carbon contents agree with the greater decomposition of cellulose. The chemical composition of the torrefied fuels also change relative to the parent fuel as shown in Table 5-6 ,where the carbon content of the fuels increase with torrefaction severity, while the oxygen and hydrogen contents decrease. This is in agreement with the results of the proximate analysis where the decrease oxygen and hydrogen can be attributed to decomposition of holocellulose.

	Condition	C % (daf)	H % (daf)	N % (daf)	S % (daf)	O % (daf)
Pine	Untreated	49.68	5.67	0.13	0.06	44.46
	250-30	51.88	6.10	0.12	0.00	41.89
	270-30	52.57	5.82	0.11	0.00	41.49
	270-60	54.12	5.84	0.10	0.00	39.94
	290-30	54.95	5.58	0.09	0.00	39.37
Eucalyptus	Untreated	51.53	5.67	0.10	0.11	42.59
	250-30	51.80	5.82	0.11	0.07	42.20
	270-30	55.25	5.47	0.10	0.00	39.28
	27060	57.19	5.67	0.10	0.00	37.05
	290-30	59.67	5.13	0.05	0.00	35.15

daf = dry-ash free basis

Table 5-6 – Ultimate analysis for untreated and torrefied pine and eucalyptus

Changes in the chemical composition of the fuel can be further shown on a Van Krevelen plot in Figure 5.8 which shows the change in atomic O/C and H/C ratios with torrefaction.

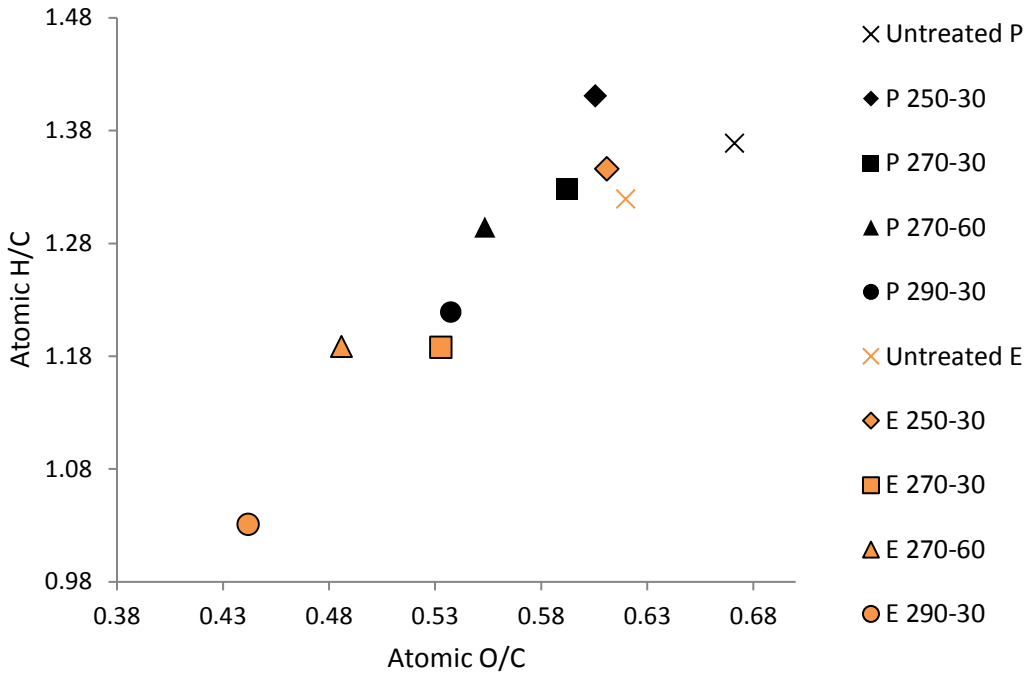

Figure 5-8 - Van Krevelen plot for untreated and torrefied pine and eucalyptus

With increasing torrefaction severity, the general trend of decreasing atomic H/C and O/C ratios is observed. It can be seen that torrefaction has a greater impact on the H/C and O/C ratios for eucalyptus than pine. The differences between the ratios for the untreated and torrefied eucalyptus fuels is also greater than the differences between ratios for the untreated and torrefied pine fuels which is in agreement with the results of the proximate analysis: there is a greater loss of volatiles upon torrefaction for eucalyptus relative to its pine analogues. The ratios for pine torrefied at 290-30 and eucalyptus at 270-30 for example yield very similar H/C and O/C ratios and have volatiles contents of 72.78% and 72.23% respectively. It can be seen therefore than eucalyptus appears to be more reactive than pine due to this greater loss of volatiles species and corresponding decrease in H/C and O/C ratios. Ibrahim et al. reported similar results for eucalyptus fuels [107].

5.3.5.2 Energy Yield of solid products

The loss of low energy oxygen-rich species from biomass and concentration of carbon results in a more energy-dense product with an increased calorific value relative to the untreated fuel. The higher heating values (HHV) and energy densification ratios for pine and eucalyptus are shown in Table 5-7 on a dry basis. The measured HHVs for pine determined by bomb calorimetry are reported in addition to the calculated HHVs for untreated and torrefied pine and eucalyptus using the Friedl equation [160].

		HHV (MJ/kg) (db)		
		Measured	Calculated	Energy Densification Ratio
Pine	Untreated	20.21	19.41	1.00
	250-30	20.72	20.44	1.03
	270-30	21.22	20.67	1.05
	270-60	22.09	21.33	1.09
	290-30	23.49	21.56	1.16
Eucalyptus	Untreated	NA	20.24	1.00
	250-30	NA	20.34	1.00
	270-30	NA	21.69	1.07
	270-60	NA	22.64	1.12
	290-30	NA	23.36	1.15

db = dry basis, NA = not analysed

Table 5-7 - Higher heating values for untreated and torrefied pine and eucalyptus

It can be seen that with torrefaction, the higher heating value of the fuels increase. As the torrefaction conditions become more severe, both the higher heating values and energy densification ratios increases. While torrefied biomass will lose some of its original energy during treatment, the ratios of the HHV torrefied fuel/untreated fuel are greater than one and the mass loss of the fuel is greater than the energy loss. This is further exemplified in comparing the mass and energy yields directly for each of the conditions. The results of the mass and energy yields for torrefied pine and eucalyptus (calculated using the equations shown in sections 4.3.3 and 4.3.4) and are shown in Figures 5-9 and 5-10 respectively.

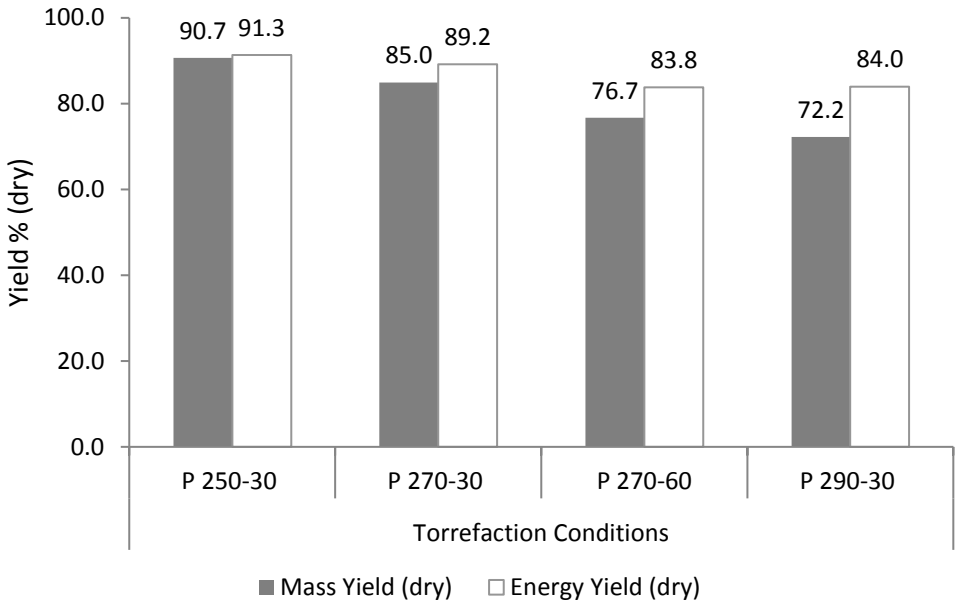

Figure 5-9 – Solid mass and energy yields for torrefied pine

With attention on pine (Figure 5-9), it can be seen that the mass and energy yields decrease with increasing torrefaction severity. Of notable interest are the yields for pine 270-60 when compared to the milder condition 270-30, as the decrease in mass yield is comparatively greater than the decrease in energy yield. Note above the changes in lignocellulose for pine at this condition highlighting the effect of residence time on pine in this treatment. For eucalyptus (Figure 5-10), the mass and energy yields decrease steadily with increasing torrefaction severity until condition 290-30 where, as discussed above, carbonisation of the cellulose fraction has begun to occur.

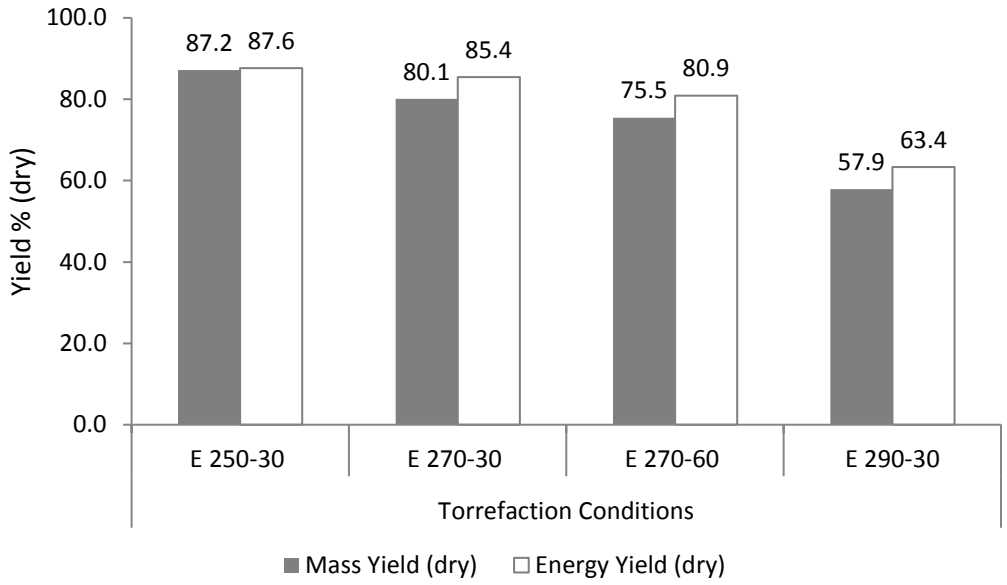

Figure 5-10 – Solid mass and energy yields for torrefied eucalyptus

5.3.5.3 Grindability

The data above shows that with torrefaction the chemical properties of torrefied fuel have improved: there is a loss of volatile materials resulting in depletion of oxygen and the enrichment of carbon, producing a more energy dense fuel. The loss of these volatiles from hemicellulose in particular affects the structural integrity of biomass particles as this fraction acts a support for cellulose. Its loss therefore contributes to improved grindability of the fuel. The HGI equivalent data for pine is shown in Table 5-8 and performed according to the methodology set out in section 4.4.6. Unfortunately the $HGI_{equivelent}$ for eucalyptus was not performed due to too little sample.

Fuel	% passed through 75µm sieve	HGI_{equiv}
Untreated	1.2	1
250-30	4.8	24
270-30	6.0	32
270-60	9.0	51
290-30	11.5	67

Table 5-8 – HGI equivalent results for untreated and torrefied pine.

The results show poor grindability for untreated pine with a small number of particles passing through the 75µm sieve. With torrefaction there is a marked improvement in grindability of the fuels which increases as torrefaction temperature and residence time increases. From a fuel perspective this has significance in terms of milling prior to combustion in a furnace as well as

milling prior to pellet production which will be discussed in more detail in the Chapter 7. Figure 5-11 shows the correlation between HGI equivalent and higher heating value. The enrichment of carbon/loss of hydrogen and oxygen as a result of reduction in hemicellulose leads to an increased calorific value fuel and improved grindability. For conditions 270-60 and 290-30, it can be seen that the trend is beginning to plateau; note that by condition 270-60 all of the hemicellulose has been devolatilised.

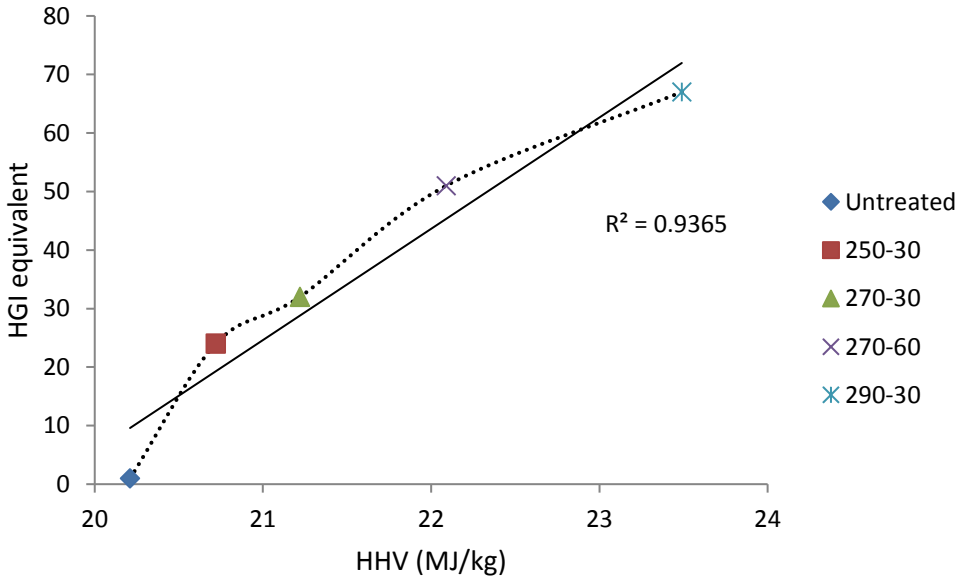

Figure 5-11 – Relationship between HGI equivalent and HHV for untreated and torrefied pine.

5.3.5.4 Particle Size Distribution

The results of the particle size distribution for untreated and torrefied pine, performed according to methodology outlined in section 4.4.7 further shows the effect torrefaction has on the grinding behaviour of fuels. Upon torrefaction, the number of particles distributed to smaller aperture sizes in the sieves increases highlighting the increased size reduction upon milling for torrefied fuels. Other researchers have found the same trend [83, 112].

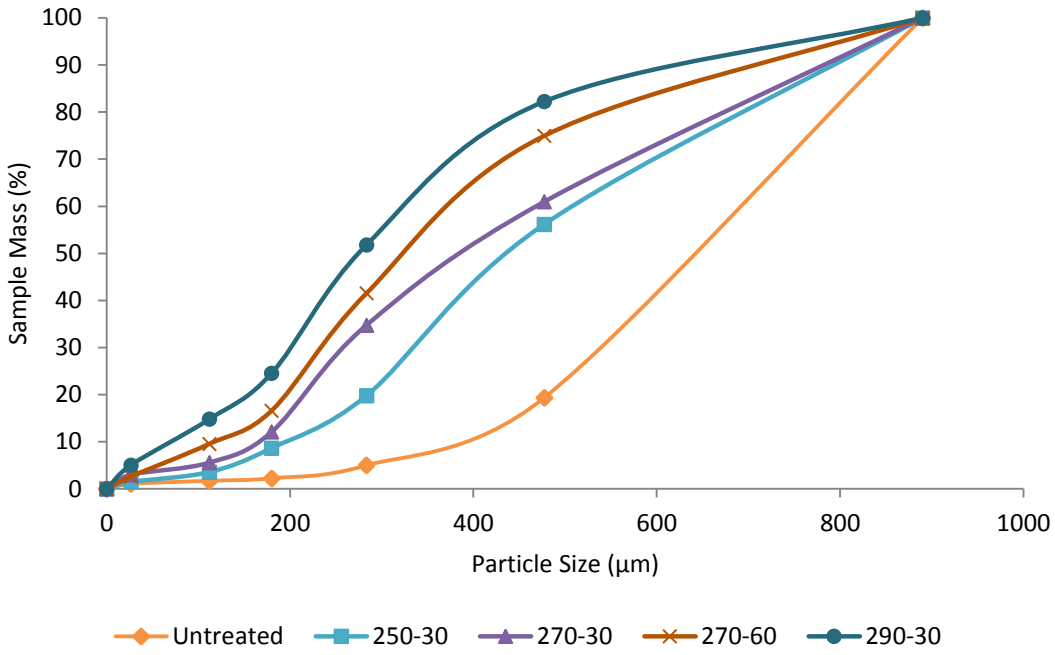

Figure 5-12 - Particle size distribution for untreated and torrefied pine

5.3.5.5 Scanning electron microscopy images

Structural and morphological changes to biomass upon torrefaction can be further understood using scanning electron microscopy where the microstructure can be examined visually. High magnification images of untreated and torrefied pine (treatments 270-30, 270-60 and 290-30) were taken using the methodology outlined in Section 4.4.9 and shown in Figure 5-13. For untreated pine, the biomass particles appear rounded and bulky; there is limited visibility of the internal cellular microstructure as expected as the xylem tissue remains intact. Upon torrefaction however, the biomass particles appear more brittle and fibrous and the cellular microstructure is more evident. This microstructure shows evidence of 'hollowing' out of particles which can be attributed to loss of hemicellulose upon torrefaction; this effect is more apparent when very high magnification images were taken. Figure 5-14 shows images taken at 1000x magnification where it becomes clear that while the cellular structure is retained, free space exists between the tubular fibres for the torrefied materials relative to the untreated fuel. The pits on the tracheid cells are also more evident on the torrefied fuels, giving an almost 'strawberry seed' effect on the surface of the biomass particles. Similar effects were identified by SEM images of torrefied eucalyptus taken by Chen et al. who also found this hollowing effect of the cellular network [118]. Figure 5-15 show torrefied pine at even greater magnification (x3000) where structural deformity can be seen in the fraying of the cell edges and the hollowing of cellular structure. These structural changes arise from changes in chemical composition and contribute to the easier grindability.

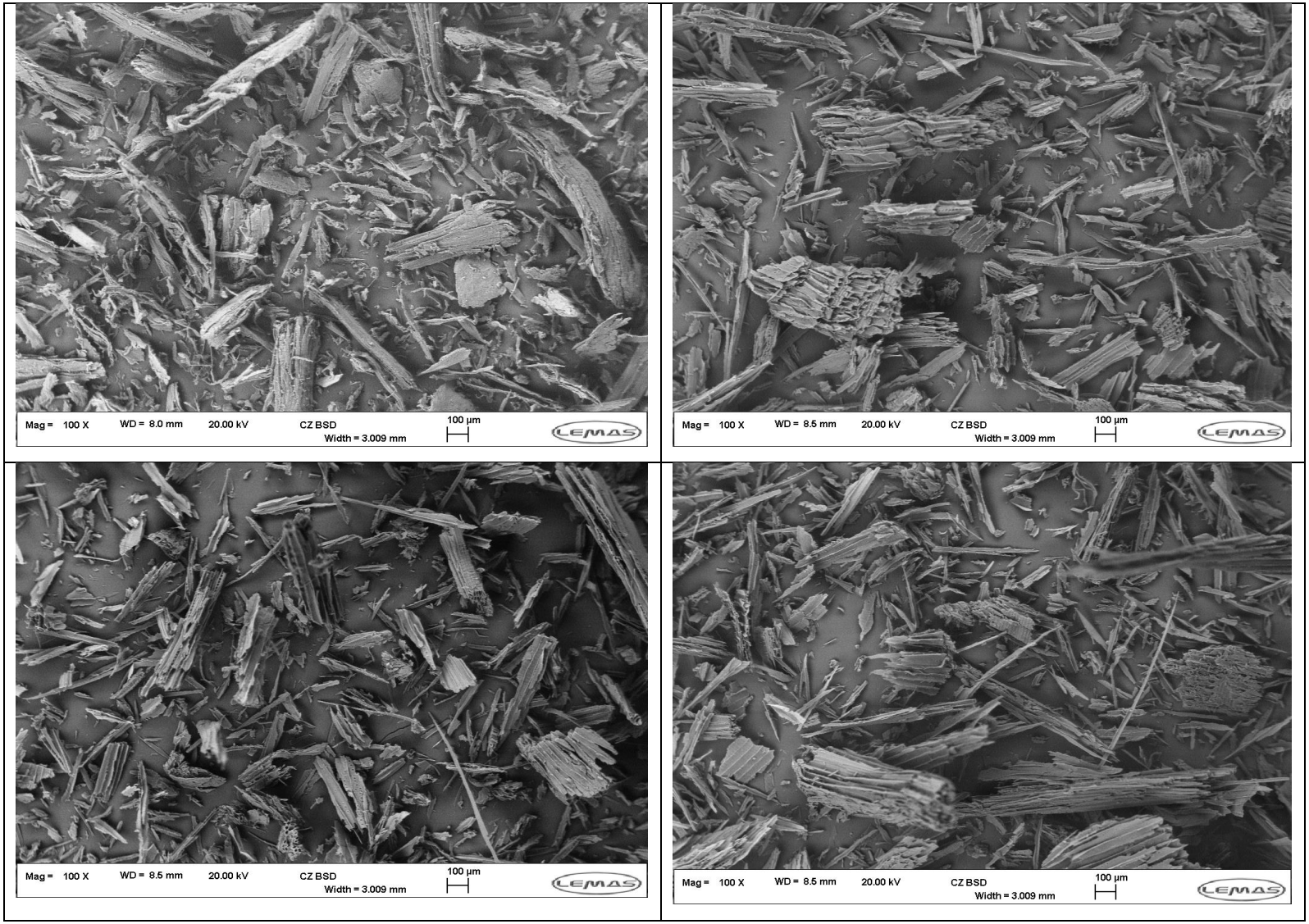

Figure 5-13 - SEM images of (clockwise): untreated pine, pine 270-30, pine 270-60 and pine 290-30 at 100x magnification

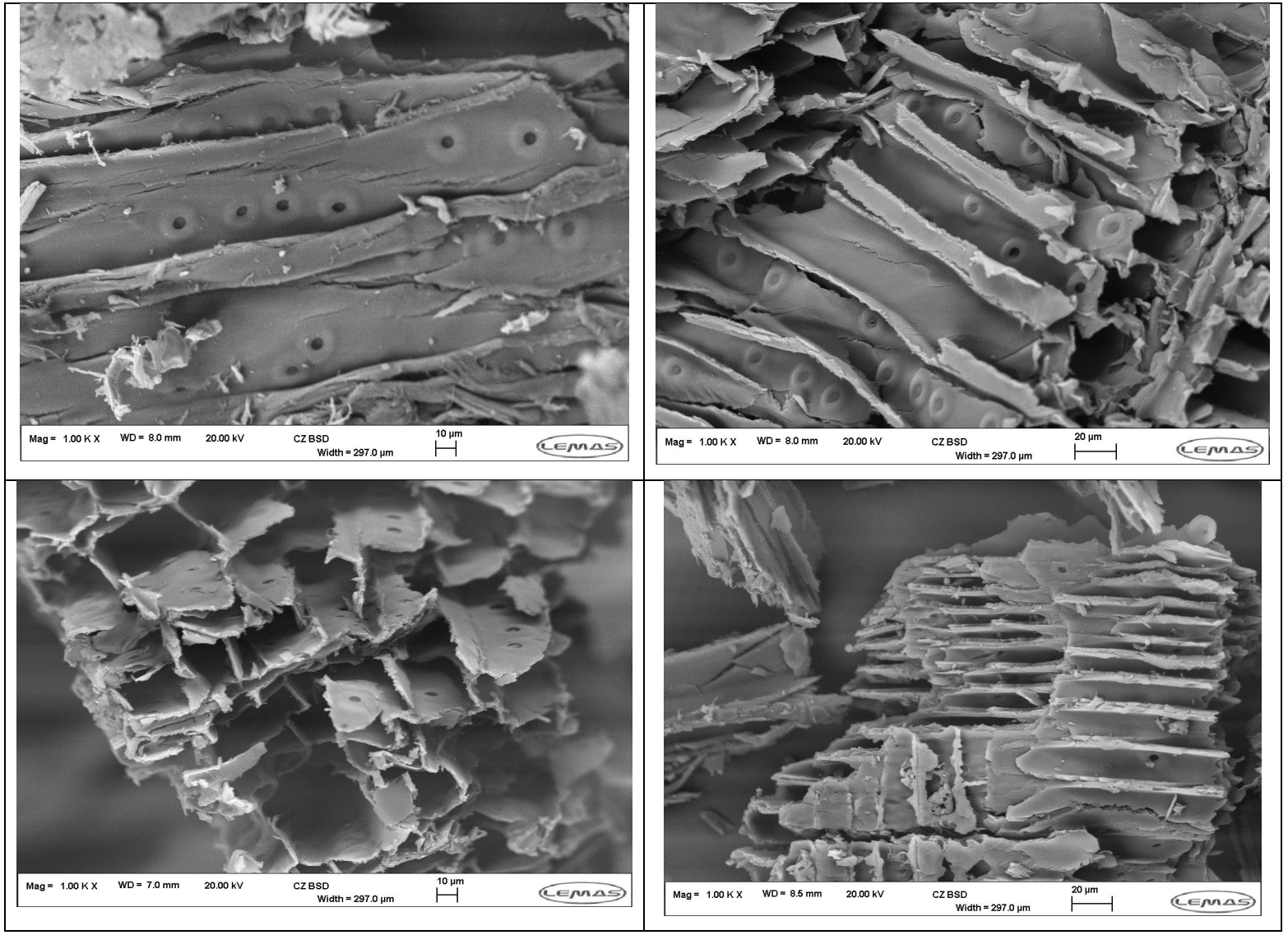

Figure 5-14 - SEM images of (clockwise): untreated pine, pine 270-30, pine 270-60 and pine 290-30 at 100x magnification

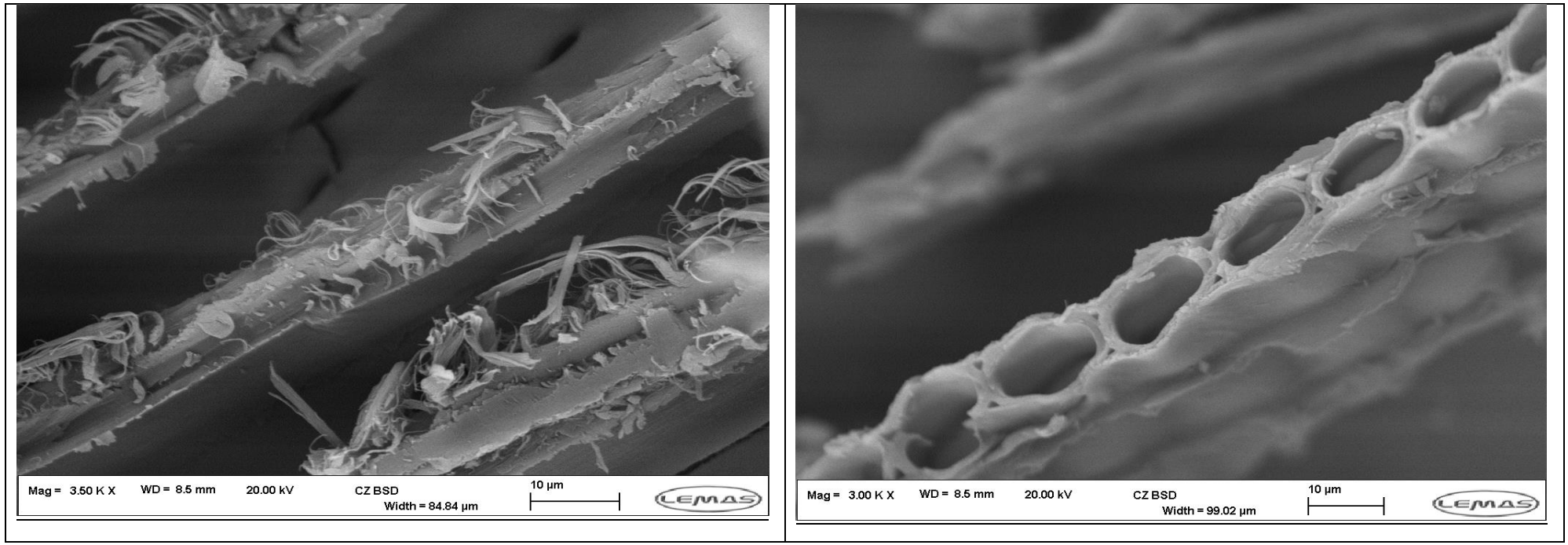

Figure 5-15 - SEM images of pine torrefied under condition 290-30 at 3500x magnification (left) and 3000x magnification (right)

5.3.5.6 Surface area analysis

Change to surface morphology of biomass particles upon torrefaction has a subsequent effect on the surface area on the particles. The degree of exposed surface on particles becomes important when reactions with oxygen are considered (e.g. combustion in air) as the oxygen will react with surface carbon atoms during reactions. The BET surface area of untreated and torrefied pine were determined according to the methodology laid out in section 4.4.8 and are shown in Table 5-9. An example adsorption isotherm and BET plot for pine 270-60 are also shown in Figures 5-16 and 5-17 respectively. With torrefaction, the BET surface area of the torrefied particles increases slightly. This can be attributed to degradation of lignocellulosic materials in the torrefied fuels, resulting in exposure of more surface and thus increased measured surface area. The loss of volatiles during torrefaction will also contribute slightly to the porosity of the biomass particles through release upon heat treatment although the slow heating rates used during treatment (10°C/minute) will not have as a great an effect on the porosity of the particles.

	BET surface area (m^2/g)	R^2 for BET plot
Untreated	0.95 +/- 0.02	0.99
270-30	0.95 +/- 0.03	0.99
270-60	1.04 +/- 0.07	0.99
290-30	1.25 +/- 0.02	0.99

Table 5-9 – BET surface areas for untreated and torrefied pine

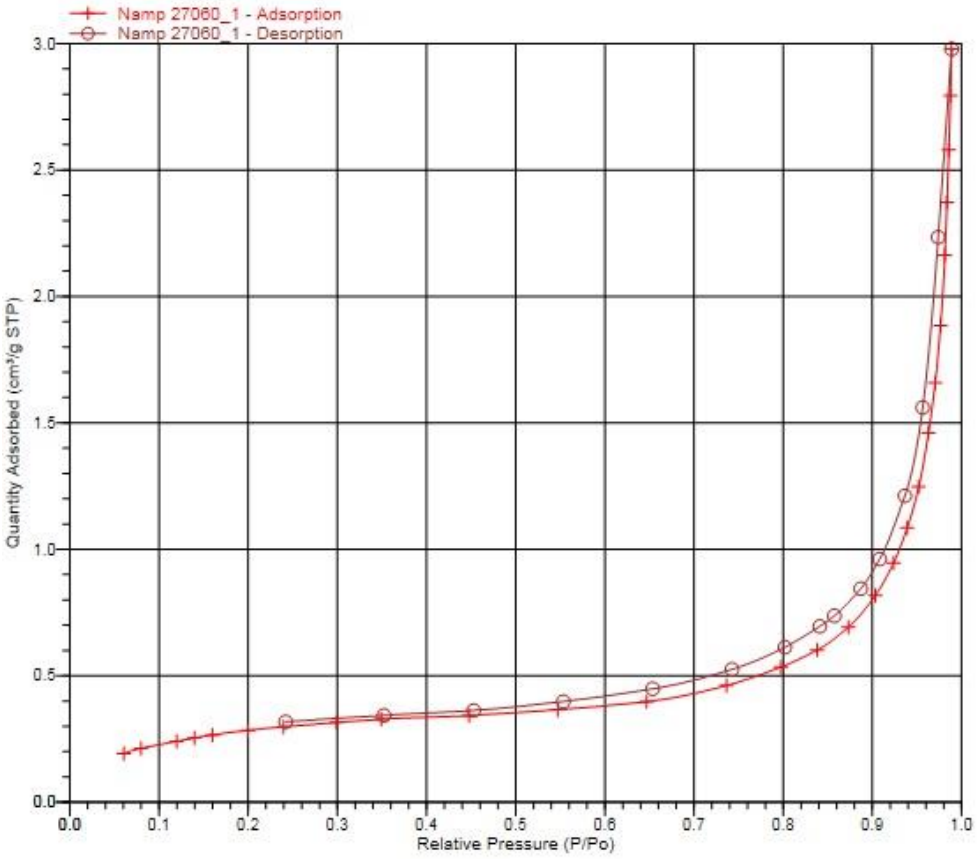

Figure 5-16 – Adsorption isotherm for pine 270-60

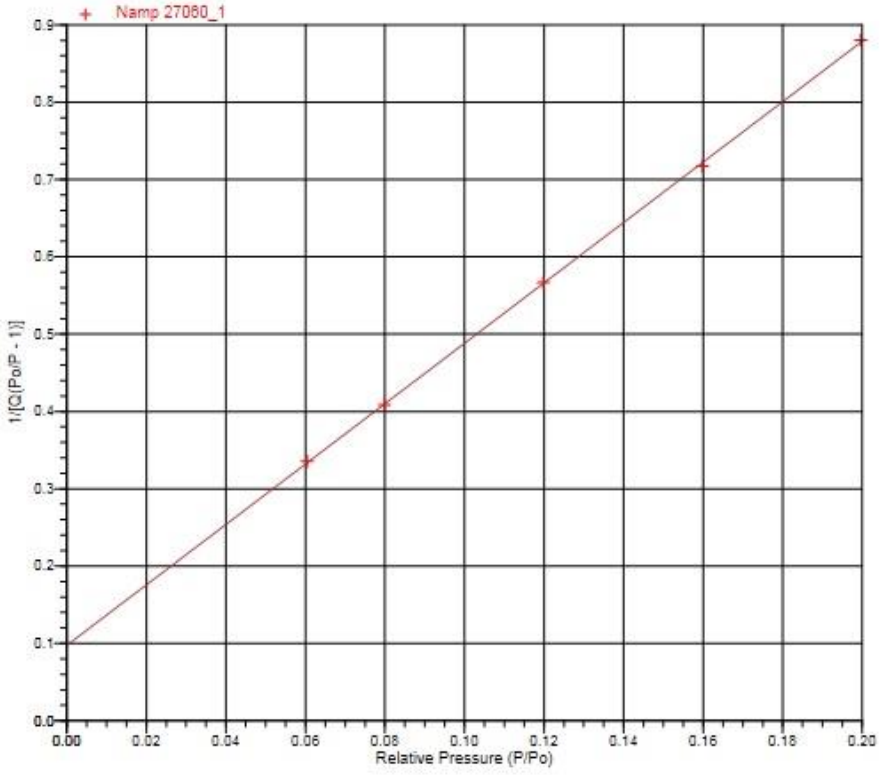

Figure 5-17 – BET plot for pine 270-60.

5.3.6 Analysis of liquid products

The liquid products of torrefaction, comprised of a mixture of liquids and condensable liquids (that were in the gas phase upon leaving the torrefaction rig) were collected according to the methodology laid out in Section 4.3. The aqueous phase products were analysed for total organic carbon (TOC) to determine the carbon content while the organic fraction was analysed for its chemical composition by ultimate analysis- these data, with the solid product carbon contents from ultimate analysis, being used to determine the carbon mass balance discussed later in section 5.3.7.1. The results for the liquids analysis are shown in Tables 5-10 and 5-11.

	Condition	TOC (g/L)
Torrefied Pine	250-30	81.7
	270-30	115.8
	270-60	126.8
	290-30	147.2
Torrefied Eucalyptus	250-30	60.6
	270-30	97.0
	270-60	99.1
	290-30	118.1

Table 5-10 – TOC analysis for the aqueous phase products of torrefied pine and eucalyptus

		C % (ar)	H % (ar)	N % (ar)	S % (ar)	O % (ar)	HHV MJ/kg (ar)
Torrefied Pine	250-30	45.94	5.89	0.13	0.00	48.03	15.4
	270-30	47.22	5.76	0.13	0.00	46.89	15.8
	270-60	48.10	6.20	0.13	0.00	45.56	17.0
	290-30	52.98	6.14	0.11	0.00	40.77	19.4
Torrefied Eucalyptus	250-30	41.74	5.19	0.02	0.00	53.05	12.1
	270-30	44.29	5.21	0.05	0.00	50.45	13.4
	270-60	47.46	5.43	0.09	0.00	46.97	15.5
	290-30	49.36	5.66	0.04	0.00	44.94	16.8

ar = as received

Table 5-11 - Ultimate analysis for the organic phase products of torrefaction

In the tar phases, the carbon weight percent increases with torrefaction severity. In comparing pine and eucalyptus, the carbon weight percents are greater for pine than eucalyptus under each condition. The corresponding oxygen weight percent for eucalyptus under each condition are greater than pine. The TOC analysis of the aqueous exhibits a similar trend to the organic phase in that the carbon content of the aqueous phase increase with torrefaction severity and

pine aqueous products contain more carbon than its eucalyptus analogues. While this trend is exhibited, the mass loss for eucalyptus is greater under each condition which suggests eucalyptus loses more oxygen and hydrogen to the aqueous phase from reactive xylan.

Previous studies on the torrefaction of woody biomass have quantified the species present in the liquid phases of woody biomasses. The main condensable products measured is reaction water from drying and dehydration reactions between organic molecules [105] and smaller amounts of acids (e.g. acetic and formic); alcohols (e.g. methanol); aldehydes (e.g. furfural); ketones (e.g. hydroxyl acetone) and aromatic alcohols (e.g. phenol) at higher temperatures [88, 105]. Bergman et al. [88, 105] quantified these products from the torrefaction of larch (softwood) and willow (hardwood) and found greater yields of water for willow when torrefied under the same conditions as larch, e.g. 7 wt% water compared with 2.7% water, produced at 250°C for 30 minutes. They also reported the main organic species present as acetic acid and methanol for willow while the main species present in the liquid phase for larch other than water was formic acid with smaller amounts of acetic acid. The differences in the composition of the liquid yields were attributed to differences in the hemicellulose composition. The formation of acetic acid and methanol are assumed to derive from acetyl, acetoxy and methoxy moieties respectively. These groups are known to branch from xylose sugars which make up xylan hemicellulose; the main polysugar found in hardwoods. This can explain the finding that eucalyptus produces a greater mass yield of liquid products with low carbon content for the aqueous phase (relative to pine), and may be attributed to similar compositional yields found by Bergman et al. Chang et al. [172] also report on the solid, liquid and gaseous products torrefaction of spruce wood and bagasse at torrefaction temperatures ranging from 260-300°C and quantified similar species in the liquid phase: the main product was water followed by acetic acid, methanol and other organic species in smaller amounts e.g. propionic acid, 1-hydroxy-2-propanone.

Chang et al. also quantified a small quantity of methoxyl-phenols in the liquid products including guaiacol, eugenol, isogenol and vanillin which derive from cleavage of the thermally unstable ether β-O-4 linkages in the lignin molecules, and these increased in quantity with increasing torrefaction severity [172]. Zheng et al. also report on the solid, liquids and gaseous yield for the torrefaction of pine, and measured lower solid mass yields and increased liquid yields with torrefaction severity [173]. In these liquid yields, water was the main liquid product, its weight percent increasing with torrefaction severity. Acetic acid was also detected as well as ketones

and furans. Similar to the work by Chang et al. the authors detected phenolic compounds which increase with torrefaction severity and are attributed to the degradation of lignin in the biomass which can occur as temperatures increase.

Mass and energy yields for the organic fraction for torrefied pine and eucalyptus are shown in Figures 5-18 and 5-19 respectively. It can be seen that mass and energy yields for the organic liquid fraction are opposite in trend to the solid yields in that, for the organic phase the mass yield is greater than the energy yield. This behaviour is expected as in torrefaction the main goal is to maximise the energy in the solid yield with as little energy distributed to the liquid and gaseous phases as possible [58].

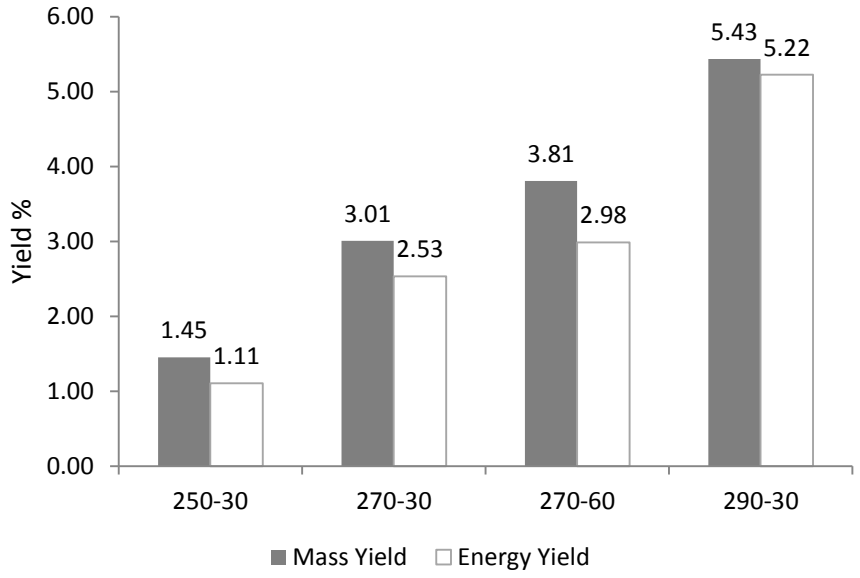

Figure 5-18 - Mass and energy yields for organic phase yields for torrefied pine

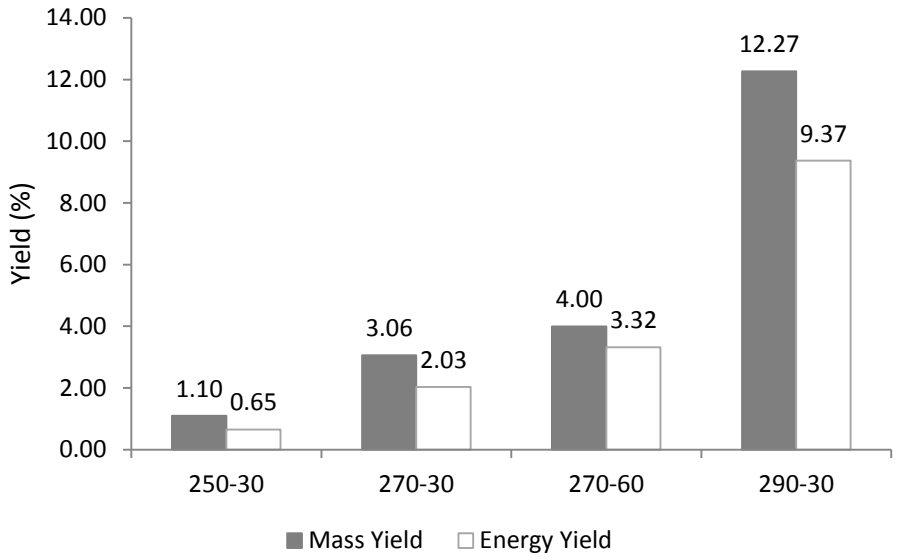

Figure 5-19 - Mass and energy yields for organic phase yields for torrefied eucalyptus

The ratios of mass loss/energy loss for the organic phase shown in Figure 5-20, reveals information on the relative changes between the two: the greater the ratio is from one signifies a greater loss of mass relative to energy. For pine, the ratios are highest for 250-30 and 270-60 highlighting that under these conditions; more mass is lost relative to the energy. For eucalyptus, the ratio shows a clearer trend with the ratio decreasing with increasing torrefaction severity until condition 290-30. Under this severe condition however, the ratio cannot be taken as an indicator of better performance (relative to 270-60) owing to the overall greater amount of mass and energy loss. As mentioned above, the sharp increase in mass yield, and subsequent energy yield for liquid products of torrefaction may be results of reactions which go beyond the optimum torrefaction reactions i.e. decomposition of the cellulose fraction. In comparing the energy yields of the organic phase for pine and eucalyptus directly, under the mildest conditions, pine retains more energy in the organic phase while under the more severe conditions, eucalyptus retains more.

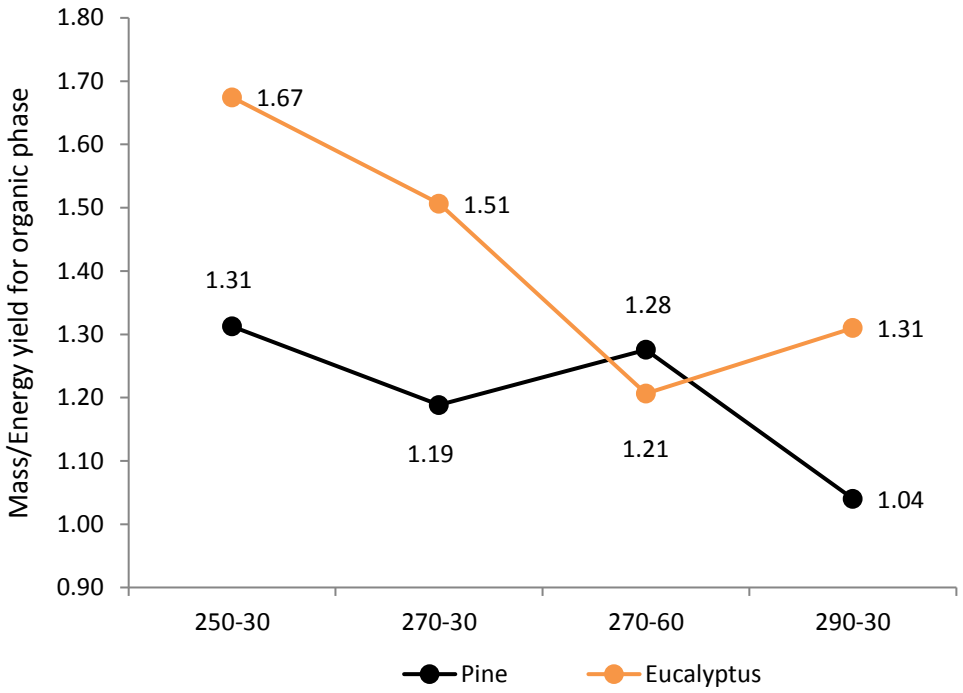

Figure 5-20 – Ratio of mass loss/energy loss for the organic phase

5.3.7 Overall Elemental Balance

5.3.7.1 Carbon balance

Using the carbon contents (wt %) derived from elemental analysis of the solid and tar phases and the carbon content of the aqueous phase derived from TOC measurements, an elemental mass balance of carbon was performed to determine its distribution between each of the solid and liquid phases. The distribution of carbon in each of the products was determined by firstly calculating the mass of carbon in the untreated fuel using the carbon weight percent from ultimate analysis and the initial mass of fuel before torrefaction. Following this, the mass of carbon in the solid, aqueous and tar product phases were calculated using the carbon contents derived from elemental analysis (solid and tar phases) and TOC (aqueous) and mass of each of the products. From this, the mass of carbon in each phase was calculated as a percentage of the initial mass of carbon to determine the distribution. Residual carbon, via the rule of conservation, was then assumed to be present in the gas phase. The results of the carbon balance for both fuels under each condition are shown in Figure 5-21.

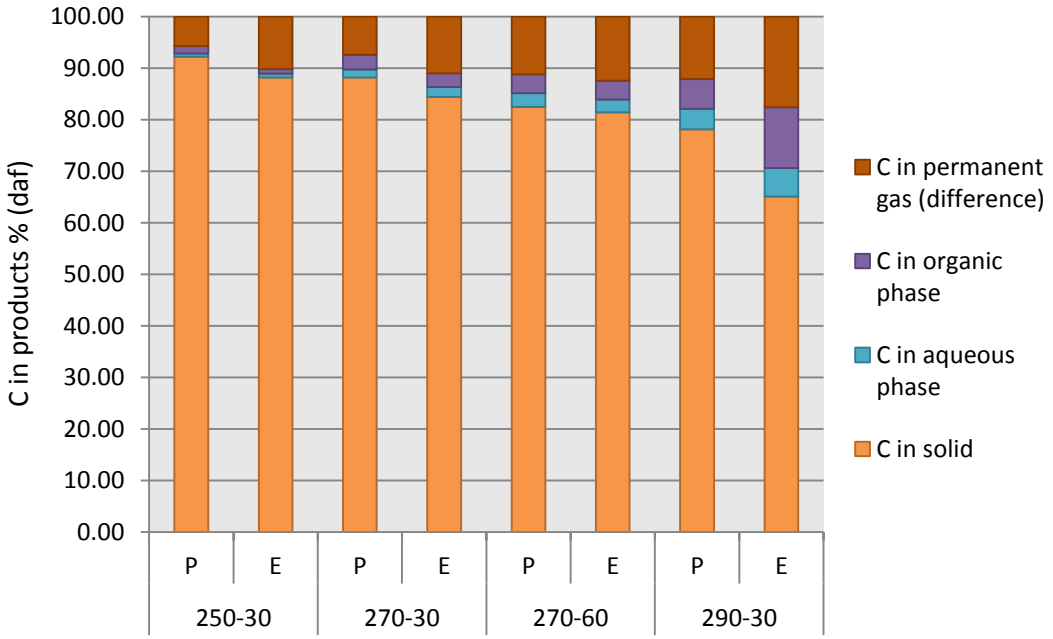

Figure 5-21: Carbon mass balance for torrefied pine (P) and eucalyptus (E) as a percentage of the original carbon mass of the untreated fuel (dry-ash free basis). C in gas phase calculated by difference.

While carbon concentrates in the solid torrefied fuel such that its weight percent increases with torrefaction severity, the carbon partitioning shows that as torrefaction conditions become more severe there is greater loss of carbon in the solid fuel with a corresponding increase in the distribution of carbon to the aqueous and tar phases. The carbon content of the gas phase, determined by difference, also increases. In comparing pine and eucalyptus, it can be seen that although the carbon weight percent of the solid eucalyptus are greater than those of pine, there is a greater loss of carbon under each condition. The differences between conditions are not significant with the exception of eucalyptus 290-30. Table 5-12 compares the ratios of carbon in product (wt %) /product yield (wt %); this providing information on the relationship between the partitioning of carbon in the fuels with respect to overall mass loss.

	250-30		270-30		270-60		290-30	
C in product/mass yield	P	E	P	E	P	E	P	E
Solid	1.044	1.005	1.058	1.072	1.089	1.11	1.106	1.158
Aqueous	0.164	0.118	0.233	0.188	0.255	0.192	0.296	0.229
Tar	0.925	0.81	0.95	0.86	0.968	0.921	1.066	0.958

Table 5-12 - Ratio of carbons in product/mass yield

Although more carbon is lost (by mass) during torrefaction of eucalyptus, Table 5-12 shows that carbon is enriched in the solid fuel to a greater degree than observed for pine under every treatment except 250-30 i.e. the ratios are greater. As mentioned above, the hemicelluloses in hardwood are more reactive than those of softwood resulting in greater mass loss and increased yield of liquid and gaseous products. So, while eucalyptus exhibits greater mass loss of carbon than pine, it exhibits a greater loss of low-energy volatile matter i.e. oxygen (and hydrogen) rich compounds. The greater ratios for pine relative to eucalyptus for the aqueous and tar yields further show the carbon enrichment of the solid fuel for the eucalyptus. This effect is in agreement with Figure 5-8; the Van Krevelen plot for the torrefied fuels where the H/C and O/C ratios for eucalyptus show greater dispersion on the plot as more H and O are lost during the torrefaction of eucalyptus.

5.3.7.2 Nitrogen Balance

The partitioning of nitrogen was performed on the solid and tar yields and the nitrogen content of these fractions were also determined using a similar methodology for carbon. Figure 5-22 shows the mass of N in the solid and tar products as a percentage of the parent fuel. As torrefaction severity increases, more nitrogen is lost from the parent fuel with a corresponding increase in the nitrogen content of the tar phase. The losses of nitrogen for pine range from 16.4 – 52.7% while the losses of nitrogen from eucalyptus range from 6.49 – 74.44%. In comparing pine and eucalyptus directly, eucalyptus retains more nitrogen in the solid product with the exception of condition 290-30. The nitrogen content of the untreated fuel for pine (0.13% d.a.f) is not significantly greater than eucalyptus (0.1%) and so the greater loss of N in likely to be result of differences in fuel-N- some studies have shown that N-content of the parent fuel is not a major factor for N-release during thermal treatment of biomass [174].

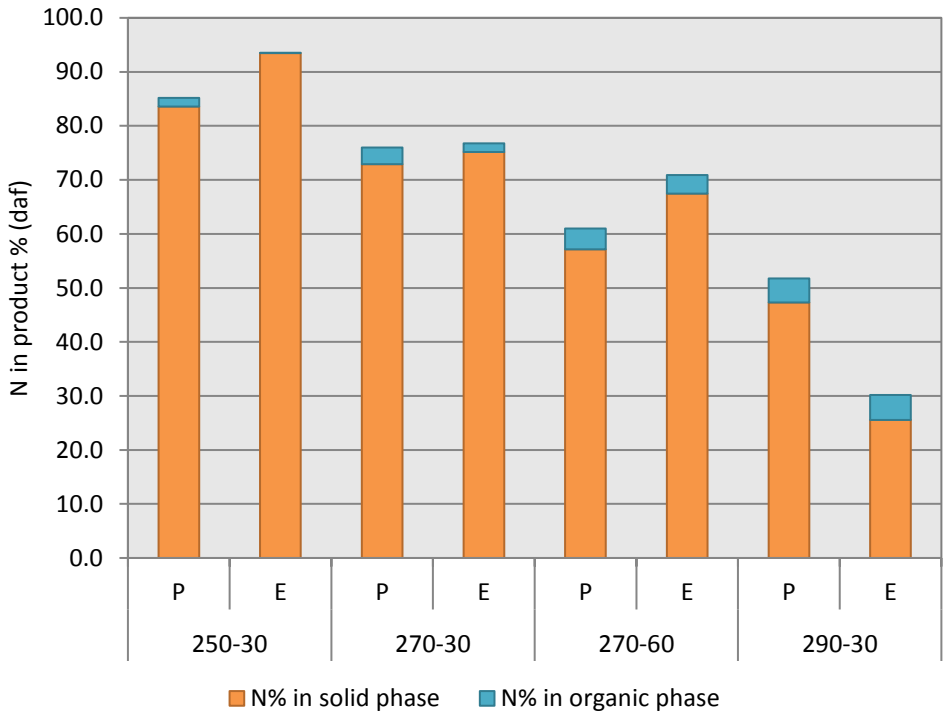

Figure 5-22: Nitrogen balance for the solid and organic phases of torrefied pine and eucalyptus.

Jones et al. [117] determined the partitioning of nitrogen during torrefaction of willow at 290°C for 10 and 60 minutes and found 0 and 40.2% of the N were lost respectively. In Figure 5-22 there is a greater loss of nitrogen in the fuels in this study. Interestingly the initial nitrogen content of the willow used by Jones et al. was greater (0.6% daf) than that found in this study and so differences in nitrogen partitioning could be due to the differences in fuel properties and composition as opposed initial nitrogen contents as mentioned above. It is important note that the balance of nitrogen detected amongst the solid and tar products does not equal 100, which could be attributed to loss of nitrogen gaseous phase discussed below.

As mentioned earlier, nitrogen in biomass exists mainly in the form of proteins and free amino acids with a small amount in the nucleic acids and enzymes [175]. Some studies have suggested that N in biomass may exist as heteroatoms in aromatic structures [176] however results of these studies are not conclusive. During thermal treatment such as torrefaction and pyrolysis, this protein-N can be retained in the wood/char or evolve in to the tar and gas phases where starts to evolve at around 200°C [175]. In the nitrogen balance above, the nitrogen in the gas/volatiles phase (calculated by difference) ranges from 6-70% as torrefaction severity increases. Studies on the release of nitrogen-species during torrefaction to the gas phase are scarce however investigations in to the partition of nitrogen to the gas phase during pyrolysis of

biomass and model compounds (i.e. proteins and amino acids reflecting the nature of nitrogen in biomass as proteins) can lend some insight in to the release of nitrogen and the nature of the species (and their reaction mechanisms) that may evolve during torrefaction. The split of nitrogen between the char and volatiles phase and the nature of nitrogen species during pyrolysis (and devolatilisation) depend on the fuel type and process temperature and residence time and tends to be preferentially retained in the char when temperature and residence time are low [154]. Thus, higher temperatures, heating rates and longer residence times promote the release of nitrogen to the gas phase during pyrolysis [154]. The main N-containing volatile species reportedly detected during biomass pyrolysis is ammonia (NH_3) with smaller amounts of hydrogen cyanide (HCN) and in some cases isocyanic acid (HCNO) [176].

The study by Leppalahti et al [177] found the dominant nitrogen species to evolve during the fixed bed pyrolysis of pine bark to be NH_3. In this study, a low heating rate (such as those used in torrefaction) of 10°C/min was applied and the pine bark pyrolysed at a final temperature of between 900-950°C in which 10-12% of fuel-N was converted to NH_3 (with 40% char yield). The authors also detected HCN however only in negligible amounts. While NH_3 was dominant in this instance, it is important to note that reaction conditions as well as the nature of N in biomass could affect the speciation of the N-containing compounds released during pyrolysis [178].

Di Nola et al [174] also investigated the partitioning of fuel-N during pyrolysis of different biomasses (woody biomass, bone meal, residues) as well as coal at different heating rates (10, 30 and 100°C/min). Results showed that more fuel-N was converted during biomass pyrolysis when compared with coal and more nitrogen was released to the volatiles phase at lower heating rates e.g. for poultry litter 21% of fuel-N was converted to NH_3 at a heating rate of 10°C/min while 15% was converted to NH_3 at 100°C/min heating rate -(HCN products for the same respective conditions were 22% and 11%, but- note the fuel and process conditions may affect the N-species evolved as mentioned above). The authors suggest that the reason for the differences in yields of N-species when increasing the heating rate from 10 to 100°C/min could be due to the introduction of heat and mass transfer limitations at higher heating rates i.e. the nitrogen volatile species may not have enough time to be released.

In drawing parallels between the nitrogen mass balance and the results of pyrolysis studies available in the literature, during torrefaction- since it can be considered as a mild pyrolysis

process, nitrogen may be evolving as either NH_3 or HCN- with more evolving as temperature and residence time increase. It is important to note at this stage that in the studies discussed above (and several others investigating the split of nitrogen during pyrolysis for biomass) the analyses are performed under dynamic conditions up to the final pyrolysis temperature. Thus, there are no significant dwell stages at or around the torrefaction temperatures such as those used in this study. It could be assumed therefore that the long the residence times in this study (30-60 minutes) along with increasing temperature (250-290°C) may have resulted in the evolution of nitrogen species to the gas phase during torrefaction. As mentioned above, Di Nola et al. [174] suggest that at low heating rates, the evolution of N containing volatiles is more likely to occur due to the absence of heat and mas transfer limitations that occur under high heating rates. The low heating rates and relatively longer residence times (when compared with the pyrolysis studies mentioned above) in torrefaction may therefore promote the release of N-volatiles.

While several studies have quantified the release of NH_3 and HCN during pyrolysis, the reaction mechanisms for their evolution are still poorly understood from review of the available literature however several mechanisms are suggested. For NH_3, its formation may result from the direct cleavage of amine groups present in the biomass [154] or the thermal cracking of N containing tar products [176]. There are also suggestions that NH_3 may derive from hydrogenation of HCN on the surface of the biomass particles however this mechanism is more dominant in coals than in biomass. HCN (and HCNO) evolution has been suggested to occur as a result of the cracking of cyclic amides formed as primary pyrolysis products [176]. Understanding of the mechanism of N-species has centred on the products of pyrolysis of model compounds (amino acids & protein), as N in biomass is known to exist in these forms. Studies on these compounds have shown that temperature and amino acid composition affect the split of nitrogen between the char and gas phases during pyrolysis as well as the NH_3/HCN selectivity [176, 178]. Using FTIR, Ren et al. [178] quantified the N-species evolved from the neat pyrolysis of several amino acids and pyrolysis of selected amino acids blended individually with hemicellulose, cellulose and lignin to determine the effect of amino acid composition and synergistic effects with the cell wall components on the nitrogen species evolved. Results of the neat pyrolysis experiments showed a great dependence on amino acid composition on the N product evolution: for some amino acids- glycine, leucine and phenylalanine - NH_3 was the dominant species while HCN was the dominant species in the pyrolysis of proline, aspartic acid, and glutamic acid although it is important to note that not all of the N was converted. To clarify with examples: almost 80% of the fuel-N in leucine was converted to NH_3 while the greatest conversion of fuel-N to HCN was only 26% for proline. Nevertheless, these variations highlight selectivity for N-volatile species

depending on the amino acid composition and by extension the nature of N in the biomass fuels. For the individual co-pyrolysis of selected amino acids (aspartic acid, leucine and proline) with hemicellulose, cellulose and lignin, the effect of these blends had varying effects on the NH_3 and HCN yields. For example, for aspartic acid, the plot of NH_3 concentration vs. time when blended with lignin was bimodal (the two peaks corresponding to deamination of aspartic acid and later secondary reaction of lignin with tar) with an overall conversion of fuel-N to NH_3 of 21%. The yield of NH_3 from aspartic acid when blended with hemicellulose and cellulose was 12 and 9% respectively. The yields of HCN showed different behaviours with yields of 22, 14 and 14% when blended with cellulose, hemicellulose and lignin respectively. As the neat pyrolysis of aspartic acid resulted in conversion of fuel-N to 0.2% NH_3 and 3% HCN, it shows greatly the effect of the cell wall components on N-volatiles yield. In the case of proline, the conversion to NH_3 increased when blended with cell wall components however the conversion to HCN decreased when blended.

While the study by Ren et al. used higher temperatures (800°C) than those used in this research, the results show that nitrogen species evolution is highly selective to cell wall species. Thus, during torrefaction, where the relative concentrations of lignocellulosic components change as the reaction progresses, this may be a factor in the evolution of nitrogen. Increasing temperature and residence time and the resultant alteration of the biomass components may be promoting the release of these N-species.

Some of the possible routes for nitrogen evolution are discussed above however it must be noted that the parent fuels have very low nitrogen content to begin with which are close to the limit of detection of the instrument (LOD = 0.1%) and so detection and subsequent evaluation at such low concentrations must be taken with caution as the room for error becomes larger.

Comparing the mass of nitrogen per unit energy provides information on the amount of nitrogen that may be released per unit energy and are shown in Table 5-13. It can be seen that with increasing torrefaction severity, there is a reduction in nitrogen per unit energy. This highlights a potential improved performance of torrefied fuels with regards to potential reduction in NO_x emissions where the mass of N per unit energy is of interest to large-scale plant with restrictions in place to the amount of NO_x that can be emitted.

		HHV MJ/kg	HHV GJ/kg	N wt% (daf)	N kg/GJ
Untreated	P	19.48	0.019	0.13	0.07
	E	20.23	0.020	0.10	0.05
250-30	P	20.55	0.021	0.12	0.06
	E	20.33	0.020	0.11	0.05
270-30	P	20.76	0.021	0.11	0.06
	E	21.59	0.022	0.10	0.05
270-60	P	21.46	0.021	0.10	0.05
	E	21.69	0.022	0.10	0.04
290-30	P	21.71	0.022	0.09	0.04
	E	22.13	0.022	0.05	0.02

daf = dry-ash free

Table 5-13 - Nitrogen in torrefied pine (P) and eucalyptus (E) on an energy basis

5.3.7.3 Hydrogen Balance

As discussed already, one of the main drivers of torrefaction is to drive off low energy volatile compounds that contribute to the low calorific value; the loss of these compounds to the benefit of energy-rich elements like carbon and non-oxidised hydrogen (i.e. H in hydroxyl groups) is desired. Figure 5-23 shows the results of the hydrogen mass balance shown as percentage of the hydrogen in the parent fuel.

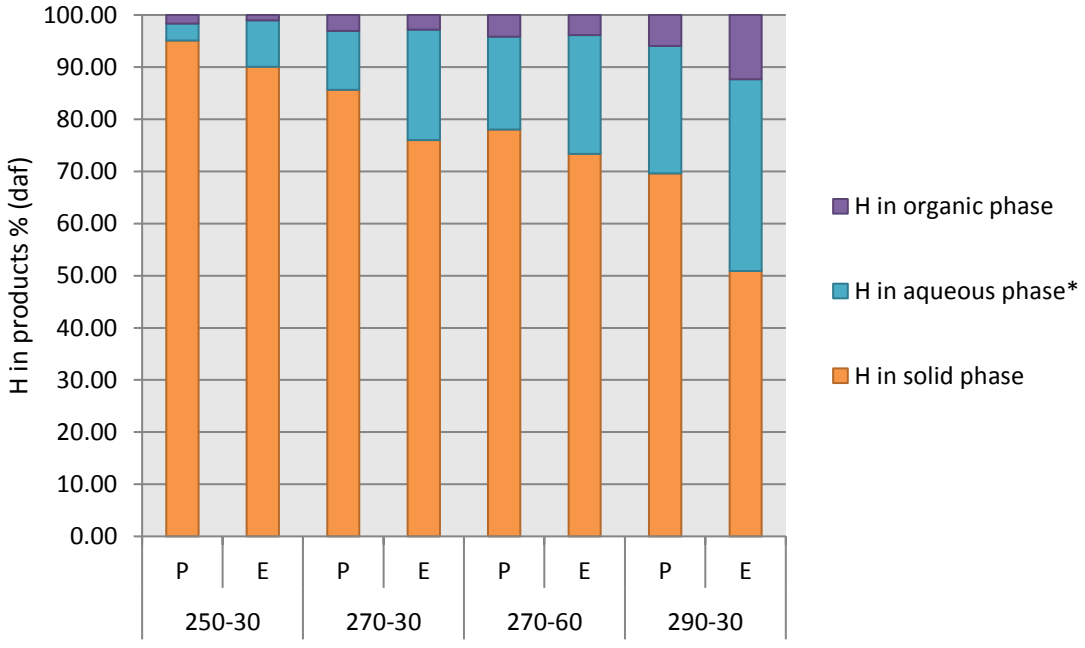

Figure 5-23 – Hydrogen mass balance for torrefied pine (P) and eucalyptus (E) as a percentage of the original mass of hydrogen in the untreated fuel (dry-ash free basis)

As expected, owing to the loss of reactive volatile materials containing hydrogen, there is greater loss of hydrogen with increasing torrefaction severity. It is important to clarify that unlike oxygen, hydrogen does contribute some energy content to solid biofuels however when covalently bonded to oxygen in the form of moisture, there is no contribution of energy from this element. The distribution also shows that eucalyptus loses more hydrogen relative to its pine analogues. Note that the calorific value for torrefied eucalyptus fuels are higher than pine for most conditions; the loss of hydrogen ascribed to oxygen one of the contributing factors. In this balance, the hydrogen content of the aqueous phase was calculated by difference. While the permanent gases of torrefaction may contain hydrogen containing gases such as methane (CH_4) or other low molecular weight alkanes such as ethene (C_2H_4), the quantities measured are often negligible [104] and so the remaining hydrogen in this instance is assumed to distribute to the aqueous phase alone.

In comparing the distribution of hydrogen in the liquid phases with the carbon distribution in the liquid phases (Figure 5-21), an inverse correlation for these elements in the aqueous and tar phases is apparent i.e. for carbon, the organic phase contains more carbon relative to the aqueous phase and for hydrogen, the aqueous phase contains more hydrogen than the organic phase. While quantification of the species present in each phase was not undertaken, the main species that would be expectedly reside in the aqueous phase is water from dehydration reactions and polar volatile species such as alcohols while the organic phase would be assumed to contains carbon rich species non-polar species.

5.4 Conclusions

The torrefaction of pine and eucalyptus under four conditions have been investigated. With increasing torrefaction severity, the mass yield of solid product decreases while the yield of liquid products increases. The solid mass yields (dry basis) for pine range from 90.7% to 72.3% while eucalyptus loses more solid mass under each condition with yields ranging from 89.4%-57.9%. The lower mass yields for eucalyptus are attributed to increased reactivity in the form of more reactive components in the hemicellulose fraction; xylan the main component of hardwoods (eucalyptus) when compared with glucomannan for softwoods (pine). The increased mass loss for eucalyptus corresponds to greater liquids yields (aqueous and organic phase) relative to pine. The permanent-gas yields were not quantified in this experimentation however caution was taken to attribute the remaining mass ‘left-over’ to permanent gases owing to any potential experimental error during mass balance.

The result of changes in lignocellulosic composition show that the hemicellulose content decreases with increasing torrefaction severity with almost all hemicellulose depleted by condition 270-60 for pine and 270-30 for eucalyptus. The cellulose contents also steadily increases before gradually starting to decrease at higher temperatures and residence times which may be a result of the onset of cellulose decomposition. Eucalyptus torrefied at 290-30 however shows greater loss of cellulose most likely as a result of carbonisation during torrefaction. The lignin contents also increase with torrefaction severity suggesting this component remains largely intact during torrefaction.

Proximate analysis of untreated and torrefied fuels show a decrease in the moisture and volatile matter with a corresponding increase in ash weight percent and fixed carbon. The results of the ultimate analysis correspond with the results from the proximate analysis as there is an increase in carbon content of the fuels and a decrease in oxygen and hydrogen content with increasing torrefaction severity. A Van Krevelen plot for the untreated and torrefied fuels shows a decrease in the H/C and O/C ratios with torrefaction with greater differences between the ratios for each condition for the eucalyptus fuels indicating that torrefaction has a greater effect on the chemical properties of eucalyptus than pine. The HHVs for the torrefied materials is higher than the untreated fuels as a result of this effect, with eucalyptus having a higher calorific value, under each condition, than pine for every condition (including untreated) with the exception of condition 250-30. The energy yields however are greater for pine under each condition although the relative difference in energy yields between pine and eucalyptus under each condition get smaller up to condition 270-60. The effect of torrefaction on the grinding behaviour of pine was investigated by measurement of the $HGI_{equiv.}$ and particle size distribution. The result for both tests show than the milling behaviour of untreated pine is very poor ($HGI_{equiv.} = 1$) however this is improved with torrefaction as the $HGI_{equiv.}$ values range from 24 for the mildest condition (250-30) to 67 (290-30) for the most severe. The particle size distribution also shows an improvement in grindability as a greater number of particles pass through smaller aperture sieves with increasing torrefaction severity.

Results of the analysis of the liquid products of torrefaction show greater carbon contents in both the organic and aqueous fractions for pine. For both fuels, the carbon in these fractions can be attributed to species arising mainly from the decomposition of hemicellulose and limited

decomposition of cellulose during torrefaction. As the results of ultimate and proximate analysis of the solid torrefied fuels show a higher carbon content and lower oxygen content for eucalyptus than pine the reciprocal is expected for the liquid yields and is shown in the measured data.

Overall elemental balances show a greater loss mass loss carbon than pine under each condition however the differences are very slim with the exception of treatment 290-30. The results also show nitrogen is retained in eucalyptus more so than for pine; the nitrogen on an energy basis decreasing for pine upon torrefaction. The hydrogen mass balance shows a greater amount of hydrogen is lost during torrefaction than for pine, again with the exception of treatment 290-30.

6 The combustion characteristics of high-heating rate chars from untreated and torrefied biomass fuels

6.1 Introduction

The previous chapter in this thesis investigated the effect of torrefaction on the chemical and physical properties of two biomass fuels. Understanding how torrefied materials behave in thermochemical conversion systems (e.g. combustion systems) represents one of the fundamental next stages in torrefaction research to understand how these materials may behave in real-life scenarios. As discussed in section 2.2 torrefaction will have an impact on the combustion properties of the resultant fuels such as the pyrolysis and oxidation kinetics, the latter largely unknown for the chars prepared with fast heating rates at high temperatures which is important when making comparisons to industrial system where these conditions are observed. Another unknown is the partitioning of potassium and nitrogen during high heating rate devolatilisation of torrefied materials. Knowledge of the partitioning of these elements is crucial as potassium is an important catalytic metal for both the pyrolysis stage and the char combustion stage and it also is a key player in dictating ash behaviour at higher temperatures. With respect to nitrogen, knowledge of the partitioning of this element is important due to potential NO_x emissions which largely arise from nitrogen retained in the char after devolatilisation. In order to understand the effects listed above, fast heating rate chars from untreated and torrefied eucalyptus and willow were prepared in drop tube furnace at 1100°C and char oxidation kinetics determined. The surface areas of the chars were also determined to yield intrinsic reactivities, yet another area where information is lacking in the literature. The nitrogen and potassium partitioning of these fuels were also investigated to determine the effect torrefaction may have. The devolatilisation kinetics of the fuel using TGA were also determined. The results are presented below.

6.1.1 Samples

Two fuels, eucalyptus and willow, and their torrefied counterparts were used in this study. These fuels were obtained from a previous study (see Ibrahim et al. [107]), and thus are not the same fuels analysed in Chapter 5 however a brief description is presented below. Both fuels, in chip form, were torrefied using the torrefaction reactor and methodology described in Section 4.4. The torrefaction conditions used in this experiment are listed in Table 6-1.

Nomenclature in text	Temperature (°C)	Residence Time (minutes)
270-30	270	30
270-60	270	60
290-30	290	30

Table 6-1 – Torrefaction conditions for willow and eucalyptus fuels

6.1.2 Experimental Methods

6.1.2.1 Char preparation

Each of the untreated and torrefied fuels were milled and sieved using the methodology described in Section 4.5.4 to obtain a size fraction of 212-355µm. High heating rate chars were then prepared at 1100°C with a residence time of ~600ms from each of the untreated and torrefied fuels in a drop tube furnace described in Section 4.5.4.

6.1.2.2 Characterisation of fuel and chars

The fuels and chars were characterised for their ultimate analysis, proximate analysis, calorific value, surface area and metals analysis using the experimental methodologies outlined in Section 4.4. Pyrolysis experiments of the untreated and torrefied fuels and the char combustion experiments of the drop tube furnace chars were performed using the methodology described in Sections 4.6 and 4.7.

6.2 Results and Discussion

6.2.1.1 Fuel and Char Characterisation

The proximate and ultimate analyses, calculated higher heating values (HHV) and specific surface areas of the untreated and torrefied woods are given in Table 6-2. As expected, torrefied fuels have lower moisture, volatiles and oxygen contents, and higher ash and carbon contents. Furthermore, the more severe the torrefaction conditions, the larger these differences become. Torrefaction appears to have a more prominent effect on the eucalyptus fuels where the decrease in oxygen and volatiles contents is greater when compared to willow torrefied at the same condition. This increased apparent reactivity of eucalyptus was also identified in Chapter 5 where torrefaction had a greater effect on eucalyptus relative to pine. While reasons for the

differences in the reactivity of pine and eucalyptus in Chapter 5 were attributed to differences in composition (i.e. softwood and hardwood respectively) - and indeed in this current study both willow and eucalyptus are hardwoods, it is likely the case that the composition of these hardwoods differ as they are different fuels. Eucalyptus may possess more reactive hemicellulose than willow which upon torrefaction, are degraded more readily. Since carbon is preferentially retained in the solid during torrefaction, HHV calculations result in higher values for the treated fuels when compared to their untreated counterparts. Again, similarities can be found between the two eucalyptus fuels in Chapters 5 and 6- notably under condition 290-30 where in both cases the carbon and fixed carbon contents increases rapidly from the previous condition 270-60 and the volatiles content decrease. While the composition of cell wall components was not undertaken for this eucalyptus fuel, it is possible that carbonisation of the cellulose fraction had begun to occur as a result of exothermic activity at 290°C as was the case for Chapter 5 eucalyptus. It can also be noted that both willow and eucalyptus are low nitrogen fuels. The sulphur contents of all fuels were below detection limits (< 0.01%).

	Willow				Eucalyptus		
Parameters	Raw	270-30	270-60	290-30	Raw	270-30	290-30
Moisture (% ar)†	6	3.9	3.8	3.6	8	4.3	4.2
Volatile (% dry)†	84.4	73.4	72.4	63.2	79.6	67.9	60.3
Fixed C (% dry)†	15.1	26.1	27.6	36.8	18.8	19.6	39.7
Ash (% dry)†	0.5	0.5	0.7	1.1	1.6	1.6	2.2
C (% daf)	49.1	54.2	54.4	58.9	50.8	55.9	59.6
H (% daf)	5.8	5.5	5.5	5.4	5.4	5.3	5.1
N (% daf)	0.5	0.2	0.3	0.3	0.4	0.3	0.2
O* (% daf)	44.6	40.1	39.8	35.5	43.4	38.5	35.1
K (% dry)	0.23	NA	0.25	0.3	0.33	0.34	0.42
Cl (% daf)	ND	0.18	0.09	0.18	0.34	0.06	0.21
HHV (MJ/kg) (daf)	19.6	22.3	22.9	24.4	19.6	23.5	28.5
Surface Area (m^2/g)†	3.8	3.4	3.1	1.9	1.1	NA	NA

† = data from Ibrahim et al [107], * = calculated by difference, NA = not analysed, ND = not detected.

Table 6-2 - Proximate and ultimate analyses of untreated and torrefied willow and eucalyptus.

The moisture and ash contents and ultimate analyses of the chars from untreated and torrefied materials are given in Table 6-3. The data listed includes the char yields obtained and specific surface areas. As the fuels enter the DTF they undergo first moisture loss followed by

devolatilisation, then begin char burnout. Using the ash tracer method described in section 4.5.5, from the ash content of the char it is possible to estimate the extent of char burnout, although this assumes that none of the ash is volatilised during char combustion. This assumption will introduce a small error since it is well known that a fraction of the potassium vaporises during pyrolysis [146, 148]. In the case of wood ash, it has been found that higher potassium losses can be expected when compared to straws, because formation of potassium silicates, like leucite ($KAlSi_2O_6$) in straw ash, results in retention of potassium in the slag [179]. The extent of char burnout will depend, among other factors, on the reactivity of the fuel, final temperature and the oxygen available for reaction with carbon deriving from both from the reaction gases (in this case ~1% O_2) and fuel-oxygen. It is noted that all chars in this study still have ~6-20% (DAF) oxygen in their structure. It can be observed that the effect of torrefaction is to slow down the char burnout (and the devolatilisation stage) such that the chars produced from the torrefied fuels have a lower extent of char burn-out. Also, the more severe the torrefaction conditions (i.e. higher final temperature and/or residence time), the lower the extent of char burnout. This indicates that the fuels have become less reactive upon torrefaction.

	Willow				**Eucalyptus**		
Parameters	Raw	270-30	270-60	290-30	Raw	270-30	290-30
Moisture (% ar)	1.4	1.39	1.47	1.6	2	1.6	1.8
Ash (% dry)	20.1	7.4	6.7	4.3	15	7.8	8
C (% daf)	80.1	84.4	87.9	84.4	87.8	89.4	87.9
H (% daf)	3	1.2	1.4	1	2.7	1.3	1.4
N (% daf)	1.4	0.3	0.4	0.4	1.1	0.3	0.2
O* (% daf)	15.6	14.1	10.3	14.2	8.4	6.5	10.5
Char Burn-Off (%) †	84	73	62	34	51	36	31
Char Yield†	3	7.1	10.5	24.4	10	20.4	27.5
Surface area (m^2/g)	57	80	17	49	94	66	10

* calculated by difference, † - calculated using the ash tracer method; see section 4.5.5

Table 6-3 - Analysis of the untreated and torrefied biomass chars.

6.2.1.2 Char Morphology

SEM images from the untreated and torrefied fuels 270-30 and 290-30 and their chars (x100 magnification) are shown in Figures 6-1 and 6-2 for willow and eucalyptus respectively. It can be seen from these images that there are apparent changes in surface morphology upon both

torrefaction and char formation. The untreated fuels for both willow and eucalyptus appear more compact with bulky xylem tissues apparent relative to their torrefied counterparts. In turn, the treated fuels seem more brittle in structure, as evidenced by the deeper fissures on the surface.

The chars produced from the untreated fuel undergo a degree of structural changes with the pointed/sharp ends of biomass particles becoming more rounded; however they maintain their apparent elongated structure. In contrast, the chars produced from torrefied biomass undergo a more severe degree of transformation and are more rounded in structure, especially in the case of fuels treated at 270-30. Disparity between the chars produced from untreated and torrefied fuels can be attributed to the alteration of the biomass structure upon torrefaction. As the fuels in this study were torrefied at 270°C and 290°C, it can be assumed the thermal treatment the fuels have undergone will have a noticeable effect on the mechanical structure of the fuels and thus the corresponding chars. In drawing parallels with the study on the changes distribution of cell wall components in Chapter 5 for eucaltypus, by condition 270-30, almost all of the hemicellulose had been degraded. As this condition is the mildest treatment used in this study, it is possible that for the willow and eucalyptus in this study, a similar loss of hemicellulose has occurred. The loss of hemicellulose, which provides structural integrity binding the cellulose macrofibrils together, may result in the changes that are observed for the torrefied chars which are more rounded in appearance. These differ from the chars prepared from untreated fuels which retain their elongate structure bearing closer resemblance to the parent fuel. In the case of the chars from torrefied fuels with a more rounded appearance, this transformation is reminiscent of that observed for high vitrinite bituminous coals during devolatilisation, whereby coal particles undergo transformation to cenosphere char particles that have melted and then re-solidified [135]. Similar findings have been reported by other researchers, such as Tolaven et al [180], who also observed a change in the appearance of torrefied particles upon pyrolysis in a DTF; the resultant char particles looked like droplets with an aspect ratio closer to one (relative to the original torrefied fuel prior to pyrolysis). Tolvanen at al. [180] suggested that formation of liquid intermediates by some of the components in the torrefied wood could be the reason for this behaviour. In all the images of char particles, there is evidence of open pores on the surface, which were not visible on the fuels prior to devolatilisation in the DTF. These pores can be attributed to volatiles escaping from the particles due to the rapid heating and relatively high temperatures the particles have been exposed to. Upon heating the particles at high-rates and relatively high temperatures, there is rapid escape of volatile gases as a result of overpressure within the particles which results in the evolution of pores across the surface. From the SEM

images, the chars produced from Willow 270-30 show pores which appear more macroporous in size, with evidence of particles with a hollowed out shell structure. Note that these chars have undergone a higher degree of burnout than the most severely torrefied biomass chars. The chars produced from willow torrefied under more severe conditions (290°C and 30 minutes) show less evidence of hollowed out structure, but a more uniform coverage of pores of varying size can be observed instead. A similar trend is observed for eucalyptus chars. These differences in surface morphologhy upon fast pyrolysis for untreated and torrefied fuels are in agreement with Fisher et al. [181], who also observed similar changes in torrefied fuels at high heating rates.

The BET surface areas for the fuels and chars are also listed in Tables 6-2 and 6-3, respectively. Upon torrefaction, willow shows a slight decrease in surface area, which becomes more significant at the more severe process conditions (290-30); this increase was unexpected, since the opposite effect has been reported previously by other researchers (e.g. [105],[182]). For the chars, whilst for eucalyptus chars the surface area decreases as the torrefaction temperature increases (up to ~10-fold in reduction is observed with respect to the parent fuel char), for willow chars, the surface area decreases in the order Willow 270-30 > Untreated Willow > Willow 290-30 > Willow 270-60. The surface areas of the willow chars do not appear to follow any trends, due to the values obtained for the the Willow 270-30 and Willow 270/60, but it should be noted that the chars have different degrees of burnout, as discussed below.

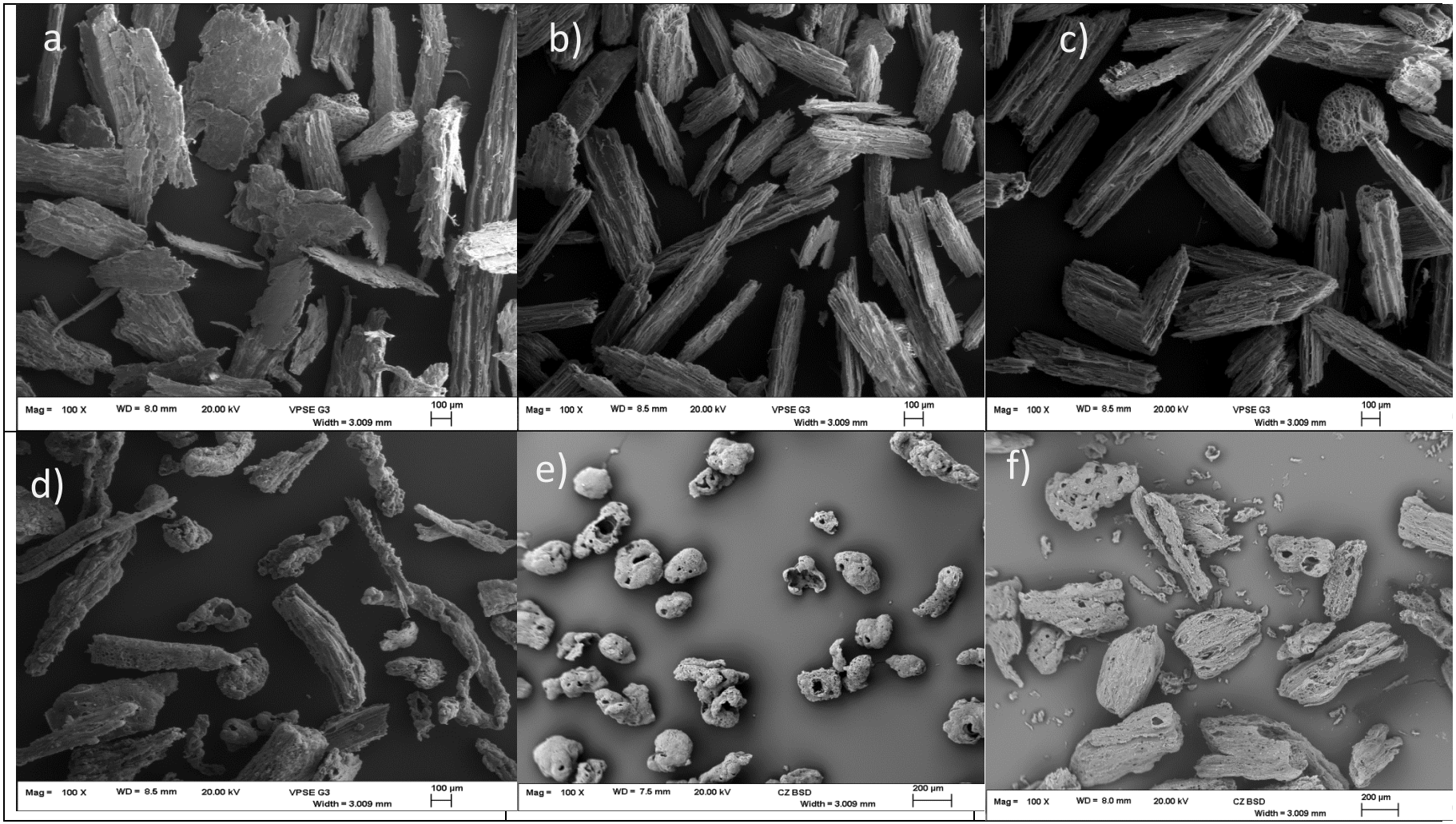

Figure 6-1 - Scanning electron micrographs x100 magnification of willow fuels (size fraction 212-355um) and chars, where: a) Untreated Willow, b) Willow 270-30, c) Willow 290-30, d) Untreated Willow char, e) Willow 270-30 char, f) Willow 290/30 char.

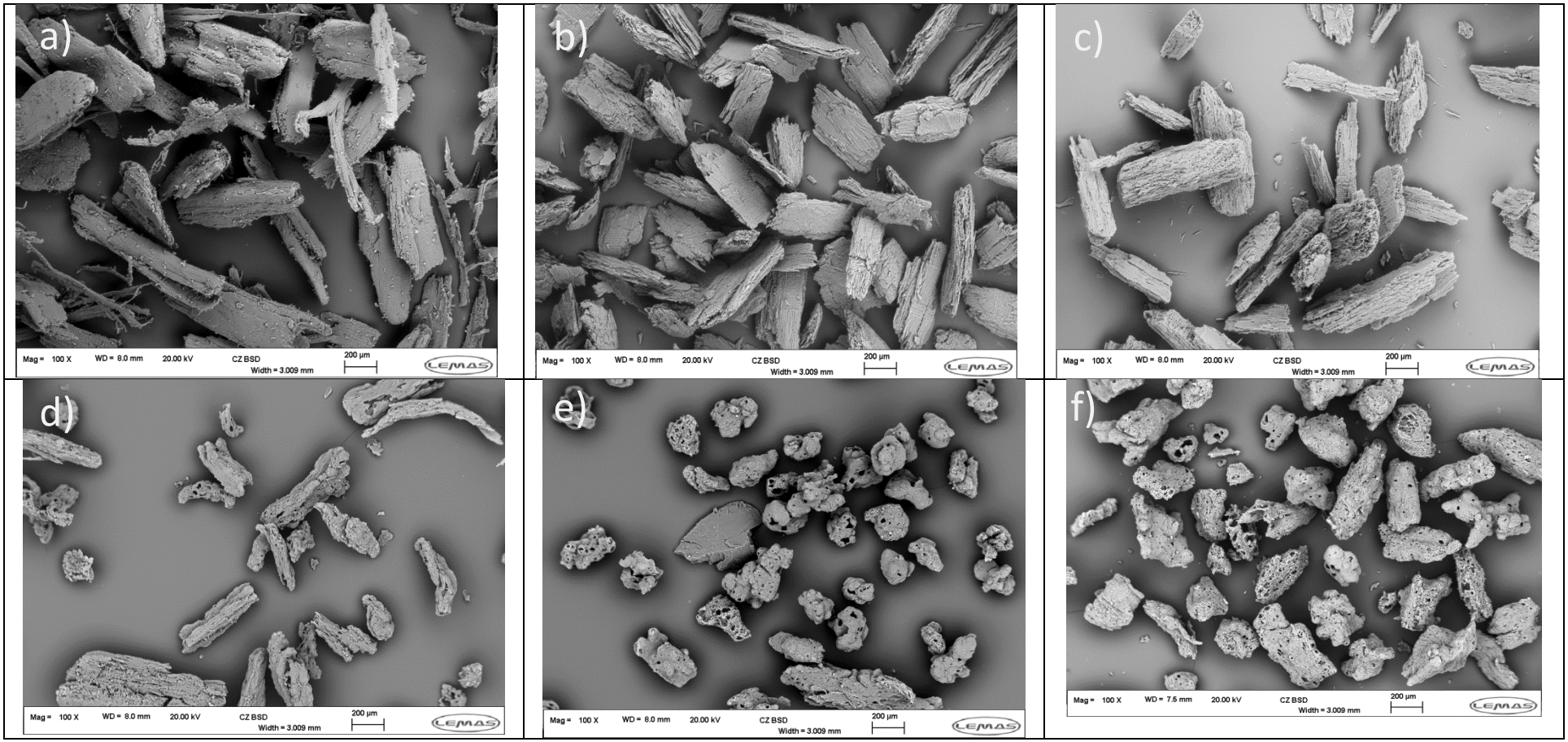

Figure 6-2 - Scanning electron micrographs x100 magnification of the eucalyptus fuels (size fraction 212-355um) and chars, where: a) Untreated Eucalyptus, b) Eucalyptus 270-30, c) Eucalyptus 290/30, d) Untreated Eucalyptus char, e) Eucalyptus 270-30 char, f) Eucalyptus 290-30 char.

The development of pores across char particles upon heating, which will develop the exposed surface area of chars, are strongly affected by the pyrolysis conditions in which the chars are prepared with heating rate being a key factor [122]. It is observed that for the chars produced from both untreated and torrefied willow and eucalyptus, the morphology and particle structure transforms significantly. This is particularly clear in the case of chars produced from all torrefied materials where the particles are clearly distinguishable from the parent fuel highlighting the impact fast-heating rates have on particle structure and specific surface area. By comparison, pyrolysis under slow-heating rates produce chars which differ in surface morphology to those produced under high heating rates as slow heating rate chars allow for escape of volatiles through 'natural' porosity and as a result often do not show notable changes in surface area from the parent fuel [138, 181, 183, 184].

The magnitude of the surface area measured for biomass chars will vary depending on a number of factors such as temperature during pyrolysis, oxygen partial pressure and residence time, i.e. parameters which affect the degree of conversion [122]. In the case of chars produced from eucalyptus, the surface areas decrease with decreasing char burnout. Untreated eucalyptus contains more volatiles than its torrefied counterparts, which, as an indicator of reactivity, could explain the increased degree of char conversion for this fuel. While this surface area trend is not shown by the chars produced from willow fuels, it should be noted that the highest surface areas reported for willow char is from the untreated fuel which undergoes the highest degree of char conversion. Additionally, because of the fibrous nature of biomass, a range of particles with varying diameters and lengths can be observed within the sieved fraction, and smaller particles will undergo a higher degree of burnoff compared to larger particles leading to heterogeniety. In this study, a 1% oxygen environment was used during pyrolysis and various degrees of burnout are observed (Table 6-3). In general, a trend for an increase in surface area as burnout decreases can be indentified. It must be noted that surface area is expected to pass through a maximum with burn-out where an initial development of porosity in the early stages of burn-out resulted in an increase in surface area while the collapse of pores towards the end of burn-out results in a decrease of surface area.

The surface area of the particles may also be affected by the annealing at high temperatures as a result of micropore coalescence [184]. At high temperatures, the biomass particles may begin to melt resulting in a loss of the cell wall structure [138]. In the case of the willow 270-30 and eucalyptus 270-30, SEM images show the particles to be smaller and more rounded relative to

the other chars. Since an unexpected lower surface area was measured ifor the illow 270-60 char, it is possible that this change in morphology could be due to annealing at high temperature

In general, surface areas of chars from torrefied biomass were found to be lower than those produced from untreated biomass. While these results are reported it is important to note that accurate surface area measurements of biomass chars are difficult to perform with high confidence due to the nature of these materials. Biomass chars may still contain volatile matter which can slowly release during analysis (effectively increasing the pressures in the reaction cells) leading to inaccurate measurements and so adequate outgassing prior to analysis is essential to avoid error as a result of this in surface area determination. In addition, for carbonaceous materials dominated by micropores, nitrogen adsorption at cryogenic analysis temperatures (-196°C) can be limited by the slow rate of diffusion of nitrogen molecules into the micropore structure, leading to an underestimation of the surface area of the particles as equilbrium is not achieved in the designated time [142]. This underestimation is especially evident when comparing measurements using a different adsorbing molecule such as CO_2 which is often used as the adsorbate in the case of biomass fuels and chars where micropores are prevalent. The figures reported using this latter method are often considerably higher than the measurements taken using N_2 [183]. For instance, Guerrero et al. [134] report very high surface areas of 528m^2/g and 539m^2/g, for eucalyptus high heating rate chars from a fluidized bed reactor at 800°C and 900°C, respectively using CO_2 adsorption. For the chars in this study however, adsorption with N_2 and the BET method was deemed appropriate as the presence of hysteresis loops characerised by type IV isotherms (as a result of capillary condensation in the mesopores) suggests the chars possess a mesoporous network structure. Measurement was still challenging and required long degassing periods and multiple repeats to give confidence in the results reported. Special care was taken during outgassing of the biomass chars and the BET values reported show linear correlation between 0.05 and 0.3 P/P_0 ($R^2 > 0.995$).

6.2.1.3 Potassium Partitioning

The concentration of potassium (K) for untreated and torrefied fuels are shown in Table 6-2. It can be seen that the potassium tends to concentrate in the torrefied fuels, as its content increases with increasing torrefaction severity for both willow and eucalyptus; with the concentrations in the eucalyptus fuels higher than the willow fuels, for both untreated and torrefied. During torrefaction, it has been suggested that potassium existing as water soluble chlorides (KCl) can react with functional groups on biomass such as carboxylic acids releasing

HCl gas whilst incorporating potassium into the fuel matrix [185]. The chlorine concentrations of the untreated and torrefied fuels are also shown in Table 6-2, where in the case of eucalyptus there is an observed decrease in chlorine concentration upon torrefaction which could be the result of these reactions taking place.

In the case of the chars metal analysis by conventional methods, such as acid-digestion and ICP-MS (as performed on the parents fuels) was not an option. This was because only small amounts are produced owing to the very low char yields associated with fast-heating rate devolatilisation and high volatile matter contents of biomass. EDX analysis was employed instead to obtain information on the metal content of both fuels and chars. For this purpose, samples were ground in order to expose the internal structure of the char; the incident electron beam on to the surface of the particles penetrates around 1-2 microns in depth making it a semi-quantitative method of analysis using the assumption that the entire particle is homogenous from centre to surface. From the char yields as listed in Table 6-2 and the potassium contents of the fuels and chars (average values calculated from a series of measurements taken using different particles from the same fuel or char), it was possible to obtain estimates of potassium partitioning, i.e. the split of potassium in the fuels between the char and volatiles upon reaction in the DTF. An example calculation for willow 270-30 is shown below:

Average K content of fuel from EDX analysis = 0.18%

Average K content of char from EDX analysis = 0.88%

Char yield using Ash Tracer Method = 7.1%

% K retained in char after devolatilisation in DTF = ((0.88/100*7.1/0.18)*100 = 34.51%

% K Evolved to the gas phase in DTF = 100 – 34.51 = 65.49%

A plot of the fraction of potassium evolved with char burnout is shown in Figure 6-3. It can be seen clearly from this plot that potassium evolves as the char combusts, and from the trend observed it can be reasonably assumed that it evolves monotonically with carbon.

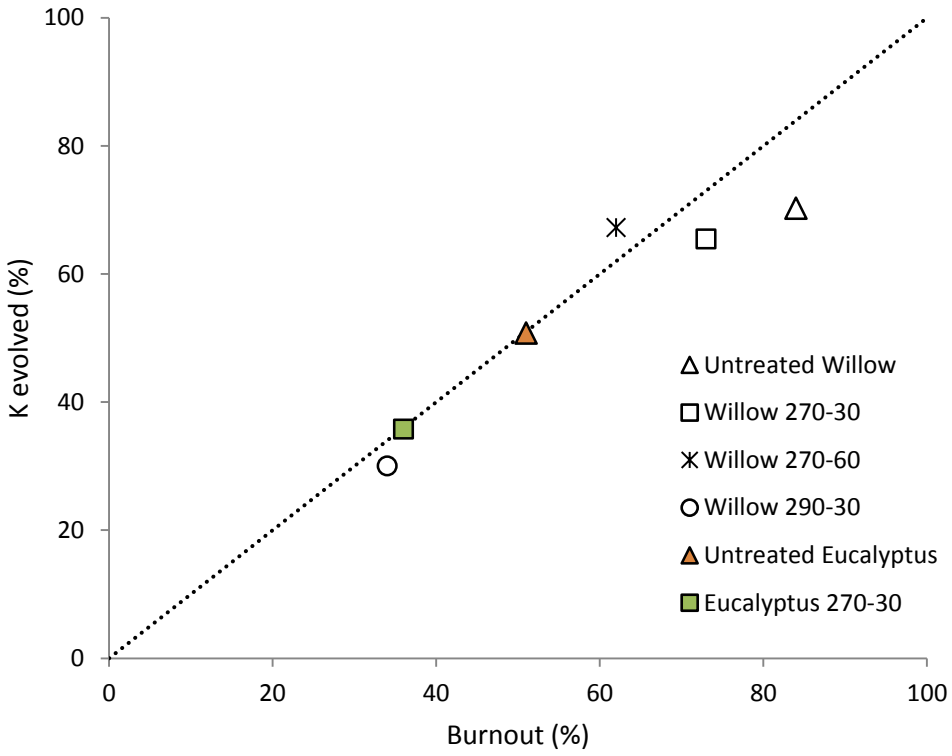

Figure 6-3 – Potassium partitioning vs. Char Burn-out for untreated and torrefied fuel

6.2.1.4 Nitrogen Partitioning

As shown in Table 6-2, there is a reduction in nitrogen content of the fuels with torrefaction. The reduction in the fuel C/N ratios upon torrefaction also highlights this effect. The partitioning of nitrogen between the volatiles and the remaining char during the devolatilisation in the DTF was calculated by a material balance from the nitrogen content of the fuel and that of the char. The results for nitrogen partitioning calculations for the willow and eucalyptus fuels and their chars are shown in Table 6-4. It can be seen that the release of nitrogen to volatile phase ranges from 72-92% across all fuels. These figures are comparable to the ones reported previously from pyrolysis of a range of untreated fuels (79-91%) [186] but higher than the ones obtained for untreated and torrefied willow (56-59%) [117] in a pyroprobe at 1000°C. It is to be noted that in the present study, the fuels have been devolatilised at a higher temperature (1100°C), which may have promoted further nitrogen release.

	Willow				Eucalyptus		
Parameters	Raw	270-30	270-60	290-30	Raw	270-30	290-30
Fuel C/N	0.009	0.003	0.005	0.004	0.007	0.005	0.003
Fuel-N in char (%)	7.9	12.7	8.7	26.7	27.8	16.9	18.9
Fuel-N in volatiles (%)	92.1	87.3	91.3	73.3	72.2	83.1	81.1

Table 6-4 – Nitrogen partitioning between the char and volatile phase during HHR pyrolysis for untreated and torrefied willow and eucalyptus

There also appears to be an opposite trend upon torrefaction for willow and eucalyptus: torrefaction of willow appears to result in retention of nitrogen in the char phase during pyrolysis whereas torrefied eucalyptus appears to promote release of nitrogen to the volatile phase during pyrolysis. It must be noted therefore that the split of nitrogen into volatiles and char are highly dependent on fuel type [154]. While the amount of nitrogen released to the volatiles phases is dependent on fuel type, the pyrolysis conditions also affect the amount of nitrogen released, with low temperatures and residence times favouring the retention of nitrogen in the char. At higher temperatures, some of the fuel-N retains in the char matrix while some is released to the volatile phase via series of reactions (e.g. rupturing, cross-linking substitution etc.) as light gases and oils [187]. Nitrogen containing species in the volatile phase can thus exist via primary and/or secondary pyrolysis reactions. In the case of the former, NH_3 can evolve as a primary pyrolysis product through direct cleavage of amino/amide groups in the biomass [154]- note speciation of N in biomass and evolution of N-species released to the volatile phase during pyrolysis were discussed in section 5.3.7.2 and will be extended for devolatilisation in this section. The evolution of NH_3 as a primary reaction product is found to be characteristic of biomass and low-rank coals [154]. In the case of nitrogen-containing species from secondary pyrolysis reactions- NH_3, HCN and HNCO can be formed via various homogenous and heterogeneous reaction mechanisms. One secondary reaction that has been identified as a route for the formation of the compounds listed above is the cracking of 2,5-diketopiperazine (DKP) [175]. This cyclic amide, formed during the dehydration of proteins (primary reaction), can yield N-containing species depending on the location of bond cleavages in the structure shown in Figure 6-4 [175].

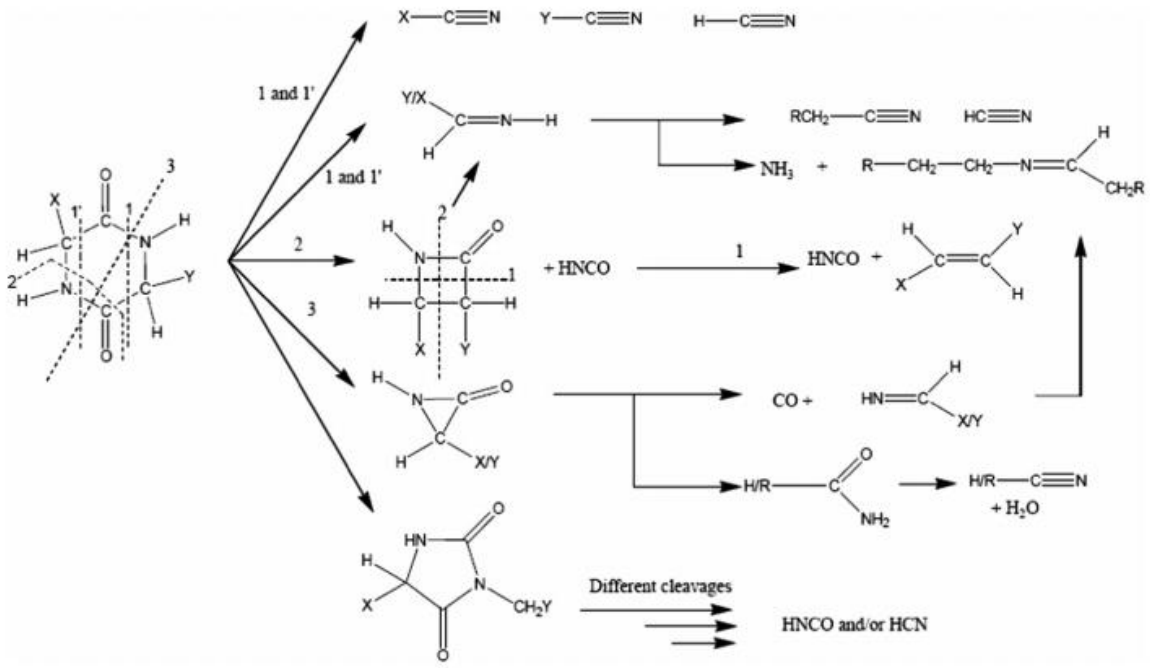

Figure 6-4 – Secondary cracking of 2,5-diketopiperazine (DKP) [188]

Ren et al. [175] state that the main products of secondary reactions are nitrile, amines, pyrroline, hydantoins and α-lactam as shown in Figure 6-4. From these products, further secondary reactions occur- NH_3 can form via secondary cracking of amine compounds while HCN and HNCO can form via cleavage of hydantoin products of DKP cleavage [175]. In addition to the mechanisms listed above, other secondary reactions include the hydrogenation of HCN to produce NH_3, more typical of slow heating rate pyrolysis where there is more time for the diffusion of NH_3 through the char pores to react with hydrogen atoms on the surface [154].

As mentioned above, the release of N-species from biomass during thermal decomposition depends on the conditions, heating rate and fuel type. As the chars in this study were produced under identical conditions, the differences in nitrogen evolution can be attributed to differences in fuel composition with torrefaction having an apparent different impact on the release of volatile-N for willow and eucalyptus.

Following devolatilisation in a combustion system, char-N can then be oxidised by O_2 to NO with some smaller quantities of HCN and HNCO released (up to 20%) although formation of HNCO

from char-N is more pronounced at temperatures <1100K [154]. Thus, the reduction of char-N is desired as this is an important route for NO_x formation.

6.2.2 Fuel and Char Reactivity

6.2.2.1 Pyrolysis Kinetics

Figures 6-5 and 6-6 show a plot of the derivative of the mass loss with time curve (DTG) against temperature during the temperature-programmed pyrolysis of (untreated and torrefied) eucalyptus and willow, respectively. For both untreated fuels, there is a shoulder present on the main decomposition peak which can mainly be attributed to hemicellulose decomposition while the main decomposition peak is attributed to cellulose decomposition and the broad underlying peak is attributed to lignin decomposition. The impact of torrefaction can clearly be seen on these plots: the hemicellulose shoulder is no longer present for the torrefied fuels and relative contribution of the lignin peak increases with increasing torrefaction severity. The lignin concentration can be correlated to the fixed carbon content [189] which increases with increasing degree of torrefaction, as shown in Table 6-2.

Note the similarity in pyrolysis behaviour for untreated willow and eucalyptus (both hardwoods) with the pyrolysis behaviour of the different untreated eucalyptus sample shown in Section 5.3.4. For the eucalyptus sample analysed in Chapter 5, under condition 270-30 almost all of the hemicellulose had been depleted which is in agreement with the samples analysed here. Apparent pyrolysis kinetics were derived from the TGA data assuming a global first order reaction rate and the Arrhenius parameters are listed in Table 6-5. A rate constant calculated at 300^{o}C (k_{573}) demonstrates firstly that eucalyptus decomposes more quickly than willow, and that pyrolysis becomes slower as the severity of torrefaction increases. The kinetic parameters obtained here are in agreement with previous work [129]. The relatively lower reactivity of the torrefied fuels compared to the untreated fuels has been observed previously by other researchers e.g. [112, 129, 190, 191] and is also consistent with the results of extent of char burnout from the drop tube studies, i.e. a higher degree of burnout is experienced for the chars prepared from the more reactive untreated fuels relative to the torrefied fuels at the same conditions and residence time.

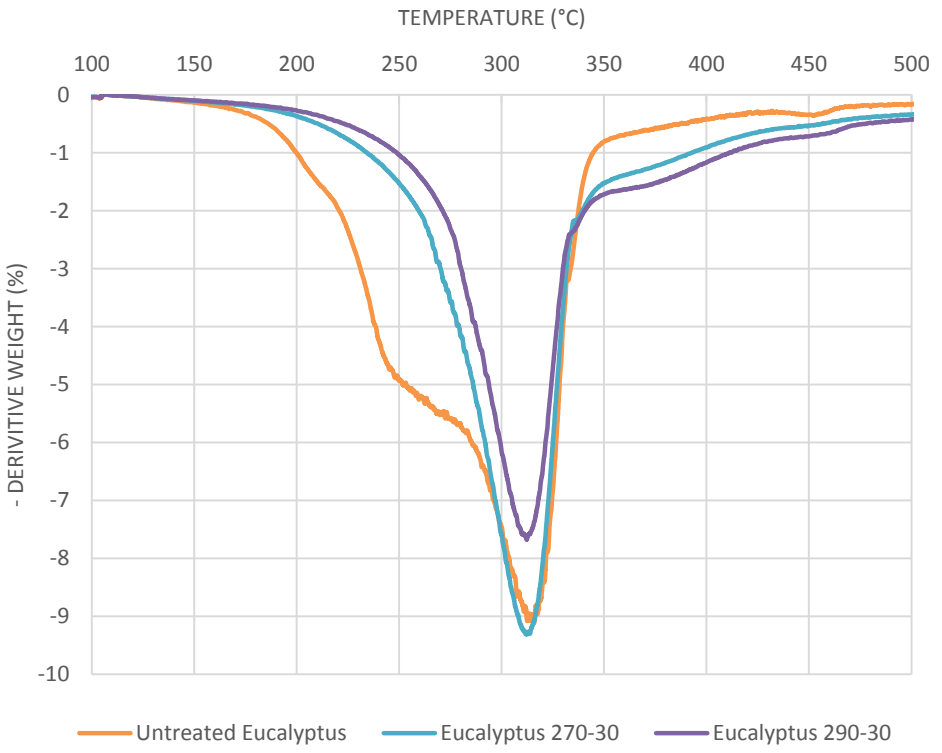

Figure 6-5 – Derivative of the mass loss-time curve during pyrolysis of untreated and torrefied eucalyptus.

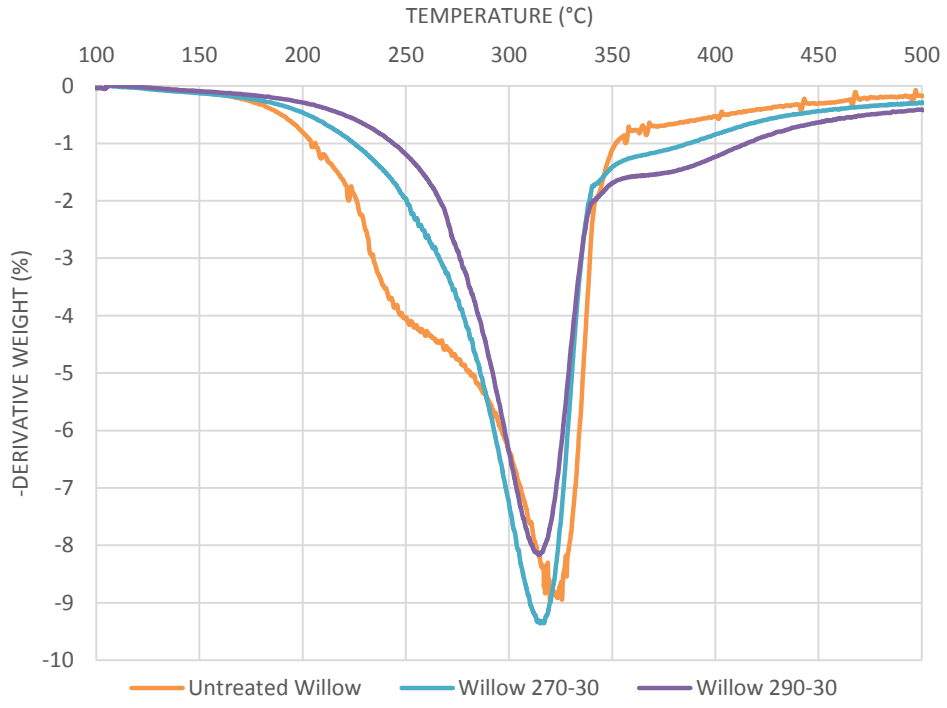

Figure 6-6 - Derivative of the mass loss-time curve during pyrolysis of untreated and torrefied willow.

The extent of char burnout can also be linked to the remaining percentage of volatiles in the parent fuels and their oxygen concentrations. Untreated willow and eucalyptus fuel have volatile contents of 84.4% and 79.6%, respectively, which decrease upon torrefaction by around 10% for willow and slightly more for eucalyptus 270-30, and by 20% for both fuels torrefied at 290°C for 30 min, consistent with the reaction rate constants calculated above.

	Willow			Eucalyptus		
Parameters	Untreated	270-30	290-30	Untreated	270-30	290-30
Pyrolysis						
Ea (kJ mol^{-1})	60.7	61.3	72.2	58.5	65.8	78.5
Ln A (s^{-1})	6.53	6.54	8.65	6.56	7.30	9.89
k_{573} (s^{-1})	0.0020	0.0018	0.0013	0.0033	0.0015	0.0013

Table 6-5: Arrhenius parameters for pyrolysis of untreated and torrefied fuels.

6.2.2.2 Char Burn out Kinetics

The oxidative reactivity of chars prepared in the drop tube furnace from untreated and torrefied willow were determined using isothermal TGA according to the methodology laid out in Section 4.5. An example of the mass loss curves obtained from the isothermal combustion experiments is shown in Figure 6-7 for the willow 290-30 char (the remaining mass loss curves can be found in Appendix A). From this plot it can be see that as the temperature at which isothermal combustion takes place increases, the greater the rate of mass loss.

The Arrhenius parameters, E_A and A, derived from an Arrhenius plot, which can be found for all fuels in Appendix A, from the reaction rate constants determined for each isothermal experiment are shown in Table 6-6. The reaction rate constant calculated at 825K, k_{825}, are also shown. Figure 6-5 shows the plot of chemical reactivity (extrapolated to higher temperatures) against reaction temperature for the untreated and torrefied chars. The chemical reactivity plot also shows an outline of the data compiled by Di Blasi [123] who plotted the chemical reactivites of a number of biomass chars as discussed in Section 2.2.5.

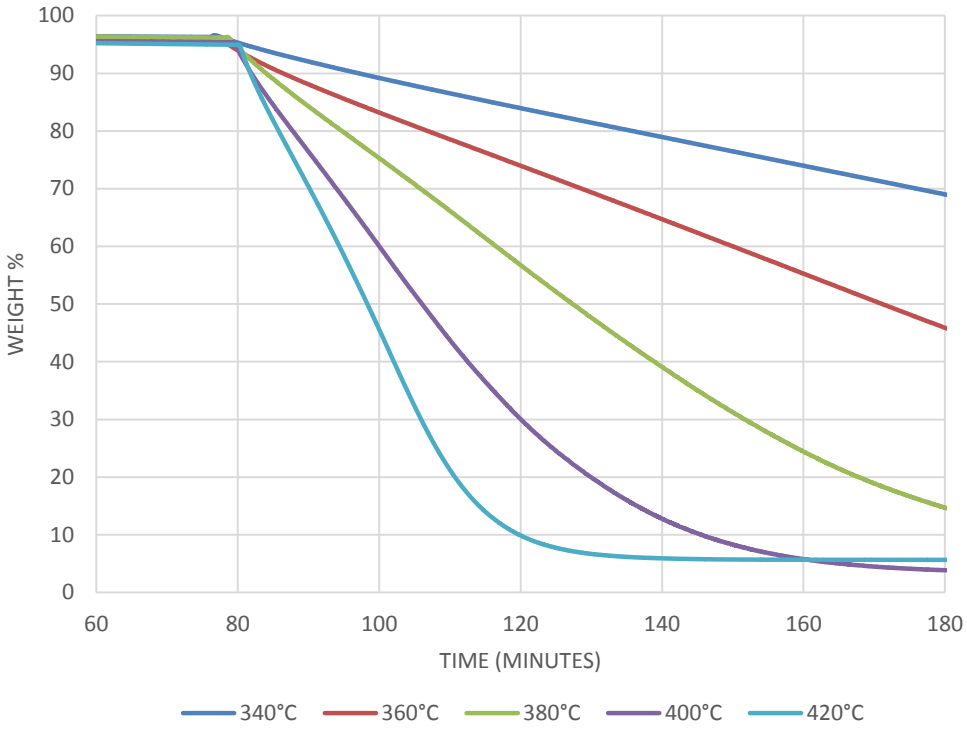

Figure 6-7 - Mass loss curves for the isothermal combustion of Willow 290-30min char

	Willow			Eucalyptus		
Parameters	Untreated	270-30	290-30	Untreated	270-30	290-30
Char Combustion						
Ea (kJ mol^{-1})	87.2	115.43	105.61	123.7	107.9	102.7
Ln A (s^{-1})	10.1	13.8	10.4	17.9	13.1	11.7
k_{825} (s^{-1})	0.067	0.049	0.009	0.918	0.068	0.0012

Table 6-6: Arrhenius parameters for the combustion of chars from untreated and torrefied fuels.

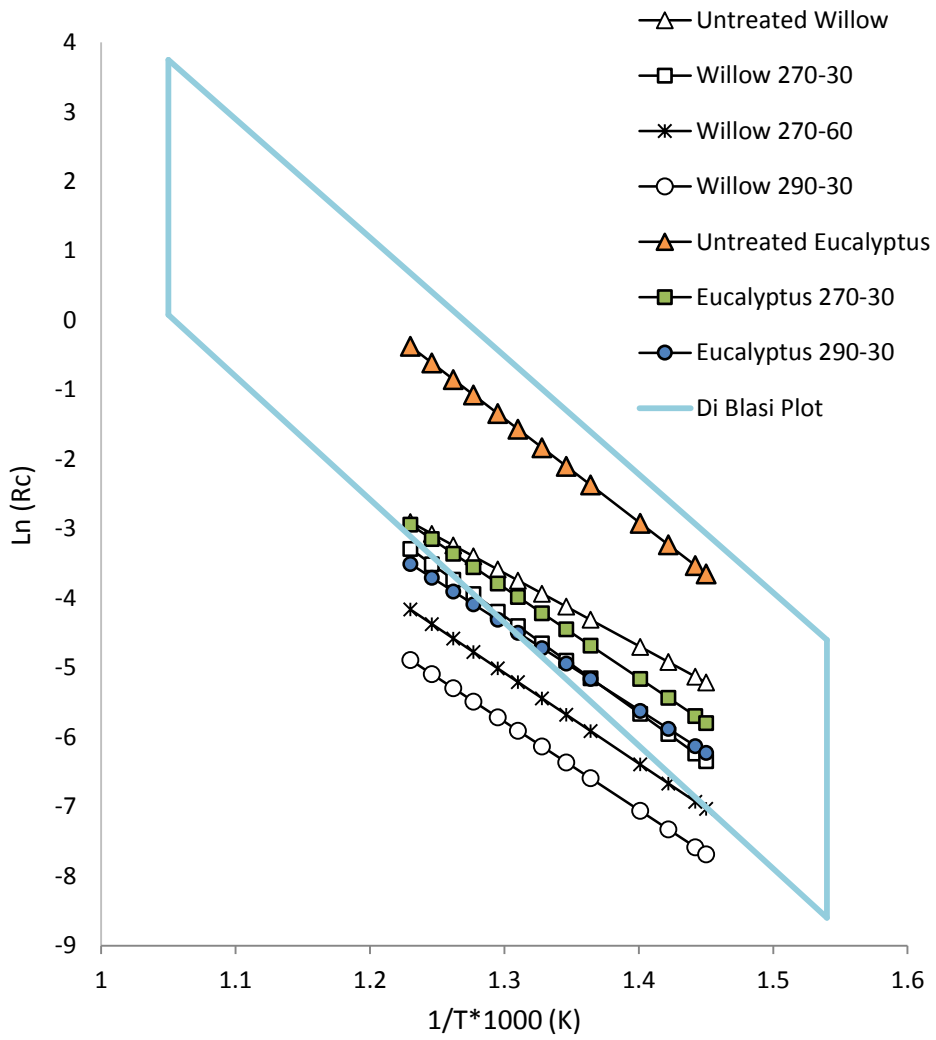

Figure 6-8 - Chemical reactivity plot for untreated and torrefied chars. Data from Di Blasi [41] outlined in the shaded area.

It can be seen from Figure 6-8 and the reaction rates calculated at 825°K (Table 6-6), that the chars prepared from untreated willow and eucalyptus are the most reactive and the chars, prepared at the same temperatures and residence time, from torrefied materials are less reactive. The reduction in reactivity becomes more prominent with increasing torrefaction severity. Torrefaction, however appears to result in a bigger drop in reactivity for the eucalyptus chars than for the willow chars. Fisher et al. [181] reported on the reactivity of untreated and torrefied DTF chars and observe a similar effect of reduced reactivity for torrefied willow chars [181]. The difference in reactivity is also in agreement with single particle combustion measurements in a methane flame of untreated and torrefied willow [117], where longer char combustion times were needed for the particles that had undergone torrefaction [105].

As dissuced in section 2.2.4, chars prepared under high-heating rates are expected to be more reactive than those pyrolysed at low heating rates [134, 181, 183] as a result of higher surface

areas and thus surface available for reactions which result from these pyrolysis conditions. As such, it would be expected that the behaviour of the chars from untreated fuels would dominate the top region of the Di Blasi [41] outline (as the majority of the chars included on this plot were prepared at low heating rates). While untreated eucalyptus occupies this position, the chars from untreated willow exhibit considerably lower reactivities. As noted above, the char combustion rate constants calculated at 552°C (k_{825}), predict that untreated eucalyptus chars would react considerably quicker than willow chars. As the surface area for untreated eucalyptus is the highest for all the chars (80m^2/g) as shown in Table 6-3, this may contribute to this fuel's higher reactivity. In comparison with untreated willow, this fuel underwent a higher degree of burn-out than eucalyptus, 84% and 51% respectively, which may also account for the reduction in reactivity measured for the untreated willow chars. In the case of eucalyptus, the degree of disparity between the untreated and torrefied chars may be in part due to the reduction in oxygen in these fuels during torrefaction. The mild torrefaction (270-30) for eucalyptus results in 10% reduction in oxygen concentration, while the most severe conditions (290-30) reduces the oxygen content by 20% with reduction in oxygen content having an impact on the reactivity of the chars. In comparing the two sets of torrefied fuels, it can be noted that eucalyptus 290-30 exhibits a similar reactivity to willow 270-30 despite this latter fuel having a 13% more volatile content as determined from proximate analysis. Potassium catalysis may therefore be a factor here as it is known potassium can affect reaction rates during pyrolysis and combustion [146, 192]. It is to be noted that due to the lower extent of burnout on the eucalyptus chars and higher original K contents than willow shown in table 6-2, eucalyptus appears to retain a larger fraction of K in the fuel which may contribute to increased reactivity.

At present, there is limited information available in the literature that focusses on the oxidation characteristics of fast heating rate chars from torrefied fuels specifically. There is even less information on the intrinsic reactivity of fast-heating chars from torrefied fuels; the intrinsic reactivity defined as the reaction rate per unit area of pore surface in the absence of any mass-transfer limitation limitations [132]. A plot of the intrinsic reactivity of the untreated and torrefied chars against reaction temperature is shown in Figure 6-8, alongside some data for bituminous coals from Jones et al. [193] and Smith [194], for comparison purposes. Similar to the chemical reactivites, the chars from untreated biomass are more reactive than the chars from torrefied fuels. However, the effect of surface area has changed the order of reactivity for the torrefied fuels whereby the most torrefied ≠ the least reactive e.g. euclyptus 270-30 is less reactive than eucalyptus 290-30. However, it is worth highlighting again, that the surface area

of chars can vary considerably depending on the devolatilisation conditions and degree of burnout [122] in addition to the method of surface area analysis. As a result, Figure 6-8 is not comparing "like with like", since all the chars have different extents of burnout. Nevertheless, it is clear that chars from torrefied biomass are less reactive than those from untreated biomass, in spite of the former having higher surface area. This is consistent with findings from previous work [37].

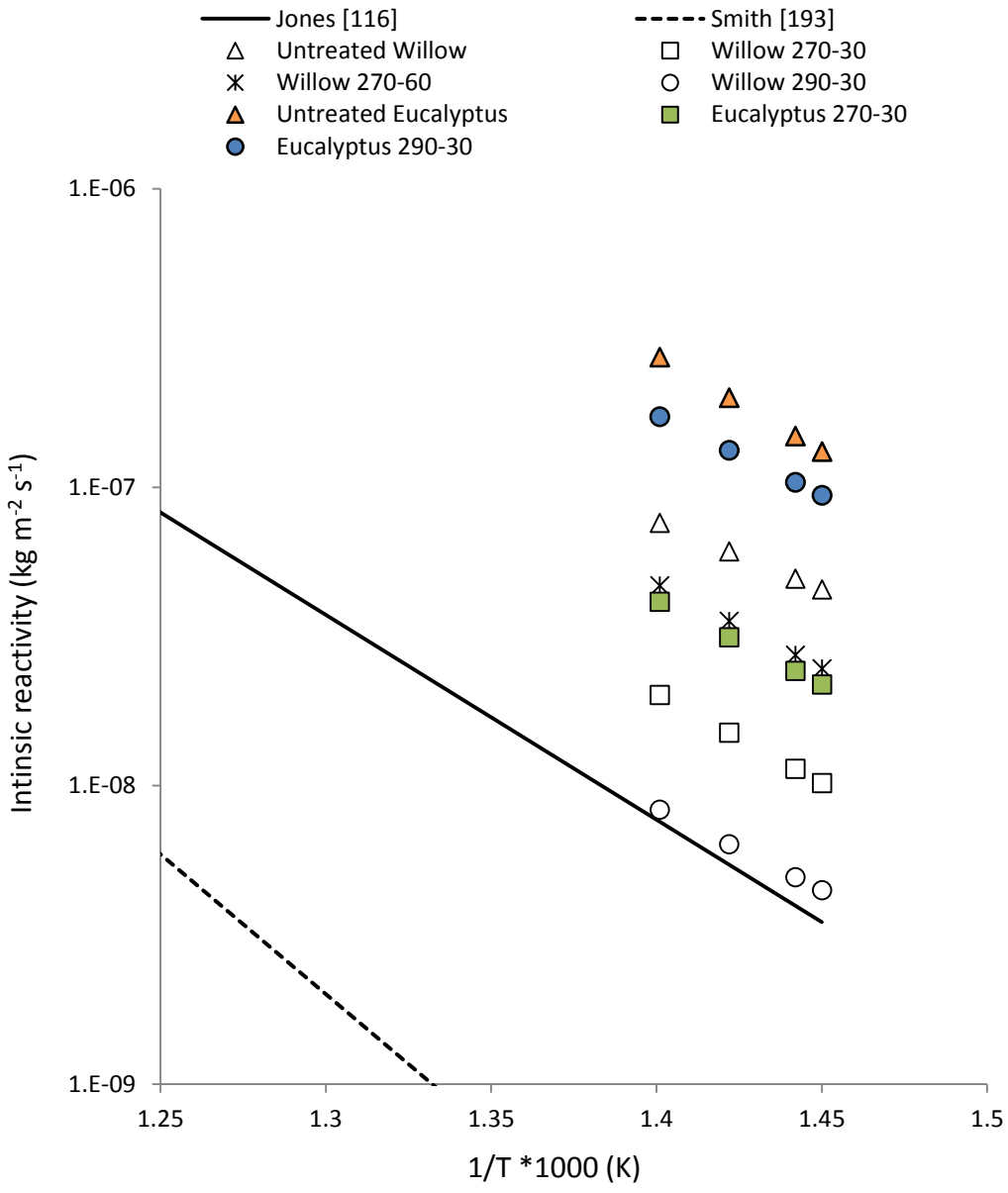

Figure 6-9 – Intrinsic reactivities for untreated and torrefied willow and eucalyptus chars. Data for bituminous coals for comparison taken from Jones et al [117] (solid line) and Smith [194] (dashed line).

6.3 Conclusions

In this study chars were prepared in a drop tube furnace from two biomass fuels: short rotation coppice willow and eucalyptus, and also from their torrefied counterparts. The fuels and chars were characterised for proximate, ultimate and surface areas and morphology by SEM/EDX. Upon fast devolatilisation in the drop tube furnace, the chars from torrefied fuels appeared more rounded in structure while the chars from untreated fuel retained their parent elongated structure more closely. These differences in morphology may be attributed to structural changes that take place during torrefaction- the loss of binding hemicellulose during torrefaction may result in increased deformation of the biomass particles during rapid devolatilisation. The measured surface areas of the chars were all greater than the parent fuels, these changes due to rapid release of volatiles in the DTF creating surface porosity.

Furthermore, the pyrolysis and char combustion kinetics were estimated from TGA experiments. It was found that the torrefied fuels were less reactive for the pyrolysis stage than the untreated fuels as demonstrated by determination of rate constants as 300°C (573°K) (k_{573})- these decreasing with increasing torrefaction severity. Similarly, the chars produced from the torrefied fuels were found to be less reactive than chars produced from the untreated materials. Differences between the combustion behaviour of the two types of wood studied were also observed. Eucalyptus chars were more reactive than willow char analogues, although they had seen a lower extent of burn off. Similar trends were also observed from their intrinsic reactivities -extrapolated to higher temperature ranges, which show that chars from the untreated fuel were more reactive than chars from torrefied woods, and in general, eucalyptus chars were more reactive than willow chars. Semi-quantitative EDX analysis analyses of the fuels and chars enabled the estimation of the partitioning of potassium during high heating rate pyrolysis. Results indicate that a monotonic correlation between potassium release and percent burnout is a reasonable assumption. With respect to the effect of torrefaction on fuel-N, it was found that the process conditions used resulted in lower fuel-N contents for the fuels studied. Moreover, ~72-92% of the fuel-nitrogen was released with the volatile fraction upon devolatilisation at 1100°C. Both findings suggest that torrefaction would be beneficial for pf combustion in terms of nitrogen emissions.

7 An assessment of the impact of torrefaction of North American Pine on life cycle greenhouse gas emissions

7.1 Introduction

While the previous two chapters have investigated the torrefaction process and the combustion properties of torrefied materials, this chapter aims to investigate the effect of torrefaction on a bioenergy supply chain, namely its effect on life-cycle GHG emissions for the production of electricity. As the use of bioenergy has been highlighted as a key technology in lowering GHG emissions in the UK, it is important that real-carbon savings are delivered when additional treatment steps such as torrefaction are implemented. Using experimental data collected and described in Chapter 5, a mass and energy model to determine the energy requirements for the torrefaction of North American Pine under 4 conditions has been performed. These data have then been incorporated in to a bespoke bioenergy supply chain to determine the life-cycle GHG emissions associated with the generation of electricity from torrefied wood pellets in the UK that have been harvested, torrefied and pelleted in North America. The GHG emissions are then compared to a traditional wood pellet supply chain and a sensitivity analysis on GHG results is performed to assess key assumptions and data uncertainties. Prior to this, a short introduction to biomass sustainability, GHG emissions accounting and feedstock supply is outlined followed by the status of torrefaction technologies and other studies which help put this aim of study in to further context.

7.2 Biomass Sustainability

One of the main drivers for using biomass for electricity generation is to reduce greenhouse gas emissions. Owing to the nature of biomass combustion, it can be incorporated in to the energy mix relatively cheaply and easily. In delivering biomass in to the energy mix however, its deployment is underpinned almost entirely by the requirement to source it sustainably. The question of biomass sustainability arises, in most part, from uncertainties within the bioenergy supply chain. These include whether carbon savings are actually achievable, the availability (as well as cost) of sustainably sourced biomass and the impact bioenergy production has on other environmental systems such as land use for food production, biodiversity and construction materials [57].

In the UK, since 2011, electricity generators using biomass with net capacity greater than 50kW have been required to provide information relating to particular sustainability criteria on the type of land biomass is sourced from and the greenhouse gas emissions associated with the generation of one MJ of delivered electricity. With respect to the RO outlined in Section 1.2.5, until April 2013 generators only had to report on these sustainability criteria which had no impact on whether or not ROCs could be attained. To ensure bioenergy used in UK is sourced sustainably, DECC has introduced a more robust a set of sustainability criteria in which solid biofuel procurement and utilisation must adhere in order to qualify for any subsidies within the RO [195]. Up to the year 2020, generators of electricity using biomass[1] must achieve a minimum of 60% GHG emissions savings compared to the EU fossil fuel average (285 $kgCO_2e/MWh$ compared to 712 $kgCO_2e/MWh$ [196]) [195]. New-build dedicated biomass have stricter GHG trajectories of 240 $kgCO_2e/MWh$ until 2020 to reflect higher efficiencies achievable in new-build plant [195]. There are also general restrictions in place on sourcing materials from land with high carbon stock or protected areas [197]. After 2020 however, all biomass generators will have the same GHG emissions trajectory of 200 $kgCO_2e/MWh$ until 2026 when it will reduce to 180 $kgCO_2e/MWh$ to 2030 [195]. While these targets will be situ, to account for difficulties that may be incurred out-with a generators control (e.g. diversion of a ship to another port) these targets represent the *annual average* GHG emissions with provision that any one consignment must not exceed a ceiling of 285, 270 and 260 $kgCO_2e/MWh$ for the periods up to 2020, 2025 and 2030 respectively [195].

7.3 Supply chain GHG emissions

The bioenergy supply chain involves several logistical considerations that can make a sizeable impact on the overall carbon intensity of a fuel chain. While using bioenergy can be considered 'carbon-neutral' at point of combustion, the harvesting, processing and transport of the fuel ultimately contribute positive emissions which must be accounted for. In order to make a full assessment of the emissions at each step in a given supply chain a 'life-cycle' approach is a useful mechanism to understand where emissions occur at each stage in production. Life Cycle Assessment (LCA) studies the potential environmental impacts throughout a product's or system's life from raw material acquisition through production, use and disposal [198, 199]. The purpose is to provide a holistic view of the emissions and resource requirements of a product system. The comprehensive view provided by LCA allows GHG emissions to be assessed on a

[1] Biomass generators include: existing dedicated biomass power, standard co-firing, enhanced co-firing, coal to biomass conversion, advanced conversion technologies or anaerobic digestion, all with or without combined heat and power (CHP).

whole system basis by life cycle stage. Emissions at each stage of the supply chain will vary depending on type of feedstock, processing and treatment steps and changes of land due to cultivation [200]. The standardised methodology for calculating life-cycle GHG emission which generators in the UK report against takes account of the recommendation outlined in the European Commission's Renewable Energy Directive (RED) [35]. The RED methodology considers the emissions from the cultivation, harvesting, processing and transport of the biomass feedstocks in addition to direct land use change where the land use has changed category since 2008 [76, 200]. Thus, the emissions at each step in the bioenergy supply chain prior to conversion to electricity are calculated according to the following equation:

$$E = e_{ec} + e_{l} + e_{p} + e_{td} + e_{u} - e_{sca} - e_{ccs} - e_{ccr}$$

Where,

- E = total emissions from the production of the fuel before energy conversion,
- e_{ec} = emissions from the extraction or cultivation of raw materials,
- e_{l} = annualised emissions from carbon stock changes caused by land use change,
- e_{p} = emissions from processing,
- e_{td} = emissions from transport and distribution,
- e_{u} = emissions from the fuel in use, that is greenhouse gases emitted during the combustion of solid and gaseous biomass,
- e_{sca} = emission savings from soil carbon accumulation via improved agricultural management,
- e_{ccs} = emission savings from carbon capture and geological storage and
- e_{ccr} = emission savings from carbon capture and replacement.

It can be seen above that emissions from each 'stage' in this equation are totalled (or subtracted in the case of savings) to give the total emissions prior to conversion to electricity. Each module therefore has its own individual emissions which are calculated using standard emissions factors and various mass inputs (e.g. fertiliser or fuel). In the case of extraction and cultivation where nitrogen fertiliser is used (taken as an arbitrary example), the emissions would be calculated as follows:

[Mass of nitrogen fertiliser (kg nutrient /ha. yr) * emissions factor (kg CO_2e / kg nutrient)] /

yield (t/ha. yr)

= total emissions (kg CO_2e/t)

The emissions for cultivation take in to account the amount of fertiliser used multiplied by a specific emissions factor averaged over the yield per year. The emissions for extraction i.e. using machinery used to uplift the biomass for this module are calculated as follows:

[(MJ diesel/ha. yr) * emissions factor (kg CO_2e / MJ diesel)] /

yield (t/ha. yr)

= total emissions (kg CO_2e/t)

Where the volume of diesel in e.g. litres is converted to MJ diesel (using the density and lower heating value) and multiplied by the diesel emissions factor averaged over the yield as above. Similar calculations, which vary depending on the fuels and inputs used, are performed for each stage from which the supply chain emissions can be totalled. From this, the emissions associated with the conversion of biomass to useful electricity are calculated using the following equation:

$$EC_{el} = \frac{E}{\eta el}$$

Where,

- EC_{el} = total greenhouse gas emissions from the final energy commodity (in this instance electricity)
- E = total emissions from the production of the fuel before energy conversion,
- ŋel = the electrical efficiency, defined as the annual electricity produced divided by the annual fuel input.

The greenhouse gas savings can then be calculated using the above and the following equation:

$$\text{Greenhouse gas saving} = (EC_{F\ (h,\ el,\ c)} - EC_{h,\ el,\ c})/EC_{F\ (h,\ el,\ c)}$$

Where,

- ECF (h, el, c) = total emissions from the fossil fuel comparator for electricity
- ECh, el, c = total emissions from the electricity

In the UK, DECC in conjunction with Ofgem have provided free software for generators using biomass to calculate their life-cycle GHG emissions in the form of the UK Solid and Gaseous Biomass Carbon Calculator [201]. This model allows generators to input their own supply chain information to determine whether the life-cycle GHG emissions are within sustainability limits and to ascertain where emissions are highest along the supply chain.

7.4 Bioenergy Feedstocks for UK electricity generation

A number of priority feedstocks have been identified by the NNFCC in conjunction with DECC which are likely to be important over the next 20 years in terms of deployment in the UK and are listed in Table 7-1 [202]. Some of the feed stocks are sourced from the UK while others are found further afield in mainland Europe, Brazil and North America.

The feedstocks from North America are particularly significant owing to the anticipated demand for bioenergy electricity generation in the years to come- it is estimated that between 9 and 16 Modt of biomass will be required for electricity generation in the UK in 2020(mainly in the form of imported wood pellets) and growth of the pellet industry in the United States and Canada. As a result, it is anticipated that a large proportion will be sourced from North America as UK forest resources cannot satisfy this demand alone. From 2009-2010, the United States underwent the greatest increase in production capacity for wood pellet production as shown in Figure 7-1 [203]. The wood pellet market is continuing to rapidly expand with total operational and planned capacity of wood pellet production in North America estimated at 22 Million tonnes pellets/year in February 2014.

Form	Biomass Type	Origin
Wood Chips	Forest Residues Round Wood	North America Europe UK Brazil
Wood Pellets	**Forest Residues** **Round wood**	**North America** Europe UK Brazil
Wood Briquettes	Forest Residues	Europe UK
Bales	Straw	UK
Chips	Miscanthus SRC	UK
Pellets	Miscanthus SRC	UK
Pellets	Olive Cake Palm Kernel Expeller	Europe Malaysia

Table 7-1: Priority feedstocks for deployment in the UK in the next 20 years

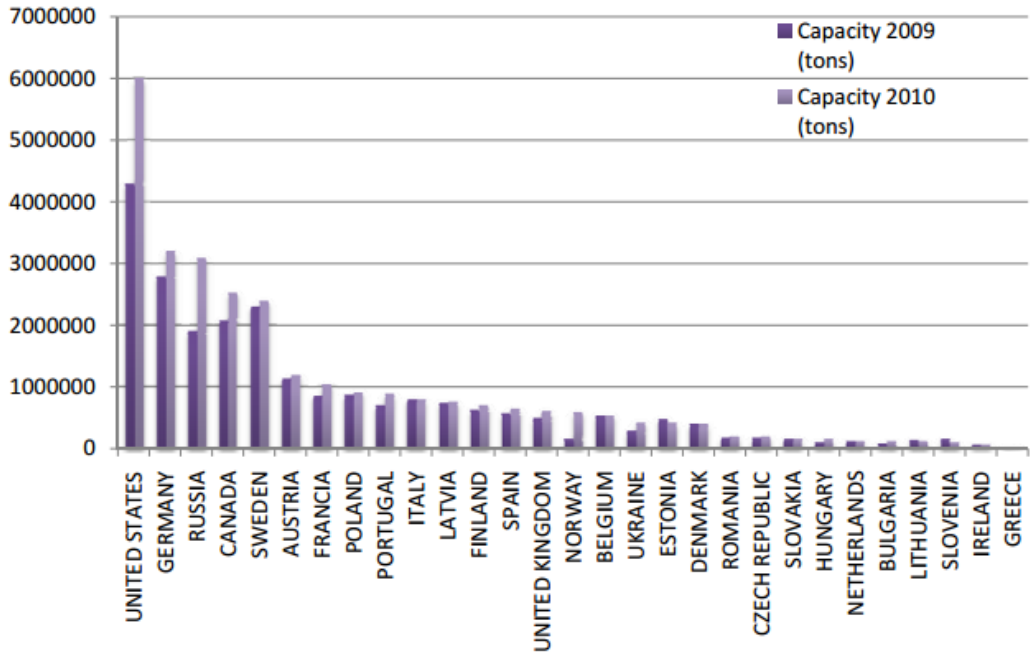

Figure 7-1 – Wood pellet production capacity by country in 2009 and 2010 [203].

Traditionally, the feedstocks for pellet production have derived from sawmill residues co-located at sawmills and are by and large still the main resource used in wood pellet production [203]. As

a result, the wood pellet market has been greatly influenced by the trends and dynamics of the wood industry. With increased demand for wood pellets however, mostly from EU member states as a result of generous subsidies available for renewable electricity and heat [204], there is a need for more stable and secure supplies of feedstock with alternatives being sought from forest residues and round-wood [203]. Other feedstocks that are currently considered for wood pellet production include diseased trees, notably beetle-killed trees which are highlighted as a potential primary feedstock owing to their availability in large volumes [76]. One of the benefits of using roundwood and forest residues for pellet production is their relative homogeneity when compared to those derived from saw-mill residues. In Southern USA at Georgia Biomass, the largest pellet facility in the world (750,000 t/pellets year), roundwood is used in pellet production with forest residues as their utility fuel to dry the wood prior to pelleting [76]. The round wood used for wood pellet production, in addition to other lower-value commodities, is normally in form of pulp-wood, as opposed to high-value sawn-timber [76].

While the wood pellet market is increasing in light of renewable electricity generation, pellets derived from raw biomass still retain some of the inherent problems commonly associated with biomass fuels such as absorption of moisture upon transportation and storage, which can cause pellets to become mouldy and disintegrate [205]. While the densification process of pelletisation does aim to ameliorate some of these problems e.g. drying before pelleting, additional treatments such as torrefaction can be considered in lieu or in combination with pelletisation to ameliorate some of these problems.

7.5 Torrefaction in the bionenergy supply chain

7.5.1 History of production scale torrefaction plant

The first pilot plant for the production of torrefied biomass was built by the French company Pechiney in the mid-1980s to produce a reducing agent in the production of aluminium [206]. The Pechiney plant had a production capacity of roughly 12,000t/annum and although it worked well in terms of technology, its low energy efficiency of 70% resulted high total production costs [206]. The main losses in energy efficiency were attributed to the production of fines during the cutting and sieving of biomass feedstocks, which without these losses, would have resulted in an energy efficiency of around 82% [103]. A schematic of the Pechiney Process is shown below in figure 7-2.

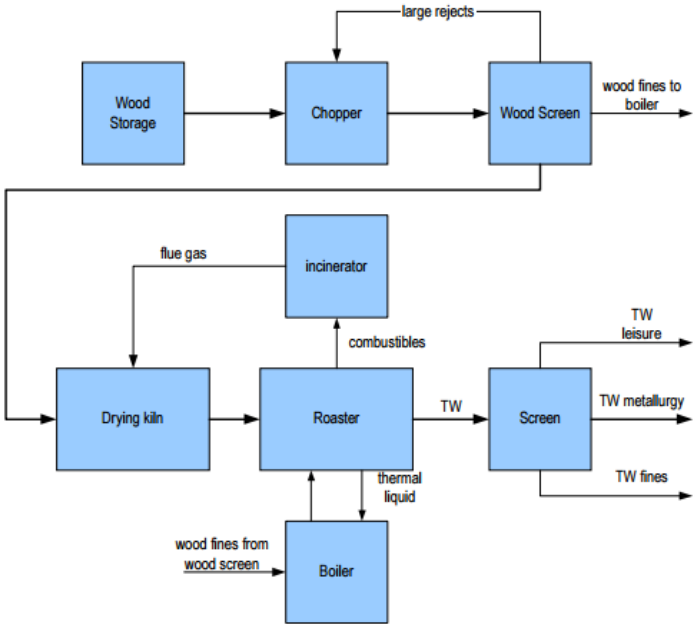

Figure 7-2 – Schematic of the Pechiney Process [103]

The reactor design for the Pechiney process was an indirectly heated screw reactor in which heat was transferred to the biomass via conductive heat transfer through the shell and screw [103]. The size of the reactor is a function of required heat duty as the area for heat transfer is limiting. As a result, the maximum moisture content of the biomass entering the reactor was limited at 15% with a throughput no greater than 2 ton/hour as a higher moisture content would drop the reactor throughput capacity [103]. Included in the Pechiney process is the utilisation of the heat from combustion of the volatile gases lost during torrefaction, reducing the amount of auxiliary fuel required to cover the heat demand of the process. In this instance, the additional auxiliary fuel is taken from fines produced from the incoming feedstock making it 'self-sustaining' provided the entire heat demand is covered. In the case where an external auxiliary fuel is required however, integration of the heat produced from the combustion of volatile gases back into the torrefaction system can become very significant when considering the potential GHG emissions savings that can be made. This heat integration will be discussed in greater detail below.

7.5.2 Torrefaction technology

The Pechiney plant was built for application in the metallurgy industry however there has been renewed interest in torrefaction technologies for production of biomass feedstocks with

improved physical and chemical properties for use in energy systems. While the Pechiney process was successful in the fact the plant operated for a number of years, Bergman et al. have discussed the potential issues with using this specific design for torrefaction on large-scales as questionable [103]. This includes a low maximum energy efficiency of 82% as well the optimisation of process parameters for products specific to the metallurgy industry [103]. A modified design proposed by Bergman et al, analogous to the Pechiney process is shown Figure 7-3 with some design considerations highlighted as well. This includes the combustion of the volatile gases released during torrefaction, as discussed above, to provide heat for both drying and torrefaction. A key consideration proposed by Bergman et al. was to design a torrefaction plant to operate as a 'stand-alone' process with its own heat inputs taking away any need for the torrefaction plant to be adjacent to a power station where it may utilise any excess heat [103]. By taking this approach, the logistical benefits of using torrefied materials can be maximised as the torrefaction plant does not need to be located geographically close to the end-user.

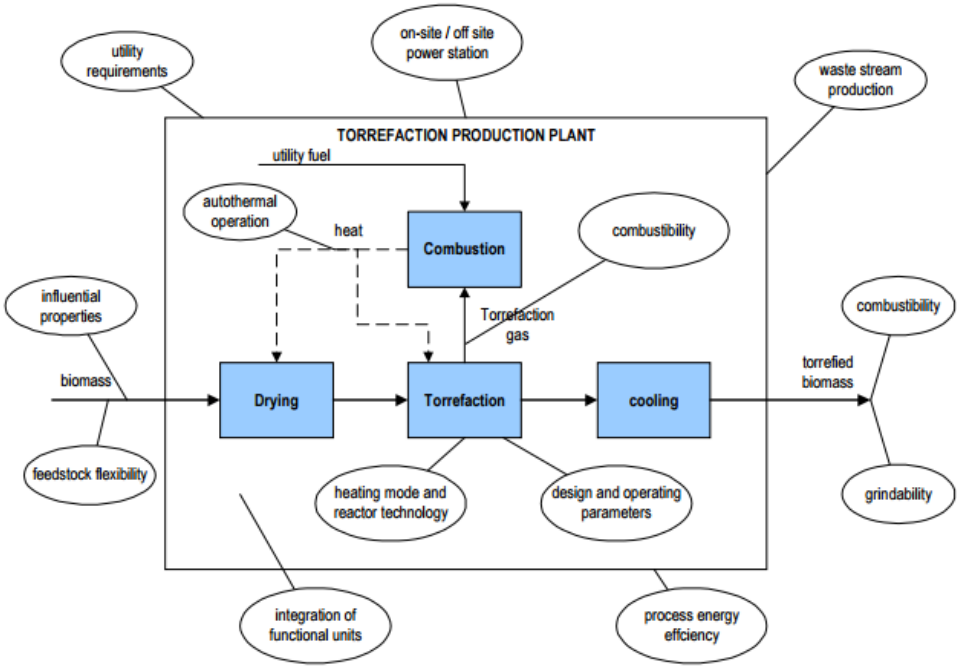

Figure 7-3 – Heat integration option for torrefaction of wood for use in energy applications [103]

Utilising the heat from the combustion of torrefaction gases to provide heat demand will ultimately be performed under three possible scenarios: autothermal operation, below the point of autothermal operation and above the point of autothermal operation. Under autothermal operation, the energy content of the torrefaction gases balances the heat duty of

drying and torrefaction. Below the point of autothermal operation, the energy content of the torrefaction gases is insufficient to cover the entire heat demand of the process requiring an auxiliary fuel to operate the process. Above the point of autothermal operation, the torrefaction gases have too much energy requiring some of this excess energy to be withdrawn. This latter scenario is particularly significant with respect to the energy efficiency of the process as too much energy in the gas stream may signify too severe torrefaction conditions resulting in the loss of valuable product [103].

The use of torrefaction gases is also underpinned by the combustion properties of the gases. As discussed in Section 2.1.7, the volatile products of torrefaction will contain mixture of various organic compounds which have some energy content. According to conservation of energy laws, the energy lost during torrefaction (deduced from an overall mass and energy balances) should be contained in the volatile stream and is in theory available for combustion. By mass however, some of the products of torrefaction however provide no useful energy and are non-combustible- namely CO_2 and water (free and reaction). As the original moisture content can be as high as 50% and the CO_2 produced as much as 10%, this may result in a 0.6 fraction of incombustible matter in the volatile stream although variations in torrefaction temperature and residence time will change this amount. When considering the use of torrefaction gases therefore, it is important to consider the adiabatic flame temperature in the combustor as the presence of CO_2 will ultimately lower it. In order to ensure combustion remains spontaneous, the flame temperature must be typically 400°C higher than the compound with the highest auto-ignition temperature. For example, CO has a high ignition temperature of 600°C and thus the flame temperature in the case where this ignition temperature is the greatest must be of the order of around 1000°C.

Fundamentally, torrefaction combines two main processes: heating of the biomass and retention of the biomass at the desired temperature for a specific residence time. In terms of reactor technology therefore, there are two main categories for heating of the biomass: Indirect and direct heating [103]. Indirect heating during torrefaction occurs when the biomass is heated by means of a wall acting as the heat carriers. Examples of this include rotary kiln dryers and indirectly heated screw reactors such as the Pechiney process. Directly heating the biomass involves biomass coming in direct contact with a gaseous heat carrier. Examples of this include rotary drum dryers and fluidised bed reactors.

7.5.3 Torrefaction and supply chain GHG emissions

At the time of writing, few torrefaction technologies are currently operating at commercial scales big enough for stand-alone incorporation in large-scale power generation however some plant are do exist in addition to several pilot and demonstration scale plants. A summary of the current status of technologies is presented in Table 7-2. It can be seen that 3 commercial scales plants are currently operation including one in the UK with a capacity of 30,000t/annum. The largest commercial plant in terms of production capacity is the Solvay/New Biomass Energy plant in the United States with a capacity of 80,000t/annum. While some large-scale plant do exist, torrefaction on wide-spread commercial scales is currently not in operation and so the effect of torrefaction on bioenergy supply chain GHG emissions is thus largely limited to modelling of emissions as only few plants exist to extract real-life emissions data. There are some technologies in pilot and small-scale operation as for smaller-scale applications such as those mentioned above however in which GHG emissions assessments have been performed. These include the study by Agar et al. [207] who studied the energy and emissions balance of torrefied pellets vs. conventional pellets to be used in co-firing based on pilot plant data and adopting the RED GHG accounting methodology. In their study, the authors developed a mass and energy balance for drying and torrefaction of logging residues scaled up against a 500kg/hour pilot plant which integrates the heat produced from combustion of the volatiles. The torrefaction plant has mass and energy yields of 80 and 90% respectively and an overall thermal efficiency (thermal out of torrefied products/thermal input of untreated products) of 86% although specific process parameters (temperature and residence time) are not discussed. The authors performed two case studies, one in which the feedstocks are supplied, produced (upgraded) and transported from Finland while the other uses the same methodology but taking place in Western Canada. Both scenarios follow with shipping to Western Spain where co-firing with coal takes place. Both scenarios were then compared with the same supply chain minus the torrefaction step. The results of CO_2 equivalent emissions/MJ electricity delivered for each stage in production for each supply chain are shown in Figure 7-4. The results show comparable overall GHG emissions for both conventional and torrefied pellet production from Finland and West Canada although the conventional pellet route from Finland is slightly lower. Expectedly, the transport emissions from Canada are greater than from Finland (shipping distances were 15500km compared with 3361km).

Developer	Technology	Location(s)	Production capacity (ton/a)	Scale and status Pilot scale: 50 kg/h - 500 kg/h Demo scale: > 500 kg/h - 2 ton/h Commercial scale: > 2ton/h)	Full integration (pre-treatment, torrefaction, combustion, heat cycle, densification)	Status
Clean Electricity Generation (UK)	Oscillating bed	Derby (UK)	30,000	Commercial scale	Yes	Available/operational
Horizon Bioenergy (NL)	Oscillating belt conveyor	Steenwijk (NL)	45,000	Commercial scale	Yes	Dismantled
Solvay (FR) / New Biomass Energy (USA)	Screw reactor	Quitman (USA/MS)	80,000	Commercial scale	Yes	Available/operational
Topell Energy (NL)	Fluidised bed	Duiven (NL)	60,000	Commercial scale	Yes	Mothballed
Torr-Coal B.V. (NL)	Rotary drum	Dilsen-Stokkem (BE)	30,000	Commercial scale	Yes	Available/operational
Airex (CAN/QC)	Cyclonic bed	Bécancour (CAN/QC)	16,000	Demonstration scale		Available/operational
Agri-Tech Producers LLC (USA/SC)	Screw reactor	Allendale (USA/SC)	13,000	Demonstration scale	Yes	Scheduled to be built
Andritz (AT)	Rotary drum	Frohnleiten (AT)	10,000	Demonstration scale	Yes	Out-of-service
Andritz (DK) / ECN (NL)	Moving bed	Stenderup (DK)	10,000	Demonstration scale		Unknown
BioEndev (SWE)	Dedicated screw reactor	Holmsund, Umea (SWE)	16,000	Demonstration scale	Yes	Available (2015)
CMI NESA (BE)	Multiple hearth	Seraing (BE)	Undefined	Demonstration scale		Unknown
Earth Care Products (USA)	Rotary drum	Independence (USA/KS)	20,000	Demonstration scale		Available/operational
Grupo Lantec (SP)	Moving bed	Urnieta (SP)	20,000	Demonstration scale		Unknown
Integro Earth Fuels, LLC (USA)	Multiple hearth	Greenville (USA/SC)	11,000	Demonstration scale		Unknown
LMK Energy (FR)	Moving bed	Mazingarbe (FR)	20,000	Demonstration scale		Unknown
River Basin Energy (USA)	Undefined	Laramie (USA/WY)	Undefined	Demonstration scale		Available/operational
Teal Sales Inc (USA)	Rotary drum	White Castle (USA/LA)	15,000	Demonstration scale		Available/operational
Torrec (FI)	Moving bed	Mikkeli (FI)	10,000	Demonstration scale		Available/operational
Agri-Tech Producers LLC (US/SC)	Screw reactor	Raleigh (USA/NC)	Undefined	Pilot stage		Available/operational
Airex (CAN/QC)	Cyclonic bed	Rouyn-Noranda (CAN/QC)	Undefined	Pilot stage		Available/operational
Airex (CAN/QC)	Cyclonic bed	Trois-Rivières (CAN/QC)	Undefined	Pilot stage		Available/operational
Arigna Fuels (IR)	Screw reactor	County Roscommon (IR)	Undefined	Pilot stage		Available/operational
CENER (SP)	Rotary drum	Aoiz (SP)	Undefined	Pilot scale		Available/operational
Terra Green Energy (USA)	Multiple hearth	McKean County (USA/PA)	Undefined	Pilot scale		Available/operational
Wyssmont (USA)	Multiple hearth	Fort Lee (USA/NJ)	Undefined	Pilot scale		Unknown
CEA (FR)	Multiple hearth	Paris (FR)	Undefined	Laboratory scale		Available/operational
Rotawave, Ltd. (UK)	Microwave	Chester (UK)	Undefined	Laboratory scale		Unknown
Bio Energy Development & Production (CAN)	Fluidised bed	Nova Scotia (CAN/NS)	Undefined	Unknown		Unknown

Table 7-2 – Overview of some torrefaction initiatives as of 2015 [208]

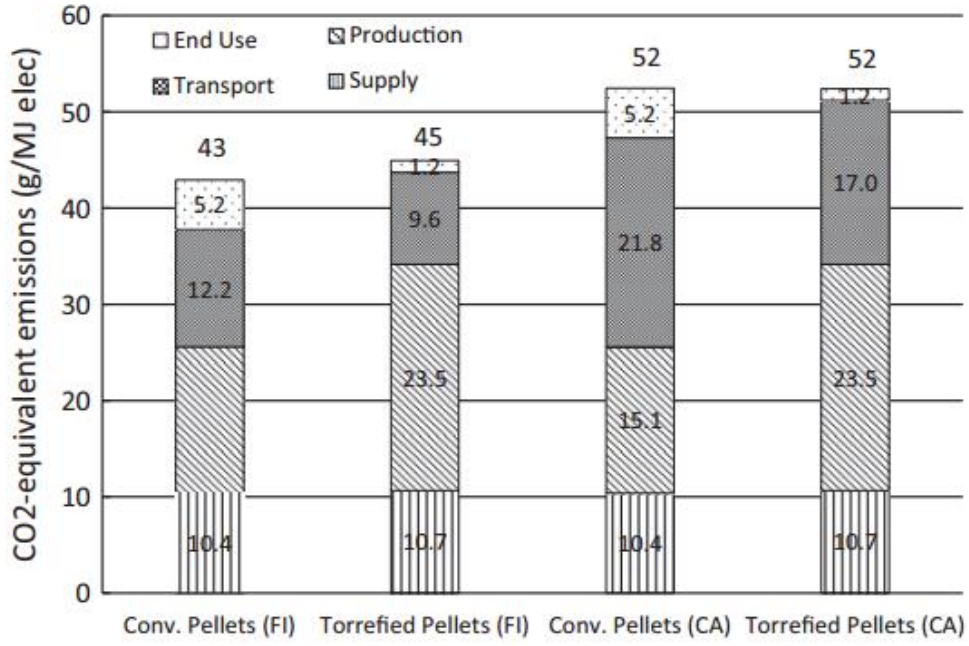

Figure 7-4 – Life cycle GHG emissions for conventional and torrefied pellet supply chains [207].

The addition of torrefaction in to the supply chain increases the production emissions: 23.5 $gCO_2e/MJ_{electricity}$ when compared with 15.1 $gCO_2e/MJ_{electricity}$ for Canadian torrefied and conventional pellets respectively. Implementing torrefaction however lowers the end use emissions from 5.2 to 1.2 $gCO_2e/MJ_{electricity}$ for the same conventional and torrefied supply chains as a result of increased calorific value. Although the life-cycle emissions are comparable for conventional and torrefied pellets, the authors highlight that the improvements in fuels properties such as increased CV and improved grindability in torrefied pellets make it overall a better fuel for use in large-scales.

Hall [209] also assessed the reduction in carbon dioxide emissions achievable from modelling the torrefaction of hardwood and softwood based on existing data available in the literature. In this study, Hall modelled the anhydrous mass loss during torrefaction and the energy requirements for torrefaction based on the latent energy of the volatile products and the enthalpy change of the reaction based on the HHV of the untreated and torrefied fuels. Two scenarios for heat integration were modelled. Firstly, the heat for torrefaction was supplied from the latent heat of syngas from an adjacent gasification plant (where torrefied material is gasified) while the other scenario combusted the volatiles produced during torrefaction at 80% efficiency. For this latter heat integration option, the following model steps included the grinding

and pelleting of the torrefied wood and transport to a separate combustion site. The results for the change in GHG emissions for this scenario are shown in Figure 7-5.

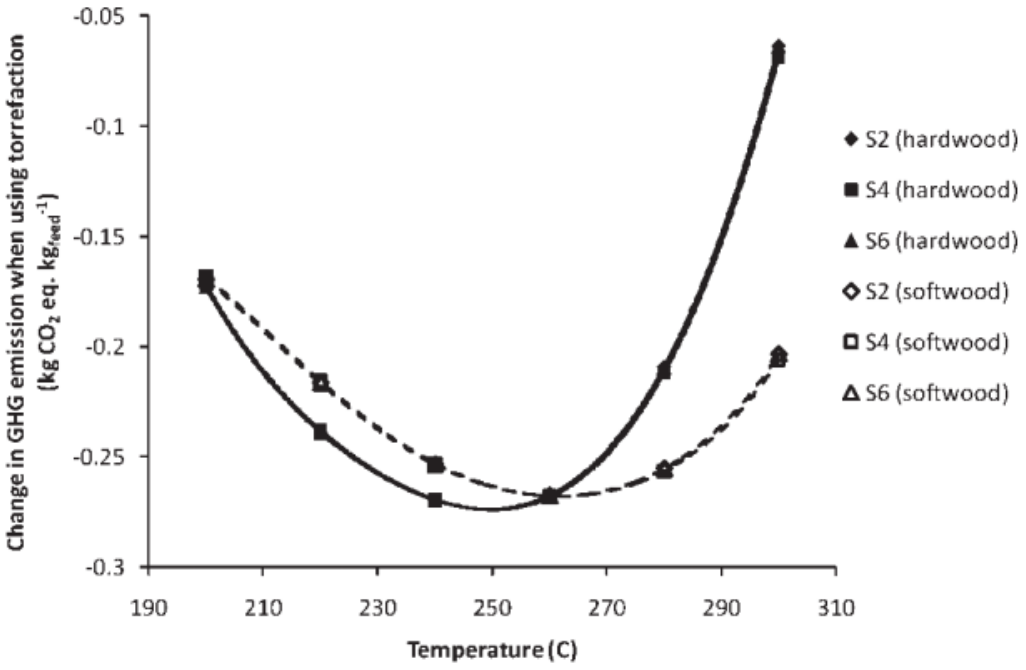

Figure 7-5 – Effect of torrefaction GHG emissions savings from the torrefaction of hardwood and softwood [209]

Under each scenario and torrefaction temperature, GHG emissions savings are made. The greatest savings are observed in the mid-torrefaction temperature ranges from around 240-260°C. The author attributes this to not using the volatiles in electricity production which would result in higher torrefaction conditions lowering overall emissions due to a greater amount of energy released in the volatiles phase. Although overall life-cycle emissions or emissions for each stage in production are not presented, Hall does discuss the relationship between the energy released by the volatiles and the energy required for grinding to be significant when determining optimum torrefaction conditions. Figure 7-6 shows the relationship between these two parameters where the temperature at which the energies cross-over corresponds with the temperature at which the greatest GHG savings are made.

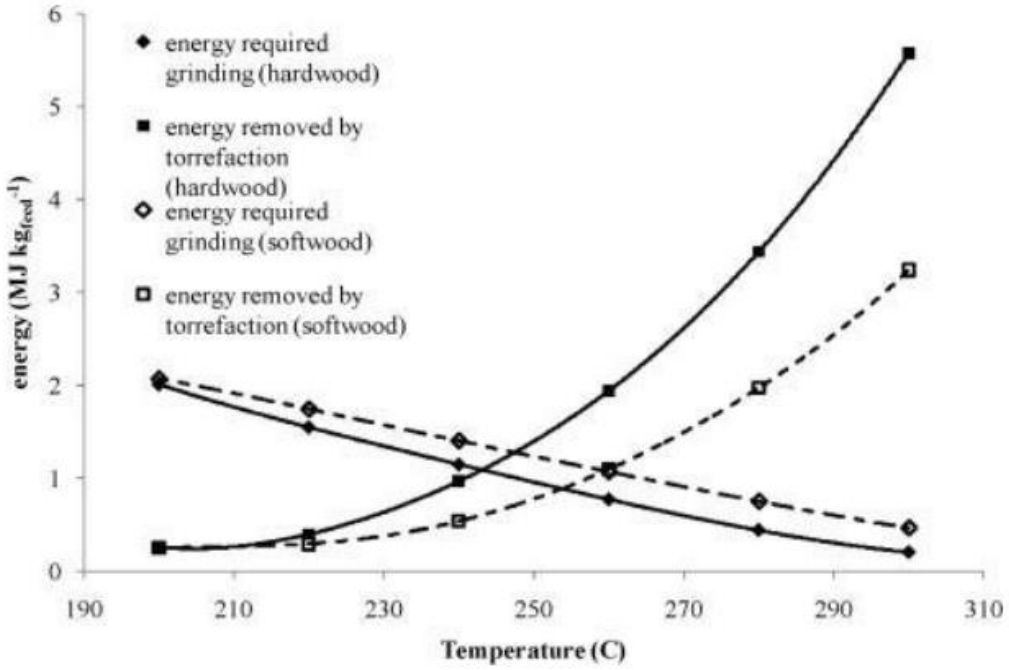

Figure 7-6 – Energy removed during torrefaction and energy required for grinding of torrefied material [209]

7.6 An assessment of the torrefaction of North American Pine and life cycle greenhouse gas emissions

7.6.1 Introduction

In order to investigate the potential emissions reductions that can be made using torrefied biomass in large-scale electricity generation further, a whole systems assessment of GHG emissions from the supply chain incorporating torrefaction has been performed. As fuel from North America is a current fuel of great interest for use in electricity generation in UK at present time, this was selected as the source of the fuels in this supply chain. Using experimental data described in Chapter 5 for the torrefaction of North American Pine, a mass and energy balance was developed and the energy requirements for each torrefaction condition determined as part of a case study comparing conventional and torrefied wood pellet production. The methodology, results and discussion are shown below. This chapter aims to fulfil Objectives 10-12 of this thesis to model the energy requirements for torrefaction, build a bioenergy supply chain and to determine the GHG emissions at each stage of production with and without the addition of torrefaction.

7.6.2 Methodology

The methodology is split in to three sections: the torrefaction of North American Pine, the modelling of energy requirements for the torrefaction of pine under 4 conditions and the greenhouse gas assessment.

7.6.2.1 Torrefaction of North American Pine

The full experimental procedure for torrefaction is described in Section 4.3 and the results and discussion are presented in Chapter 5. To summarise briefly, de-barked wood chips of North American pine sourced from a local power station were torrefied under 4 conditions: 250°C for 30 minutes, 270°C for 30 and 60 minutes and 290°C for 30 minutes. The untreated and torrefied samples were analysed for their ultimate and proximate analysis and their HHV determined using bomb calorimetry. The mass and energy yields were also determined.

7.6.2.2 Mass Balance

To calculate the GHG emissions associated with the drying and torrefaction process, a mass and energy balance reflecting a real-life system was modelled based on experimental results obtained from the torrefaction of pine under each of the conditions listed above. The initial mass flow in to the dryer was calculated as the mass of wet biomass required to produce 1000kg of torrefied product and varied depending on the torrefaction condition i.e. more severe conditions required a greater mass flow in owing to a greater mass loss during torrefaction to produce 1000kg of torrefied product. The mass inputs for each torrefaction condition are shown below in Table 7-5. Using the results from proximate and ultimate analysis for untreated pine, the weight percent of each of the species C, H, N, O and ash were interpolated at 35% moisture to determine the flow of each of these species (plus moisture) entering the dryer using the following equation:

Mass flow of each species in to dryer (kg) =

Weight percent of species (at 35% moisture) (%) * basis (kg)

This was done firstly, to reflect the true composition of harvested biomass entering a dryer in a real-life system and secondly, as 35% was considered the minimum moisture content that could be achieved through storage in outdoor piles through natural drying after harvest [66].

After drying at 110°C, it was assumed that the moisture content of the biomass was reduced to 10% (with moisture exiting the dryer system) with no other changes to the fuel occurring. At 10% moisture, the biomass then enters the torrefier where it is torrefied under the conditions listed above. Once torrefied, the mass flow of each of the species (C, H, N, O, ash and moisture) exiting the torrefier were based on the ultimate and proximate analysis and dry mass yields obtained for the torrefied materials using the following equation:

Mass flow of each species out of the torrefier (excluding moisture) (kg) =

(Weight percent of torrefied species (dry basis) (%) * [Experimental Mass Yield (dry) * Mass flow (dry) (kg)])

To close the mass balance the volatile species and gases were calculated by difference. The elemental composition of the volatiles stream was determined from the mass balance, however the individual species were estimated using the FG-Biomass model [210] to determine the latent heat of vaporisation for each species as discussed below. For this, heating rates, residence times and final temperatures and a specific fuel file were used as inputs. This provided yields of solids, condensable and gaseous products and their composition.

7.6.2.3 Energy Balance

An energy balance was performed to determine the energy flows in to the torrefaction system and the energy contained in the torrefied product and volatiles stream. The HHVs were determined from bomb calorimetry and thus the LHVs were calculated for the untreated pine (at 35% moisture) and each of the torrefied materials using the following equations:

$$HHV_{(dry)} = HHV_{(ar)} * \frac{100 - M_{ar}}{100}$$

$$LHV_{(dry)} = HHV_{(dry)} - 212.2 * H\%_{(dry)} - 0.8 * (O\%_{(dry)} + N\%_{(dry)})$$

$$LHV_{(ar)} = LHV_{(dry)} * (1\text{-}MC\%/100) - 2.443 * (MC\%/100)$$

In order to mimic a real-life system, the LHV of fuels were used as the HHVs account for the energy that would be recovered from the condensation of steam upon combustion which is not applicable in industrial scenarios. The energy flow into the system was calculated using the LHV of the untreated biomass (at 35% moisture) and the mass flow into the dryer using the following equation:

$$\text{Energy Flow in (kJ)} = \text{LHV untreated fuel}_{(35\%\ \text{moisture})}\ \text{(kJ/kg)} * \text{Mass flow in (kg)}$$

The energy exiting the system was calculated using the LHV of the torrefied product (at each condition) and the mass flow out of the torrefier using the following equation:

$$\text{Energy Flow in (kJ)} =$$

$$\text{LHV torrefied fuel (kJ/Kg)} * [\text{Experimental Mass Yield (dry)} * \text{Mass flow (kg)}])$$

The remaining energy by rule of conservation was assumed to all be contained in the volatile stream. Complete mass and energy balances for each of the scenarios can be found in Appendix B.

7.6.2.4 Energy requirements

Knowledge of the energy requirements for the overall torrefaction process is crucial in determining the GHG emissions associated with the process. The total energy required was split in to two stages: drying and torrefaction and calculated as the sum of the energies required to heat the dry biomass and moisture contained in the biomass (both accounting for the sensible energy requirements) and the latent heats of vaporisation of the moisture and volatile species. The energy requirements were calculated using the following equations:

$$Q \text{ dry wood} = m_{\text{dry wood}} * Cp_{\text{wet wood}} * (T_f°C - T_i°C)$$

$$Q \text{ torrefy wood} = m_{\text{dry wood}} * Cp_{\text{dry wood}} * (T_f°C - T_i°C)$$

$$Q \text{ torrefy wood} > 250°C = m_{\text{dry wood}} * Cp_{\text{torrefied wood}} * (T_f°C - 250°C)$$

$$Q \text{ moisture} = m_{\text{moisture}} * Cp_{\text{moisture}} * (T_f°C - T_i°C)$$

$$Q \text{ latent heat of vaporisation} = m_{\text{species}} * \Delta H_{\text{species}}$$

Where,

$m_{\text{dry wood}}$ = mass flow of dry wood in to the dryer or torrefier (kg)

m_{moisture} = mass flow of moisture in to the dryer or torrefier (kg)

m_{species} = mass flow of species in volatiles stream (including moisture) out of the torrefier (kg)

$Cp_{\text{wet wood}}$ = heat capacity of wet pine (kJ/kg. K)

$Cp_{\text{dry wood}}$ = heat capacity of dry pine (kJ/kg. K)

$Cp_{\text{torrefied wood}}$ = heat capacity of torrefied pine (kJ/kg. K)

Cp_{moisture} = heat capacity of water (kJ/kg. K)

$T_i°C$ = initial temperature for drying (20°C) or torrefaction (110°C)

$T_f°C$ = final temperature for drying (110°C) or torrefaction (250°C; 270°C; 290°C)

$\Delta H_{\text{species}}$ = latent heat of vaporisation of each of the volatile species (including water)

The thermodynamic constants used in the above equations are shown in Tables 7.3 and 7.4 below:

Species in volatiles stream	H_{vap} (kJ/kg)
Water	2199
Phenol	612.77
Acetone	539.66
Methanol	1100.00
Formaldehyde	810.00
Formic Acid	493.48
Acetic Acid	395.00
Acetaldehyde	593.18

Table 7-3 – Enthalpies of vaporisation used in determination of the latent energy requirements for drying and torrefaction

Species	C_p (kJ/kg. K)
Specific heat capacity water	4.18
Specific heat capacity wet pine	1.31
Specific heat capacity of dry pine	1.64
Specific heat capacity of torrefied pine	1.29

Table 7-4 – Specific heat capacities used to determine the sensible energy requirements for drying and torrefaction

The specific heat capacities for wet wood, dry wood and torrefied wood were calculated using correlations in Gupta et al. [211]. The duties for torrefaction are also shown in Table 7-5. The overall energy for drying and torrefaction are the sum of all of these duties. As some of initial energy content of the fuel is lost during torrefaction, by conservation this energy is contained in the volatile stream. All of this energy was assumed to be available for combustion at an efficiency of 95% to provide some of the heat demand required for the torrefaction. For each condition, the energy available in this stream was less than the energy required for drying and torrefaction i.e. below the point of autothermal operation and so the additional energy required was provided by a utility fuel: wood chips (WC) or natural gas (NG). The energy available in the volatiles stream is also shown in Table 7-5. The overall thermal efficiency of the process was calculated using the following equation:

Thermal efficiency =

[Flow of energy out of the torrefier (kJ)/

(Flow of energy in to torrefier (kJ) + Energy required for drying and torrefaction (kJ)]*100

	250-30	270-30	270-60	290-30
Mass input for 1000kg torrefied material output (kg)	1655.72	1777.34	1982.89	2086.35
Mass Yield (Dry) (%)	90.7	85.0	76.7	72.3
Dryer Duty (MJ)	344.85	370.18	413.00	434.54
Torrefier Duty (MJ)	317.06	380.89	424.94	431.45
Latent Energy of vaporisation of volatiles* (MJ)	1240.06	1400.77	1558.21	1628.85
Total Duty (MJ)	1901.98	2151.84	2396.15	2494.84
CV of Torgas (MJ/kg)	2.00	3.24	4.85	4.04
Total energy in Torgas (MJ) at 95% efficiency	371.35	872.96	1988.90	1946.62
Percentage of total duty available in volatile stream	19.52	40.57	83.00	78.03
Additional energy required from auxiliary fuel (MJ)	1530.63	1278.88	407.25	548.22
Thermal Efficiency (%)	89.0	86.3	82.1	82.74

*including moisture

Table 7-5 – Summary of mass and energy data for the GHG emissions assessment

7.6.2.5 Greenhouse Gas Emissions Assessment

In accordance with the EU Renewable Energy Directive (RED) methodology [35], the life-cycle GHG emissions associated with the generation of electricity using pellets from torrefied pellets (TPs) were determined. Therefore, the functional unit in this study is $kgCO_2e/MJ_{electricity}$ delivered. These emissions were then compared with the emissions associated with conventional wood pellet (WP) production without the torrefaction step for comparative purposes. Impacts of activities considered in the torrefied wood pellet production include biomass cultivation, harvesting and collection, transportation, size reduction and screening, drying, torrefaction, pelletisation, storage, distribution and use of TP/WP to the end-user. To model GHG emissions for the torrefaction system it was necessary to define the key parameters of the supply chain. This was done by delineating the key resources, energy inputs and emissions from each life cycle stage. The following provides a description of the torrefied pellet (TP) production and use i.e. the process from pine forest through to electricity production. A detailed summary of the main inventory data and assumptions used in the study is provided in Table 7-6.

7.6.2.6 Pine feedstock supply – cultivation, harvesting, chipping, and transport

Existing pine forests are well established and managed for wood supply. The pine wood was assumed to be cultivated in Amory, Mississippi (MS), South-East USA [212]. The total land

required was calculated as the amount of wood required to produce 100,000 tonnes of pellets and normalised to against the CV of the least torrefied fuel. This was done to account for changes in mass loss upon torrefaction with increase in CV. A plant capacity of 100,000 tonnes of pellets was derived from the review of 170 pellet plants in the USA [213] and 49 in Canada [214] which have a calculated average capacity of 102,792t per year of pellet output. This number was reduced to 100,398t per year when the outliers (e.g. plants ≤ 50kt or ≥ 200kt per year) were excluded. Hence, for this study an operational capacity of 100,000t of pellets was considered a realistic scale of operation. It was assumed that no fertilisers or pesticides are required, so the main emission source was the diesel consumed in cultivation and harvesting [215]. In accordance with the RED methodology GHG emissions as a result of land use change (LUC) are not required to be calculated where a LUC has not occurred from 2008 [35, 216]. Consequently, soil carbon and land-use change emissions are not considered in the inventory, but are discussed later in the text. It is recognised that these are important issues for the carbon balance of biomass supply chains [217]. However, the primary focus of this assessment is the biomass processing and logistics. The feedstock supply is a secondary consideration here, and detailed assessment of forestry is outside the scope.

Pine roundwood yields are given as 8.03 t/ha at a moisture content (MC) of 50%; modelled as a 70 year rotation using roundwood only [218]. Natural drying reduces the MC to 35% following which they are chipped at the forest roadside using diesel wood-chippers and incurring losses of 2.5% [219, 220]. Wood chips are then transported to the torrefaction pellet facility from the forest with a density of 385kg/m^3 [221]. Diesel was consumed for transportation assuming an energy intensity of 0.81 MJ(fuel)/t.km [222]. Transport distances were calculated based on the feedstock input required to produce 100,000 tonnes per annum of torrefied pellets (TP). This assumes that 80% of the circular area surrounding the processing facility is used to supply biomass as some land is likely used for other purposes such as roads. A tortuosity factor of 1.3 was applied as this accounts for the fact that roads are not straight hence the average distance from A to B is 1.3 by road, whereas it would be 1 as the bird flies. The average transport distance was two thirds of the radius using circle geometry. In order to calculate the average transport distance, the mass required to produce 100,000 tonnes of pellets in one year was determined (see above) and assumes that the pellet facility is located in the centre of a circle. The distances covered do not consider the wood required for wood chip as a utility fuel as these would not be applied in the supply chain where natural gas is used as the utility fuel. It also only considers one year of operation, hence for more years of operation the distances would increase as more forests are required from a greater area.

7.6.2.7 Drying, torrefaction & storage

Once received at the torrefaction pellet facility, wood chip is stored on site before being dried to reduce the moisture content to 10% as mentioned above. The energy required for the drying and torrefaction processes are modelled using experimental data (See Section 7.6.2.4) and the energy contained in the volatile species evolved during torrefaction (from now on will be referred to as 'torgas') are assumed to undergo combustion at a combustion efficiency of 95% to provide some of the process energy required with the remaining energy required provided by a utility fuel. Two types of utility fuel are assessed in the results: WC and NG. Some electricity is also required for cooling, control equipment, and to meet the parasitic load.

7.6.2.8 Torrefied pellet production

After drying and torrefaction, the torrefied wood is cooled to prevent combustion between the torrefied wood and atmospheric oxygen during subsequent processing operations [223]. This can occur at the elevated temperatures of 250°C at which torrefied wood leaves the reactor [224]. Once cooled the torrefied wood enters a hammermill to reduce particle size to allow for pelleting using a pellet mill [225]. Both the hammermill and industrial pellet mill processes are assumed to be driven using a USA grid electricity mix [226]. Electricity demand for the base case was assumed to be 15kWh/t for the hammermill and 80 kWh/t for pelleting [205].There are conflicting data in the literature for the energy requirements of pelleting torrefied biomass; hence this parameter is further assessed in the sensitivity analysis (see 7.7.5.2).

7.6.2.9 Transport & logistics to end-user

Once the torrefied pellets (TP) are produced they are then exported to the UK using existing transport logistics and infrastructure. As an existing exporting pellet facility exists in Amory, MS, [212] it is assumed the infrastructure is already in situ. Pellets are assumed to be transported by truck on road from Amory, MS to the port in Mobile, Alabama (AL) over a distance of 415km. At the port, pellets are loaded onto an ocean-going vessel with 50kt capacity. A product tanker transports the pellets for 8,912km (4812 nautical miles) to the Port of Hull, UK. This port was selected as it is currently operating as a receiving port for wood pellets arriving from North America for use in a large UK biomass power station [227]. From the port, pellets are transported to a Power Plant by road over a distance of 51km. As one of the main benefits of torrefaction is around improved transport logistics it was considered crucial to the accuracy of the results to

use actual locations and take into account the volumes of biomass and land available, thereby allowing the calculation of actual distances.

7.6.2.10 Electricity production

Pellets are assumed to be used for electricity production in a large scale power plant with 40% electrical efficiency [228].

7.6.2.11 Conventional wood pellet production

For comparative assessment, a conventional wood pellet (WP) supply chain was modelled using the same biomass as TP without the torrefaction stage. As shown in Table 7-4, most of the assumptions for WP remain the same as TP to allow for comparability. Key differences are summarised as:

- No torrefaction process involved, therefore all utility fuel from external sources
- Additional energy requirement for grinding biomass prior to pelletisation
- Lower calorific value and bulk density

Key assumptions and input data for the GHG model described in sections 7.6.2.6 to 7.6.2.11 are summarised in Table 7-6 by life cycle stage.

Life Cycle Stage	Parameter	Units	Value					
	Torrefaction Condition/Wood Pellet		250-30	270-30	270-60	290-30	WP	Ref.
Cultivation	MC at collection	%	50	50	50	50	50	[66]
	LHV	MJ/kg	8.22	8.22	8.22	8.22	8.22	†
	Yield	tonnes/ha	8.03	8.03	8.03	8.03	8.03	[218]
	Diesel Use	L/ha	0.3	0.3	0.3	0.3	0.3	[229]
Harvesting	Diesel Use	L/t of feedstock	2.96	2.96	2.96	2.96	2.96	[229]
Chipping	Losses	%	2.5	2.5	2.5	2.5	2.5	[219]
	Diesel	L/t of feedstock	1.01	1.01	1.01	1.01	1.01	[230]
	MC (of output)	%	35	35	35	35	35	[66]
	LHV	MJ/kg	11.43	11.43	11.43	11.43	11.43	†
Transport to Pellet Facility	Density of 35% MC wood chip	kg/m^3	269	269	269	269	269	[231]*
	Energy intensity of transport	MJ(fuel)/t.km	0.81	0.81	0.81	0.81	0.81	[222]
	Average distance transported	km	8.95	9.07	9.30	9.27	8.60	‡
Drying, torrefaction & storage	Losses	%	1	1	1	1	1	[201]
	MC after drying	%	10	10	10	10	10	[66]
	MC after torrefaction	%	2.43	1.86	1.13	2.02	n/a	ς
	Electricity use	MJ/ton	12.1	12.1	12.1	12.1	12.1	[232]
	Electricity emissions factor	$kgCO_2e/MJ_{electricity}$	0.145	0.145	0.145	0.145	0.145	[226]
	Utility fuel requirement	MJ(fuel)/ton feedstock	1530.6	1278.9	407.2	548.2	1134.2	†
	LHV	MJ/kg	18.5	19.4	20.6	21.8	16.8	γ
Pellet Production	Losses	%	2	2	2	2	2	[222]
	Electricity use	MJ/ton	342	342	342	342	530	[205]
	Electricity emissions factor	$kgCO_2e/MJ_{electricity}$	0.145	0.145	0.145	0.145	0.145	[226]
	Density of dry product	kg/m^3	725	725	725	725	540	[233]
Transport to Port	Energy intensity of transport	MJ(fuel)/t.km	0.81	0.81	0.81	0.81	0.81	[222]
	Distance transported	km	415	415	415	415	415	‡
Shipping	Energy intensity of transport	MJ(fuel)/t.km	0.13	0.13	0.13	0.13	0.13	[222]
	Distance transported	km	8912	8912	8912	8912	8912	‡
Transport to Power Plant	Energy intensity of transport	MJ(fuel)/t.km	0.81	0.81	0.81	0.81	0.81	[222]
	Distance transported	km	51	51	51	51	51	‡
End-use	Electrical Efficiency	%	40%	40%	40%	40%	40%	[228]

† = See methodology, ‡ = See Supplementary Information, ς= determined: see section 2.1.3.1, γ = Calculated: see section 2.2.2, * = calculated from density of wood chips at 30% MC which = $250kg/m^3$

Table 7-6 - Summary of input data and key assumptions for modelling the GHG emissions of 4 TPs and conventional W

7.6.2.12 Scenarios and Sensitivity Analysis

Some aspects of this study were not based on experimental work or have uncertainties associated with them. To assess these further some different scenarios are considered in the results along with a sensitivity analysis of uncertain parameters, these can be summarised as follows:

- Use of torgas – results for the base case are assessed when no torgas is utilised (see section 7.7.5.1)
- Electricity required for pelleting torrefied wood – low and high values from literature (see section 7.7.5.2)
- Transport type (to port) – different options for land transport are considered (see section 7.7.5.3)

7.6.2.13 Limitations

The energy requirements presented above are based on modelled information from laboratory experiments. These data are then applied to a large-scale system for the production of torrefied pellets in an industrial scale plant. It is recognised that applying laboratory scale data to model the energy requirements does have limitations and will not exactly match the working conditions of a large-scale plant where several other factors are at play. For example, in a large-scale plant, such as the 100,000/annum output modelled in this study, there is a much greater throughput of fuel compared with the a laboratory-scale torrefaction rig. As such, heat transfer through to the centre of the biomass bed in an industrial plant may not be as great as in a bench-scale reactor. Furthermore, moisture losses from the biomass during the drying stage may not be as efficient as in a bench-scale reactor where in an industrial plant different levels moisture contents in the biomass may be entering the torrefier.

Nevertheless, the lack of industrial scale data due to few commercial torrefaction plants operating ultimately mean that modelling energy requirements based on laboratory data can be used to provide an assessment of what may take place at large-scales.

7.7 Results

7.7.1 Torrefaction of North American Pine

A full description of the results of the torrefaction of North American Pine can be found in Chapter 5. To summarise briefly here, torrefaction resulted in the loss of moisture and volatile matter from the biomass samples while increasing the fixed carbon content. These changes corresponded with an increase in the carbon content of the fuel while the oxygen and hydrogen contents decreased. These effects became more pronounced as the torrefaction condition severity increased. The loss of oxygen and enrichment of carbon upon torrefaction had a marked effect on the heating value of the fuels which increased from 20.21MJ/kg for untreated pine (dry basis) to 23.49MJ/kg for pine treated 290-30. Also, increasing torrefaction severity resulted in greater mass and energy loss having a resultant effect on the mass and energy yields shown in Chapter 5. The energy yields are greater than the mass yields under each condition resulting in an overall increasing trend of energy densification for the torrefied fuels with increased HHVs. The increasing mass loss corresponds to a greater energy loss despite the increase in HHV, which becomes significant when scaling up and economics of processes are considered. Typical mass and energy yields for torrefaction are often cited as 70% and 90% respectively [103] and if these criteria were to be considered as optimal, the two mildest conditions: 250-30 and 270-30 are within acceptable limits. The most severe conditions: 270-60 and 290-30 however may be considered inefficient as while the mass yields are within range, almost 15% and 20% of the original energy content of the fuel is lost resulting in lower energy yields despite the marked improvement in CV. The energy loss during torrefaction has further implications when analysing the potential for utilising energy in the volatile stream ('torgas') for heat to power the torrefaction process, which will be discussed later in the text.

7.7.2 Composition of volatile species determined using FG-Biomass

The composition of the volatile species was modelled using the FG-Biomass model and shown are Figure 7-7 below. It can be seen that for each species, the yields increases with increasing torrefaction severity. Reaction water represents the highest yield for all conditions followed by carbon dioxide then acetic acid. These results are comparable with the volatile species quantified experimentally by Prins et al. [104] in which the authors ascribe the formation of these species to occur as a result of decomposition of the hemicellulose fraction. The small amounts of carbon monoxide present, as noted by Prins et al, cannot be explained by decomposition reactions involving the cell wall species. The authors thus attribute the formation

of carbon monoxide as a result of the reaction of carbon dioxide and steam with char as temperatures increase [104].

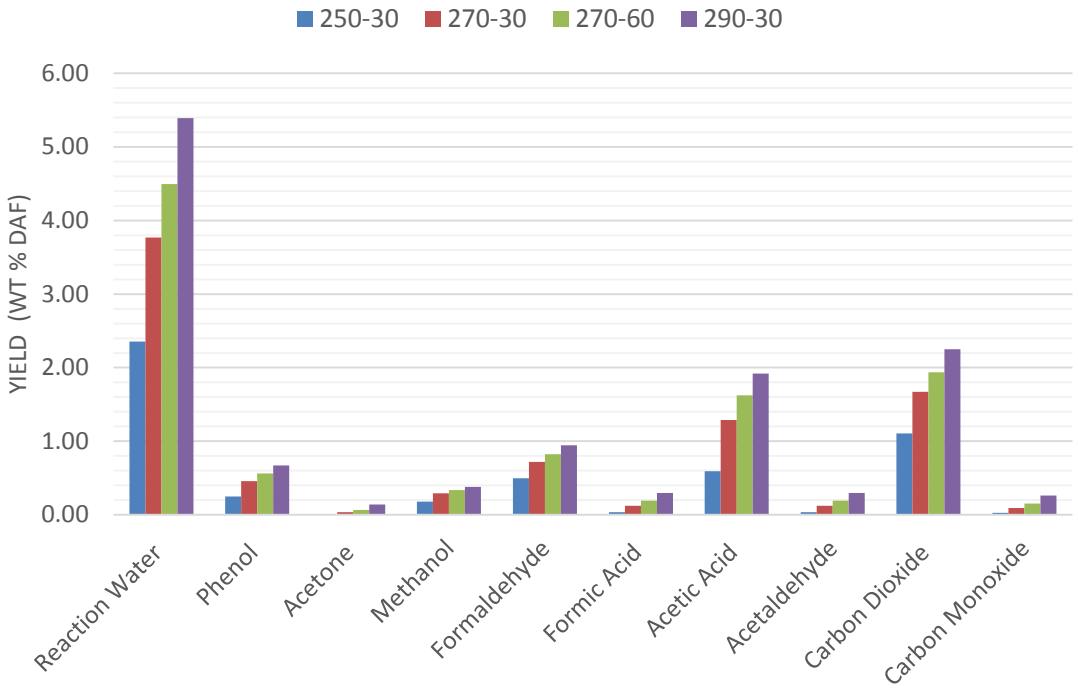

Figure 7-7 - Species contained in the volatiles stream modelled using FG-Biomass (dry-ash free basis).

7.7.3 Land Required

The results for the amount of land required for pellet production and additional wood for utility fuel are shown Table 7-7.

The land required for production of torrefied pellets increases with the trend 250-30 < 270-30 < 290-30 < 270-60. As torrefaction severity increases there is greater mass loss which would correspond to more input fuel required and thus more land to produce the same amount of feedstock. However, as torrefaction increases the CV of the resultant fuel, there is a compensation effect as there is more energy contained in the most torrefied fuels and accounting for this increase with respect to mass loss allows the land requirements to be calculated assuming the same energy output in the torrefied pellets.

	250-30	270-30	270-60	290-30	WP
Mass input (wet) to make 1000kg of TPs (kg)	1656	1777	1983	2086	1385
Total annual wood required (kilotons)	165.5	177.7	198.3	208.6	138.5
Total annual land required* (ha)	26805	27501	28930	28726	24730
Biomass required for drying**					
Utility fuel required (MJ/t output)	1531	1279	407	548	1394
Utility fuel required (GJ/year)	153060	127888	40725	54822	139400
Wood chip required (t)***	13391	11188	3562	4796	12195
Land required for WC utility fuel (ha)	2167	1811	577	776	1974
Total land required (ha)	**29,444**	**29,313**	**29,507**	**29,503**	**26,705**

* For 100,000 tonnes annual output and normalised against lowest CV fuel,

** Where biomass is used for utility fuel,

*** based on wood pellet CV of 11.43MJ/kg

Table 7-7- Land requirements for torrefied and untreated wood pellet production

This evident when comparing the land required for pellet production for conditions 270-60 and 290-30 as there is greater input mass required to make 1000kg of torrefied pellets for condition 290-30 however less land required as a result of higher CV. The additional mass required to account for using this feedstock as a utility fuel is also shown in Table 7-7. Condition 250-30 requires more additional utility fuel as there is less energy available in the volatile stream to be used for combustion to heat the torrefaction process. In combining the land requirements for pellet production and utility fuel, condition 270-30 requires the least amount of land overall. When comparing the land required for untreated wood pellets however, it can be seen that less land is required when compared to each torrefaction condition.

7.7.4 Greenhouse gas emissions assessment

Greenhouse gas (GHG) emission results are presented for the base case using the assumptions outlined in Section 7.6. For each of the four torrefaction conditions two options were considered for utility fuel being wood chips (WC) and natural gas (NG) to produce torrefied pellets (TP). Results are also presented for a conventional wood pellet (WP) for comparison purposes. Figure7-8 shows the results for these different pellets broken down into the 9 life cycle stages.

Figure 7-8 shows that treatment 250-30 result in 29.4CO_2e/MJ for WC and 43.1 CO_2e/MJ for NG which has the highest emissions when compared to other TPs on a 'per MJ' basis. The primary reason for this is the limited amount of torgas available from the volatiles from the less severe conditions which result in a fuel with lower calorific value (CV). By increasing the temperature by 20°C the emissions for 270-30 are reduced to 27.9 gCO_2e/MJ for WC and 38.8 gCO_2e/MJ for NG. Even greater GHG savings are obtained when the torrefaction severity increases to conditions 270-60 and 290-30. This trend is observed due to an increased CV of the torgas produced as a result of longer residence times and temperature respectively, requiring less additional utility fuel. While the reduction in consumption of additional fuel is desirable from a GHG emissions perspective, the additional energy available in the torgas stream for the more severe conditions is available at the expense of the energy contained in the parent fuel as discussed above. The parameters with which torrefaction optimisation are to be ascribed must therefore be clearly defined when making assessments of GHG emissions. In this instance, if the mass and energy yields are to remain within traditional guidelines, torrefaction under conditions 270-60 and 290-30 may be considered uneconomic as greater amounts of feedstock will be required, which may result in potential rejection despite lower overall emissions. The emissions associated with the utility fuel subsequently play a crucial role when looking at GHG emissions- if a higher proportion of heat for torrefaction is sourced externally. Differences in results are less pronounced when WC are used for drying and torrefaction, showing that the torrefaction condition is more significant (from a GHG emissions perspective) when NG is used as utility fuel. Combustion of NG has much higher emissions factor than WC as a fossil derived energy carrier, whereas carbon emitted from WC is considered to be biogenic with an emissions factor close to zero [226].

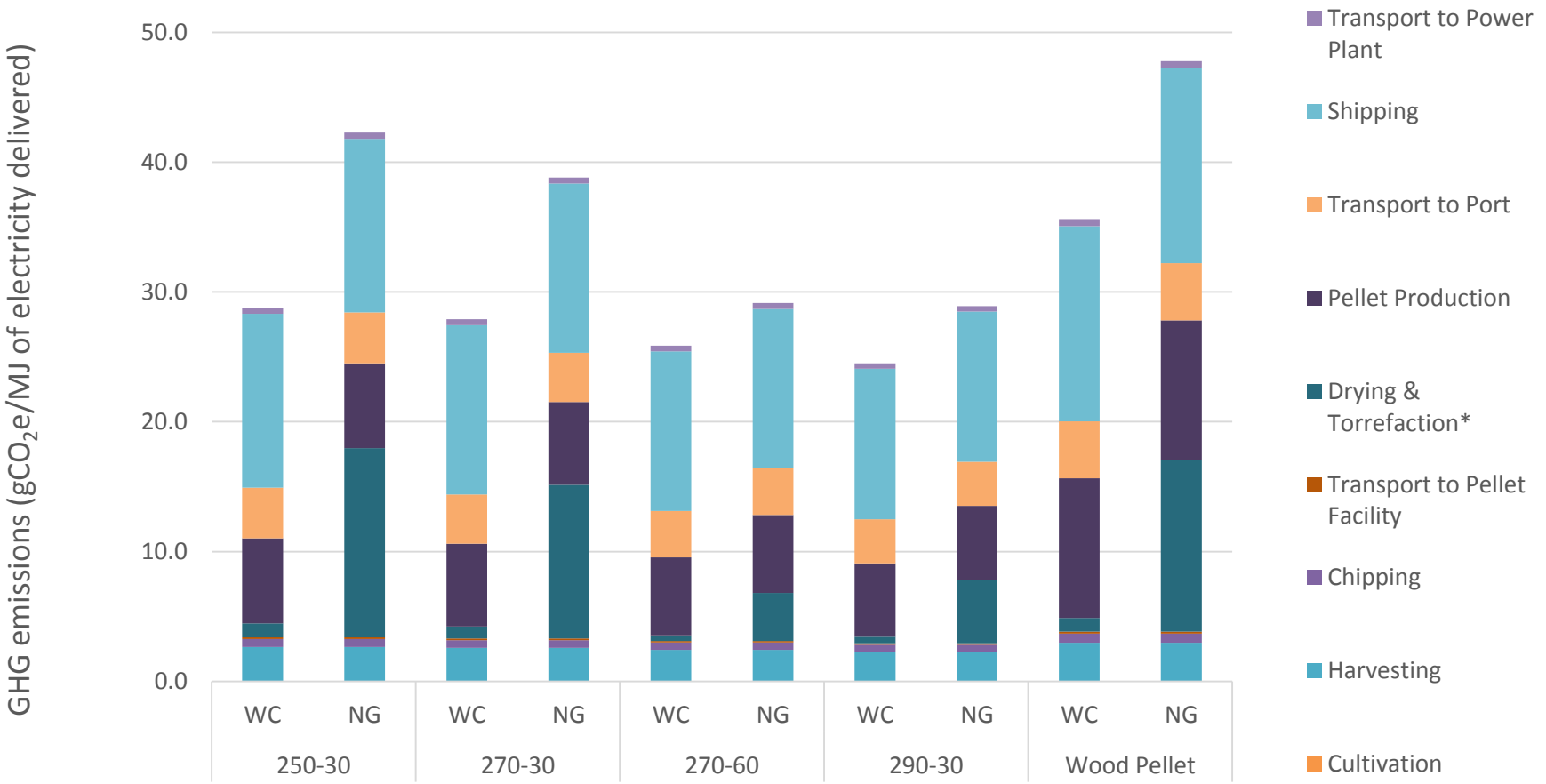

Figure 7-8 - Greenhouse gas (GHG) emissions per MJ of electricity delivered for 4 different torrefied pellets and conventional wood pellets (WP) using wood chips (WC) and natural gas (NG) as utility fuel. *For wood pellets = drying only.

With biomass sustainability criteria becoming increasingly important, the GHG emissions from biomass electricity are required to meet thresholds of 79.2gCO_2e/$MJ_{electricity}$; a saving of 60% against the EU fossil average for electricity generation [234]. This threshold has been implemented following recommendations from the EU [235], and under current UK legislation will reduce over time [234]. All pellets presented in Figure 3 would meet the existing GHG criteria, and show that using biomass rather than fossil fuels for utility fuel is crucial to maximise GHG savings of the supply chain.

All 4 TPs produce lower GHG emissions than conventional WP showing that despite the additional processing step, the use of torgas and increased calorific value of the TPs lowers their GHG emissions on a 'per MJ' basis. When the different life cycle stages of production are assessed, it is apparent that cultivation, harvesting, chipping, and transport to the pellet plant (collectively grouped as 'feedstock supply') have broadly the same emissions for all pellets considered. Feedstock supply contributes approximately 2.9-3.8gCO_2e/$MJ_{electricity}$ to each pellet supply chain and is therefore not further analysed here. It should however be reiterated that emissions from biomass feedstock supply can vary substantially depending on wider factors such as land use change, carbon debt, soil carbon and system boundary definition, and also specific variables; for example fertiliser inputs, fuel use, processing, and transportation distance [215, 236-241].

The contribution of drying and torrefaction are of crucial importance when considering the life cycle GHG emissions, particularly with regard to the choice of utility fuel. Figure 3 portrays that emissions from drying and torrefaction could be as low as 0.5gCO_2e/$MJ_{electricity}$ (<3% of total) for 290-30 (WC) or as high as 14.9gCO_2e/$MJ_{electricity}$ (~43% of total) for 250-30 (NG). For WPs the contribution from drying using WC and NG is 2.9 and 27.7% of the total respectively.

The emissions from pellet production derive from the energy required to grind the wood to smaller particles before pelleting followed by compression and extrusion in the pellet press. During torrefaction, decomposition of the lignocellulosic components in biomass occurs, with hemicellulose the most reactive under thermal treatment. As this polysugar provides structural integrity in the pine wood cells, its full or partial degradation leads to improved grindability and thus lower amounts of energy required in particle size reduction. The emissions for pellet production for the TPs range from 5.7 to 6.5gCO_2e/$MJ_{electricity}$ while the emissions for production

of WP (with no torrefaction) are 10.8gCO_2e/$MJ_{electricity.}$ The assumptions for electricity use vary in the literature and are therefore assessed further in the sensitivity analysis (Section 7.7.5.2).

Emissions from road transportation of pellets to the shipping port reduce with higher torrefaction severity due to the increased CV and bulk density. The contribution of road transport to the port for WP is the highest at 4.4gCO_2e/MJ with this reducing to the lowest of 3.4gCO_2e/MJ for 290-30. Utility fuel type influences emissions up to the point of pellet production; however for the transportation logistics it is primarily the energy content of the fuel that determines the GHG balance. For densified biomass such as pellets, transport is usually mass restricted whereas unprocessed biomass (e.g. wood chips) with higher moisture and lower bulk density, the volume is frequently the limiting factor.

Shipping is the biggest emission source for all scenarios, except for 250-30 where drying and torrefaction is larger when natural gas is used. Shipping emissions reduce as the calorific value of the pellet increases therefore 290-30 has lowest emissions from transport with WP the highest, representing one of the key potential advantages of torrefaction. Emissions for drying are higher for WP due to the assumption that no torgas is available to reduce demand for utility fuel.

7.7.5 Sensitivity Analysis

For the sensitivity analysis 3 main areas were highlighted for additional assessment. Feedstock supply was considered outside the scope for further analysis as all pellets assessed have the same emissions up to the point of delivery to the pellet processing plant. The sensitivity cases focus on i) the use of torgas; ii) electricity required for pelleting torrefied wood; iii) transport type (to port).

7.7.5.1 Use of torgas

Making use of the torgas is of key importance when assessing the GHG emissions from different torrefaction conditions [233]. There are limits to the degree of mass and energy loss that should occur in torrefaction that will affect the amount of energy contained in the volatile fuel stream as discussed in sections 7.7.1. Higher temperature and longer residence time means that more

energy is available in the torgas reducing the utility fuel requirement. Nonetheless, the increased torrefaction conditions presented here result in higher mass loss and consequently more biomass is required, thereby increasing the land required and associated economic cost. While the energy available in the torgas is modelled in this study and assumed to be all available for combustion (at 95% efficiency) its application in real-life scenarios is accompanied with several design and process considerations which would be factored in the event of a pilot or production-scale torrefaction plant being built. Such considerations include whether the combustion of torgas provides heat directly or indirectly to the incoming fuel where in each case the fuel to be torrefied either comes in contact with the heat carrier or is heated via a physical separation (e.g. a wall) respectively [103]. Other design considerations could also include utilising the heat from the torrefied product exiting the torrefier to reduce the amount of additional utility fuel required. The design and considerations mentioned here are beyond the scope of this study, however the impact of using no torgas was considered as part of the sensitivity analysis and to demonstrate its significance, emissions were calculated for a scenario with no torgas available. Figure 7.9 depicts how the calculated GHG emissions change for 'drying and torrefaction' when all of the thermal energy requirements are assumed to be supplied by utility fuel with zero torgas. It is observed that not using torgas makes results for natural gas drying much higher than the base case results, particularly for 270-60 and 290-30. All torrefaction cases show similar results when no torgas is available, with results comparable to WP when natural gas is used. Using wood chips for 'drying and torrefaction' has less more of an impact on results with these out-performing WPs under each condition.

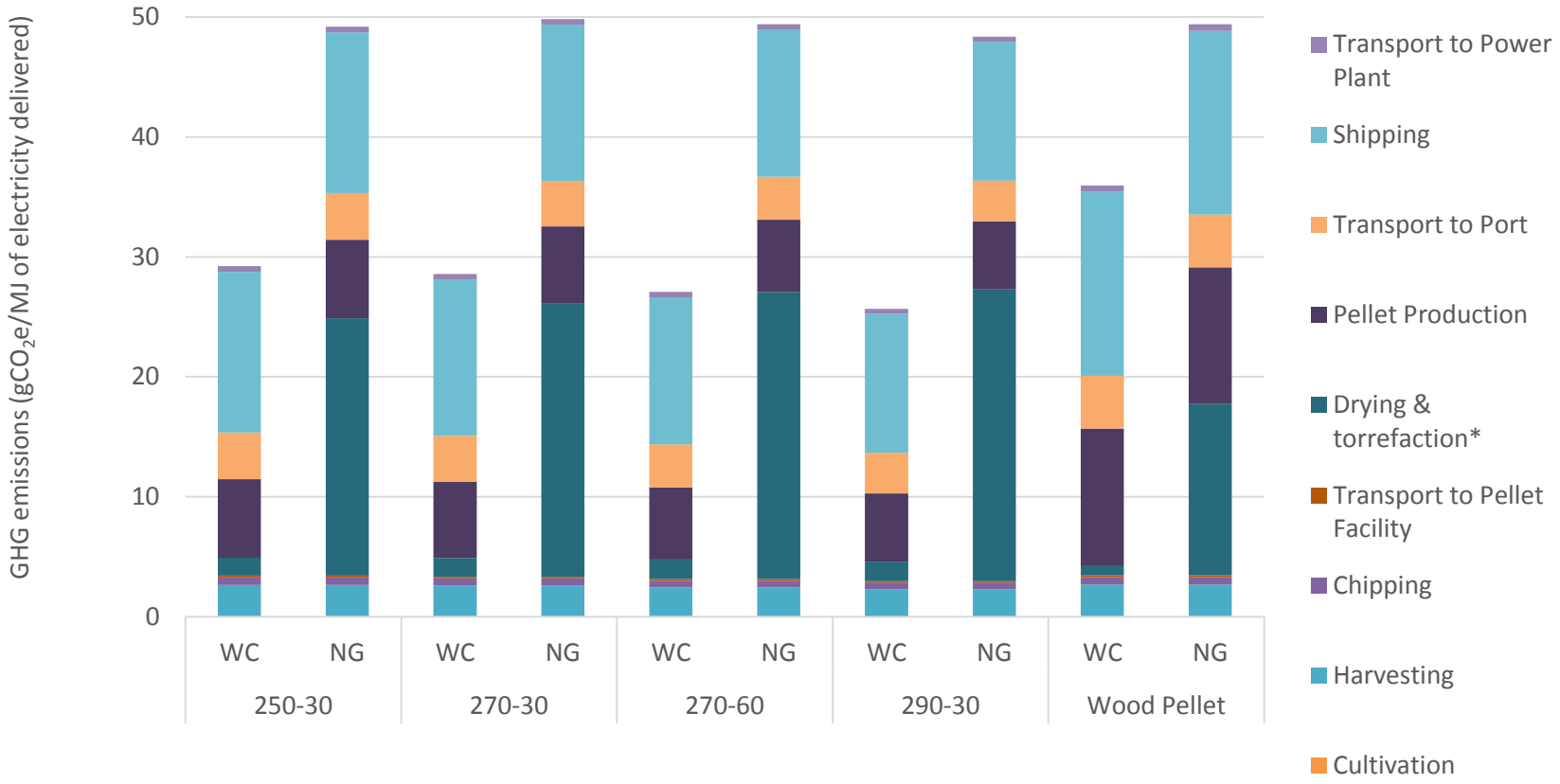

Figure 7-9 – Greenhouse gas (GHG) emissions per MJ of electricity delivered for 4 different torrefied pellets with no torgas using wood chips (WC) or natural gas (NG) only. *For wood pellets = drying only

Table 7-8 summarises how the results change for the 2 scenarios of torgas use for the different pellets.

	Total GHG Emissions $gCO_2e/MJ(electricity)$			Emissions from drying and torrefaction $gCO_2e/MJ(electricity)$			
	With torgas	No torgas	Difference (%)	With torgas	% of total	No torgas	% of total
Wood chips							
250-30	29.4	29.6	0.7	1.1	3.8	1.3	4.4
270-30	27.9	28.4	1.7	0.9	3.3	1.4	4.9
270-60	25.9	26.9	3.9	0.4	1.7	1.4	5.3
290-30	24.5	25.4	3.7	0.5	2.0	1.4	5.5
Wood Pellet	N.A	36	N.A	N.A	N.A	1.1	3.0
Natural gas							
250-30	43.1	46.6	8.1	17.6	38.9	18.0	39.4
270-30	38.8	46.7	20.3	11.8	30.5	19.7	42.2
270-60	29.1	46.1	58.2	3.7	12.7	20.7	44.8
290-30	28.9	44.3	53.3	4.9	17.0	20.3	45.8
Wood Pellet	N.A	47.8	N.A	N.A	N.A	13.2	27.7

N.A = not applicable

Table 7-8 – Results for the sensitivity analysis for no torgas

7.7.5.2 Electricity required for pelleting torrefied wood

As mentioned in section 7.6.2.8, there is a lack of agreement in the literature regarding data on the electricity required for pellet production, which will vary depending on the nature of the feedstock, degree of torrefaction, and type of mill and pellet pressed used to determine consumption. It is generally known that less energy is required to reduce torrefied wood chips to smaller particles prior to pelleting than untreated wood chips, since torrefaction can result of improved grindability and thus has an impact on the overall electricity consumption of the process when torrefaction is combined with pelleting [90]. However, uncertainties lie in the energy required for compression and extrusion of pellets from torrefied biomass. Some

researchers, such as Stelte et al. [242], argue that the loss of moisture (which acts as a plasticizer) and extractives during torrefaction increase friction in the channel press resulting in higher pelletizing pressures and subsequent energy uptake of the mill (which increases as torrefaction severity increases). In agreement with this notion is the study by Li et al. [243] which also attributed reduced plasticity, and therefore increased extrusion and compression in the pellet press, to the degradation of hemicellulose and lignin during torrefaction thus resulting in greater energy requirements when compared to pelleting untreated wood. Similar trends have been reported from pilot-scale pelletizing of spruce torrefied at 270°C and 300°C for 16.5 minutes by Larsson et al. [244], where 100% more energy was required for pelleting torrefied material when compared to pelleting of untreated fuel. Moreover, it was also found that torrefied pellets were less durable and had only comparable bulk densities to untreated pellets.

In contrast, Bergman et al. [245] report lower overall power consumptions are required for pelleting torrefied biomass when compared to untreated biomass. The authors also report higher bulk densities for torrefied pellets compared with conventional pellets (750-850kg/m^3 and 500-650 kg/m^3 respectively) and that the torrefied pellets obtained showed improved mechanical strength- with crushing tests demonstrating that torrefied pellets could withstand 1.5-2 times more force than traditional wood pellets. The authors attribute this to alterations to fatty structures during torrefaction, which serve as binding agents, as well increased lignin weight percent providing mechanical strength. The role of lignin in WPs is very important as it acts as a binder in pellet production and contributes to pellet mechanical strength. It is generally agreed that upon heating through compaction, the lignin in wood particles, with aid of moisture, undergoes softening and transitions from a 'glassy to rubbery' composition acting as a glue between particles via hydrogen bonding on the surface with hemicellulose [205, 246]. Although there are different views on the role of lignin in torrefied pellet production, it is known that in the case of severely torrefied materials (i.e. T >280°C) the resultant pellets have less mechanical strength than those torrefied under milder conditions (e.g. [242]) in some cases not producing viable pellets at all. It has been suggested that only low molecular weight polymers are involved in glass transition and binding in wood pellets and as these can degrade during torrefaction, pellets produced under certain torrefaction conditions lack mechanical strength and durability [243]. These problems may be overcome from increasing the die temperature in the pellet press to encourage glass transition of higher weight lignin polymers or the addition of a binding agent; however these will have implications on energy consumption and subsequent GHG emissions.

Furthermore, the values for electricity consumption found in the literature are based on laboratory-scale mills and single pellet presses, which are not synonymous with large-scale industrials mills. As pointed out by Jarvinen et al. [205], industrial data is scarce as pelleting of torrefied wood on large scale is often performed internally; requiring large amounts of feedstock that are not often produced in academic institutions. This leads to a gap in the information available resulting in the use of laboratory or semi-industrial scale data, which may not reflect real-life scenarios and affect the results of GHG emissions assessments.

Due to the lack of large scale data and issues discussed above, a sensitivity analysis for the electricity consumption for pelleting torrefied wood was deemed necessary as any uncertainties may have a sizeable impact on associated GHG emissions. The results of the sensitivity analysis for the electricity required to pelletise torrefied wood are shown in Figure 7-10. The low and high case scenarios were taken from Batidzirai et al. [247] and are 18kWh/t and 395kWh/t respectively. The results show little change in GHG emissions for each torrefaction condition under the low case scenarios (18 kWh/t) when WCs are used with values ranging between 19.9 and 23.7 $gCO_2e/MJ_{electricity.}$ When NG is utilised the emissions range from 40.0 $gCO_2e/MJ_{electricity}$ to 24.3 $gCO_2e/MJ_{electricity}$ for biomass torrefied at 250-30 and 270-60, respectively. Under the high case scenario (395kWh/t) a similar trend is observed. However, the emissions using WC range from 42.4-49.7 $gCO_2e/MJ_{electricity}$ while the NG emissions are much higher ranging from 46.8-66.0 $gCO_2e/MJ_{electricity.}$ Comparing to conventional WP emissions, when WCs are used, the low case scenarios outperforms the WP emissions- although under the high scenario the reverse is shown. When comparing TP and WP supply chain emissions where NG is used as utility fuel, the low case scenarios for all TPs outperform WP emissions. Under the high case scenario, only the 270-60 and 290-30 life-cycle emissions outperform the WP emissions.

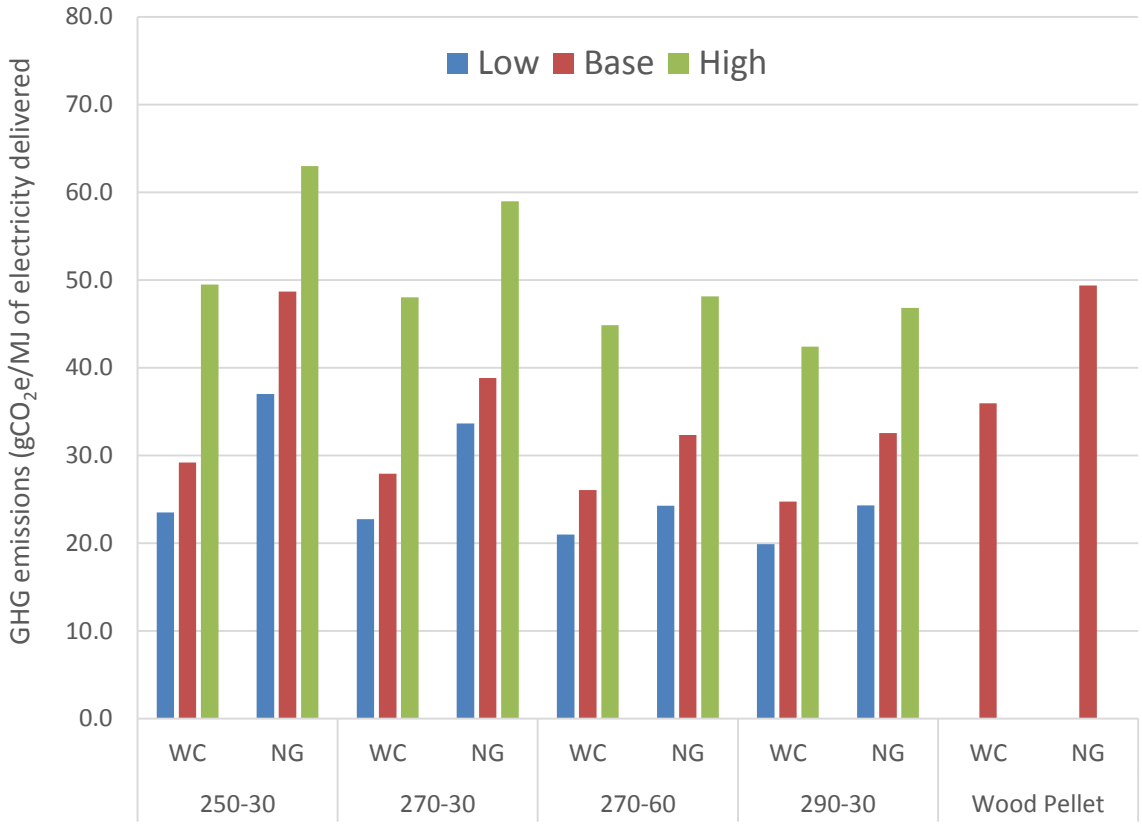

Figure 7-10 - Results of the sensitivity analysis for low, base and high case electricity requirements for pellet production

7.7.5.3 Transport type (to port)

The base case assumes that road transport is used for transporting pellets to/from transatlantic shipping ports; however in several locations alternative options include freight-trains or inland water barges. In particular the pellet facility chosen for this case study uses inland barges [212]. The sensitivity analysis results for wood chip (WC) only, assuming a distance of 415km is displayed in Table 7-9.

Transport Mode Fuel utilised	Truck Diesel	Rail Electricity	Rail Diesel	Inland Water Barge Heavy Fuel Oil
250-30				
Transport Emissions ($gCO2_e/MJ_{electricity}$)	3.9	1.5	1.7	1.6
Total Supply Chain Emissions ($gCO2_e/MJ_{electricity}$)	28.8	26.4	26.6	26.5
Contribution of transport to supply chain	13.5%	5.7%	6.4%	6.0%
Change from base case	-	-8.4%	-7.7%	-8.0%
270-30				
Transport Emissions ($gCO2_e/MJ_{electricity}$)	3.8	1.4	1.6	1.5
Total Supply Chain Emissions ($gCO2_e/MJ_{electricity}$)	27.9	25.5	25.7	25.6
Contribution of transport to supply chain	13.6%	5.5%	6.2%	5.9%
Change from base case	-	-8.6%	-7.9%	-8.3%
270-60				
Transport Emissions ($gCO2_e/MJ_{electricity}$)	3.6	1.4	1.5	1.4
Total Supply Chain Emissions ($gCO2_e/MJ_{electricity}$)	25.9	23.7	23.8	23.7
Contribution of transport to supply chain	13.9%	5.9%	6.3%	5.9%
Change from base case	-	-8.5%	-8.1%	-8.5%
290-30				
Transport Emissions ($gCO2_e/MJ_{electricity}$)	3.4	1.3	1.4	1.3
Total Supply Chain Emissions ($gCO2_e/MJ_{electricity}$)	24.5	22.4	22.5	22.4
Contribution of transport to supply chain	13.9%	5.8%	6.2%	5.8%
Change from base case	-	-8.5%	-8.1%	-8.5%
Wood Pellet				
Transport Emissions ($gCO2_e/MJ_{electricity}$)	4.4	1.6	1.9	1.7
Total Supply Chain Emissions ($gCO2_e/MJ_{electricity}$)	35.6	32.8	33.1	32.9
Contribution of transport to supply chain	12.4%	4.9%	5.7%	5.2%
Change from base case	-	-7.8%	-7.0%	-7.6%

Table 7-9 - Results for the transport sensitivity analysis

Fuel use and emission factors are taken from Biograce [222]. These results show that reductions in GHG emissions of 7.0-8.6% are achievable with rail (electric), rail (diesel), and inland water barges. Over the distance of 415km, the GHG emissions from transport using alternative transport to road trucks can reduce from 3.4-4.4 $gCO_2e/MJ_{electricity}$ (12.4-13.9% of the total) to 1.4-1.9 $gCO_2e/MJ_{electricity}$ (4.9-6.4% of the total).

7.7.6 Other aspects

7.7.6.1 Land use change and soil carbon

The life-cycle emissions determined in this study adopt the RED methodology which considers the emissions associated with harvesting, processing, transport and combustion and consequently do not consider the emissions associated with LUC/ILUC prior to 2008 [44]. The inclusion of LUC and ILUC within the system boundaries is often challenging as specific data

pertaining to LUC/ILUC change is difficult to determine with certainty [217]. It can also be difficult to relate changes in LUC/ILUC with bioenergy systems being assessed i.e. the model outputs measuring carbon stocks are not strictly related to the functional units used for bionenergy systems; in this instance $gCO_2e/MJ_{electricity}$ [236].

Several studies have attempted to include changes in carbon stock within the system boundaries of bioenergy LCA e.g. [236, 237, 248]. The UK Department of Energy and Climate Change's 2014 report also considers the implication of changes to carbon stock, foregone sequestration and indirect changes on carbon fluxes and GHG emissions and present life-cycle GHG emissions from a range of scenarios and their counterfactuals where bioenergy is used for electricity production [249]. The results reported for electricity from round wood (in addition to wood residues and energy crops) under different harvesting and management regimes and under different time periods (40 and 100 years) varied significantly (depending on whether the forests were naturally re-generated or intensively managed; with the latter's emissions subsequently depending on whether demand for wood is high or low) from negative emissions to emissions higher than coal life-cycle emissions. Caution must therefore be administered when including LUC and ILUC within system boundaries, as it can severely under or overestimate emissions. As a result, while the authors acknowledge the importance of changes in carbon stock as a result of LUC/ILUC in life-cycle GHG emissions assessments, as no standardised methodology is utilised that accounts for these changes carbon stock in LCA, the RED methodology was selected as this is the approved methodology adopted in the EU.

Changes in LUC/ILUC also have an impact on soil carbon stocks which are not included in the RED methodology. Similar to changes in forest carbon, impacts on soil carbon are difficult to determine with absolute certainty. Nevertheless, some studies have attempted to quantify the change in soil carbon as a result of harvest temperate forests e.g. [238] and growth of energy crops e.g. [250].

7.7.6.2 Emissions from outdoor drying

Emissions can arise from storage of biomass that can contribute to GHG emissions including CO_2, nitrous oxide (N_2O) and methane (CH_4). The gaseous emissions from storage are linked to dry

matter loss which occurs as a result of degradation of the wood. The extent of degradation depends on the nature of the feedstock, storage environment and moisture content [82, 251]. CO_2 emissions from wood can occur from thermal oxidation and aerobic and anaerobic biodegradation, while action of micro-organisms in anaerobic conditions results in CH_4 evolution [251]. N_2O emissions occur as the end product of incomplete ammonium oxidation of incomplete denitrification [82]. He et al. report on the emissions of CO_2 and CH_4 from Canadian Douglas fir branches with higher emissions for both gases at higher temperatures (35°C when compared to 15°C) and peak concentrations of 138,000ppm and 1500ppm respectively, most likely as a results of increased microbial activity at higher temperatures [251]. The authors also noted a decrease in oxygen concentrations to between 1-2% after 10 days storage. Theoretical methane and nitrous oxides losses from wood residues were calculated by Wihersaari who calculated daily emissions rates of 24g/m^3 and 0.6g/m^3 for methane and nitrous oxide respectively [82]. The conclusion of this study was that forest residue should be utilised as quickly as possible to avoid emissions from this source. These emissions may present an issue when natural of drying wood occurs, particularly in the summer months where outdoors the climate is warmer leading to increased microbial activity.

7.8 Conclusions

The use of bioenergy is increasingly being deployed as a means of reducing GHG emissions and to meet emission reductions targets. While this is apparent, the biomass used in energy applications must be sourced sustainably with stringent regulations set in place in many countries which cap the overall life-cycle GHG emissions for approved bioenergy supply chains. In the UK, generators using bioenergy are now required to report their life-cycle GHG emissions using the European Commission RED methodology, with subsequent emissions reported required to adhere to regulatory limits set in place in order to qualify for subsidies in the RO: one of the main government incentives for using renewable technologies. The magnitude of GHG emissions reported by UK generators are becoming increasingly more important as feedstocks sourced from overseas, notably North America are increasingly being sought after to supply demand. The feedstocks sought from North America for use in the UK are mainly in form of wood pellets with the wood pellet market expanding to accommodate the demand from not only the UK but other EU states. While wood pellets are an adequate densified product, their suitability as a fuel can be limited by low calorific value, energy and bulk density when compared with fossil fuels and problems during transportation and logistics. Torrefaction can alleviate

some of these issues by addressing the problems listed above. In combination with pelletisation, torrefied pellets may represent an overall superior fuel. As torrefaction is an endothermic process however, there is a trade-off between energy input and improved fuel characteristics. This can be come significant when life-cycle GHG emissions are considered.

An assessment of the effect of torrefaction on life-cycle GHG emissions for a priority fuel chain importing North American pine pellets to the UK was performed to determine any changes that occur with the addition of this pre-treatment step. Using real-life experimental date for the torrefaction of North American pine under 4 conditions, mass and energy balances for each condition were performed and the energy requirements for drying and torrefaction modelled. The torgas was assumed to be available for combustion at 95% efficiency with remained heat demand provided by either wood chips or natural gas. These data were then incorporated in to a bespoke bioenergy supply chain and the GHG emissions calculated in line with the RED methodology and compared with a traditional wood pellet supply chain without torrefaction. Results showed that based on experimental results and assumptions described above, potential GHG savings could be made by implantation of torrefaction. The lowest life-cycle emissions per MJ of electricity delivered were found when pine was torrefied at 290°C for 30 minutes and wood chips were used as the utility fuel where emissions were 24.7g $CO_2e/MJ_{electricity}$. The life-cycle emissions where wood chips were used as the utility fuel ranged from 24.7 to 29.2g $CO_2e/MJ_{electricity.}$ When natural gas was used, the emissions were expectedly higher than the wood chip fuel chains ranging from 32.5 to 48.7g $CO_2e/MJ_{electricity.}$ Without torrefaction, conventional wood pellet life-cycle emissions were 36.0 and 49.4g $CO_2e/MJ_{electricity}$ when wood chips and natural gas were used for drying respectively. The largest emissions by life-cycle stage is caused by shipping is followed by the torrefaction and drying stages while several stages of production i.e. cultivation and transport to pellet facility have a relatively small contribution to overall supply chain emissions.

Sensitivity analysis for using no torgas for drying and torrefaction showed all torrefaction cases to have similar life-cycle emissions with results comparable to conventional wood pellets when natural gas is used. Using wood pellets however, the torrefied pellet supply chains outperform wood pellet supply chain emissions. When, using no torgas and natural gas as the utility fuel, the emissions for conditions 270/60 and 290/30 are notably higher than when torgas is used.

Wood chips are thus preferred as a utility fuel overall owing to their lower life-cycle GHG emissions. The sensitivity analysis for the electricity required for pelleting showed that little variation in life-cycle emissions when wood chips are used elsewhere in the supply chain for the low case scenario (18 kWh/t) however notable reduction overall were observed. The high case scenario showed the same trend however with greater overall emissions. This sensitivity analysis was selected due to the lack of industrial data for the electricity required to pelletise torrefied wood and due to conflicting data in the literature. Transport sensitivity analysis showed that emissions can be lowered when alternative transport methods such as rail or inland barge are used in transporting the pellets to port.

8 Conclusions and Future Work

8.1 Conclusions

Since the 1990s as the dangers of climate change rose on the social and political agenda, so have the governmental measures, domestically and in the EU, to introduce renewable technologies in to the energy mix. This has been achieved with the implementation of market-mechanism such as the RO to the reform of the electricity market effective in increased deployment of various low carbon technologies. The use of bioenergy is one such technology which, as a carbon carrier that can exist in solid, liquid and gaseous form, has undergone increased deployment in the UK. Bioenergy in large-scale electricity generation has undergone rapid growth in part due to its easy incorporation in to existing energy supply chains such as coal. Initially, the focus of bioenergy in UK electricity generation was in co-firing with coal however policy changes such as reforming of governmental subsidies has shifted the focus to stand alone generation through dedicated plant and conversion of coal mills. While the use of bioenergy, specifically solid biofuels such as wood pellets can be utilised in such capacities, inherent problems with their deployment do exist. These include high moisture content and low calorific value relative to fossil fuels, poor grindability owing to the lignocellulosic make-up of biomass and issues using solid biomass in the supply chain such as disintegration (owing to high moisture contents) when stored and ignition risks.

Torrefaction is pre-treatment step that aims to address some of these issues. By heating biomass at relatively low temperatures in the absence of oxygen for a desired residence time (typically up to one hour), the biomass loses moisture and oxygen-rich volatiles while improving the calorific value and grindability via degradation of the structures that give biomass its tenacity. Torrefaction thus enhances the physical and chemical properties of the fuel. As a result of these changes, the pyrolysis and combustion properties are enhanced too including reducing reactivity through a decrease in volatiles content.

The above provides the foundation for the focus of this research. The first topic of investigation was the effect of torrefaction, using four sets of conditions, on the physical and chemical properties of pine and eucalyptus fuels and to determine the overall mass and energy balances of the processes. Results showed that increasing the torrefaction severity (i.e. increasing

temperature and residence time) results in decreased moisture content and increased calorific value; these changes becoming more pronounced as conditions become more severe. Increasing severity also results in decreased solid mass yields. As such, while properties such as calorific value increase as torrefaction temperature and residence time are greater, too great a mass loss could uneconomic if greater input masses are required to achieve the desired results. The same can be said for the energy losses where implementing too severe conditions can result in too much energy loss. As a result, the improvements in fuel properties must be considered alongside mass and energy losses in order to evaluate the optimum process conditions.

It was also demonstrated that fuels containing more reactive hemicelluloses such as eucalyptus (in the case of hardwoods) result in greater mass loss relative to pine (softwood) under the same condition. From this, eucalyptus may be better suited for torrefaction than pine under some circumstances, as a greater mass loss can potentially achieve a more energy dense fuel under the same conditions. Results also showed that torrefaction temperature has a greater impact on solid mass loss than residence time for both pine and eucalyptus, which follows results found by other researchers. This information can be used to elucidate optimum torrefaction conditions by comparing the results of each condition and testing conditions which yield the greatest overall results.

Ultimate and proximate analysis of untreated and torrefied pine and eucalyptus show the carbon weight percent, fixed carbon and ash contents to increase while moisture, oxygen weight percent and volatiles concentration decrease. Results also show that nitrogen is lost to the organic and gaseous phase during torrefaction which increases as torrefaction conditions become more severe. The loss of nitrogen resulted in a decrease in nitrogen per unit energy signifying the potential for using torrefied fuels in reducing NO_x emissions. Grindability studies on untreated and torrefied pine fuels show that grindability progressively increases as torrefaction temperature and residence time increase. Particle size distribution studies which complement grindability tests further show increase in smaller particles as torrefaction conditions become more severe. Chapter 6 investigated the pyrolysis and combustion properties of untreated and torrefied willow and eucalyptus. Results showed that torrefied fuels are less reactive than their untreated analogues at the onset of pyrolysis (as determined from TGA studies). These results demonstrate that torrefaction results in the loss of the most reactive

volatile components in biomass and increase in more stable, fixed carbon. From a fuels perspective, the loss of low energy products and enrichment of carbon-rich materials is desired as essentially higher calorific value and more energy dense fuel is created. Results of the nitrogen partitioning during rapid devolatisation in the drop tube furnace showed opposite trends for willow and eucalyptus. In general, torrefaction appeared to result in the retention of nitrogen in the char during fast-heating rate devolatilisation of willow while for eucalyptus, torrefaction appeared to promote the release of N to the volatiles phase. Thus, from a NO_x emissions perspective, torrefied eucalyptus fuels may be favourable. Investigation of the partitioning of potassium during fast-devolatilisation suggest that potassium evolves at the same rate as carbon for both untreated and torrefied fuels, potentially having a catalytic effect of char burn-out.

The final section of this work investigated the effect of torrefaction on life-cycle GHG emissions for the production electricity using torrefied pine pellets. The results of the GHG assessment, performed using the standardised RED methodology, give an important conclusion that GHG emissions could be saved using torrefied pellets when compared to conventional wood pellet. The increased calorific value and utilisation of the volatile gases or 'torgas' for heat production are key factors although more initial feedstock and thus more land is required in producing torrefied pellets. For the sensitivity analysis where no torgas was utilised, the utility fuel selected, either wood chips or natural gas had a considerable impact on GHG emissions, with natural gas resulting in increased emissions due to its higher emissions factor. Overall, results showed that introducing torrefaction in to the supply chain can result in lower life-cycle emissions than conventional pellets and life-cycle emissions that fall within current and future sustainability guidelines.

8.2 Future Work

8.2.1 Torrefaction studies

An area of future work to follow on from the torrefaction studies on pine and eucalyptus could include the extension of the mass and energy balance work to determine experimentally the permanent gas products of torrefaction. In this study, the permanent gases were calculated by difference however future work could include determining the gaseous species (CO_2, CO and other light volatiles) using Gas Chromatography. This could be achieved by connected the

exhaust line of the torrefaction rig to a GC during experiments for on-line determination or collection of gases using gas-bags for off-line determination.

Further work on torrefaction could include quantification of the species present in the aqueous and tar phases. By employing techniques such as high pressure liquid chromatography (HPLC) and gas-chromatography mass spectrometry (GC-MS), the species presents in liquid products could be determined. Species expected to be included in aqueous phase products include methanol and acetic acid while the tar phase species are expected to include non-polar compounds such as aromatics. The lignocellulosic origin of some of the compounds could also be estimated as part of this work e.g. the presence of phenolics originating from the lignin fraction.

Lastly, an interesting work could include extending the cell wall component analysis to investigate the differences in hemicellulose and lignin composition for the fuels and their changes in concentration with torrefaction- and how this impacts on pelleting and briquetting. As the torrefaction conditions, notably severe torrefaction conditions (>280C), may impact on the fuel's ability to make viable pellets- further work linking torrefaction condition and pellet production could be undertaken marking an important next step in commercialisation.

8.2.2 Char work

The main area for further work on char combustion studies would be to include the North American pine fuel as part this work. By preparing fast-heating rate chars from the untreated and torrefied pine fuels analysed in Chapter 5 and studying the isothermal oxidation kinetics on these chars would provide information on the behaviour of these fuels in industrial application. This would allow a 'full-circle' assessment of the torrefaction of pine, the combustion behaviour and a GHG emissions assessment. As work present in this thesis was not performed chronologically and so this was unfortunately not feasible. However char combustion studies of pine would be the first study to continue this work.

Another option for future work could be to vary the residence time of particles in the drop tube furnace by altering the flow rate of gases in to the reactor tube. By increasing or decreasing the residence time, this will affect the degree of devolatilisation and burn-out and thus the surface area. The rate of char oxidation could then be calculated to determine char combustion rates at high temperature as well develop a correlation between burn-out and surface area for the char particles.

8.2.3 GHG emissions assessment

The GHG emissions assessment could be extended by including a further sensitivity analysis to include different location. As shipping contributes the greatest emissions in the supply chain, varying this to include closer (e.g. Europe) and further (e.g. Western Canada) locations could provide insight in to impact of torrefaction on overall emissions. That is to say, as distance contributes the most emissions, implementing torrefaction could benefit transporting fuels greater distances or reduce emissions even more by torrefying closer to the UK.

Further studies could include performing a GHG emissions assessment for the electricity produced from torrefied eucalyptus as this was also investigated in Chapter 5. This could include domestic or international feedstock supply of eucalyptus to broaden the study more.

The research could be developed further by extending the modelling of the torrefier energy requirements to include different dryer and torrefier design considerations. This could include an investigation in to the various heat integration options for the torgas e.g. indirect and direct heating. In addition, it could include investigation of the various dryer and torrefier technologies e.g. rotary drum or microwave technologies and their associated energy demands.

References

1. Houghton, J., *Global Warming*. 1997: Cambridge University Press.
2. UNFCC. *Kyoto Protocol*. 2015; Available from: http://unfccc.int/kyoto_protocol/items/3145.php.
3. IPCC, *Summary for Policymakers. In: Climate Change 2013: The Physical Science Basis. Contribution of Working Group I to the Fifth Assessment Report of the Intergovernmental Panel on Climate Change* 2013.
4. IPCC, *Black Carbon Aerosol from Fossil Fuels* 2007.
5. IEA, *CO2 Emissions from Fuel Combustion - Highlights*. 2014.
6. U.S Department of Commerce. *Earth System Research Laboratory: Global Monitoring Devision - Full Mauna Loa CO2 record*. 2015; Available from: http://www.esrl.noaa.gov/gmd/ccgg/trends/.
7. UNFCC. *Background on the UNFCCC: The internation response to climate change*. 2015; Available from: http://unfccc.int/essential_background/items/6031.php.
8. UNFCCC. *Cancun Climate Change Conference - November 2010* 2015; Available from: http://unfccc.int/meetings/cancun_nov_2010/meeting/6266/php/view/documents.php.
9. IEA, *Energy and Climate Change - World Energy Outlook Speical Report* 2015.
10. Netherlands Environmental Assessment Agency and *Meeting the 2°C target - From climate objectiove to emission reduction mesaures* 2009.
11. IPCC, *Principles Governing IPCC work* 2013.
12. DECC, *2013 UK Greenhouse Gas Emissions, Final Figures.* 2015.
13. Newbery, D.M. and M.G. Pollitt, *The restructuring and privatisation of Britain's CEGB - Was it worth it?* Journal of Industrial Economics, 1997. **45**(3): p. 269-303.
14. Domah, P. and M.G. Pollitt, *The restructuring and privatisation of electricity distribution and supply businesses in England and Wales: A social cost-benefit analysis.* Fiscal Studies, 2001. **22**(1): p. 107-146.
15. Simmonds, G., *Regulation of the UK electricity industry*, in *Centre for the study of regulated industries*. 2002.
16. Chesshire, J. and J. Surrey, *UK electricity privatization.* Energy Policy, 1988. **16**(2): p. 98-101.
17. Green, R., *Reshaping the CEGB.* Utilities Policy, 1991. **1**(3): p. 245-254.
18. Beggs, C., *Energy: Management, Supply and Conservation*. 2012: Routledge.
19. Green, R., *Draining the Pool: The Reform of Electricity trading in England and Wales*. 1998, University of Cambridge: Cambridge.
20. Bower, J., *Why Did Electricity Prices Fall in England and Wales? Market Mechanism or Market Structure?* 2002, Oxford Institute for Energy Studies.
21. Mitchell, C., *The renewables NFFO - A review.* Energy Policy, 1995. **23**(12): p. 1077-1091.
22. Mitchell, C., *The England and Wales non-fossil fuel obligation: History and lessons.* Annual Review of Energy and the Environment, 2000. **25**: p. 285-312.
23. Mitchell, C. and P. Connor, *Renewable energy policy in the UK 1990-2003.* Energy Policy, 2004. **32**(17): p. 1935-1947.
24. Elliott, D., *RENEWABLES AND THE PRIVATIZATION OF THE UK-ESI - A CASE-STUDY.* Energy Policy, 1992. **20**(3): p. 257-268.
25. Agnolucco. P., *Opportunism and competition in the non-fossil fuel obligation*. 2005, Tyndall Centre for Climate Change Research.
26. Newbery, D., *Electricity liberalisation in Britain: The quest for a satisfactory wholesale market design.* Energy Journal, 2005: p. 43-70.
27. Pearson, P., and Watson, J., , *UK Energy Policy 1980-2010: A history and lessons to be learnt*. 2012, The Institue of Engineering and Technology.

28. UN, *United Nations Framework Convention on Climate Change*. 1992.
29. UN, *Kyoto Protocol to the United Nations Framework Conventio on Climate Change*. 1998, United Nations: Kyoto.
30. Woodman, B. and C. Mitchell, *Learning from experience? The development of the Renewables Obligation in England and Wales 2002-2010.* Energy Policy, 2011. **39**(7): p. 3914-3921.
31. Woodman, B. and C. Mitchell, *Learning from experience? The development of the Renewables Obligation in England and Wales 2002–2010.* Energy Policy, 2011. **39**(7): p. 3914-3921.
32. Ofgem, *Renewables Obligation: Guidance for generators*. 2013.
33. Wood, G. and S. Dow, *What lessons have been learned in reforming the Renewables Obligation? An analysis of internal and external failures in UK renewable energy policy.* Energy Policy, 2011. **39**(5): p. 2228-2244.
34. Parliament, U., *Climate Change Act 2008.* London: The Stationery Office Limited, 2008.
35. European Comission, *DIRECTIVE 2009/28/EC OF THE EUROPEAN PARLIAMENT AND OF THE COUNCIL of 23 April 2009 on the promotion of the use of energy from renewable sources and amending and subsequently repealing Directives 2001/77/EC and 2003/30/EC*. 2009.
36. Ofgem, *Renewables Obligation: Guidance for generators*. 2011.
37. DECC, *Consultation on proposals for the levels of banded support under the Renewables Obligation for the period 2013-2017 and the Renewables Obligation Order 2012*, DECC, Editor. 2011: London.
38. European Comission. *The EU Emissions Trading System (EU ETS)*. Available from: http://ec.europa.eu/clima/publications/docs/factsheet_ets_en.pdf.
39. Stone, M., *Bad Politics: Do renewable energy targets undermine the european union's emissions trading scheme?*, University of Dundee.
40. Ofgem, *The BETTA way forward*. 2005.
41. House of Commons: Energy and Climate Change committee, *Electricity Market Reform*. 2011.
42. Fairuz, A.J.A., *Market Power in the Great Britain Wholesale Electricity Market*, in *Mechanical Engineering*. 2007, University of Glasgow: Glasgow.
43. Tovey, K., *Developments in the Electricity Markets in the UK: the move towards BETTA*. 2005, School if Environmental Sciences, University of East Anglia.
44. European Comission, *DIRECTIVE 2001/80/EC OF THE EUROPEAN PARLIAMENT AND OF THE COUNCIL of 23 October 2001 on the limitation of emissions of certain pollutants into the air from large combustion plants*. 2001.
45. DECC, *Special feature - Large Combustion Plant Directive: Running hours udring winter 2011/12 for plants opted-out of the Large Combustion Plant Directive (LCPD)*, DECC, Editor. 2012: London.
46. National Grid, *Large Combustion Plant Directive*. 2007.
47. DECC. *Policy: Maintaining UK energy security*. 2012; Available from: https://www.gov.uk/government/policies/maintaining-uk-energy-security--2/supporting-pages/electricity-market-reform.
48. Parliment of United Kingdom, *Energy Act 2013, Chaoter 32*, DECC, Editor. 2013: London.
49. DECC, *Implementing Electricity Market Reform (EMR)*, DECC, Editor. 2014: London.
50. DECC, *Special Feature - Renewable Energy in 2014*. 2015.
51. McKendry, P., *Energy production from biomass (part 1): overview of biomass.* Bioresource Technology, 2002. **83**(1): p. 37-46.
52. Bain, R.L., R.P. Overend, and K.R. Craig, *Biomass-fired power generation.* Fuel Processing Technology, 1998. **54**(1–3): p. 1-16.

53. Thornley, P., *Increasing biomass based power generation in the UK.* Energy Policy, 2006. **34**(15): p. 2087-2099.
54. IEA. *About Bioenergy* 2015; Available from: https://www.iea.org/topics/renewables/subtopics/bioenergy/.
55. Heinimo, J. and M. Junginger, *Production and trading of biomass for energy - An overview of the global status.* Biomass & Bioenergy, 2009. **33**(9): p. 1310-1320.
56. Bridgwater, A.V., *Renewable fuels and chemicals by thermal processing of biomass.* Chemical Engineering Journal, 2003. **91**(2–3): p. 87-102.
57. DECC, *UK Bioenergy Strategy*. 2012.
58. Basu, P., *Biomass Gasification, Pyrolysis and Torrefaction: Practical Design and Theory.* . Second Edition ed. 2013: Elsevier.
59. Tuck, G., et al., *The potential distribution of bioenergy crops in Europe under present and future climate.* Biomass and Bioenergy, 2006. **30**(3): p. 183-197.
60. Morris, J.R., *CourseSmart International E-book for Biology: How Life Works*. 2013, Palgrave Macmillan.
61. Hon, D., and Shiraishi, N., , *Wood and Cellulosic Chemistry: second edition, revised and expanded*. 2001: Marcel Dekker
62. Tumuluru, J.S., Sokhansanj, S., Hess, J.R., Wright, C., and Boardman, R.D., , *A Reviw on biomass torrefaction process and product properties for energy applications.* Industrial Biotechnology, 2011.
63. Novaes, E., et al., *Lignin and Biomass: A Negative Correlation for Wood Formation and Lignin Content in Trees.* Plant Physiology, 2010. **154**(2): p. 555-561.
64. Scheller, H.V. and P. Ulvskov, *Hemicelluloses.* Annual Review of Plant Biology, Vol 61, 2010. **61**: p. 263-289.
65. Sjostrom, E., *Wood Chemistry: Fundamentals and Applications*. Second Edition ed. 1993, San Diego: Acadmic Press
66. Van Loo, S. and J. Koppejan, *The Handbook of Biomass Combustion & Co-firing*. 2008, London: Earthscan.
67. DECC, *Digest of United Kingdom Energy Statistics 2015*. 2015: London.
68. Oxera, *What is the impact of changes to the co-firing cap?* 2009.
69. DECC, *Government response to the consultation on propoals for the levels of banded support undere the Renewables Obligation for the period 2013-17 and the Renewable Obligation Order 2012*. 2012: London.
70. DECC, *Fact Sheet: Grandfathering and cost-control for biomass co-firing and conversions*.
71. DECC, *Digest of United Kingdom Energy Statistics 2013*. 2014: London.
72. DECC, *Digest of United Kingdom Energy Statistics 2007*. 2008: London.
73. DECC, *Digest of United Kingdom Energy Statistics 2008*. 2009: London.
74. Drax, *Regulatory Briefing - Capital Markets Day*. 2013.
75. Ofgem, *Renewables Obligation: Annual Report 2013-2014*. 2015.
76. DECC, *Life-Cycle Impacts of Biomass Electricity in 2020 - Scenarios for Assessing the Greenhouse Gas Impacts and Energy Input Requirements of Using North American Woody Biomass for Electricity Generation in the UK*. 2014: London.
77. Jenkins, B.M., L.L. Baxter, and T.R. Miles, *Combustion properties of biomass.* Fuel Processing Technology, 1998. **54**(1-3): p. 17-46.
78. Kaupp, A., *Small Scale Gas Producer-Engine Systems* 1984: Vieweg.
79. Quaak, P., Knoef, H., and Stassen, H.E., , *Energy from Biomass: A review of Combustion and Gasification Technologies* 1999: World Bank Publications.
80. Jones, J.M., Lea-Langton A. R., Ma, L., Pourkashanian, M., Williams, A.,, *Pollutants Generated by the Combustion of Solid Biomass Fuels*. 2014, London: Springer-Verlag.

81. Jones, J.M., et al., *Low temperature ignition of biomass.* Fuel Processing Technology, 2015. **134**: p. 372-377.
82. Wihersaari, M., *Evaluation of greenhouse gas emission risks from storage of wood residue.* Biomass & Bioenergy, 2005. **28**(5): p. 444-453.
83. Bridgeman, T.G., et al., *An investigation of the grindability of two torrefied energy crops.* Fuel, 2010. **89**(12): p. 3911-3918.
84. Kumar, P., et al., *Methods for Pretreatment of Lignocellulosic Biomass for Efficient Hydrolysis and Biofuel Production.* Industrial & Engineering Chemistry Research, 2009. **48**(8): p. 3713-3729.
85. Harmsen, P.F.H., Huijgen, W.J.J., Bermudez Lopez, L.M., and Bakker, R.R.C., , *Literature Review of Physical and Chemical Pretreatment Processes for Lignocellulosic Biomass* 2010, ECN.
86. Stelte, W., *Steam explosion for biomass pre-treatment*, Danish Technological Institute.
87. Yang, H.P., et al., *Characteristics of hemicellulose, cellulose and lignin pyrolysis.* Fuel, 2007. **86**(12-13): p. 1781-1788.
88. Bergman, P.C.A., Boersma, A.R., Kiel, J.H.A., Prins, M.J., Ptasinski, K.J., Jansse, F.J.J.G., , *Torrefaction for entrained-flow gasification of biomass*. 2005
89. Prins, M.J., K.J. Ptasinski, and F. Janssen, *More efficient biomass gasification via torrefaction.* Energy, 2006. **31**(15): p. 3458-3470.
90. Bergman, P.C.A., et al., *Torrefaction for biomass co-firing in existing coal-power stations*. 2005, ECN Biomass. p. 1-71.
91. Park, J., et al., *Transformation of lignocellulosic biomass during torrefaction.* Journal of Analytical and Applied Pyrolysis, 2013. **100**: p. 199-206.
92. Chen, W.H. and P.C. Kuo, *Torrefaction and co-torrefaction characterization of hemicellulose, cellulose and lignin as well as torrefaction of some basic constituents in biomass.* Energy, 2011. **36**(2): p. 803-811.
93. Shen, D.K., S. Gu, and A.V. Bridgwater, *Study on the pyrolytic behaviour of xylan-based hemicellulose using TG–FTIR and Py–GC–FTIR.* Journal of Analytical and Applied Pyrolysis, 2010. **87**(2): p. 199-206.
94. Werner, K., L. Pommer, and M. Brostrom, *Thermal decomposition of hemicelluloses.* Journal of Analytical and Applied Pyrolysis, 2014. **110**: p. 130-137.
95. Ramiah, M.V., *THERMOGRAVIMETRIC AND DIFFERENTIAL THERMAL ANALYSIS OF CELLULOSE, HEMICELLULOSE, AND LIGNIN.* Journal of Applied Polymer Science, 1970. **14**(5): p. 1323-&.
96. Demirbaş, A., *Mechanisms of liquefaction and pyrolysis reactions of biomass.* Energy Conversion and Management, 2000. **41**(6): p. 633-646.
97. Shen, D.K. and S. Gu, *The mechanism for thermal decomposition of cellulose and its main products.* Bioresource Technology, 2009. **100**(24): p. 6496-6504.
98. Mohan, D., C.U. Pittman, and P.H. Steele, *Pyrolysis of wood/biomass for bio-oil: A critical review.* Energy & Fuels, 2006. **20**(3): p. 848-889.
99. Di Blasi, C. and M. Lanzetta, *Intrinsic kinetics of isothermal xylan degradation in inert atmosphere.* Journal of Analytical and Applied Pyrolysis, 1997. **40–41**: p. 287-303.
100. Shafizadeh, F., *Introduction to pyrolysis of biomass.* Journal of Analytical and Applied Pyrolysis, 1982. **3**(4): p. 283-305.
101. Prins, M.J., K.J. Ptasinski, and F. Janssen, *Torrefaction of wood - Part 1. Weight loss kinetics.* Journal of Analytical and Applied Pyrolysis, 2006. **77**(1): p. 28-34.
102. Melkior, T., et al., *NMR analysis of the transformation of wood constituents by torrefaction.* Fuel, 2012. **92**(1): p. 271-280.
103. Bergman, P., et al., *Torrefaction for biomass co-firing in existing coal-fired power stations: BIOCOAL. ECN report.* Renewable energy in the Netherlands. ECN-C-05-013, 2005.

104. Prins, M.J., K.J. Ptasinski, and F. Janssen, *Torrefaction of wood - Part 2. Analysis of products.* Journal of Analytical and Applied Pyrolysis, 2006. **77**(1): p. 35-40.
105. Bridgeman, T.G., et al., *Torrefaction of reed canary grass, wheat straw and willow to enhance solid fuel qualities and combustion properties.* Fuel, 2008. **87**(6): p. 844-856.
106. Nocquet, T., et al., *Volatile species release during torrefaction of wood and its macromolecular constituents: Part 1 – Experimental study.* Energy, 2014. **72**: p. 180-187.
107. Ibrahim, R.H.H., et al., *Physicochemical characterisation of torrefied biomass.* Journal of Analytical and Applied Pyrolysis, 2013. **103**: p. 21-30.
108. Chen, W.H., et al., *Thermal pretreatment of wood (Lauan) block by torrefaction and its influence on the properties of the biomass.* Energy, 2011. **36**(5): p. 3012-3021.
109. Nachenius, R.W., et al., *Torrefaction of pine in a bench-scale screw conveyor reactor.* Biomass and Bioenergy, 2015. **79**: p. 96-104.
110. van der Stelt, M.J.C., et al., *Biomass upgrading by torrefaction for the production of biofuels: A review.* Biomass & Bioenergy, 2011. **35**(9): p. 3748-3762.
111. Medic, D., et al., *Effects of torrefaction process parameters on biomass feedstock upgrading.* Fuel, 2012. **91**(1): p. 147-154.
112. Arias, B., et al., *Influence of torrefaction on the grindability and reactivity of woody biomass.* Fuel Processing Technology, 2008. **89**(2): p. 169-175.
113. Peng, J.H., et al., *Torrefaction and densification of different species of softwood residues.* Fuel, 2013. **111**(0): p. 411-421.
114. Wannapeera, J., B. Fungtammasan, and N. Worasuwannarak, *Effects of temperature and holding time during torrefaction on the pyrolysis behaviors of woody biomass.* Journal of Analytical and Applied Pyrolysis, 2011. **92**(1): p. 99-105.
115. Meetani, M.A., F. Basile, and K.J. Voorhees, *Investigation of pyrolysis residues of poly(amino acids) using matrix assisted laser desorption ionization-time of flight-mass spectrometry.* Journal of Analytical and Applied Pyrolysis, 2003. **68–69**: p. 101-113.
116. Galbiati, M., et al., *Mild combustion for fuel-NOx reduction.* Combustion Science and Technology, 2004. **176**(7): p. 1035-1054.
117. Jones, J.M., et al., *Combustion properties of torrefied willow compared with bituminous coals.* Fuel Processing Technology, 2012. **101**: p. 1-9.
118. Chen, W.-H., et al., *Non-oxidative and oxidative torrefaction characterization and SEM observations of fibrous and ligneous biomass.* Applied Energy, 2014. **114**: p. 104-113.
119. Phanphanich, M. and S. Mani, *Impact of torrefaction on the grindability and fuel characteristics of forest biomass.* Bioresource Technology, 2011. **102**(2): p. 1246-1253.
120. Repellin, V., et al., *Energy requirement for fine grinding of torrefied wood.* Biomass & Bioenergy, 2010. **34**(7): p. 923-930.
121. Jones, J.M., Waldron, D., and Bridgeman, T, *Applying Coal Milling Technologies to Thermally Treated Biomass: Proof of Concept*. 2009.
122. Williams, A., et al., *Pollutants from the combustion of solid biomass fuels.* Progress in Energy and Combustion Science, 2012. **38**(2): p. 113-137.
123. Di Blasi, C., *Combustion and gasification rates of lignocellulosic chars.* Progress in Energy and Combustion Science, 2009. **35**(2): p. 121-140.
124. Saddawi, A., et al., *Kinetics of the Thermal Decomposition of Biomass.* Energy & Fuels, 2010. **24**: p. 1274-1282.
125. Hayhurst, A.N., *The kinetics of the pyrolysis or devolatilisation of sewage sludge and other solid fuels.* Combustion and Flame, 2013. **160**(1): p. 138-144.
126. Atkins, P. and J. de Paula, *Elements of Physical Chemistry*. 5th Edition ed. 2009, London: Oxford.
127. Safi, M.J., I.M. Mishra, and B. Prasad, *Global degradation kinetics of pine needles in air.* Thermochimica Acta, 2004. **412**(1–2): p. 155-162.

128. Agrawal, R.K. and M.S. Sivasubramanian, *INTEGRAL APPROXIMATIONS FOR NONISOTHERMAL KINETICS.* Aiche Journal, 1987. **33**(7): p. 1212-1214.
129. Saddawi, A., et al., *Commodity Fuels from Biomass through Pretreatment and Torrefaction: Effects of Mineral Content on Torrefied Fuel Characteristics and Quality.* Energy & Fuels, 2012. **26**(11): p. 6466-6474.
130. Marsh, H., *Introduction to Carbon Science*. 1989: Butterworths.
131. Janse, A.M.C., et al., *Combustion kinetics of char obtained by flash pyrolysis of pine wood.* Industrial & Engineering Chemistry Research, 1998. **37**(10): p. 3909-3918.
132. Smith, I.W., *INTRINSIC REACTIVITY OF CARBONS TO OXYGEN.* Fuel, 1978. **57**(7): p. 409-414.
133. Guerrero, M., et al., *Characterization of biomass chars formed under different devolatilization conditions: Differences between rice husk and eucalyptus.* Energy & Fuels, 2008. **22**(2): p. 1275-1284.
134. Guerrero, A., et al., *Pyrolysis of eucalyptus at different heating rates: studies of char characterization and oxidative reactivity.* Journal of Analytical and Applied Pyrolysis, 2005. **74**(1-2): p. 307-314.
135. Biagini, E., M. Simone, and L. Tognotti, *Characterization of high heating rate chars of biomass fuels.* Proceedings of the Combustion Institute, 2009. **32**: p. 2043-2050.
136. Cetin, E., et al., *Influence of pyrolysis conditions on the structure and gasification reactivity of biomass chars.* Fuel, 2004. **83**(16): p. 2139-2150.
137. Borrego, A.G., L. Garavaglia, and W.D. Kalkreuth, *Characteristics of high heating rate biomass chars prepared under N2 and CO2 atmospheres.* International Journal of Coal Geology, 2009. **77**(3–4): p. 409-415.
138. Pottmaier, D., et al., *Comparison of Rice Husk and Wheat Straw: From Slow and Fast Pyrolysis to Char Combustion.* Energy & Fuels, 2013. **27**(11): p. 7115-7125.
139. Brunauer, S., P.H. Emmett, and E. Teller, *Adsorption of gases in multimolecular layers.* Journal of the American Chemical Society, 1938. **60**: p. 309-319.
140. Yuan, S.A., et al., *CO2 Gasification Kinetics of Biomass Char Derived from High-Temperature Rapid Pyrolysis.* Energy & Fuels, 2011. **25**(5): p. 2314-2321.
141. Lowell, S., Shields, J.E., Thomas, M.A., and Thommes, M., , *Characterisation of Porous Solids: Surface Area, Pore Size and Density*. 2004: Kluwer Academic Publishers.
142. Marsh, H. and W.F.K. Wynnejones, *THE SURFACE PROPERTIES OF CARBON .1. THE EFFECT OF ACTIVATED DIFFUSION IN THE DETERMINATION OF SURFACE AREA.* Carbon, 1964. **1**(3): p. 269-279.
143. Aarna, I. and E.M. Suuberg, *Changes in reactive surface area and porosity during char oxidation.* Symposium (International) on Combustion, 1998. **27**(2): p. 2933-2939.
144. Rocca, P.A.D., et al., *Pyrolysis of hardwoods residues: on kinetics and chars characterization.* Biomass and Bioenergy, 1999. **16**(1): p. 79-88.
145. Li, J., et al., *High-temperature rapid devolatilization of biomasses with varying degrees of torrefaction.* Fuel, 2014. **122**: p. 261-269.
146. Jones, J.M., et al., *An investigation of the thermal and catalytic behaviour of potassium in biomass combustion.* Proceedings of the Combustion Institute, 2007. **31**: p. 1955-1963.
147. Fahmi, R., et al., *The effect of alkali metals on combustion and pyrolysis of Lolium and Festuca grasses, switchgrass and willow.* Fuel, 2007. **86**(10–11): p. 1560-1569.
148. Olsson, J.G., et al., *Alkali metal emission during pyrolysis of biomass.* Energy & Fuels, 1997. **11**(4): p. 779-784.
149. Westberg, H.M., M. Bystrom, and B. Leckner, *Distribution of potassium, chlorine, and sulfur between solid and vapor phases during combustion of wood chips and coal.* Energy & Fuels, 2003. **17**(1): p. 18-28.

150. Adanez, J., et al., *Determination of biomass char combustion reactivities for FBC applications by a combined method.* Industrial & Engineering Chemistry Research, 2001. **40**(20): p. 4317-4323.
151. Mason, P.E., et al., *Single particle flame-combustion studies on solid biomass fuels.* Fuel, 2015. **151**: p. 21-30.
152. European Environment Agency, *Nitrogen oxides (NOx) emissions*. 2010: Copenhagen.
153. Di Nola, G., *Biomass fuel characterisation for NOx emissions in Co-firing applications*, in *Department of Mechanical Engineering*. 2007, University of Naples Naples.
154. Glarborg, P., A.D. Jensen, and J.E. Johnsson, *Fuel nitrogen conversion in solid fuel fired systems.* Progress in Energy and Combustion Science, 2003. **29**(2): p. 89-113.
155. Ndibe, C., J. Maier, and G. Scheffknecht, *Combustion, cofiring and emissions characteristics of torrefied biomass in a drop tube reactor.* Biomass and Bioenergy, 2015. **79**: p. 105-115.
156. C.E.N Standard, *BS EN 14774-3:2009 - Solid biofuels – determination of the moisture content* 2009.
157. C.E.N Standard, *BS EN 14775:2009 - Solid biofuels – determination of ash content*. 2009.
158. C.E.N Standard, *BS EN 15148:2009 - Solid biofuels – determination of the content of volatile matter*. 2009.
159. C.E.N Standard, *BS EN 15104: 2011 - Solid biofuels – Determination of total content of carbon, hydrogen and nitrogen – instrumental methods*. 2011.
160. Friedl, A., et al., *Prediction of heating values of biomass fuel from elemental composition.* Analytica Chimica Acta, 2005. **544**(1-2): p. 191-198.
161. C.E.N Standard, *BS EN 14918: 2009 - Solid biofuels – Determination of calorific value*. 2009.
162. British Standard, *BS ISO 5074:2015 - Methods for analysis and testing of coal and coke. Determination of Hardgrove grindability index of hard coal*. 2015.
163. Sing, K., *The use of nitrogen adsorption for the characterisation of porous materials.* Colloids and Surfaces a-Physicochemical and Engineering Aspects, 2001. **187**: p. 3-9.
164. Russ, J.C., *Chapter 1 - X-Ray Emission*, in *Fundamentals of Energy Dispersive X-ray Analysis*, J.C. Russ, Editor. 1984, Butterworth-Heinemann. p. 1-9.
165. Central Facility for Advanced Microscopy and Microanalysis, U.o.C., *Introduction to Energy Dispersive X-ray Spectrometry (EDS)* 2015.
166. Vansoest, P.J., J.B. Robertson, and B.A. Lewis, *METHODS FOR DIETARY FIBER, NEUTRAL DETERGENT FIBER, AND NONSTARCH POLYSACCHARIDES IN RELATION TO ANIMAL NUTRITION.* Journal of Dairy Science, 1991. **74**(10): p. 3583-3597.
167. Allison, G.G., et al., *Effect of nitrogen fertiliser application on cell wall composition in switchgrass and reed canary grass.* Biomass and Bioenergy, 2012. **40**: p. 19-26.
168. Jung, H.J.G., et al., *Accuracy of Klason lignin and acid detergent lignin methods as assessed by bomb calorimetry.* Journal of Agricultural and Food Chemistry, 1999. **47**(5): p. 2005-2008.
169. Hatfield, R. and R.S. Fukushima, *Can lignin be accurately measured?* Crop Science, 2005. **45**(3): p. 832-839.
170. Couhert, C., S. Salvador, and J.M. Commandre, *Impact of torrefaction on syngas production from wood.* Fuel, 2009. **88**(11): p. 2286-2290.
171. Pach, M., Zansi R., amd Bjornbom E, *Torrefied biomass as a substitute for wood* in *6th Asia Pacific International Symposium on Combustion and Energy utilisation*. 2002: Kuala Lumpur.
172. Chang, S., et al., *Characterization of Products from Torrefaction of Sprucewood and Bagasse in an Auger Reactor.* Energy & Fuels, 2012. **26**(11): p. 7009-7017.

173. Zheng, A.Q., et al., *Effect of Torrefaction Temperature on Product Distribution from Two-Staged Pyrolysis of Biomass.* Energy & Fuels, 2012. **26**(5): p. 2968-2974.
174. Di Nola, G., W. de Jong, and H. Spliethoff, *TG-FTIR characterization of coal and biomass single fuels and blends under slow heating rate conditions: Partitioning of the fuel-bound nitrogen.* Fuel Processing Technology, 2010. **91**(1): p. 103-115.
175. Ren, Q.Q. and C.S. Zhao, *Evolution of fuel-N in gas phase during biomass pyrolysis.* Renewable & Sustainable Energy Reviews, 2015. **50**: p. 408-418.
176. Hansson, K.-M., et al., *Formation of HNCO, HCN, and NH3 from the pyrolysis of bark and nitrogen-containing model compounds.* Combustion and Flame, 2004. **137**(3): p. 265-277.
177. Leppälahti, J., *Formation of NH3 and HCN in slow-heating-rate inert pyrolysis of peat, coal and bark.* Fuel, 1995. **74**(9): p. 1363-1368.
178. Ren, Q., et al., *NOx and N2O precursors (NH3 and HCN) from biomass pyrolysis: Co-pyrolysis of amino acids and cellulose, hemicellulose and lignin.* Proceedings of the Combustion Institute, 2011. **33**(2): p. 1715-1722.
179. Thy, P., et al., *Compositional constraints on slag formation and potassium volatilization from rice straw blended wood fuel.* Fuel Processing Technology, 2006. **87**(5): p. 383-408.
180. Tolvanen, H., L. Kokko, and R. Raiko, *Fast pyrolysis of coal, peat, and torrefied wood: Mass loss study with a drop-tube reactor, particle geometry analysis, and kinetics modeling.* Fuel, 2013. **111**: p. 148-156.
181. Fisher, E.M., et al., *Combustion and gasification characteristics of chars from raw and torrefied biomass.* Bioresource Technology, 2012. **119**: p. 157-165.
182. Xue, G., et al., *Impact of torrefaction on properties of Miscanthus x giganteus relevant to gasification.* Fuel, 2014. **121**: p. 189-197.
183. Cetin, E., R. Gupta, and B. Moghtaderi, *Effect of pyrolysis pressure and heating rate on radiata pine char structure and apparent gasification reactivity.* Fuel, 2005. **84**(10): p. 1328-1334.
184. Paethanom, A. and K. Yoshikawa, *Influence of Pyrolysis Temperature on Rice Husk Char Characteristics and Its Tar Adsorption Capability.* Energies, 2012. **5**(12): p. 4941-4951.
185. Shoulaifar, T.K., et al., *Ash-Forming Matter in Torrefied Birch Wood: Changes in Chemical Association.* Energy & Fuels, 2013. **27**(10): p. 5684-5690.
186. Darvell, L.I., et al., *Combustion properties of some power station biomass fuels.* Fuel, 2010. **89**(10): p. 2881-2890.
187. Mura, E., et al., *Pyrolysis of biomass in a semi-industrial scale reactor: Study of the fuel-nitrogen oxidation during combustion of volatiles.* Biomass and Bioenergy, 2013. **59**: p. 187-194.
188. Samuelsson, J., *Conversion of Nitrogen in a Fixed Burning Biofuel Bed*, in *Department of Energy and Environment* 2006, CHALMERS UNIVERSITY OF TECHNOLOGY: Gotehnburg.
189. Demirbas, A., *Relationships between lignin contents and fixed carbon contents of biomass samples.* Energy Conversion and Management, 2003. **44**(9): p. 1481-1486.
190. Brostrom, M., et al., *Influence of torrefaction on the devolatilization and oxidation kinetics of wood.* Journal of Analytical and Applied Pyrolysis, 2012. **96**: p. 100-109.
191. Ren, S.J., et al., *Thermal behaviour and kinetic study for woody biomass torrefaction and torrefied biomass pyrolysis by TGA.* Biosystems Engineering, 2013. **116**(4): p. 420-426.
192. Nowakowski, D.J., et al., *Potassium catalysis in the pyrolysis behaviour of short rotation willow coppice.* Fuel, 2007. **86**(15): p. 2389-2402.
193. Jones, J.M., et al., *Conversion of char nitrogen to NO during combustion.* Journal of the Energy Institute, 2004. **77**(513): p. 82-89.

194. Smith, I.W., *The Combustion Rates of Coal Chars: A Review.* Nineteenth Symposium (International) on Combustion/The Combustion Institute, 1982: p. 1045-1065.
195. DECC, *Government Response to the consultation on proposals to enhance the sustainability criteria for the use of biomass feedstocks under the Renewables Obligation (RO).* 2013.
196. DECC, *Proposals to enhance the sustainability criteria for the use of solid and gaseous biomass feedstocks under the Renewables Obligation (RO)* 2013.
197. DECC, *Sustainability standards for electricity generation from biomass.* 2013.
198. International Standards Organisation (ISO), *Environmental management – life cycle assessment – principles and framework, Second Edition, EN ISO 14040*. 2006: Geneva.
199. International Standards Organisation (ISO), *Environmental management – life cycle assessment – requirements and guidelines, Second Edition, EN ISO 14044*. 2006: Geneva.
200. European comission, *REPORT FROM THE COMMISSION TO THE COUNCIL AND THE EUROPEAN PARLIAMENT on sustainability requirements for the use of solid and gaseous biomass sources in electricity, heating and cooling*. 2010: Brussels.
201. Ofgem. *The UK Solid and Gaseous Biomass Carbon Calculator*. 2012; Available from: https://www.ofgem.gov.uk/publications-and-updates/uk-solid-and-gaseous-biomass-carbon-calculator.
202. NNFCC, *RO Sustainability Standards*. 2013.
203. IEA, *Global Wood Pellet Industry Market and Trade Study* 2011.
204. Lamers, P., et al., *Developments in international solid biofuel trade-An analysis of volumes, policies, and market factors.* Renewable & Sustainable Energy Reviews, 2012. **16**(5): p. 3176-3199.
205. Jarvinen, T. and D. Agar, *Experimentally determined storage and handling properties of fuel pellets made from torrefied whole-tree pine chips, logging residues and beech stem wood.* Fuel, 2014. **129**: p. 330-339.
206. Schorr C., M., M., and Nurminen, F., , *Torrefaction of Biomass*. 2012, Miktech.
207. Agar, D., et al., *Torrefied versus conventional pellet production – A comparative study on energy and emission balance based on pilot-plant data and EU sustainability criteria.* Applied Energy, 2015. **138**: p. 621-630.
208. IEA Bioenergy, *Status Overview of torrefaction technologies: A review of the commercialisation status of biomass torrefaction* 2015.
209. Hall, W.J., *Assessment of carbon dioxide emissions reductions achievable by using torrefaction.* Journal of the Energy Institute, 2012. **85**(2): p. 103-113.
210. Advanced Fuel Research, *User's guide to the FG-Biomass pyrolysis model - Version 10.0.15 for Windows*. 2013.
211. Gupta, M., J. Yang, and C. Roy, *Specific heat and thermal conductivity of softwood bark and softwood char particles ☆.* Fuel, 2003. **82**(8): p. 919-927.
212. Enviva. *Enviva Pellets Amory, Enviva LP, Bethesda, USA*. 2015; Available from: http://www.envivabiomass.com/manufacturing-operations/amory/.
213. Biomass Magazine. *Pellet Plants - USA*. 2015; Available from: http://biomassmagazine.com/plants/listplants/pellet/US
214. Biomass Magazine, *Biomass Plants - Canada* 2015.
215. Forest Research, *Understanding the carbon and greenhouse gas balance of forests in Britain*. 2012: Edinburgh.
216. Ofgem, *Renewables Obligation: Sustainability Criteria Guidance. Office for Gas and Electricity Markets* 2014.
217. Adams, P.W.R., Bows, A., Gilbert, P., Howard, D., Lee, R., McNamara, N., Thornley, P., Whittaker, C., and Whitaker, J., *Understanding Greehnhouse Gas Balances of Bioenergy Syetems*. 2013 Supergen Bioenergy Hub

218. Forestry Commission, *C-Sort Model.* . 2012, Forestry Commission Edinburgh.
219. Hamelinck, C.N., R.A.A. Suurs, and A.P.C. Faaij, *International bioenergy transport costs and energy balance.* Biomass & Bioenergy, 2005. **29**(2): p. 114-134.
220. European Comission, *Well-to-Wheels Analysis of Future Automotive and Powertrains in the European Context* Luxembourg.
221. Centre, B.E. *Typical Calorific Value of fuels*. 2015; Available from: http://www.biomassenergycentre.org.uk/portal/page?_pageid=75,20041&_dad=portal&_schema=PORTAL.
222. Biograce II. *Harmonised Greenhouse Gas Calculations for Electricity, Heating and Cooling for Biomass*. 2015; Available from: http://www.biograce.net/app/webroot/biograce2/
223. Koppejan, J., Sokhansank, S., Jess, J., Wright, C., Boardman, R., , *Status overview of torrefaction technologies*. 2012, Internation Energy Agency (IEA): Enschede.
224. Tumuluru, J.S., et al., *A review of biomass densification systems to develop uniform feedstock commodities for bioenergy application.* Biofuels Bioproducts & Biorefining-Biofpr, 2011. **5**(6): p. 683-707.
225. Stelte, W., et al., *Pelletizing properties of torrefied wheat straw.* Biomass & Bioenergy, 2013. **49**: p. 214-221.
226. DEFRA. *Government GHG Conversion Factors for Company Reporting. Department for Environment, Food & Rural Affairs (DEFRA), London*. 2015; Available from: http://www.ukconversionfactorscarbonsmart.co.uk/
227. BBC. *Hull's new biomass fuel plant for Drax power station* 2014; Available from: http://www.bbc.co.uk/news/uk-england-30309861.
228. IEA-ETSAP, I., *Biomass Co-firing: Technology Brief*. 2013.
229. Commission, F., *Understanding thecarbon and greenhouse gas balance of forests in Britain*. 2012: Edinburgh.
230. Edwards, R., Larive, J.F., and Beziat, J.C., , *Well-to-wheels Analysis of Future Automotive Fuels and Powertrains in the European Context*. 2011: Luxembourg.
231. Biomass Energy Centre. *Typical Calorific Value of Fuels, taken from http://www.biomassenergycentre.org.uk/portal/page?_pageid=75,20041&_dad=portal*. Available from: http://www.biomassenergycentre.org.uk/portal/page?_pageid=75,20041&_dad=portal.
232. Defra & Environmental Agency. *Biomass Environmental Assessment Tool (BEAT2), AEA & North Energy, Available from http://www.biomassenergycentre.org.uk/portal/page?_pageid=74,153193&_dad=portal&_schema=PORTAL*. 2008.
233. Adams, P.W.R., J.E.J. Shirley, and M.C. McManus, *Comparative cradle-to-gate life cycle assessment of wood pellet production with torrefaction.* Applied Energy, 2015. **138**: p. 367-380.
234. Ofgem, *Renewables Obligation: Sustainability Criteria*. 2014 Ofgem: London.
235. European Comission, *Sustainability requirements for the use of solid and gaseous biomass sources in electricity, heating and cooling*. 2010: Brussels
236. McKechnie, J., et al., *Forest Bioenergy or Forest Carbon? Assessing Trade-Offs in Greenhouse Gas Mitigation with Wood-Based Fuels.* Environmental Science & Technology, 2011. **45**(2): p. 789-795.
237. Ter-Mikaelian, M.T., et al., *Carbon debt repayment or carbon sequestration parity? Lessons from a forest bioenergy case study in Ontario, Canada.* Global Change Biology Bioenergy, 2015. **7**(4): p. 704-716.
238. Nave, L.E., et al., *Harvest impacts on soil carbon storage in temperate forests.* Forest Ecology and Management, 2010. **259**(5): p. 857-866.

239. Röder, M., C. Whittaker, and P. Thornley, *How certain are greenhouse gas reductions from bioenergy? Life cycle assessment and uncertainty analysis of wood pellet-to-electricity supply chains from forest residues.* Biomass and Bioenergy, 2015. **79**: p. 50-63.
240. Haberl, H., et al., *Correcting a fundamental error in greenhouse gas accounting related to bioenergy.* Energy Policy, 2012. **45**: p. 18-23.
241. Cherubini, F., et al., *Energy- and greenhouse gas-based LCA of biofuel and bioenergy systems: Key issues, ranges and recommendations.* Resources, Conservation and Recycling, 2009. **53**(8): p. 434-447.
242. Stelte, W., et al., *Pelletizing properties of torrefied spruce.* Biomass & Bioenergy, 2011. **35**(11): p. 4690-4698.
243. Li, H., et al., *Pelletization of torrefied sawdust and properties of torrefied pellets.* Applied Energy, 2012. **93**: p. 680-685.
244. Larsson, S.H., et al., *Effects of moisture content, torrefaction temperature, and die temperature in pilot scale pelletizing of torrefied Norway spruce.* Applied Energy, 2013. **102**: p. 827-832.
245. Bergman, P.C.A., *Combined torrefaction and pelletisation: The TOP process*. 2005, ECN: Petten.
246. Stelte, W., Sanadi, A. R., Shanf, L., Holm, J. K., Ahrenfeldt, J. and Henrikson, U. B., , *Recent Developments in Biomass Pelletization - A Review.* BioResources, 2012. **7**(3).
247. Batidzirai, B., et al., *Biomass torrefaction technology: Techno-economic status and future prospects.* Energy, 2013. **62**: p. 196-214.
248. Djomo, S.N., et al., *Impact of feedstock, land use change, and soil organic carbon on energy and greenhouse gas performance of biomass cogeneration technologies.* Applied Energy, 2015. **154**: p. 122-130.
249. Stephenson, A.L. and D.J.C. MacKay, *Life Cycle Impacts of Biomass Electricity in 2020: Scenarios for Assessing the Greenhous Gas Impacts and Energy Input Requirements of Using North American Woody Biomass for Electricity Generation in the UK*. 2004, Department of Energy & Climate Change London.
250. Harris, Z.M., Spake, R., and Taylor, G. , *Land use change to bioenergy: A meta-analysis of soil carbon and GHG emissions.* Biomass and Bioenergy, 2015.
251. He, X., et al., *Dry matter losses in combination with gaseous emissions during the storage of forest residues.* Fuel, 2012. **95**(1): p. 662-664.

APPENDIX A – Isothermal combustion and Arrhenius plots for untreated and torrefied chars

- Isothermal combustion runs for fast heating rate chars prepared in a DTF at 1100°C for untreated willow:

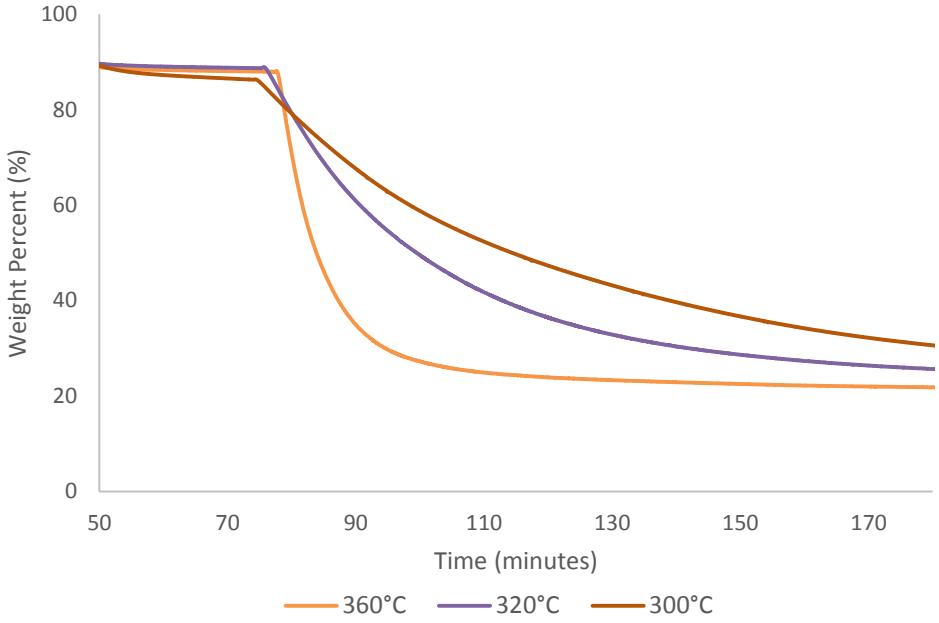

- Isothermal combustion runs for fast heating rate chars prepared in a DTF at 1100°C for willow torrefied at 270°C for 30 minutes:

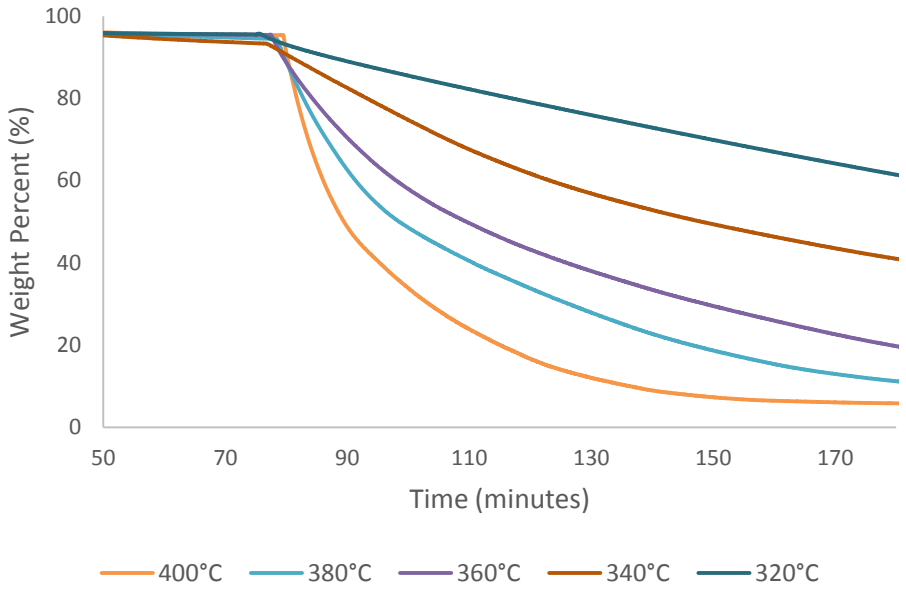

- Isothermal combustion runs for fast heating rate chars prepared in a DTF at 1100°C from willow torrefied at 290°C for 30 minutes:

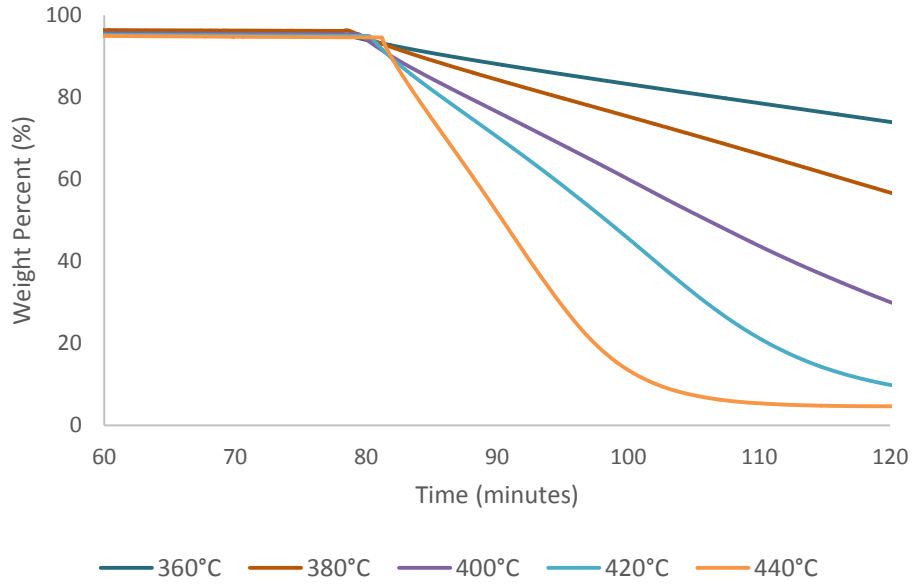

- Arrhenius plot for the chemical reactivities for oxidation of fast heating rates chars prepared from untreated and torrefied willow:

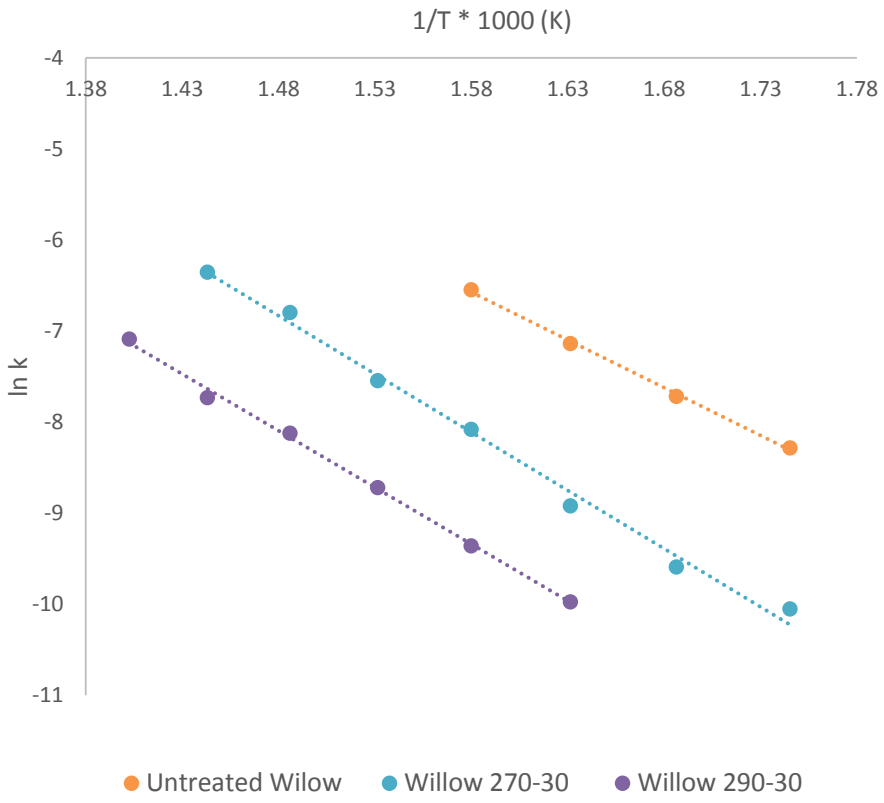

- Isothermal combustion runs for fast heating rate chars prepared in a DTF at 1100°C from untreated eucalyptus:

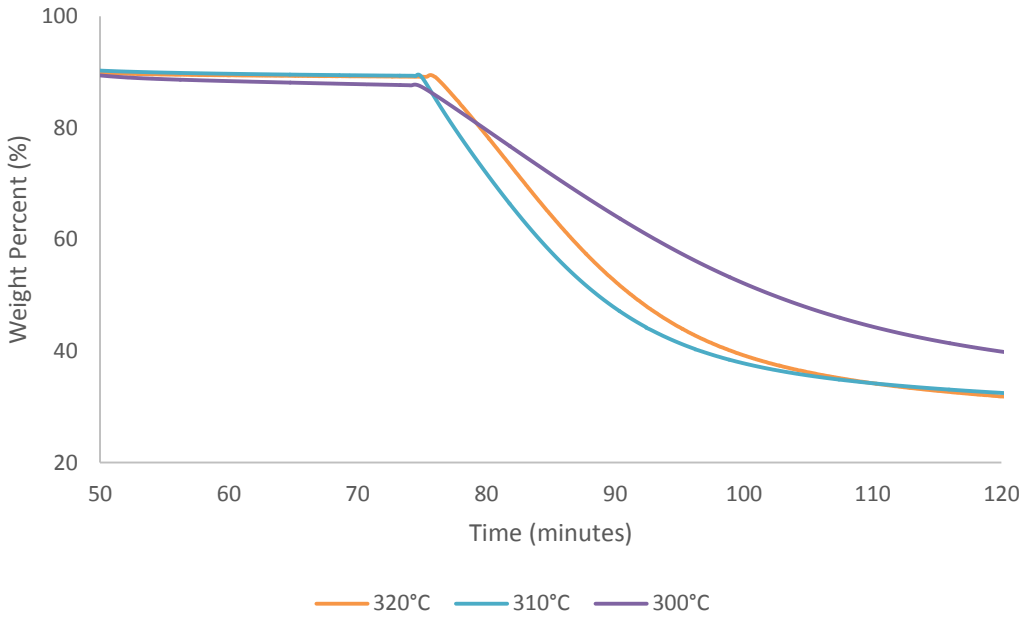

- Isothermal combustion runs for fast heating rate chars prepared in a DTF at 1100°C from eucalyptus torrefied at 270°C for 30 minutes:

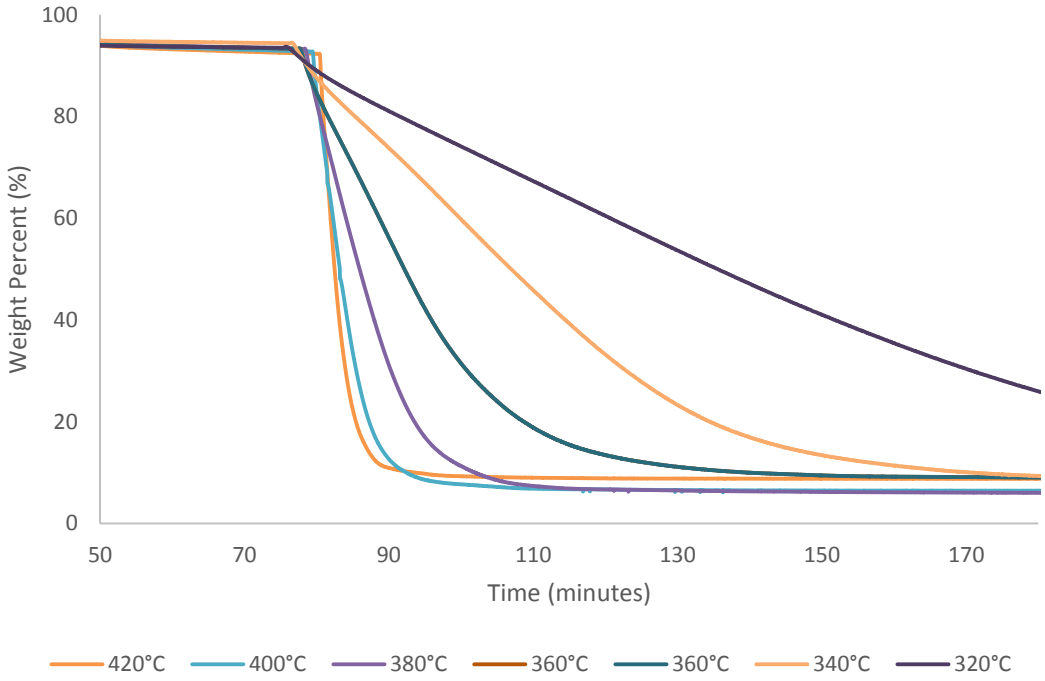

- Isothermal combustion runs for fast heating rate chars prepared in a DTF at 1100°C from eucalyptus torrefied at 290°C for 30 minutes:

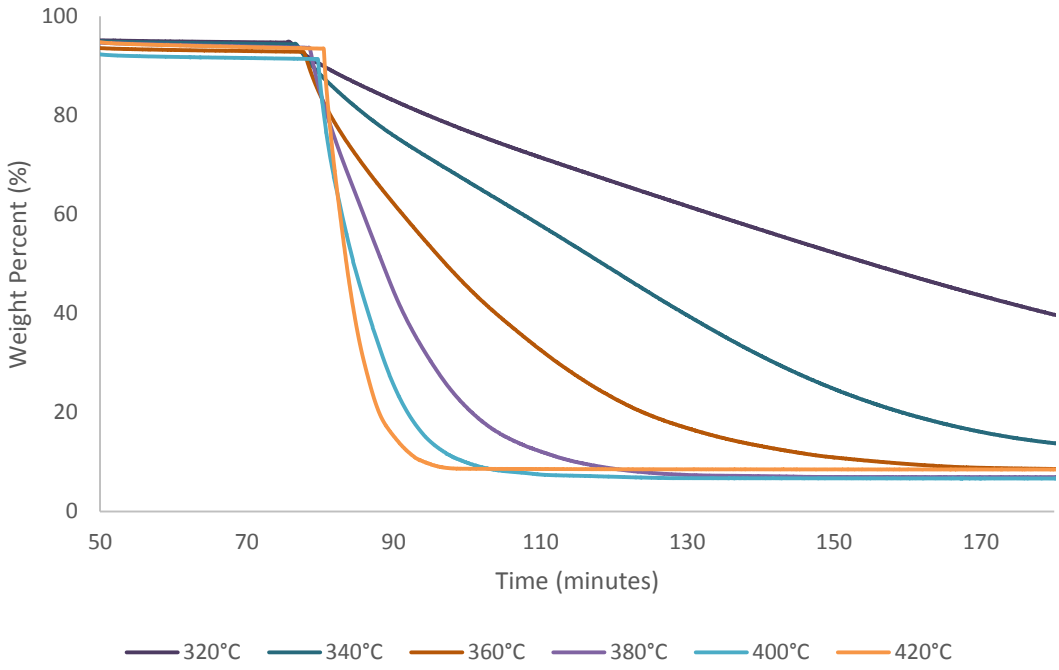

- Arrhenius plot for the chemical reactivities for oxidation of fast heating rates chars prepared from untreated and torrefied eucalyptus:

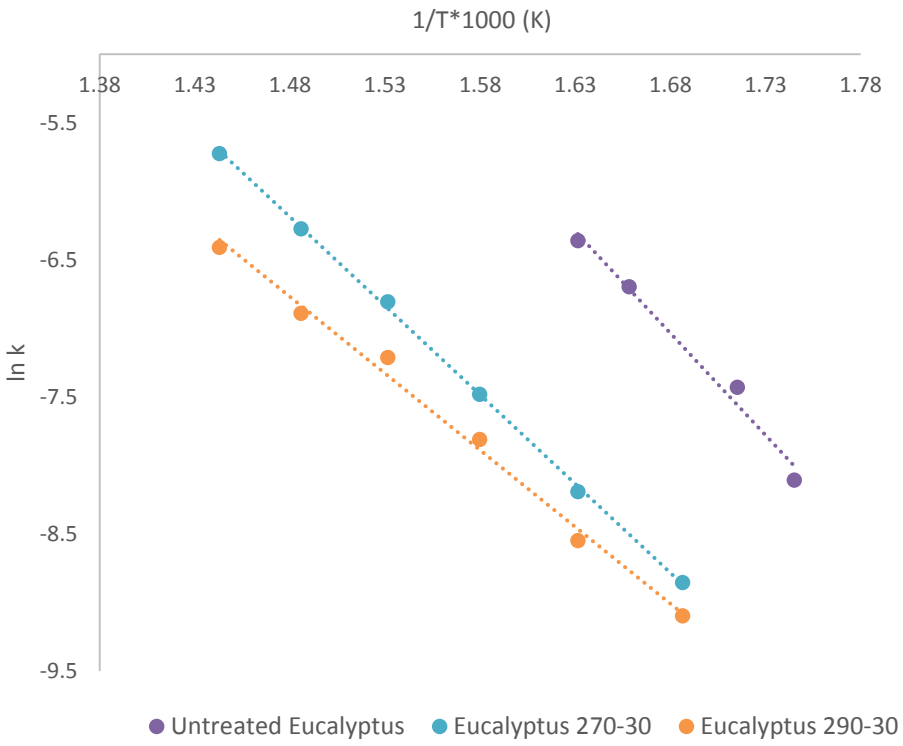

APPENDIX B – Mass and Energy Balances for the torrefaction scenarios in the GHG emissions assessment

- Mass Balance for North American Pine torrefied at 250°C for 30 minutes:

	Weight (%)	Fuel in to dryer (kg)
Moisture	35.00	579.50
C	32.18	532.74
H	4.22	69.95
N	0.08	1.41
S	0.03	0.58
O	28.24	467.60
Ash	0.24	3.94
Total	100.00	1655.72

	Weight (%)	Fuel exiting dryer (kg)
Moisture	10.00	119.58
C	44.55	532.74
H	5.85	69.95
N	0.12	1.41
S	0.05	0.58
O	39.10	467.60
Ash	0.33	3.94
Total	100.00	1195.80
Total Dry		1076.22

	Weight (%)	Fuel exiting torrefier (kg)
Moisture	2.43	24.30
C	50.39	503.88
H	6.20	61.96
N	0.00	0.00
S	0.00	0.00
O	40.54	405.36
Ash	0.45	4.50
Total	100.00	1000.00
Total Dry		975.70

Moisture exiting dryer (kg)
459.92

	Volatile stream (kg)
Moisture	95.28
C	28.86
H	7.99
N	1.41
S	0.58
O	62.25

- Mass Balance for North American Pine torrefied at 270°C for 30 minutes:

	Weight (%)	Fuel in to dryer (kg)
Moisture	35.00	622.07
C	32.18	571.87
H	4.22	75.09
N	0.08	1.51
S	0.03	0.62
O	28.24	501.95
Ash	0.24	4.23
Total	100.00	1777.34

	Weight (%)	Fuel exiting dryer (kg)
Moisture	10.00	128.36
C	44.55	571.87
H	5.85	75.09
N	0.12	1.51
S	0.05	0.62
O	39.10	501.95
Ash	0.33	4.23
Total	100.00	1283.63
Total Dry		1155.27

	Weight (%)	Fuel exiting torrefier (kg)
Moisture	1.86	18.60
C	51.41	514.09
H	5.90	59.00
N	0.00	0.00
S	0.00	0.00
O	40.48	404.81
Ash	0.35	3.50
Total	100.00	1000.00
Total Dry		981.40

Moisture exiting dryer (kg)
493.70

	Volatile stream (kg)
Moisture	109.76
C	57.78
H	16.09
N	1.51
S	0.62
O	97.14

- Mass Balance for North American Pine torrefied at 270°C for 60 minutes:

	Weight (%)	Fuel in to dryer (kg)
Moisture	35.00	694.01
C	32.18	638.01
H	4.22	83.77
N	0.08	1.68
S	0.03	0.69
O	28.24	560.00
Ash	0.24	4.72
Total	100.00	1982.89

	Weight (%)	Fuel exiting dryer (kg)
Moisture	10.00	143.21
C	44.55	638.01
H	5.85	83.77
N	0.12	1.68
S	0.05	0.69
O	39.10	560.00
Ash	0.33	4.72
Total	100.00	1432.09
Total Dry		1288.88

	Weight (%)	Fuel exiting torrefier (kg)
Moisture	1.13	11.30
C	53.25	532.54
H	5.87	58.73
N	0.10	0.97
S	0.00	0.00
O	39.18	391.76
Ash	0.47	4.70
Total	100.00	1000.00
Total Dry		988.70

Moisture exiting dryer (kg)
550.80

	Volatile stream (kg)
Moisture	131.91
C	105.47
H	25.05
N	0.71
S	0.69
O	168.24

Mass Balance for North American Pine torrefied at 290°C for 30 minutes:

	Weight (%)	Fuel in to dryer (kg)
Moisture	35.00	730.22
C	32.18	671.30
H	4.22	88.14
N	0.08	1.77
S	0.03	0.73
O	28.24	589.22
Ash	0.24	4.96
Total	100.00	2086.35

	Weight (%)	Fuel exiting dryer (kg)
Moisture	10.00	150.68
C	44.55	671.30
H	5.85	88.14
N	0.12	1.77
S	0.05	0.73
O	39.10	589.22
Ash	0.33	4.96
Total	100.00	1506.81
Total Dry		1356.12

	Weight (%)	Fuel exiting torrefier (kg)
Moisture	2.02	20.20
C	53.54	535.40
H	5.67	56.67
N	0.09	0.86
S	0.00	0.00
O	38.14	381.37
Ash	0.55	5.50
Total	100.00	1000.00
Total Dry		979.80

Moisture exiting dryer (kg)
579.54

	Volatile stream (kg)
Moisture	130.48
C	135.89
H	31.47
N	0.92
S	0.73
O	207.85

Energy Balances for the torrefaction scenarios used in GHG emissions assessment:

250-30

Untreated pine LHV (kJ/kg)	11425.1
Mass flow in to dryer (kg)	1655.72
Energy in to drier (kJ)	18916781.33

Torrefied pine (250-30) LHV	18525.9
Mass flow out of torrefier (kg)	1000.00
Energy out of torrefier (kJ)	18525900

Energy in volatile stream (kJ)	390881.33
% of original energy in stream	2.1

270-30

Untreated pine LHV (kJ/kg)	11425.1
Mass flow in to dryer (kg)	1777.34
Energy in to drier (kJ)	20306231.07

Torrefied pine (250-30) LHV	19387.32056
Mass flow out of torrefier (kg)	1000.00
Energy out of torrefier (kJ)	19387320.56

Energy in volatile stream (kJ)	918910.513
% of original energy in stream	4.5

270-60

Untreated pine LHV (kJ/kg)	11425.1
Mass flow in to dryer (kg)	1982.89
Energy in to drier (kJ)	22654746.4

Torrefied pine (250-30) LHV	20561.17
Mass flow out of torrefier (kg)	1000.00
Energy out of torrefier (kJ)	20561169

Energy in volatile stream (kJ)	2093577.39
% of original energy in stream	9.2

290-30

Untreated pine LHV (kJ/kg)	11425.1
Mass flow in to dryer (kg)	2086.35
Energy in to drier (kJ)	23836705.8

Torrefied pine (250-30) LHV	21787.63
Mass flow out of torrefier (kg)	1000.00
Energy out of torrefier (kJ)	21787628.38

Energy in volatile stream (kJ)	2049077.46
% of original energy in stream	8.6